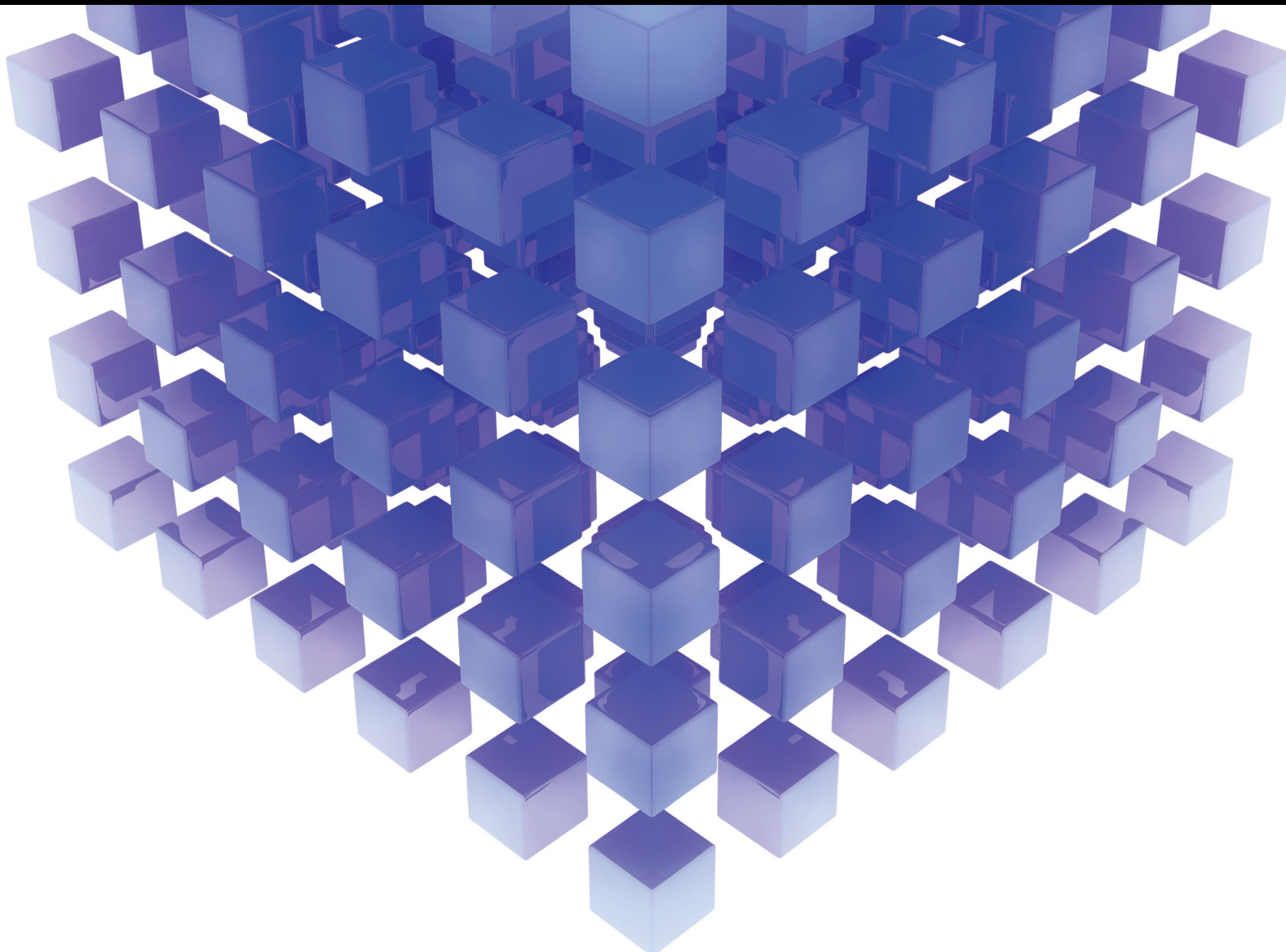# Modelling and Design Optimization of Complex Engineering Systems considering Mixed Uncertainties

Lead Guest Editor: Debiao Meng
Guest Editors: Xin Liu, Ning-Cong Xiao, and José A. F. O. Correia

Modelling and Design Optimization of Complex Engineering Systems considering Mixed Uncertainties

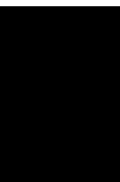# Modelling and Design Optimization of Complex Engineering Systems considering Mixed Uncertainties

Lead Guest Editor: Debiao Meng
Guest Editors: Xin Liu, Ning-Cong Xiao, and José A. F. O. Correia

Chief Editor

Paolo Boscariol, Italy
Daniela Boso (iD), Italy
Guillermo Botella-Juan, Spain
Abdesselem Boulkroune (iD), Algeria
Boulaïd Boulkroune, Belgium
Fabio Bovenga (iD), Italy
Francesco Braghin (iD), Italy
Ricardo Branco, Portugal
Julien Bruchon (iD), France
Matteo Bruggi (iD), Italy
Michele Brun (iD), Italy
Maria Elena Bruni, Italy
Maria Angela Butturi (iD), Italy
Bartłomiej Błachowski (iD), Poland
Dhanamjayulu C (iD), India
Raquel Caballero-Águila (iD), Spain
Filippo Cacace (iD), Italy
Salvatore Caddemi (iD), Italy
Zuowei Cai (iD), China
Roberto Caldelli (iD), Italy
Francesco Cannizzaro (iD), Italy
Maosen Cao (iD), China
Ana Carpio, Spain
Rodrigo Carvajal (iD), Chile
Caterina Casavola, Italy
Sara Casciati, Italy
Federica Caselli (iD), Italy
Carmen Castillo (iD), Spain
Inmaculada T. Castro (iD), Spain
Miguel Castro (iD), Portugal
Giuseppe Catalanotti (iD), United Kingdom
Alberto Cavallo (iD), Italy
Gabriele Cazzulani (iD), Italy
Fatih Vehbi Celebi, Turkey
Miguel Cerrolaza (iD), Venezuela
Gregory Chagnon (iD), France
Ching-Ter Chang (iD), Taiwan
Kuei-Lun Chang (iD), Taiwan
Qing Chang (iD), USA
Xiaoheng Chang (iD), China
Prasenjit Chatterjee (iD), Lithuania
Kacem Chehdi, France
Peter N. Cheimets, USA
Chih-Chiang Chen (iD), Taiwan
He Chen (iD), China

Kebing Chen (iD), China
Mengxin Chen (iD), China
Shyi-Ming Chen (iD), Taiwan
Xizhong Chen (iD), Ireland
Xue-Bo Chen (iD), China
Zhiwen Chen (iD), China
Qiang Cheng, USA
Zeyang Cheng, China
Luca Chiapponi (iD), Italy
Francisco Chicano (iD), Spain
Tirivanhu Chinyoka (iD), South Africa
Adrian Chmielewski (iD), Poland
Seongim Choi (iD), USA
Gautam Choubey (iD), India
Hung-Yuan Chung (iD), Taiwan
Yusheng Ci, China
Simone Cinquemani (iD), Italy
Roberto G. Citarella (iD), Italy
Joaquim Ciurana (iD), Spain
John D. Clayton (iD), USA
Piero Colajanni (iD), Italy
Giuseppina Colicchio, Italy
Vassilios Constantoudis (iD), Greece
Enrico Conte, Italy
Alessandro Contento (iD), USA
Mario Cools (iD), Belgium
Gino Cortellessa, Italy
Carlo Cosentino (iD), Italy
Paolo Crippa (iD), Italy
Erik Cuevas (iD), Mexico
Guozeng Cui (iD), China
Mehmet Cunkas (iD), Turkey
Giuseppe D'Aniello (iD), Italy
Peter Dabnichki, Australia
Weizhong Dai (iD), USA
Zhifeng Dai (iD), China
Purushothaman Damodaran (iD), USA
Sergey Dashkovskiy, Germany
Adiel T. De Almeida-Filho (iD), Brazil
Fabio De Angelis (iD), Italy
Samuele De Bartolo (iD), Italy
Stefano De Miranda (iD), Italy
Filippo De Monte (iD), Italy

José António Fonseca De Oliveira Correia, Portugal
Jose Renato De Sousa, Brazil
Michael Defoort, France
Alessandro Della Corte, Italy
Laurent Dewasme, Belgium
Sanku Dey, India
Gianpaolo Di Bona, Italy
Roberta Di Pace, Italy
Francesca Di Puccio, Italy
Ramón I. Diego, Spain
Yannis Dimakopoulos, Greece
Hasan Dinçer, Turkey
José M. Domínguez, Spain
Georgios Dounias, Greece
Bo Du, China
Emil Dumic, Croatia
Madalina Dumitriu, United Kingdom
Premraj Durairaj, India
Saeed Eftekhar Azam, USA
Said El Kafhali, Morocco
Antonio Elipe, Spain
R. Emre Erkmen, Canada
John Escobar, Colombia
Leandro F. F. Miguel, Brazil
FRANCESCO FOTI, Italy
Andrea L. Facci, Italy
Shahla Faisal, Pakistan
Giovanni Falsone, Italy
Hua Fan, China
Jianguang Fang, Australia
Nicholas Fantuzzi, Italy
Muhammad Shahid Farid, Pakistan
Hamed Faroqi, Iran
Yann Favennec, France
Fiorenzo A. Fazzolari, United Kingdom
Giuseppe Fedele, Italy
Roberto Fedele, Italy
Baowei Feng, China
Mohammad Ferdows, Bangladesh
Arturo J. Fernández, Spain
Jesus M. Fernandez Oro, Spain
Francesco Ferrise, Italy
Eric Feulvarch, France
Thierry Floquet, France

Eric Florentin, France
Gerardo Flores, Mexico
Antonio Forcina, Italy
Alessandro Formisano, Italy
Francesco Franco, Italy
Elisa Francomano, Italy
Juan Frausto-Solis, Mexico
Shujun Fu, China
Juan C. G. Prada, Spain
HECTOR GOMEZ, Chile
Matteo Gaeta, Italy
Mauro Gaggero, Italy
Zoran Gajic, USA
Jaime Gallardo-Alvarado, Mexico
Mosè Gallo, Italy
Akemi Gálvez, Spain
Maria L. Gandarias, Spain
Hao Gao, Hong Kong
Xingbao Gao, China
Yan Gao, China
Zhiwei Gao, United Kingdom
Giovanni Garcea, Italy
José García, Chile
Harish Garg, India
Alessandro Gasparetto, Italy
Stylianos Georgantzinos, Greece
Fotios Georgiades, India
Parviz Ghadimi, Iran
Ştefan Cristian Gherghina, Romania
Georgios I. Giannopoulos, Greece
Agathoklis Giaralis, United Kingdom
Anna M. Gil-Lafuente, Spain
Ivan Giorgio, Italy
Gaetano Giunta, Luxembourg
Jefferson L.M.A. Gomes, United Kingdom
Emilio Gómez-Déniz, Spain
Antonio M. Gonçalves de Lima, Brazil
Qunxi Gong, China
Chris Goodrich, USA
Rama S. R. Gorla, USA
Veena Goswami, India
Xunjie Gou, Spain
Jakub Grabski, Poland

Francisco J. Martos (iD), Spain
Elio Masciari (iD), Italy
Paolo Massioni (iD), France
Alessandro Mauro (iD), Italy
Jonathan Mayo-Maldonado (iD), Mexico
Pier Luigi Mazzeo (iD), Italy
Laura Mazzola, Italy
Driss Mehdi (iD), France
Zahid Mehmood (iD), Pakistan
Roderick Melnik (iD), Canada
Xiangyu Meng (iD), USA
Jose Merodio (iD), Spain
Alessio Merola (iD), Italy
Mahmoud Mesbah (iD), Iran
Luciano Mescia (iD), Italy
Laurent Mevel (iD), France
Constantine Michailides (iD), Cyprus
Mariusz Michta (iD), Poland
Prankul Middha, Norway
Aki Mikkola (iD), Finland
Giovanni Minafò (iD), Italy
Edmondo Minisci (iD), United Kingdom
Hiroyuki Mino (iD), Japan
Dimitrios Mitsotakis (iD), New Zealand
Ardashir Mohammadzadeh (iD), Iran
Francisco J. Montáns (iD), Spain
Francesco Montefusco (iD), Italy
Gisele Mophou (iD), France
Rafael Morales (iD), Spain
Marco Morandini (iD), Italy
Javier Moreno-Valenzuela (iD), Mexico
Simone Morganti (iD), Italy
Caroline Mota (iD), Brazil
Aziz Moukrim (iD), France
Shen Mouquan (iD), China
Dimitris Mourtzis (iD), Greece
Emiliano Mucchi (iD), Italy
Taseer Muhammad, Saudi Arabia
Ghulam Muhiuddin, Saudi Arabia
Amitava Mukherjee (iD), India
Josefa Mula (iD), Spain
Jose J. Muñoz (iD), Spain
Giuseppe Muscolino, Italy
Marco Mussetta (iD), Italy

Hariharan Muthusamy, India
Alessandro Naddeo (iD), Italy
Raj Nandkeolyar, India
Keivan Navaie (iD), United Kingdom
Soumya Nayak, India
Adrian Neagu (iD), USA
Erivelton Geraldo Nepomuceno (iD), Brazil
AMA Neves, Portugal
Ha Quang Thinh Ngo (iD), Vietnam
Nhon Nguyen-Thanh, Singapore
Papakostas Nikolaos (iD), Ireland
Jelena Nikolic (iD), Serbia
Tatsushi Nishi, Japan
Shanzhou Niu (iD), China
Ben T. Nohara (iD), Japan
Mohammed Nouari (iD), France
Mustapha Nourelfath, Canada
Kazem Nouri (iD), Iran
Ciro Núñez-Gutiérrez (iD), Mexico
Wlodzimierz Ogryczak, Poland
Roger Ohayon, France
Krzysztof Okarma (iD), Poland
Mitsuhiro Okayasu, Japan
Murat Olgun (iD), Turkey
Diego Oliva, Mexico
Alberto Olivares (iD), Spain
Enrique Onieva (iD), Spain
Calogero Orlando (iD), Italy
Susana Ortega-Cisneros (iD), Mexico
Sergio Ortobelli, Italy
Naohisa Otsuka (iD), Japan
Sid Ahmed Ould Ahmed Mahmoud (iD),
Saudi Arabia
Taoreed Owolabi (iD), Nigeria
EUGENIA PETROPOULOU (iD), Greece
Arturo Pagano, Italy
Madhumangal Pal, India
Pasquale Palumbo (iD), Italy
Dragan Pamučar, Serbia
Weifeng Pan (iD), China
Chandan Pandey, India
Rui Pang, United Kingdom
Jürgen Pannek (iD), Germany
Elena Panteley, France
Achille Paolone, Italy

Yong (Aaron) Tan, United Kingdom
Marco Antonio Taneco-Hernández (iD), Mexico
Lu Tang (iD), China
Tianyou Tao, China
Hafez Tari (iD), USA
Alessandro Tasora (iD), Italy
Sergio Teggi (iD), Italy
Adriana del Carmen Téllez-Anguiano (iD), Mexico
Ana C. Teodoro (iD), Portugal
Efstathios E. Theotokoglou (iD), Greece
Jing-Feng Tian, China
Alexander Timokha (iD), Norway
Stefania Tomasiello (iD), Italy
Gisella Tomasini (iD), Italy
Isabella Torcicollo (iD), Italy
Francesco Tornabene (iD), Italy
Mariano Torrisi (iD), Italy
Thang nguyen Trung, Vietnam
George Tsiatas (iD), Greece
Le Anh Tuan (iD), Vietnam
Nerio Tullini (iD), Italy
Emilio Turco (iD), Italy
Ilhan Tuzcu (iD), USA
Efstratios Tzirtzilakis (iD), Greece
FRANCISCO UREÑA (iD), Spain
Filippo Ubertini (iD), Italy
Mohammad Uddin (iD), Australia
Mohammad Safi Ullah (iD), Bangladesh
Serdar Ulubeyli (iD), Turkey
Mati Ur Rahman (iD), Pakistan
Panayiotis Vafeas (iD), Greece
Giuseppe Vairo (iD), Italy
Jesus Valdez-Resendiz (iD), Mexico
Eusebio Valero, Spain
Stefano Valvano (iD), Italy
Carlos-Renato Vázquez (iD), Mexico
Martin Velasco Villa (iD), Mexico
Franck J. Vernerey, USA
Georgios Veronis (iD), USA
Vincenzo Vespri (iD), Italy
Renato Vidoni (iD), Italy
Venkatesh Vijayaraghavan, Australia

Anna Vila, Spain
Francisco R. Villatoro (iD), Spain
Francesca Vipiana (iD), Italy
Stanislav Vítek (iD), Czech Republic
Jan Vorel (iD), Czech Republic
Michael Vynnycky (iD), Sweden
Mohammad W. Alomari, Jordan
Roman Wan-Wendner (iD), Austria
Bingchang Wang, China
C. H. Wang (iD), Taiwan
Dagang Wang, China
Guoqiang Wang (iD), China
Huaiyu Wang, China
Hui Wang (iD), China
J.G. Wang, China
Ji Wang (iD), China
Kang-Jia Wang (iD), China
Lei Wang (iD), China
Qiang Wang, China
Qingling Wang (iD), China
Weiwei Wang (iD), China
Xinyu Wang (iD), China
Yong Wang (iD), China
Yung-Chung Wang (iD), Taiwan
Zhenbo Wang (iD), USA
Zhibo Wang, China
Waldemar T. Wójcik, Poland
Chi Wu (iD), Australia
Qiuhong Wu, China
Yuqiang Wu, China
Zhibin Wu (iD), China
Zhizheng Wu (iD), China
Michalis Xenos (iD), Greece
Hao Xiao (iD), China
Xiao Ping Xie (iD), China
Qingzheng Xu (iD), China
Binghan Xue (iD), China
Yi Xue (iD), China
Joseph J. Yame (iD), France
Chuanliang Yan (iD), China
Xinggang Yan (iD), United Kingdom
Hongtai Yang (iD), China
Jixiang Yang (iD), China
Mijia Yang, USA
Ray-Yeng Yang, Taiwan

Zaoli Yang ⓘ, China
Jun Ye ⓘ, China
Min Ye ⓘ, China
Luis J. Yebra ⓘ, Spain
Peng-Yeng Yin ⓘ, Taiwan
Muhammad Haroon Yousaf ⓘ, Pakistan
Yuan Yuan, United Kingdom
Qin Yuming, China
Elena Zaitseva ⓘ, Slovakia
Arkadiusz Zak ⓘ, Poland
Mohammad Zakwan ⓘ, India
Ernesto Zambrano-Serrano ⓘ, Mexico
Francesco Zammori ⓘ, Italy
Jessica Zangari ⓘ, Italy
Rafal Zdunek ⓘ, Poland
Ibrahim Zeid, USA
Nianyin Zeng ⓘ, China
Junyong Zhai ⓘ, China
Hao Zhang ⓘ, China
Haopeng Zhang ⓘ, USA
Jian Zhang ⓘ, China
Kai Zhang, China
Lingfan Zhang ⓘ, China
Mingjie Zhang ⓘ, Norway
Qian Zhang ⓘ, China
Tianwei Zhang ⓘ, China
Tongqian Zhang ⓘ, China
Wenyu Zhang ⓘ, China
Xianming Zhang ⓘ, Australia
Xuping Zhang ⓘ, Denmark
Yinyan Zhang, China
Yifan Zhao ⓘ, United Kingdom
Debao Zhou, USA
Heng Zhou ⓘ, China
Jian G. Zhou ⓘ, United Kingdom
Junyong Zhou ⓘ, China
Xueqian Zhou ⓘ, United Kingdom
Zhe Zhou ⓘ, China
Wu-Le Zhu, China
Gaetano Zizzo ⓘ, Italy
Mingcheng Zuo, China

Contents

Research Article

An Overview on Modelling of Complex Interconnected Nonlinear Systems

Mourad Elloumi [1,2] **Hamdi Gassara** [1] **and Omar Naifar** [3,4]

[1]*Laboratory of Sciences and Technology of Automatic Control and Computer Engineering, National School of Engineering of Sfax, University of Sfax, P. O. Box 1173, Sfax 3038, Tunisia*
[2]*Faculty of Sciences of Gafsa, University of Gafsa, Gafsa, Tunisia*
[3]*Control and Energy Management Laboratory, National School of Engineering, Sfax University, Sfax, Tunisia*
[4]*Higher Institute of Applied Science and Technology of Kairouan, University of Kairouan, Kairouan, Tunisia*

Correspondence should be addressed to Omar Naifar; email.naifar@gmail.com

This paper proposes new mathematical models of representation, which can describe the dynamic behavior of large-scale nonlinear systems, such as an extended mathematical model of Volterra series, interconnected Hammerstein structures, and interconnected Wiener structures. In this research, we focus on the class of large-scale nonlinear systems, which are composed of several interconnected nonlinear subsystems. In this context, a discrete nonlinear mathematical model with unknown time-varying parameters, mono-variable, characterizes each interconnected subsystem operating in a deterministic or stochastic environment. An illustrative numerical simulation example of two interconnected nonlinear processes is provided to prove the validity and the performance of the developed theoretical results.

1. Introduction

In the literature, the description of a dynamical system by a mathematical model (MM) can be carried out from two different approaches: the first approach is based on a theoretical analysis which allows the system to be described by a MM based on the universal laws that govern it. As for the second, it is realized by experimental analysis which makes it possible to describe the system by a MM based on the results of the experimental tests carried out of this system. The first step in any system study undoubtedly requires representing it by a model that can characterize its dynamic behavior. Thus, this step is essential in the synthesis of a control scheme, with a view to solving either a tracking problem, or a regulation problem, or a joint tracking and regulation problem, of a dynamic system (mechanical, electrical, biological), since it determines the targeted control performance (rapidity, stability, accuracy). It can present difficulties of practical implementation, more particularly in the case of complex systems.

In both the scientific and social sciences, the study of complex systems is becoming increasingly relevant. It is widely assumed that there is such a thing as a complex system, with many instances examined across a variety of fields. However, there is no succinct description of a complex system, much less one that is agreed upon by all scientists. Various attempts have been made to describe a complex system and examine a core set of characteristics that are generally identified with complex systems in the literature and by specialists. Some of these characteristics are neither required nor sufficient for complexity, while others are too imprecise or ambiguous to be analytically useful. To add mathematical development to the topic, various common measures of complexity are undertaken from the scientific literature, and taxonomy for them is offered, before claiming that the statistical complexity best reflects the qualitative idea of the order generated by complex systems. In this context, requirements as a characterization of complexity might be provided. These are qualitative requirements that may or may not be adequate for complexity when taken together. It is a ripe research field with a plethora

of viewpoints to consider. With the increasing use of complex systems in real-world applications, especially biomedical, finance, and engineering, the study and analysis of complex behavior and dynamic response of complex systems have become increasingly essential. The development of the estimation and the control strategies for a complex system is based on the description of its dynamic behavior by a MM. This description may essentially be carried out using two ways of analysis, the theoretical technique and the experimental one. These MMs can be expressed by difference equations (IOMMs), transfer functions, or state equations (state MMs). The complex systems modelling (nonlinear, nonstationary, high dimensional) from a theoretical analysis can lead to a failure. Indeed, these systems are complex enough for us to be able to apply universal laws to them, in order to formulate theoretically MMs allowing them to describe correctly their dynamic behavior. However, the obtained MM, which is based on theoretical analysis, will not be useable in general for the synthesis of a control law, in particular a digital control law. This is due, on the one hand, to the equations resolution complexity of this MM and, on the other hand, to the disregard of disturbances acting on different points in the system. To overcome the problems relating to the modelling of a dynamic system based on a method of theoretical analysis, we seek to apprehend this system in a phenomenological way, by establishing a mathematical model from experimental analysis. Therefore, we seek to link the measured quantities of the system (input, output, state) by a certain combination.

The study of dynamical high dimensional systems has attracted the attention of many researchers and automation engineers worldwide. Every large-scale system can be envisaged as a system consisting of a large number of interacting interconnected systems. Since such a system normally comprises several interconnected systems (power network system and set of coupled tanks), the formulation problem of their parametric estimation or their control is too intricate. Several studies dealing with different themes (modelling, identification, control, stability, and optimization) have been developed and published in the literature [1–3]. In fact, the study [1] is motivated by the desire to build decentralized control for a class of large-scale systems that do not meet the matching condition criterion. The author of [2] discusses the topic of implicit self-tuning control for a class of large-scale systems that have been deconstructed into linked subsystems. The authors look at plants with unknown characteristics that are characterized by a linear invariant or slowly variable model. In addition, the development of recursive estimation techniques for large-scale stochastic systems utilizing the maximum likelihood method was given in [3]. The findings of this research concentrated on large-scale linear systems that can be defined as either continuous or discrete MM. However, certain results concerning large-scale nonlinear systems have been developed and published [4–13]. Indeed, the author of [4] proposes a fault-tolerant control of a class of linked feedback linearizable nonlinear systems via a decentralized adaptive approximation architecture. An adaptive approximation strategy for

decentralized fault-tolerant control for a class of nonlinear large-scale systems with unknown multiple time-delayed interaction faults is proposed in [5]. Using the input-output linearization idea, the author of [6] suggested a resilient adaptive fuzzy semidecentralized control for a class of large-scale nonlinear systems. The author of [7] investigates the topic of decentralized adaptive control in large-scale non-strict-feedback nonlinear systems with a dynamic interaction and unmeasurable states, where the dynamic interaction is connected to both input and output items. A unique extended modal series approach for tackling the infinite horizon optimal control issue of nonlinear linked large-scale dynamic systems is presented in [8]. The infinite horizon nonlinear large-scale two-point boundary value problem (TPBVP), derived from Pontryagin's maximum principle, is converted into a series of linear time-invariant TPBVPs using this approach. An adaptive fuzzy decentralized output-feedback control issue for a class of nonlinear large-scale systems is discussed in [9]. The parametric absolute stability of linked Lurie systems with several subsystems is studied in [10], where the parametric stability refers to the difficulty of determining the feasibility and stability of equilibrium states when the unknown parameters change. A decentralized fuzzy control problem for asymptotic stabilization of a class of nonlinear large-scale systems using an observer-based output-feedback method has been presented in [11]. A PD-type iterative learning control has been developed and applied for uncertain spatially interconnected systems [12]. Tao et al. were proposed a robust PD-type iterative learning control for discrete systems with multiple time delays subjected to polytopic uncertainty and restricted frequency domain [13]. The most of these works concerned the large-scale systems which can be described by a linear MM (input-output MM and state MM) with constant or slow time-varying parameters. However, a few results were published concerning the large-scale nonlinear systems which are described by nonlinear state MMs. Furthermore, we may use other MMs to characterize these nonlinear dynamic systems. The traditional structure relies on the nonlinear system's approximation by the Volterra series. Other forms of representations, like input-output models and linked block models, allow us to characterize the dynamic behavior of considered systems.

Consequently, we shall build a variety of nonlinear discrete MMs capable of describing the dynamic behavior of large-scale nonlinear systems in this study. The emphasis will be on the class of large-scale nonlinear systems that composed of several linked mono-variable nonlinear systems with unknown time-varying parameters. We suppose that these complex systems can operate in a deterministic or stochastic environment.

The remainder of this research is organized as follows: Section 2 is devoted to the description of large-scale nonlinear systems by MMs in a series of functions, where two forms of MMs are developed. In Section 3, input-output MMs for modelling the dynamic behavior of linked nonlinear systems, operating in a deterministic or stochastic environment, are proposed. The modelling of linked nonlinear mono-variable systems, based on interconnected Hammerstein and Wiener structures, is derived in Section 4.

Finally, some simulation results and concluding remarks are provided in Sections 5 and 6.

2. MMs in Series of Functions

Serial models of functions are one of the MMs that may represent the dynamic behavior of a nonlinear system. This family of models allows its output at a given moment to be described by an infinite sum of polynomial functions dependent on the input at the same and previous instants. As a result, the Volterra series representation and the Volterra parametric representation may be extended to describe nonlinear systems with huge dimensions. These two representations are commonly used in the study and description of nonlinear systems [14–17], particularly those defined by discrete MMs. In fact, this is the second installment of a two-volume guidebook [14] that provides a detailed review of nonlinear dynamic system identification. Many elements of nonlinear processes are covered in the books, including modelling, parameter estimates, structure search, nonlinearity, and model validity testing. Not only nonparametric models but also parametric models with a restricted number of parameters are included in the book. The estimate of time-domain parameters is covered in depth, as well as frequency domain and power spectrum processes. This work is aimed towards postgraduate students, researchers, and engineers working in the field of nonlinear systems. There are numerous instances, case studies, and experimental identifications of genuine processes. The study [15] gives an overview of works in the field of mathematical modelling of nonlinear input-output dynamic systems with Volterra polynomials that were undertaken at systems. The author of [16] presents a method for identifying nonlinear aeroelastic systems based on the Volterra theory of nonlinear systems. The theory's recent applicability to difficulties in computational and experimental aeroelasticity is discussed. The book [17] covers simple, brief, and easy-to-understand methods for identifying nonlinear systems, as well as new research discoveries in the field of adaptive nonlinear system identification. These approaches make use of adaptive filter algorithms, which are well-known for identifying linear systems. They can be used to simulate nonlinear systems that polynomials can efficiently model.

2.1. MM in a Series of Volterra.
The Volterra series represent nonlinear MMs without output feedback. Thus, a nonlinear system can be described by the following MM in a series of Volterra:

$$y(k) = f(u(k-1), u(k-2), \ldots, u(k-\tau)). \tag{1}$$

The previous model can be extended to describe the dynamics of an INS.

$$y_\alpha(k) = f_\alpha\left(u_\alpha(k-1), u_\alpha(k-2), \ldots, u_\alpha(k-\tau), u_\beta(k-1), u_\beta(k-2), \ldots, u_\beta(k-\tau)\right), \tag{2}$$

where $y_\alpha(k)$ and $u_\alpha(k)$ represent, respectively, the output and input of the INS S_α, $\alpha = 1, \ldots, N$; $u_\beta(k)$ indicates the inputs from the other connected subsystems S_β, $\beta = 1, \ldots, N$; $\beta \neq \alpha$; N represents the number of INSs; and $f_\alpha(.)$ is a nonlinear function, which is approximated by a polynomial for the case of the Volterra model.

An approximation of the MM (2) allowing to describe an INS of order M, which is composed of N INSs, can be obtained using the second-order nuclei, such as

$$
\begin{aligned}
y_\alpha(k) = \mu_\alpha &+ \sum_{r=1}^{M} \zeta_{\alpha,r}\, u_\alpha(k-r) + \sum_{r=1}^{M}\sum_{s=1}^{M} \zeta_{\alpha,rs}\, u_\alpha(k-r)\, u_\alpha(k-s), \\
&+ \sum_{\beta=1,\beta\neq\alpha}^{N}\sum_{r=1}^{M} \zeta_{\alpha\beta,r}\, u_\beta(k-r) + \sum_{\beta=1,\beta\neq\alpha}^{N}\sum_{r=1}^{M}\sum_{s=1}^{M} \zeta_{\alpha\beta,rs}\, u_\alpha(k-r)\, u_\beta(k-s),
\end{aligned}
\tag{3}
$$

where $\alpha, \beta = 1, \ldots, N$; $\beta \neq \alpha$, μ_α is a constant, and $\zeta_{\alpha,r}$, $\zeta_{\alpha,rs}$, $\zeta_{\alpha\beta,r}$, and $\zeta_{\alpha\beta,rs}$ are positive parameters. These parameters are called Volterra kernels.

2.2. Parametric Model of Volterra.
This MM family is distinguished by linear feedback of outputs and a polynomial function of inputs. In the literature, the Volterra parametric model is used to describe a nonlinear system.

$$
\begin{aligned}
y(k) = f(u(k-1), u(k-2), \ldots, u(k-m)) \\
- \sum_{h=1}^{m} a_h\, y(k-h).
\end{aligned}
\tag{4}
$$

Thereby, we propose the following parametric model of Volterra in order to describe the dynamic of an INS:

$$y_\alpha(k) = f_\alpha\Big(u_\alpha(k-1), u_\alpha(k-2), \ldots, u_\alpha(k-m), u_\beta(k-1), u_\beta(k-2), \ldots, u_\beta(k-m)\Big),$$
$$-\sum_{h=1}^{m} a_{\alpha,h}\, y_\alpha(k-h) + \sum_{\beta=1,\beta\neq\alpha}^{N} \sum_{h=1}^{m} a_{\alpha\beta,h}\, y_\beta(k-h), \tag{5}$$

with $u_\alpha(k)$ is the input and $y_\alpha(k)$ is the output of the INS S_α; $y_\beta(k)$ and $u_\beta(k)$ represent, respectively, the outputs and inputs from the other INSs S_β, $\beta = 1, \ldots, N; \beta \neq \alpha$; $a_{\alpha,h}$ and $a_{\alpha\beta,h}$ are constant parameters; and m is a positive

parameter which corresponds to the order of the considered system.

In the case of an order system M and a polynomial of degree 2, the expression of the output $y_\alpha(k)$ is written in the following form:

$$y_\alpha(k) = \mu_\alpha - \sum_{h=1}^{M} a_{\alpha,h}\, y_\alpha(k-h) + \sum_{r=1}^{M} \zeta_{\alpha,r}\, u_\alpha(k-r) + \sum_{r=1}^{M}\sum_{s=1}^{M} \zeta_{\alpha,rs}\, u_\alpha(k-r)\, u_\alpha(k-s),$$
$$+ \sum_{\beta=1,\beta\neq\alpha}^{N}\sum_{r=1}^{M} \zeta_{\alpha\beta,r}\, u_\beta(k-r) + \sum_{\beta=1,\beta\neq\alpha}^{N}\sum_{h=1}^{M} a_{\alpha\beta,h}\, y_\beta(k-h) + \sum_{\beta=1,\beta\neq\alpha}^{N}\sum_{r=1}^{M}\sum_{s=1}^{M} \zeta_{\alpha\beta,rs}\, u_\alpha(k-r)\, u_\beta(k-s). \tag{6}$$

We can notice that these different representations of MMs become more and more complex by increasing the order of the system or the nonlinearity degree.

3. IOMMs

The use of input-output MMs to describe nonlinear systems is a popular strategy in industrial settings [15, 17]. In fact, the paper [15] provides an overview of work done at systems in the subject of mathematical modelling of nonlinear input-output dynamic systems with Volterra polynomials. Based on the Volterra theory of nonlinear systems, the author of [16] proposes a technique for finding nonlinear aeroelastic systems. The theory's current relevance to computational and experimental aeroelasticity problems is reviewed. The book [17] discusses simple, concise, and simple-to-understand approaches for identifying nonlinear systems, as well as recent research findings in the field of adaptive nonlinear system identification. These methods employ adaptive filter techniques, which are well-known for finding linear systems. These methods can be used to simulate nonlinear systems whose models are approximated by polynomial functions.

This paragraph is concerned with the description of large-scale nonlinear systems, which are made up of multiple linked mono-variable nonlinear systems functioning in a deterministic or stochastic environment [18]. We can differentiate three types of nonlinearities, which are as follows:

(1) Nonlinearity with respect to the parameters

(2) Nonlinearity with respect to the observations

(3) Nonlinearity with respect to the parameters and the observations

We are particularly interested in input-output MMs with linear parameters and nonlinear data.

3.1. Nonlinearity with respect to the Inputs. In this part, we will present input-output MMs that can be used to characterize the dynamics of INSs with nonlinearity with respect to the inputs. We will concentrate on linked nonlinear dynamical systems that may be characterized by the class of deterministic or stochastic input-output MMs, which are nonlinear with respect to inputs, mono-variables, with time-varying parameters.

3.1.1. Deterministic Input-Output MMs. We are interested here in the description of INSs by deterministic input-output MMs. In this context, we consider an INS S_α, $1 \leq \alpha \leq N$, coupled with other interconnected subsystems S_β, $\beta = 1, \ldots, N; \beta \neq \alpha$, having a nonlinearity with respect to the inputs, which can be modeled by the following IOMM INDARMA (interconnected nonlinear deterministic autoregressive moving average) [18]:

$$A_\alpha\big(q^{-1},k\big) y_\alpha(k) = q^{-d_\alpha} B_\alpha\big(q^{-1},k\big) u_\alpha(k) + \sum_{\beta=1,\beta\neq\alpha}^{N} q^{-d_{\alpha\beta}} B_{\alpha\beta}\big(q^{-1},k\big) u_\beta(k) + \sum_{\beta=1,\beta\neq\alpha}^{N} q^{-t_{\alpha\beta}} A_{\alpha\beta}\big(q^{-1},k\big) y_\beta(k),$$
$$+ f_g^u\big[u_\alpha(k-1), u_\alpha(k-2), \ldots, u_\alpha(k-n_\alpha), u_\beta(k-1), u_\beta(k-2), \ldots, u_\beta(k-n_\alpha)\big], \tag{7}$$

where $y_\alpha(k)$ and $u_\alpha(k)$ represent, respectively, the output and input of the INS S_α; $u_\alpha(k)$ and $u_\beta(k)$ denote,

respectively, the outputs and inputs from the other interconnected nonlinear subsystems S_β, $\beta = 1, \ldots, N; \beta \neq \alpha$; d_α

presents the intrinsic delay of the considered system; $t_{\alpha\beta}$ and $d_{\alpha\beta}$ represent the delays of the interactions, which are relative to the outputs and the inputs of the other INSs S_β; and $A_\alpha(q^{-1}, k)$, $B_\alpha(q^{-1}, k)$, $B_{\alpha\beta}(q^{-1}, k)$, and $A_{\alpha\beta}(q^{-1}, k)$ are time-varying polynomials, defined as follows:

$$
\begin{aligned}
A_\alpha\left(q^{-1}, k\right) &= 1 + a_{\alpha,1}(k)q^{-1} + \ldots + a_{\alpha,n_{A_\alpha}}(k)q^{-nAa}, \\
B_\alpha\left(q^{-1}, k\right) &= b_{\alpha,1}(k)q^{-1} + \ldots + b_{\alpha,n_{B,a}}(k)q^{-n_{Ba}}, \\
B_{\alpha\beta}\left(q^{-1}, k\right) &= b_{\alpha\beta,1}(k)q^{-1} + \ldots + b_{\alpha\beta,n_{B_{\alpha\beta}}}(k)q^{-n_{B_{\alpha\beta}}},
\end{aligned} \quad (8)
$$

and

$$
A_{\alpha\beta}\left(q^{-1}, k\right) = 1 + a_{\alpha\beta,1}(k)q^{-1} + \ldots + a_{\alpha\beta,n_{A_{\alpha\beta}}}(k)q^{-n_{A_{\alpha\beta}}}, \quad (9)
$$

with $\alpha, \beta = 1, \ldots, N; \beta \neq \alpha$, and $n_{A_\alpha}, n_{B_\alpha}, n_{B_{\alpha\beta}}$, and $n_{A_{\alpha\beta}}$ are the orders of the polynomials $A_\alpha(q^{-1}, k)$, $B_\alpha(q^{-1}, k)$, $B_{\alpha\beta}(q^{-1}, k)$, and $A_{\alpha\beta}(q^{-1}, k)$.

The term $f_g^u[.]$ represents a nonlinear function with nonlinearity degree p, which depends on the input sequences of the interconnected system (IS) S_α, $1 \leq \alpha \leq N$, and the other INSs S_β, $\beta = 1, \ldots, N; \beta \neq \alpha$, defined as follows [18]:

$$
\begin{aligned}
f_g^u[.] = & \sum_{r_1=1}^{n_{g_{\alpha\alpha,r_1}}} \sum_{r_2=1}^{n_{g_{\alpha\alpha,r_1 r_2}}} g_{\alpha\alpha,r_1 r_2}(k) u_\alpha(k-r_1)u_\alpha(k-r_2), \\
& + \sum_{r_1=1}^{n_{g_{\alpha\alpha,r_1}}} \sum_{r_2=1}^{n_{g_{\alpha\alpha,r_1 r_2}}} \sum_{r_3=1}^{n_{g_{\alpha\alpha,r_1 r_2 r_3}}} g_{\alpha\alpha,r_1 r_2 r_3}(k) u_\alpha(k-r_1)u_\alpha(k-r_2)u_\alpha(k-r_3), \\
& + \cdots + \sum_{r_1=1}^{n_{g_{\alpha\alpha,r_1}}} \sum_{r_2=1}^{n_{g_{\alpha\alpha,r_1 r_2}}} \cdots \sum_{r_p=1}^{n_{g_{\alpha\alpha,r_1 r_2 \ldots r_p}}} g_{\alpha\alpha,r_1 \ldots r_p}(k) u_\alpha(k-r_1) \ldots u_\alpha(k-r_p), \\
& + \sum_{\beta=1,\beta\neq\alpha}^{N} \sum_{r_1=1}^{n_{g_{\alpha\beta,r_1}}} \sum_{r_2=1}^{n_{g_{\alpha\beta,r_1 r_2}}} g_{\alpha\beta,r_1 r_2}(k)u_\alpha(k-r_1) u_\beta(k-r_2), \\
& + \sum_{\beta=1,\beta\neq\alpha}^{N} \sum_{r_1=1}^{n_{g_{\alpha\beta,r_1}}} \sum_{r_2=1}^{n_{g_{\alpha\beta,r_1 r_2}}} \sum_{r_3=1}^{n_{g_{\alpha\beta,r_1 r_2 r_3}}} g_{\alpha\beta,r_1 r_2 r_3}(k) u_\alpha(k-r_1)u_\alpha(k-r_2)u_\beta(k-r_3), \\
& + \cdots + \sum_{\beta=1,\beta\neq\alpha}^{N} \sum_{r_1=1}^{n_{g_{\alpha\beta,r_1}}} \sum_{r_2=1}^{n_{g_{\alpha\beta,r_1 r_2}}} \cdots \sum_{r_p=1}^{n_{g_{\alpha\beta,r_1 r_2 \ldots r_p}}} g_{\alpha\beta,r_1 \ldots r_p}(k) u_\alpha(k-r_1) \ldots u_\beta(k-r_p).
\end{aligned} \quad (10)
$$

Note that each IS S_α, $\alpha = 1, \ldots, N$, is coupled with the outputs and the inputs of the other INSs S_β, by the polynomials $A_{\alpha\beta}(q^{-1}, k)$ and $B_{\alpha\beta}(q^{-1}, k)$.

3.1.2. Stochastic Input-Output MMs. This subsection deals with the description of the INSs, which are described by stochastic IOMMs. Consider a stochastic INS S_α, $1 \leq \alpha \leq N$, which is coupled to other ISs S_β, $\beta = 1, \ldots, N; \beta \neq \alpha$, nonlinear with respect to the inputs. This system can be qualified by the following mathematical input-output model INAR-MAX (interconnected nonlinear autoregressive moving average with exogenous) [18]:

$$
\begin{aligned}
A_\alpha\left(q^{-1}, k\right) y_\alpha(k) = & q^{-d_\alpha} B_\alpha\left(q^{-1}, k\right)u_\alpha(k) + \sum_{\beta=1,\beta\neq\alpha}^{N} q^{-d_{\alpha\beta}} B_{\alpha\beta}\left(q^{-1}, k\right) u_\beta(k) + \sum_{\beta=1,\beta\neq\alpha}^{N} q^{-t_{\alpha\beta}} A_{\alpha\beta}\left(q^{-1}, k\right) y_\beta(k), \\
& + f_g^u\left[u_\alpha(k-1), u_\alpha(k-2), \ldots, u_\alpha(k-n_\alpha), u_\beta(k-1), u_\beta(k-2), \ldots, u_\beta(k-n_\alpha)\right], \\
& + f_\gamma^{ue}\left[u_\alpha(k-1), u_\alpha(k-2), \ldots, u_\alpha(k-n_\alpha), e_\alpha(k-1), e_\alpha(k-2), \ldots, e_\alpha(k-n_\alpha)\right] \\
& + f_c^e\left[e_\alpha(k-1), e_\alpha(k-2), \ldots, e_\alpha(k-n_\alpha)\right] + C_\alpha\left(q^{-1}\right) e_\alpha(k),
\end{aligned} \quad (11)
$$

where $\{e_\alpha(k)\}$ represents the set of random variables acting on the IS S_α, which can be assimilated to a Gaussian distribution with zero mean and constant variance σ_α^2, $f_g^u[.]$ is a nonlinear function of degree p given by (10), $A_\alpha(q^{-1}, k)$, $B_\alpha(q^{-1}, k)$, $B_{\alpha\beta}(q^{-1}, k)$, and $A_{\alpha\beta}(q^{-1}, k)$ are time-varying polynomials defined by (8), (9), (10), and (9), and $C_\alpha(q^{-1})$ is a polynomial with constant parameters, defined as follows:

$$C_\alpha\left(q^{-1}\right) = 1 + c_{\alpha,1}q^{-1} + \ldots + c_{\alpha,n_{Ca}}q^{-n_{C_\alpha}}, \qquad (12)$$

where n_{C_α} denotes the order of $C_\alpha(q^{-1})$.

The term $f_\gamma^{ue}[\,.\,]$ denotes a nonlinear function of degree p, which is determined by the IS's input sequences S_α and the disturbance $e_\alpha(k)$. This function can be expressed as follows:

$$
\begin{aligned}
f_\gamma^{ue}[.] &= \sum_{r_1=1}^{n_{\gamma_{\alpha\alpha,r_1}}} \sum_{r_2=1}^{n_{\gamma_{\alpha\alpha,r_1 r_2}}} \gamma_{\alpha\alpha,r_1 r_2} u_\alpha(k-r_1)e_\alpha(k-r_2) + \ldots \quad \ldots +, \\
&\quad \sum_{r_1=1}^{n_{\gamma_{\alpha\alpha,r_1}}} \sum_{r_2=1}^{n_{\gamma_{\alpha\alpha,r_1 r_2}}} \cdots \sum_{r_p=1}^{n_{\gamma_{\alpha\alpha,r_1 r_2 \ldots r_p}}} \gamma_{\alpha\alpha,r_1 \ldots r_p} u_\alpha(k-r_1) \ldots e_\alpha(k-r_p).
\end{aligned}
\tag{13}
$$

The term $f_c^e[\,.\,]$ represents a nonlinear function of degree p, which depends only on the noise sequence $\{e_\alpha(k)\}$. This term is defined as follows:

$$
\begin{aligned}
f_c^e[.] &= \sum_{r_1=1}^{n_{c_{\alpha\alpha,r_1}}} \sum_{r_2=1}^{n_{c_{\alpha\alpha,r_1 r_2}}} c_{\alpha\alpha,r_1 r_2} e_\alpha(k-r_1)e_\alpha(k-r_2) + \ldots \quad \ldots +, \\
&\quad \sum_{r_1=1}^{n_{c_{\alpha\alpha,r_1}}} \sum_{r_2=1}^{n_{c_{\alpha\alpha,r_1 r_2}}} \cdots \sum_{r_p=1}^{n_{c_{\alpha\alpha,r_1 r_2 \ldots r_p}}} c_{\alpha\alpha,r_1 \ldots r_p} e_\alpha(k-r_1) \ldots e_\alpha(k-r_p).
\end{aligned}
\tag{14}
$$

As an example, we consider a large-scale nonlinear dynamic system composed of two INSs S_1 and S_2. Each subsystem can be modeled by the INARMAX mathematical model of the second order, nonlinear with respect to the inputs and having a degree of nonlinearity equal to 2. Thus, the output $y_\alpha(k)$ of each INS S_α is demonstrated by the following expression:

$$
\begin{aligned}
y_\alpha(k) &= -\sum_{r=1}^{2} a_{\alpha,r}(k)y_\alpha(k-r) + \sum_{r=1}^{2} b_{\alpha,r}(k)u_\alpha(k-d_\alpha-r) + \sum_{r=1}^{2} c_{\alpha,r}\, e_\alpha(k-r), \\
&\quad + \sum_{\beta=1,\beta\neq\alpha}^{2} \sum_{r=1}^{2} b_{\alpha\beta,r}(k)\, u_\beta\left(k-d_{\alpha\beta}-r\right) + \sum_{\beta=1,\beta\neq\alpha}^{2} \sum_{r=1}^{2} a_{\alpha\beta,r}(k)\, y_\beta\left(k-t_{\alpha\beta}-r\right), \\
&\quad + \sum_{r_1=1}^{2} \sum_{r_2=1}^{2} g_{\alpha\alpha,r_1 r_2}(k)u_\alpha(k-r_1)u_\alpha(k-r_2) + \sum_{\beta=1,\beta\neq\alpha}^{2} \sum_{r_1=1}^{2} \sum_{r_2=1}^{2} g_{\alpha\alpha,r_1 r_2}(k)\, u_\alpha(k-r_1)u_\beta(k-r_2),
\end{aligned}
\tag{15}
$$

with $\alpha, \beta = 1, 2; \beta \neq \alpha$.

3.2. Nonlinearity with respect to the Outputs.

This section is dedicated to the description of INSs with nonlinearity in their outputs. This type of dynamical system may be characterized by input-output MMs that are nonlinear in terms of the outputs, mono-variable, deterministic, or stochastic and include time-varying parameters.

3.2.1. Deterministic Input-Output MMs.

Let us consider an INS operating in a deterministic environment, mono-variable and having a nonlinearity with respect to the outputs. The

general structure of the considered system can be described by the following INDARMA mathematical model [18]:

$$
\begin{aligned}
A_\alpha\left(q^{-1},k\right) y_\alpha(k) = q^{-d_\alpha} B_\alpha\left(q^{-1},k\right) u_\alpha(k) &+ \sum_{\beta=1,\beta\neq\alpha}^{N} q^{-d_{\alpha\beta}} B_{\alpha\beta}\left(q^{-1},k\right) u_\beta(k) + \sum_{\beta=1,\beta\neq\alpha}^{N} q^{-t_{\alpha\beta}} A_{\alpha\beta}\left(q^{-1},k\right) y_\beta(k), \\
&+ f^{y}_{f_{\alpha\beta}}\left[y_\alpha(k-1), y_\alpha(k-2), \ldots, y_\alpha(k-n_\alpha), y_\beta(k-1), y_\beta(k-2), \ldots, y_\beta(k-n_\alpha)\right], \\
&- f^{y}_{f_{\alpha\alpha}}\left[y_\alpha(k-1), y_\alpha(k-2), \ldots, y_\alpha(k-n_\alpha)\right],
\end{aligned}
\tag{16}
$$

where the terms $f^{y}_{f_{\alpha\alpha}}[\,.\,]$ and $f^{y}_{f_{\alpha\beta}}[\,.\,]$ are nonlinear functions of nonlinearity degree p, which depend on the output sequences of the IS S_α and the other ISs S_β, respectively. These functions can be defined by the following expressions:

$$
\begin{aligned}
f^{y}_{f_{\alpha\alpha}}[.] = \sum_{r_1=1}^{n_{f_{\alpha\alpha,r_1}}} \sum_{r_2=1}^{n_{f_{\alpha\alpha,r_1 r_2}}} & f_{\alpha\alpha,r_1 r_2}(k)\, y_\alpha(k-r_1) y_\alpha(k-r_2), \\
+ \sum_{r_1=1}^{n_{f_{\alpha\alpha,r_1}}} \sum_{r_2=1}^{n_{f_{\alpha\alpha,r_1 r_2}}} \sum_{r_3=1}^{n_{f_{\alpha\alpha,r_1 r_2 r_3}}} & f_{\alpha\alpha,r_1 r_2 r_3}(k)\, y_\alpha(k-r_1) y_\alpha(k-r_2) y_\alpha(k-r_3), \\
+ \ldots + \sum_{r_1=1}^{n_{f_{\alpha\alpha,r_1}}} \sum_{r_2=1}^{n_{f_{\alpha\alpha,r_1 r_2}}} \cdots \sum_{r_p=1}^{n_{f_{\alpha\alpha,r_1 r_2 \ldots r_p}}} & f_{\alpha\alpha,r_1 \ldots r_p}(k)\, y_\alpha(k-r_1) \ldots y_\alpha(k-r_p),
\end{aligned}
\tag{17}
$$

and

$$
\begin{aligned}
f^{y}_{f_{\alpha\beta}}[.] = \sum_{\beta=1,\beta\neq\alpha}^{N} \sum_{r_1=1}^{n_{f_{\alpha\beta,r_1}}} \sum_{r_2=1}^{n_{f_{\alpha\beta,r_1 r_2}}} & f_{\alpha\beta,r_1 r_2}(k)\, y_\alpha(k-r_1) y_\beta(k-r_2), \\
+ \sum_{\beta=1,\beta\neq\alpha}^{N} \sum_{r_1=1}^{n_{f_{\alpha\beta,r_1}}} \sum_{r_2=1}^{n_{f_{\alpha\beta,r_1 r_2}}} \sum_{r_3=1}^{n_{f_{\alpha\beta,r_1 r_2 r_3}}} & f_{\alpha\beta,r_1 r_2 r_3}(k)\, y_\alpha(k-r_1) y_\alpha(k-r_2) y_\beta(k-r_3), \\
+ \ldots + \sum_{\beta=1,\beta\neq\alpha}^{N} \sum_{r_1=1}^{n_{f_{\alpha\beta,r_1}}} \sum_{r_2=1}^{n_{f_{\alpha\beta,r_1 r_2}}} \cdots \sum_{r_p=1}^{n_{f_{\alpha\beta,r_1 r_2 \ldots r_p}}} & f_{\alpha\beta,r_1 \ldots r_p}(k)\, y_\alpha(k-r_1) \ldots y_\beta(k-r_p).
\end{aligned}
\tag{18}
$$

3.2.2. Stochastic Input-Output MMs. We consider an INS S_α, $1 \leq \alpha \leq N$, which is coupled to other INSs S_β, $\beta = 1, \ldots, N; \beta \neq \alpha$, exhibiting nonlinearity in outputs and working in a stochastic environment. We suppose that the noise operating on the investigated system is made up of a sequence of independent random variables with a zero mean and a finite variance, σ_α^2. The general structure of this MM is given by the following expression [18]:

$$
\begin{aligned}
A_\alpha\left(q^{-1},k\right) y_\alpha(k) = q^{-d_\alpha} B_\alpha\left(q^{-1},k\right) u_\alpha(k) &+ \sum_{\beta=1,\beta\neq\alpha}^{N} q^{-d_{\alpha\beta}} B_{\alpha\beta}\left(q^{-1},k\right) u_\beta(k) + \sum_{\beta=1,\beta\neq\alpha}^{N} q^{-t_{\alpha\beta}} A_{\alpha\beta}\left(q^{-1},k\right) y_\beta\left(q^{-1},k\right), \\
&+ f^{y}_{f_{\alpha\beta}}\left[y_\alpha(k-1), y_\alpha(k-2), \ldots, y_\alpha(k-n_\alpha), y_\beta(k-1), y_\beta(k-2), \ldots, y_\beta(k-n_\alpha)\right], \\
&- f^{y}_{f_{\alpha\alpha}}\left[y_\alpha(k-1), y_\alpha(k-2), \ldots, y_\alpha(k-n_\alpha)\right] + f^{e}_{c}\left[e_\alpha(k-1), e_\alpha(k-2), \ldots, e_\alpha(k-n_\alpha)\right], \\
&+ f^{ye}_{\lambda}\left[y_\alpha(k-1), y_\alpha(k-2), \ldots, y_\alpha(k-n_\alpha), e_\alpha(k-1), e_\alpha(k-2), \ldots, e_\alpha(k-n_\alpha)\right] + C_\alpha\left(q^{-1}\right) e_\alpha(k),
\end{aligned}
\tag{19}
$$

where $A_\alpha(q^{-1},k)$, $B_\alpha(q^{-1},k)$, $B_{\alpha\beta}(q^{-1},k)$, and $A_{\alpha\beta}(q^{-1},k)$ are time-varying polynomials, defined by (8), (9), (10), and (9); $C_\alpha(q^{-1})$ is a polynomial with constant parameters, given by (14); and the nonlinear functions $f_c^e[.]$, $f_{f_{\alpha\alpha}}^y[.]$, and $f_{f_{\alpha\beta}}^y[.]$ are defined by (16), (19), and (20), respectively.

The term $f_\lambda^{ye}[.]$ denotes a nonlinear function of degree p, which depends on the output sequences of the IS S_α and the noise $\{e_\alpha(k)\}$. This function can be defined as follows:

$$f_\lambda^{ye}[.] = \sum_{r_1=1}^{n_{\lambda_{\alpha\alpha,r_1}}} \sum_{r_2=1}^{n_{\lambda_{\alpha\alpha,r_1 r_2}}} \lambda_{\alpha\alpha,r_1 r_2} y_\alpha(k-r_1) e_\alpha(k-r_2) + \dots \dots +,$$

$$\sum_{r_1=1}^{n_{\lambda_{\alpha\alpha,r_1}}} \sum_{r_2=1}^{n_{\lambda_{\alpha\alpha,r_1 r_2}}} \dots \sum_{r_p=1}^{n_{\lambda_{\alpha\alpha,r_1 r_2 \dots r_p}}} \lambda_{\alpha\alpha,r_1 \dots r_p} y_\alpha(k-r_1) \dots e_\alpha(k-r_p).$$

$$(20)$$

For example, the following model corresponds to an IOMMINARMAX of the second order with a nonlinearity degree equal to 2, making it possible to describe the dynamic behavior of a large-scale nonlinear process composed of two interconnected nonlinear subsystems S_1 and S_2. The output $y_\alpha(k)$ of each interconnected nonlinear subsystem S_α is described as

$$y_\alpha(k) = -\sum_{r=1}^{2} a_{\alpha,r}(k) y_\alpha(k-r) - \sum_{r_1=1}^{2} \sum_{r_2=1}^{2} f_{\alpha\alpha,r_1 r_2}(k) y_\alpha(k-r_1) y_\alpha(k-r_2),$$

$$+ \sum_{r=1}^{2} b_{\alpha,r}(k) u_\alpha(k-d_\alpha-r) + \sum_{\beta=1,\beta\neq\alpha}^{2} \sum_{r=1}^{2} b_{\alpha\beta,r}(k) u_\beta(k-d_{\alpha\beta}-r),$$

$$+ \sum_{\beta=1,\beta\neq\alpha}^{2} \sum_{r=1}^{2} a_{\alpha\beta,r}(k) y_\beta(k-t_{\alpha\beta}-r) + \sum_{\beta=1,\beta\neq\alpha}^{2} \sum_{r_1=1}^{2} \sum_{r_2=1}^{2} f_{\alpha\beta,r_1 r_2}(k) y_\alpha(k-r_1) y_\beta(k-r_2),$$

$$+ \sum_{r=1}^{2} c_{\alpha,r} e_\alpha(k-r),$$

$$(21)$$

with $\alpha, \beta = 1, 2; \beta \neq \alpha$.

3.3. Nonlinearity with respect to the Observations.
In this part, we will create input-output MMs of representation that allow us to describe ISs that are nonlinear with respect to the observations, are mono-variable, and have unknown time-varying parameters [18].

3.3.1. Deterministic Input-Output MMs.
We consider a dynamical system, which is composed of N ISs, working in a predictable environment and being nonlinear with regard to the observations. The input-output MMINDARMA, making it possible to describe the considered system, is given as follows [18]:

$$A_\alpha\left(q^{-1},k\right) y_\alpha(k) = q^{-d_\alpha} B_\alpha\left(q^{-1},k\right) u_\alpha(k) + \sum_{\beta=1,\beta\neq\alpha}^{N} q^{-d_{\alpha\beta}} B_{\alpha\beta}\left(q^{-1},k\right) u_\beta(k) + \sum_{\beta=1,\beta\neq\alpha}^{N} q^{-t_{\alpha\beta}} A_{\alpha\beta}\left(q^{-1},k\right) y_\beta(k),$$

$$+ f_g^u\left[u_\alpha(k-1), u_\alpha(k-2), \dots, u_\alpha(k-n_\alpha), u_\beta(k-1), u_\beta(k-2), \dots, u_\beta(k-n_\alpha)\right],$$

$$+ f_{f_{\alpha\beta}}^y\left[y_\alpha(k-1), y_\alpha(k-2), \dots, y_\alpha(k-n_\alpha), y_\beta(k-1), y_\beta(k-2), \dots, y_\beta(k-n_\alpha)\right],$$

$$- f_{f_{\alpha\alpha}}^y\left[y_\alpha(k-1), y_\alpha(k-2), \dots, y_\alpha(k-n_\alpha)\right] + f_{h\ell}^{uy}\left[y_\alpha(k-1), y_\alpha(k-2), \dots, y_\alpha(k-n_\alpha), u_\alpha(k-1),\right.$$

$$\left. u_\alpha(k-2), \dots, u_\alpha(k-n_\alpha), u_\beta(k-1), u_\beta(k-2), \dots, u_\beta(k-n_\alpha), y_\beta(k-1), y_\beta(k-2), \dots, y_\beta(k-n_\alpha)\right],$$

$$(22)$$

where $A_\alpha(q^{-1},k)$, $B_\alpha(q^{-1},k)$, $A_{\alpha\beta}(q^{-1},k)$, and $B_{\alpha\beta}(q^{-1},k)$ are polynomials defined by (8), (9), (10), and (9), respectively; $f_g^u[.]$, $f_{f_{\alpha\alpha}}^y[.]$, and $f_{f_{\alpha\beta}}^y[.]$ are nonlinear functions given by (12), (19), and (20), respectively, and $f_{\lambda hl}^{uy}[.]$ is described by the following nonlinear function:

$$f_{h\ell}^{uy}[.] = \sum_{\beta=1}^{N} \sum_{r_1=1}^{n_{h_{\alpha\beta,r_1}}} \sum_{r_2=1}^{n_{h_{\alpha\beta,r_1 r_2}}} h_{\alpha\beta,r_1 r_2}(k)\, u_\alpha(k-r_1) y_\beta(k-r_2),$$

$$+ \sum_{\beta=1}^{N} \sum_{r_1=1}^{n_{h_{\alpha\beta,r_1}}} \sum_{r_2=1}^{n_{h_{\alpha\beta,r_1 r_2}}} \sum_{r_3=1}^{n_{h_{\alpha\beta,r_1 r_2 r_3}}} h_{\alpha\beta,r_1 r_2 r_3}(k)\, u_\alpha(k-r_1) u_\alpha(k-r_2) y_\beta(k-r_3) + \ldots +,$$

$$+ \sum_{\beta=1}^{N} \sum_{r_1=1}^{n_{h_{\alpha\beta,r_1}}} \sum_{r_2=1}^{n_{h_{\alpha\beta,r_1 r_2}}} \cdots \sum_{r_p=1}^{n_{h_{\alpha\beta,r_1 r_2 \cdots r_p}}} h_{\alpha\beta,r_1 \cdots r_p}(k)\, u_\alpha(k-r_1) \ldots y_\beta(k-r_p),$$

$$(23)$$

$$+ \sum_{\beta=1,\beta\neq\alpha}^{N} \sum_{r_1=1}^{n_{\ell_{\alpha\beta,r_1}}} \sum_{r_2=1}^{n_{\ell_{\alpha\beta,r_1 r_2}}} \ell_{\alpha\beta,r_1 r_2}(k)\, y_\alpha(k-r_1) u_\beta(k-r_2),$$

$$+ \sum_{\beta=1,\beta\neq\alpha}^{N} \sum_{r_1=1}^{n_{\ell_{\alpha\beta,r_1}}} \sum_{r_2=1}^{n_{\ell_{\alpha\beta,r_1 r_2}}} \sum_{r_3=1}^{n_{\ell_{\alpha\beta,r_1 r_2 r_3}}} \ell_{\alpha\beta,r_1 r_2 r_3}(k)\, y_\alpha(k-r_1) y_\alpha(k-r_2) u_\beta(k-r_3) + \ldots +,$$

$$+ \sum_{\beta=1,\beta\neq\alpha}^{N} \sum_{r_1=1}^{n_{\ell_{\alpha\beta,r_1}}} \sum_{r_2=1}^{n_{\ell_{\alpha\beta,r_1 r_2}}} \cdots \sum_{r_p=1}^{n_{\ell_{\alpha\beta,r_1 r_2 \cdots r_p}}} \ell_{\alpha\beta,r_1 \cdots r_p}(k)\, y_\alpha(k-r_1) \ldots u_\beta(k-r_p).$$

3.3.2. Stochastic Input-Output MMs. Let us consider an INS S_α, $1 \leq \alpha \leq N$, which is coupled to the other IS S_β, $\beta = 1, \ldots, N; \beta \neq \alpha$. This system is nonlinear with respect to the observations and can be described by the class of IOMMs. The considered structure of the INARMAX MM is given by the following expression [18]:

$$A_\alpha\big(q^{-1},k\big)\, y_\alpha(k) = q^{-d_\alpha} B_\alpha\big(q^{-1},k\big) u_\alpha(k) + \sum_{\beta=1,\beta\neq\alpha}^{N} q^{-d_{\alpha\beta}} B_{\alpha\beta}\big(q^{-1},k\big) u_\beta(k),$$

$$+ \sum_{\beta=1,\beta\neq\alpha}^{N} q^{-t_{\alpha\beta}} A_{\alpha\beta}\big(q^{-1},k\big) y_\beta(k) + C_\alpha\big(q^{-1}\big) e_\alpha(k),$$

$$+ f_g^{u}\big[u_\alpha(k-1), u_\alpha(k-2), \ldots, u_\alpha(k-n_\alpha), u_\beta(k-1), u_\beta(k-2), \ldots, u_\beta(k-n_\alpha)\big],$$

$$+ f_{f_{\alpha\beta}}^{y}\big[y_\alpha(k-1), y_\alpha(k-2), \ldots, y_\alpha(k-n_\alpha), y_\beta(k-1), y_\beta(k-2), \ldots, y_\beta(k-n_\alpha)\big],$$

$$- f_{f_{\alpha\alpha}}^{y}\big[y_\alpha(k-1), y_\alpha(k-2), \ldots, y_\alpha(k-n_\alpha)\big] + f_{h\ell}^{uy}\big[y_\beta(k-1), y_\beta(k-2), \ldots, y_\beta(k-n_\alpha), u_\alpha(k-1),$$

$$u_\alpha(k-2), \ldots, u_\alpha(k-n_\alpha), u_\beta(k-1), u_\beta(k-2), \ldots, u_\beta(k-n_\alpha), y_\beta(k-1), y_\beta(k-2), \ldots, y_\beta(k-n_\alpha)\big],$$

$$+ f_\gamma^{ue}\big[u_\alpha(k-1), u_\alpha(k-2), \ldots, u_\alpha(k-n_\alpha), e_\alpha(k-1), e_\alpha(k-2), \ldots, e_\alpha(k-n_\alpha)\big],$$

$$+ f_\lambda^{ye}\big[y_\alpha(k-1), y_\alpha(k-2), \ldots, y_\alpha(k-n_\alpha), e_\alpha(k-1), e_i(k-2), \ldots, e_\alpha(k-n_\alpha)\big]$$

$$+ f_c^{e}\big[e_\alpha(k-1), e_\alpha(k-2), \ldots, e_\alpha(k-n_\alpha)\big],$$

$$(24)$$

where $f_g^u[\,.\,]$, $f_\beta^{ue}[\,.\,]$, $f_c^e[\,.\,]$, $f_{f_{\alpha\alpha}}^y[\,.\,]$, $f_{f_{\alpha\beta}}^y[\,.\,]$, , and $f_{h\ell}^{uy}[\,.\,]$ are nonlinear functions defined by (12), (15), (16), (19), (20), (22), and (23), respectively.

For the reason of simplicity, we consider the following dynamical system, which consists of N INSs, running in a deterministic environment and defined by an

IOMM INDARMA with a nonlinearity degree equal to 2, such as

$$
\begin{aligned}
A_{\alpha 1}\left(q^{-1}\right) y_\alpha(k) + A_{\alpha 2}\left(q_1^{-1}, q_2^{-1}\right) y_\alpha^2(k) = {} & B_{\alpha 1}\left(q^{-1}\right) u_\alpha(k) + B_{\alpha 2}\left(q_1^{-1}, q_2^{-1}\right) u_\alpha^2(k) + A_{\alpha\beta 1}\left(q^{-1}\right) y_\beta(k), \\
& + B_{\alpha\beta 1}\left(q^{-1}\right) u_\beta(k) + A_{\alpha\beta 2}\left(q_1^{-1}, q_2^{-1}\right) y_\alpha(k) y_\beta(k), \\
& + B_{\alpha\beta 2}\left(q_1^{-1}, q_2^{-1}\right) u_\alpha(k) u_\beta(k) + F_{\alpha\beta}\left(q_1^{-1}, q_2^{-1}\right) u_\alpha(k) y_\beta(k), \\
& + H_{\alpha\beta}\left(q_1^{-1}, q_2^{-1}\right) y_\alpha(k) u_\beta(k),
\end{aligned}
\tag{25}
$$

where

$$
\begin{aligned}
B_{\alpha 1}\left(q^{-1}\right) &= \sum_{r=1}^{n_{B_{\alpha 1}}} b_{\alpha 1, r} q^{-r}, \\[2mm]
A_{\alpha 1}\left(q^{-1}\right) &= 1 + \sum_{r=1}^{n_{A_{\alpha 1}}} a_{\alpha 1, r} q^{-r}, \\[2mm]
B_{\alpha 2}\left(q_1^{-1}, q_2^{-1}\right) u_\alpha^2(k) &= \sum_{r=1}^{n_{B_{\alpha 21}}} \sum_{s=1}^{n_{B_{\alpha 22}}} b_{\alpha 2, rs} u_\alpha(k-r) u_\alpha(k-s), \\[2mm]
A_{\alpha 2}\left(q_1^{-1}, q_2^{-1}\right) y_\alpha^2(k) &= \sum_{r=1}^{n_{A_{\alpha 21}}} \sum_{s=1}^{n_{A_{\alpha 22}}} a_{\alpha 2, rs} y_\alpha(k-r) y_\alpha(k-s), \\[2mm]
B_{\alpha\beta 1}\left(q^{-1}\right) u_\beta(k) &= \sum_{\beta=1, \beta \neq \alpha}^{N} \sum_{r=1}^{n_{B_{\alpha\beta 1}}} b_{\alpha\beta 1, r} u_\beta(k-r), \\[2mm]
A_{\alpha\beta 1}\left(q^{-1}\right) y_\beta(k) &= \sum_{\beta=1, \beta \neq \alpha}^{N} \sum_{r=1}^{n_{A_{\alpha\beta 1}}} a_{\alpha\beta 1, r} y_\beta(k-r), \\[2mm]
B_{\alpha\beta 2}\left(q_1^{-1}, q_2^{-1}\right) u_\alpha(k) u_\beta(k) &= \sum_{\beta=1, \beta \neq \alpha}^{N} \sum_{r=1}^{n_{B_{\alpha\beta 21}}} \sum_{s=1}^{n_{B_{\alpha\beta 22}}} b_{\alpha\beta 2, rs} u_\alpha(k-r) u_\beta(k-s), \\[2mm]
A_{\alpha\beta 2}\left(q_1^{-1}, q_2^{-1}\right) y_\alpha(k) y_\beta(k) &= \sum_{\beta=1, \beta \neq \alpha}^{N} \sum_{r=1}^{n_{A_{\alpha\beta 21}}} \sum_{s=1}^{n_{A_{\alpha\beta 22}}} a_{\alpha\beta 2, rs} y_\alpha(k-r) y_\beta(k-s), \\[2mm]
F_{\alpha\beta}\left(q_1^{-1}, q_2^{-1}\right) u_\alpha(k) y_\beta(k) &= \sum_{\beta=1}^{N} \sum_{r=1}^{n_{F_{\alpha\beta 1}}} \sum_{s=1}^{n_{F_{\alpha\beta 2}}} f_{\alpha\beta, rs} u_\alpha(k-r) y_\beta(k-s),
\end{aligned}
\tag{26}
$$

and

$$
H_{\alpha\beta}\left(q_1^{-1}, q_2^{-1}\right) y_\alpha(k) u_\beta(k) = \sum_{\beta=1, \beta \neq \alpha}^{N} \sum_{r=1}^{n_{H_{\alpha\beta 1}}} \sum_{s=1}^{n_{H_{\alpha\beta 2}}} h_{\alpha\beta, rs} y_\alpha(k-r) u_\beta(k-s),
\tag{27}
$$

with $\alpha, \beta = 1, \ldots, N; \beta \neq \alpha$.

From the developed MM, we can distinguish special cases of input-output MM, based on various representations, such as the following:

$$A_{\alpha 1}\left(q^{-1}\right) = 0, A_{\alpha 2}\left(q_1^{-1}, q_2^{-1}\right) = 0, A_{\alpha\beta 1}\left(q^{-1}\right) = 0, A_{\alpha\beta 2}\left(q_1^{-1}, q_2^{-1}\right) = 0, F_{\alpha\beta}\left(q_1^{-1}, q_2^{-1}\right) = 0, H_{\alpha\beta}\left(q_1^{-1}, q_2^{-1}\right) = 0. \tag{28}$$

(1) Serial model of Volterra:

(2) Parametric model of Volterra:

$$A_{\alpha 2}\left(q_1^{-1}, q_2^{-1}\right) = 0, A_{\alpha\beta 2}\left(q_1^{-1}, q_2^{-1}\right) = 0, F_{\alpha\beta}\left(q_1^{-1}, q_2^{-1}\right) = 0, H_{\alpha\beta}\left(q_1^{-1}, q_2^{-1}\right) = 0. \tag{29}$$

(3) Bilinear model:

$$A_{\alpha 2}\left(q_1^{-1}, q_2^{-1}\right) = 0, B_{\alpha 2}\left(q_1^{-1}, q_2^{-1}\right) = 0. \tag{30}$$

(4) Linear model with respect to the input signal:

$$B_{\alpha 2}\left(q_1^{-1}, q_2^{-1}\right) = 0, B_{\alpha\beta 2}\left(q_1^{-1}, q_2^{-1}\right) = 0, F_{\alpha\beta}\left(q_1^{-1}, q_2^{-1}\right) = 0, H_{\alpha\beta}\left(q_1^{-1}, q_2^{-1}\right) = 0. \tag{31}$$

(5) Linear model with respect to the output signal:

$$A_{\alpha 2}\left(q_1^{-1}, q_2^{-1}\right) = 0, A_{\alpha\beta 2}\left(q_1^{-1}, q_2^{-1}\right) = 0, F_{\alpha\beta}\left(q_1^{-1}, q_2^{-1}\right) = 0, H_{\alpha\beta}\left(q_1^{-1}, q_2^{-1}\right) = 0. \tag{32}$$

For example, we consider a large-scale nonlinear process, which is constituted of two INS S_1 and S_2. Each interconnected subsystem can be defined by the INDARMA mathematical model of the second order with time-varying parameters and having a nonlinearity degree equal to 2.

Figure 1 shows the interaction structure diagram of the considered nonlinear process:

Thus, the output $y_\alpha(k)$ of the INS S_α can be expressed as

$$
\begin{aligned}
y_\alpha(k) = &-\sum_{r=1}^{2} a_{\alpha,r}(k) y_\alpha(k-r) - \sum_{r_1=1}^{2}\sum_{r_2=1}^{2} f_{\alpha\alpha,r_1 r_2}(k)\, y_\alpha(k-r_1) y_\alpha(k-r_2), \\
&+ \sum_{r=1}^{2} b_{\alpha,r}(k) u_\alpha(k-d_\alpha-r) + \sum_{\beta=1,\beta\neq\alpha}^{2}\sum_{r=1}^{2} b_{\alpha\beta,r}(k)\, u_\beta\left(k-d_{\alpha\beta}-r\right), \\
&+ \sum_{\beta=1,\beta\neq\alpha}^{2}\sum_{r=1}^{2} a_{\alpha\beta,r}(k)\, y_\beta\left(k-t_{\alpha\beta}-r\right) + \sum_{r_1=1}^{2}\sum_{r_2=1}^{2} g_{\alpha\alpha,r_1 r_2}(k)\, u_\alpha(k-r_1) u_\alpha(k-r_2), \\
&+ \sum_{\beta=1,\beta\neq\alpha}^{2}\sum_{r_1=1}^{2}\sum_{r_2=1}^{2} g_{\alpha\beta,r_1 r_2}(k)\, u_\alpha(k-r_1) u_\beta(k-r_2) + \sum_{\beta=1,\beta\neq\alpha}^{2}\sum_{r_1=1}^{2}\sum_{r_2=1}^{2} f_{\alpha\beta,r_1 r_2}(k)\, y_\alpha(k-r_1) y_\beta(k-r_2), \\
&+ \sum_{\beta=1}^{2}\sum_{r_1=1}^{2}\sum_{r_2=1}^{2} h_{\alpha\beta,r_1 r_2}(k)\, u_\alpha(k-r_1) y_\beta(k-r_2) + \sum_{\beta=1,\beta\neq\alpha}^{2}\sum_{r_1=1}^{2}\sum_{r_2=1}^{2} \ell_{\alpha\beta,r_1 r_2}(k)\, y_\alpha(k-r_1) u_\beta(k-r_2),
\end{aligned}
\tag{33}
$$

with $\alpha, \beta = 1, 2; \beta \neq \alpha$.

We notice that these different representations of developed MMs become more and more complex by increasing the nonlinearity degree p and/or the order of the IS.

4. MMs in Connected Blocks

The linked block MMs explain the dynamic behavior of a nonlinear system composed of a linear dynamic element and a nonlinear static element. This form of MM is widely used
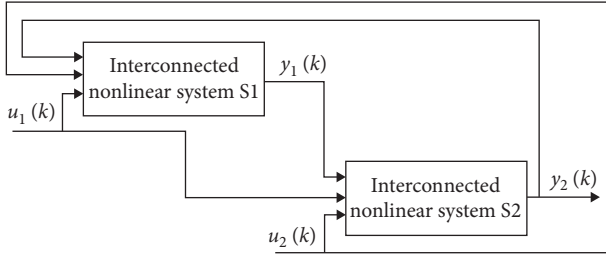
Figure 1: Interaction structure diagram of the considered process.

in a variety of industrial applications for the description of nonlinear systems with tiny dimensions [17, 19–22]. In fact, the authors of [19] provided an approach for identifying nonlinear dynamic systems using extended Hammerstein and Wiener models. Following that, the author of [20] refined a strategy for identifying the Hammerstein model. Similarly, the authors of [21] produced promising findings for Hammerstein system identification. Around ten years later, the authors of [17] proposed an adaptive nonlinear system identification approach to the Volterra and Wiener Models. The author of [22] proposes a significant improvement in the identification of Hammerstein–Wiener models. The use of MMs to describe this type of dynamic system in linked blocks simplifies the construction of parametric estimates and control strategies. In linked blocks,

there are two types of MMs, Hammerstein MM and Wiener MM.

Two structures of linked block MMs are developed in this part for the description of mono-variable INSs. This type of system can be represented by discrete MMs of Hammerstein or Wiener, which can be deterministic or stochastic, and has unknown time-varying parameters.

4.1. Interconnected Hammerstein MMs.
A Hammerstein MMs description of an interconnected nonlinear dynamic system relates to the interconnection of many MM structures, each of which consists of a static nonlinear portion followed by a dynamic linear part [23]. This family of models includes two types of MMs: a deterministic Hammerstein MM, in which an IDARMA input-output model defines the dynamic linear component of the investigated system, and a stochastic Hammerstein MM, in which an IARMAX input-output model describes the dynamic linear part.

4.1.1. Deterministic Interconnected Hammerstein MMs.
The structure of an INS S_α, $1 \le \alpha \le N$, operating in a deterministic environment and that can be defined by Hammerstein MM, is represented in Figure 2.

Figure 2 depicts the dynamic linear component of Hammerstein MM, which is characterized by the following formula [23]:

$$A_\alpha\left(q^{-1},k\right) y_\alpha(k) = B_\alpha\left(q^{-1},k\right) h_\alpha^{u_\alpha}(k) + \sum_{\beta=1,\beta\neq\alpha}^{N} B_{\alpha\beta}\left(q^{-1},k\right) h_\beta^{u_\beta}(k) + \sum_{\beta=1,\beta\neq\alpha}^{N} A_{\alpha\beta}\left(q^{-1},k\right) h_\beta^{y_\beta}(k), \tag{34}$$

where $y_\alpha(k)$ and $h_\alpha^{u_\alpha}(k)$ denote, respectively, the output and the input of the dynamic linear block of the IS S_α; $y_\beta(k)$, $u_\beta(k)$, and $u_\alpha(k)$ are the inputs of the static nonlinear blocks; $h_\beta^{u_\beta}(k)$ and $h_\beta^{y_\beta}(k)$ represent the inputs of the dynamic linear blocks of the other ISs S_β, $\beta = 1, \ldots, N; \beta \neq \alpha$; and $A_\alpha(q^{-1},k)$, $B_\alpha(q^{-1},k)$, $B_{\alpha\beta}(q^{-1},k)$, and $A_{\alpha\beta}(q^{-1},k)$ are time-varying polynomials, defined by (8), (9), (10), and (9). We must note that the INS S_α, $1 \le \alpha \le N$, is linked to other INS S_β, $\beta = 1, \ldots\infty, N; \beta \neq \alpha$, by the polynomials $A_{\alpha\beta}(q^{-1},k)$ and $B_{\alpha\beta}(q^{-1},k)$.

The following equations represent the static nonlinear sections of the analyzed Hammerstein MM:

$$h_\alpha^{u_\alpha}(k) = f_{h_\alpha^{u_\alpha}}\left[u_\alpha(k)\right], \tag{35}$$

$$h_\beta^{u_\beta}(k) = f_{h_\beta^{u_\beta}}\left[u_\beta(k)\right], \tag{36}$$

$$h_\beta^{y_\beta}(k) = f_{h_\beta^{y_\beta}}\left[y_\beta(k)\right], \tag{37}$$

where $f_{h_\alpha^{u_\alpha}}[.]$, $f_{h_\beta^{u_\beta}}[.]$, and $f_{h_\beta^{y_\beta}}[.]$ represent nonlinear functions.

Equations (40), (41), and (42) can be approximated by the following functions, such as

$$h_\alpha^{u_\alpha}(k) = \sum_{r_1=1}^{p_1} \eta_{\alpha,r_1} u_\alpha^{r_1}(k) + \Delta h_\alpha^{u_\alpha}\left[u_\alpha(k)\right], \tag{38}$$

$$h_\beta^{u_\beta}(k) = \sum_{r_2=1}^{p_2} \lambda_{\beta,r_2} u_\beta^{r_2}(k) + \Delta h_\beta^{u_\beta}\left[u_\beta(k)\right], \tag{39}$$

$$h_\beta^{y_\beta}(k) = \sum_{r_3=1}^{p_3} \gamma_{\beta,r_3} y_\beta^{r_3}(k) + \Delta h_\beta^{y_\beta}\left[y_\beta(k)\right], \tag{40}$$

where $\Delta h_\alpha^{u_\alpha}[u_\alpha(k)]$, $\Delta h_\beta^{u_\beta}[u_\beta(k)]$, and $\Delta h_\beta^{y_\beta}[y_\beta(k)]$ represent the approximation errors of nonlinear functions $f_{h_\alpha^{u_\alpha}}[.]$, $f_{h_\beta^{u_\beta}}[.]$, and $f_{h_\beta^{y_\beta}}[.]$, respectively, which can be assimilated to a disturbance acting on the output of the INS S_α, η_{α,r_1}, λ_{α,r_2}, and γ_{β,r_3}, $r_t = 1, \ldots, p_t$, $t = 1, 2, 3$ are unknown parameters, and p_t denotes the degree of nonlinearity. Note that the variances values of these approximation errors depend on the chosen of the nonlinearity degrees values p_t for the nonlinear functions.

From (40), which are related to the linear and the nonlinear parts of the Hammerstein model, we can describe the considered system by the following expression:
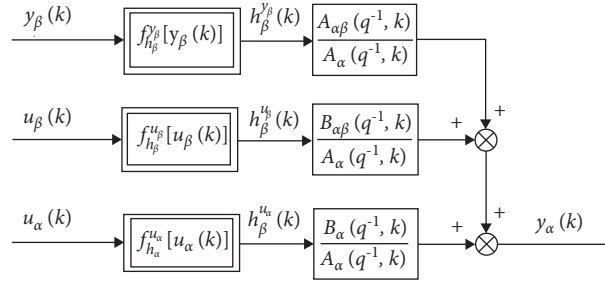
Figure 2: Deterministic structure of the interconnected Hammerstein MM.

$$y_\alpha(k) = -\sum_{r=1}^{n_{A_\alpha}} a_{\alpha,r}(k) y_\alpha(k-r) + \sum_{s=1}^{n_{B_\alpha}} \sum_{r_1=1}^{p_1} b_{\alpha,s}(k) \eta_{\alpha,r_1} u_\alpha^{r_1}(k-s) + \sum_{s=1}^{n_{B_\alpha}} \Delta h_\alpha^{u_\alpha}[u_\alpha(k-s)],$$

$$+ \sum_{\beta=1,\beta \neq \alpha}^{N} \sum_{s=1}^{n_{B_{\alpha\beta}}} \sum_{r_2=1}^{p_2} b_{\alpha\beta,s}(k) \lambda_{\beta,r_2} u_\beta^{r_2}(k-s) + \sum_{s=1}^{n_{B_{\alpha\beta}}} \Delta h_\beta^{u_\beta}[u_\beta(k-s)], \tag{41}$$

$$+ \sum_{\beta=1,\beta \neq \alpha}^{N} \sum_{s=1}^{n_{A_{\alpha\beta}}} \sum_{r_3=1}^{p_3} a_{\alpha\beta,s}(k) \gamma_{\beta,r_3} y_\beta^{r_3}(k-s) + \sum_{s=1}^{n_{A_{ij}}} \Delta h_\beta^{y_\beta}[y_\beta(k-s)].$$

4.1.2. Stochastic Interconnected Hammerstein MMs. This second form of Hammerstein MM is distinguished by IARMAX input-output MM, which describes the dynamic linear component of the system under consideration [23]. We suppose that there is a disturbance operating on the output of the considered system and that it may be characterized by a moving average MM.

As a result, Figure 3 depicts the Hammerstein MM's structure:

The following formula describes the dynamic linear component of the examined Hammerstein MM [23]:

$$A_\alpha\left(q^{-1},k\right) y_\alpha(k) = B_\alpha\left(q^{-1},k\right) h_\alpha^{u_\alpha}(k) + \sum_{\beta=1,\beta \neq \alpha}^{N} B_{\alpha\beta}\left(q^{-1},k\right) h_\beta^{u_\beta}(k) + \sum_{\beta=1,\beta \neq \alpha}^{N} A_{\alpha\beta}\left(q^{-1},k\right) h_\beta^{y_\beta}(k) + C_\alpha\left(q^{-1}\right) e_\alpha(k), \tag{42}$$

where $h_\alpha^{u_\alpha}(k)$, $h_\beta^{u_\beta}(k)$, and $h_\beta^{y_\beta}(k)$ represent the outputs of the static nonlinear blocks of the considered MM, which are defined by equations (43), (44), and (45); $e_\alpha(k)$ designates the set of disturbances acting on the output of the IS, which consists of an independent random variables sequence with zero mean and constant variance σ_α^2; and $C_\alpha(q^{-1})$ is a polynomial with constant parameters, given by (12).

Taking into account the polynomials (43), (44), and (45), the output $y_\alpha(k)$, which is defined by (47), can be written as [26]

$$y_\alpha(k) = -\sum_{r=1}^{n_{A_\alpha}} a_{\alpha,r}(k) y_\alpha(k-r) + \sum_{s=1}^{n_{B_\alpha}} \sum_{r_1=1}^{p_1} b_{\alpha,s}(k) \eta_{\alpha,r_1} u_\alpha^{r_1}(k-s) + \sum_{s=1}^{n_{B_\alpha}} \Delta h_\alpha^{u_\alpha}[u_\alpha(k-s)],$$

$$+ \sum_{\beta=1,\beta \neq \alpha}^{N} \sum_{s=1}^{n_{B_{\alpha\beta}}} \sum_{r_2=1}^{p_2} b_{\alpha\beta,s}(k) \lambda_{\beta,r_2} u_\beta^{r_2}(k-s) + \sum_{s=1}^{n_{B_{\alpha\beta}}} \Delta h_\beta^{u_\beta}[u_\beta(k-s)], \tag{43}$$

$$+ \sum_{\beta=1,\beta \neq \alpha}^{N} \sum_{s=1}^{n_{A_{\alpha\beta}}} \sum_{r_3=1}^{p_3} a_{\alpha\beta,s}(k) \gamma_{\beta,r_3} y_\beta^{r_3}(k-s) + \sum_{s=1}^{n_{A_{\alpha\beta}}} \Delta h_\beta^{y_\beta}[y_\beta(k-s)] + \sum_{r=1}^{n_{C_\alpha}} c_{\alpha,r} e_\alpha(k-r) + e_\alpha(k).$$

Other forms of Hammerstein MMs may be distinguished in order to represent the dynamics of INSs, depending on different configurations of static nonlinear elements.

For reason of simplicity, we assume that the polynomials $B_\alpha(q^{-1},k)$, $A_\alpha(q^{-1},k)$, $A_{\alpha\beta}(q^{-1},k)$, $B_{\alpha\beta}(q^{-1},k)$, and $C_\alpha(q^{-1})$ of Hammerstein MMs, which are given by (41) and
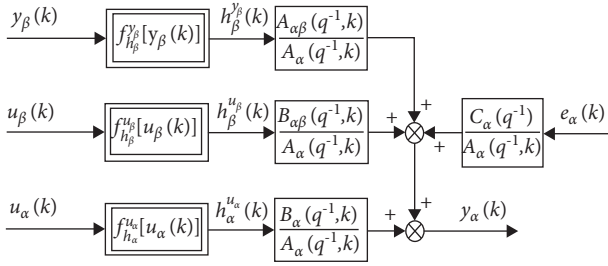
FIGURE 3: Stochastic structure of the interconnected Hammerstein MM.

(43), have the same order n_α $(n_\alpha = n_{A_\alpha} = n_{B_\alpha} = n_{B_{\alpha\beta}} = n_{A_{\alpha\beta}})$. We make also a choice of the nonlinearity degrees p_t, $t = 1, 2, 3$, in such a way that the approximation errors $\Delta h_\alpha^{u_\alpha}[u_\alpha(k)]$, $\Delta h_\beta^{u_\beta}[u_\beta(k)]$, and $\Delta h_\beta^{y_\beta}[y_\beta(k)]$ become negligible $(\Delta h_\alpha^{u_\alpha}[u_\alpha(k)] = \Delta h_\beta^{u_\beta}[u_\beta(k)] = \Delta h_\beta^{y_\beta}[y_\beta(k)] = 0)$. These assumptions allow us to further simplify the formulation of the parametric estimation and the control problems for the INSs, which are described by the two types of the developed Hammerstein MMs, which are given by (46) and (48).

4.2. Interconnected Wiener MMs.

The creation of Wiener MMs for characterizing the INSs is discussed in this section. This model's class relates to the interconnection of numerous MM structures, each of which has a dynamic linear and a static nonlinear component. In this class of MMs, we may distinguish between two forms of Wiener MMs: deterministic Wiener MMs and stochastic Wiener MMs [24].

4.2.1. Deterministic Interconnected Wiener MM.
This section is intended for Wiener MMs [24] to describe INSs working in a deterministic environment. As a result, we investigate a nonlinear time-varying system made up of deterministic ISs. The deterministic Wiener MM may be used to explain each IS, and its structure is depicted in Figure 4.

The previous structure, which is illustrated by Figure 4, can be expressed by the following MM [24]:

$$A_\alpha\left(q^{-1}, k\right) w_\alpha(k) = B_\alpha\left(q^{-1}, k\right) u_\alpha(k) + \sum_{\beta=1, \beta \neq \alpha}^{N} B_{\alpha\beta}\left(q^{-1}, k\right) u_\beta(k) + \sum_{\beta=1, \beta \neq \alpha}^{N} A_{\alpha\beta}\left(q^{-1}, k\right) y_\beta(k), \tag{44}$$

where $w_\alpha(k)$ and $u_\alpha(k)$ are, respectively, the output and input of the dynamic linear block of the IS S_α, $y_\beta(k)$, and $u_\beta(k)$ denote, respectively, the outputs and inputs, which arise from the other ISs S_β, $\beta = 1, \ldots, N; \beta \neq \alpha$, and $A_\alpha(q^{-1}, k)$, $B_\alpha(q^{-1}, k)$, $B_{\alpha\beta}(q^{-1}, k)$, and $A_{\alpha\beta}(q^{-1}, k)$ are time-varying polynomials, as given by (8), (9), (10), and (9), respectively.

The following equation describes the static nonlinear component of the considered MM:

$$y_\alpha(k) = f_{w_\alpha}[w_\alpha(k)], \tag{45}$$

where $f_{w_\alpha}[.]$ represents the nonlinear function.

The following polynomial can be used to approximate (45):

$$y_\alpha(k) = \sum_{r=1}^{p} \eta_{\alpha,r} w_\alpha^r(k) + \Delta y_\alpha[w_\alpha(k)], \tag{46}$$

where p represents the nonlinearity degree of the nonlinear function, which can be chosen in an appropriate way; $\eta_{\alpha,r}$, $r = 1, \ldots, p$, are unknown parameters; and $\Delta y_\alpha[w_\alpha(k)]$ signifies the nonlinear function's approximation error. This approximation error, which is dependent on the nonlinearity degree p chosen, might be compared to noise operating on the output of the IS in question. For an appropriate choice of the nonlinearity degree value p, this approximation error $\Delta y_\alpha[w_\alpha(k)]$ can be neglected.

The output of the IS $y_\alpha(k)$ can be written as follows, taking into consideration the dynamic linear component of the investigated Wiener MM, as stated by (44) [24]:

$$y_\alpha(k) = \sum_{r=1}^{p} \eta_{\alpha,r}\left[-\sum_{s=1}^{n_{A_\alpha}} a_{\alpha,s}(k)w_\alpha(k-s) + \sum_{h=1}^{n_{B_\alpha}} b_{\alpha,h}(k)u_\alpha(k-h),\right.$$
$$\left. + \sum_{\beta=1, \beta \neq \alpha}^{N} B_{\alpha\beta}\left(q^{-1}, k\right) u_\beta(k) + \sum_{\beta=1, \beta \neq \alpha}^{N} A_{\alpha\beta}\left(q^{-1}, k\right) y_\beta(k)\right]^r + \Delta y_\alpha[w_\alpha(k)]. \tag{47}$$

4.2.2. Stochastic Interconnected Wiener MM.
In this part, we suppose that the output of the considered system is subjected to noise, which is composed of an independent random variable sequence. As a result, the Wiener MM's dynamic linear portion is of type IARMAX.

The structure of this model is depicted in Figure 5.
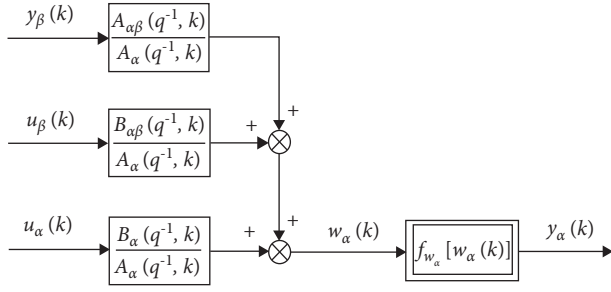
FIGURE 4: Deterministic structure of the interconnected Wiener MM.
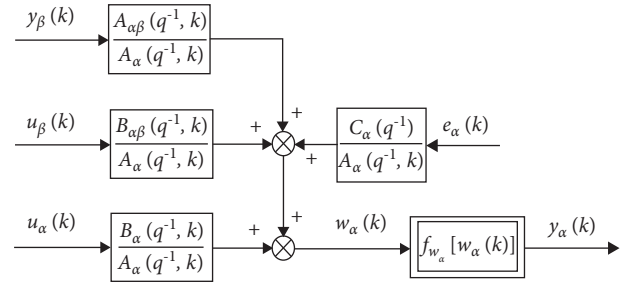
FIGURE 5: Stochastic structure of the interconnected Wiener MM. The following formula describes the dynamic linear portion of Wiener MM [24].

$$A_\alpha\left(q^{-1},k\right)w_\alpha(k) = B_\alpha\left(q^{-1},k\right)u_\alpha(k) + \sum_{\beta=1,\beta\neq\alpha}^{N} B_{\alpha\beta}\left(q^{-1},k\right)u_\beta(k) + \sum_{\beta=1,\beta\neq\alpha}^{N} A_{\alpha\beta}\left(q^{-1},k\right)y_\beta(k) + C_\alpha\left(q^{-1}\right)e_\alpha(k), \qquad (48)$$

where $e_\alpha(k)$ designates all disturbances acting on the IS S_α, $C_\alpha(q^{-1})$ is a polynomial defined by (12), and $y_\alpha(k)$ corresponds to the output of the static nonlinear part of the stochastic Wiener MM, which is given by (46).

The output of the system $y_\alpha(k)$ may be represented in the following manner based on the dynamic linear component of the investigated Wiener MM, as given by (48).

$$y_\alpha(k) = \sum_{r=1}^{P} \eta_{\alpha,r}\left[-\sum_{s=1}^{n_{A_\alpha}} a_{\alpha,s}(k)w_\alpha(k-s) + \sum_{h=1}^{n_{B_\alpha}} b_{\alpha,h}(k)u_\alpha(k-h) + \sum_{\beta=1,\beta\neq\alpha}^{N} B_{\alpha\beta}\left(q^{-1},k\right)u_\beta(k),\right.$$
$$\left. + \sum_{\beta=1,\beta\neq\alpha}^{N} A_{\alpha\beta}\left(q^{-1},k\right)y_\beta(k) + \sum_{t=1}^{n_{C_\alpha}} c_{\alpha,t}e_\alpha(k-t) + e_\alpha(k)\right]^r + \Delta y_\alpha\left[w_\alpha(k)\right]. \qquad (49)$$

In the description of the INSs, we may use a variety of Wiener MMs, which are based on various forms of the static nonlinear portion.

We assume that the polynomials $A_\alpha(q^{-1},k)$, $B_\alpha(q^{-1},k)$, $B_{\alpha\beta}(q^{-1},k)$, $A_{\alpha\beta}(q^{-1},k)$, and $C_\alpha(q^{-1})$ intervening in the two types of Wiener MMs, given by (47) and (49), have the same order n_α ($n_\alpha = n_{A_\alpha} = n_{B_\alpha} = n_{A_{\alpha\beta}} = n_{B_{\alpha\beta}}$). We also assume that the approximation error $\Delta y_\alpha[w_\alpha(k)]$ is negligible, to reduce the formulation of the parametric estimation issue for large-scale dynamical systems defined by the Wiener MMs created.

5. Case Study

In this section, we present a numerical example to illustrate the feasibility and effectiveness of the developed theoretical results. This example corresponds to a stochastic large-scale nonlinear system, composed of two interconnected subsystems S_1 and S_2, and can be described by the class of interconnected Hammerstein MM.

Figure 6 shows the general structure interaction of the considered process.

The system output $y_i(k)$, $i = 1, 2$, can be expressed as

$$y_i(k) = -a_{i,1}(k)y_i(k-1) - a_{i,2}(k)y_i(k-2) + \alpha_{i,1}u_i(k-1) + b_{i,2}(k)\alpha_{i,1}u_i(k-2),$$
$$+ \alpha_{i,2}u_i^2(k-1) + b_{i,2}(k)\alpha_{i,2}u_i^2(k-2) + \beta_{j,1}u_j(k-1) + b_{ij,2}(k)\beta_{j,1}u_j(k-2), \qquad (50)$$
$$+ \beta_{j,2}u_j^2(k-1) + b_{ij,2}(k)\beta_{j,2}u_j^2(k-2) + e_i(k) + c_{i,1}e_i(k-1),$$

where the relative data are selected as follows: $a_{1,1}(k) = -0.88 + 0.03\sin(0.2k)$, $c_{1,1} = 0.25$, $\alpha_{1,1} = 0.32$, $a_{1,2}(k) = 0.45 + 0.02\cos(0.2k)$, $b_{1,2}(k) = 0.32 + 0.02\sin(0.2k)$, $\alpha_{1,2} = 0.23$, $\beta_{2,1} = 0.33$, $\beta_{2,2} = 0.22$, $b_{12,2}(k) = 0.33 + 0.03\sin(0.2k)$, $a_{2,1}(k) = -0.85 + 0.03\sin(0.2k)$, $c_{2,1} = 0.27$, $\alpha_{2,1} = 0.31$, $a_{2,2}(k) = 0.42 + 0.02\cos(0.2k)$, $b_{2,2}(k) = 0.45 + 0.04\sin(0.2k)$, $\alpha_{2,2} = 0.21$, $\beta_{1,1} = 0.33$, $\beta_{1,2} = 0.24$,

$b_{21,2}(k) = 0.43 + 0.03\sin(0.2k)$. Adding that the input $u_i(k)$ that applied to the INS is a high level pseudo-random binary sequence [-1.5, +1.5], and the variances values of the noise sequence $\{e_i(k), i = 1, 2\}$ are $\sigma_1^2 = 0.0937$ and $\sigma_2^2 = 0.0853$.

Some results of this simulation example of the considered system are given. Thereby, Figures 7 and 8 illustrate the
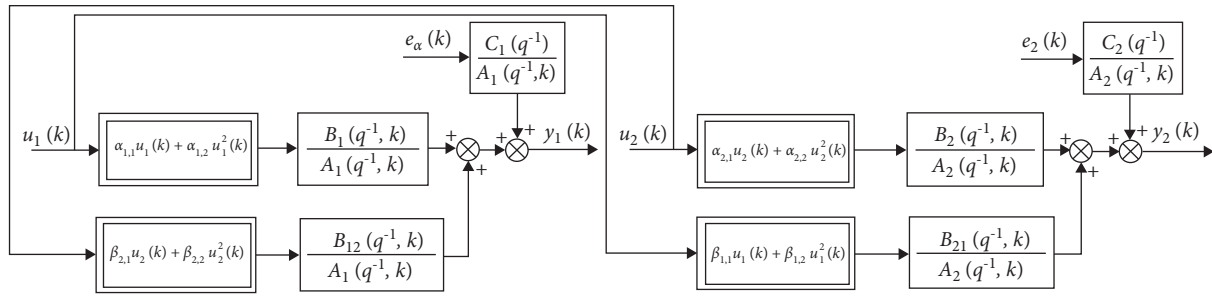
FIGURE 6: General structure interaction of the considered process.
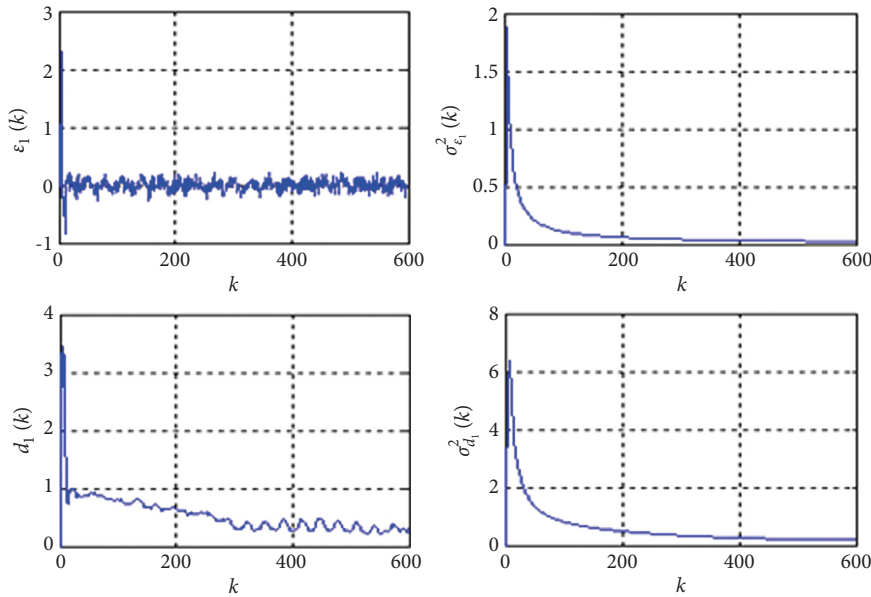
FIGURE 7: Evolution of the prediction error $\varepsilon_1(k)$, the parametric distance $d_1(k)$, and their overall variances $\sigma_{\varepsilon_1}^2(k)$ and $\sigma_{d_1}^2(k)$.

evolution of the prediction error, the parametric distance, and their overall variances for each interconnected non-linear subsystem.

The obtained results indicate the good quality of the estimate, based on an iterative algorithm. This estimate quality ensures the exact choice of the parametric estimation algorithm and the mathematical model of representation that describe the best behavior of the considered interconnected nonlinear system, despite the parameters variations, the presence of interactions signals, and disturbances interim on each system output.

Note that the mathematical model of representation, which is also called the mathematical model of control or mathematical model of behavior, corresponds to the mathematical model of the "black box". Let's add that the mathematical model of representation is most often described by difference equations; this, therefore, corresponds to an input-output type mathematical model. However, the parameters involved in this type of mathematical model have

no physical meaning. In fact, the theoretical mathematical model is much richer in physical meaning than the representation model, since it contains all the useful information about the real process.

It should also be noted that the mathematical model of representation is the most currently used in the control of dynamic systems, in particular in the synthesis of numerical control laws. However, the choice of a mathematical model, from this set of models, may depend on several criteria, such as the type of application, the desired performance indices, and the strategy of the control law envisaged. Therefore, we must classify mathematical models according to their ability to approximate the system. Thus, they can be classified from the simplest mathematical model to the most complex mathematical model. The selection of a "good" mathematical model for the formulation of the control law is made according to the targeted control objectives (accuracy, robustness, and rapidity).
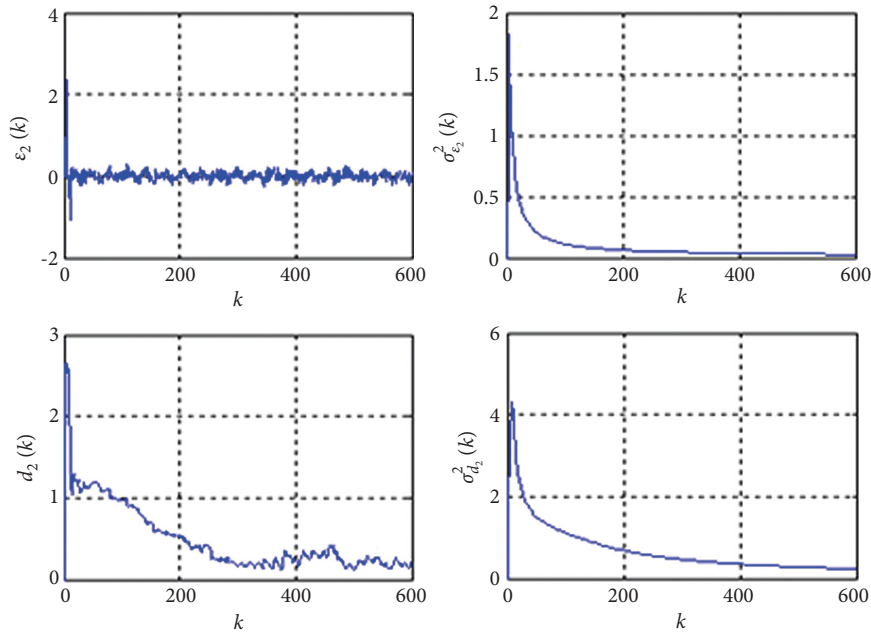
Figure 8: Evolution of the prediction error $\varepsilon_2(k)$, the parametric distance $d_2(k)$, and their overall variances $\sigma_{\varepsilon_2}^2(k)$ and $\sigma_{d_2}^2(k)$.

6. Conclusions

This paper has proposed new input-output MMs of representation, which can describe the dynamic behavior of large-scale nonlinear systems, such as the extended MM of Volterra series, the interconnected Hammerstein structures, and the interconnected Wiener structures. In this research, we considered the class of large-scale nonlinear systems, which are decomposed into several interconnected nonlinear subsystems. Each interconnected subsystem is described by discrete nonlinear MM, mono-variable, operating in a deterministic or stochastic environment, and with unknown time-varying parameters. An illustrative numerical simulation example of two interconnected nonlinear processes was treated to test the performance and the effectiveness of the developed theoretical results.

Let us note that, in certain practical situations, the formulation of a representation mathematical model based on experimental method, describing an industrial system, becomes difficult or impossible in certain cases due to the difficulty in carrying out or analyzing experimental tests on the considered process (unmeasurable inputs and outputs variables and dangerous experimental measurements of certain real process). Besides, it can be remarked that the developed mathematical model becomes more complex with the increase of the dimension and the nonlinearity degree of the considered system. In this case, the synthesis of the adequate control design will be difficult.

In future works, we will address to develop extended versions of different methods, which permit us to estimate the structure variables and the parameters of the interconnected nonlinear systems. The formulation of the control problem of this class of dynamical systems will be investigated in future research by developing various controllers based on different control approaches. [25].

Data Availability

No data were used to support the study.

Conflicts of Interest

The authors declare that they have no conflicts of interest.

References

[1] S. Jain and F. Khorrami, "Decentralized adaptive control of a class of large-scale interconnected nonlinear systems," *IEEE Transactions on Automatic Control*, vol. 42, no. 2, pp. 136–154, 1997.

[2] M. Kamoun and A. Titli, "Implicit self-tuning control for a class of large-scale systems," *International Journal of Control*, vol. 49, no. 2, pp. 713–722, 1989.

[3] S. Kamoun, "Development of recursive estimation algorithms for large-scale stochastic system using the maximum likelihood method," *International Review of Modelling and Simulations (IREMOS)*, vol. 1, no. 2, pp. 248–261, 2008.

[4] P. Panagiotis and M. Polycarpou, "Decentralized fault tolerant control of a class of Interconnected Nonlinear Systems," *IEEE Transactions on Automatic Control*, vol. 56, no. 1, pp. 178–184, 2011.

[5] S. J. Yoo, "Neural-network-based Decentralized Fault-Tolerant Control for a Class of Nonlinear Large-Scale Systems with Unknown Time-Delayed Interaction Faults," *Journal of the Franklin Institute*, vol. 351, no. 3, pp. 1615–1629, 2013.

[6] S. H. Yousef, M. Hamdy, and E. El-Madbouly, "Robust adaptive fuzzy semi-decentralized control for a class of large-scale nonlinear systems using input-output linearization concept," *International Journal of Robust and Nonlinear Control*, vol. 20, no. 1, pp. 27–40, 2010.

[7] S. J. Yoo, N. Hovakimyan, and C. Cao, "Decentralized adaptive control for large-scale nonlinear systems with

interconnected unmodelled dynamics," *IET Control Theory & Applications*, vol. 4, no. 10, pp. 1972–1988, 2010.

[8] A. Jajarmi, N. Pariz, S. Effati, and A. V. Kamyad, "Infinite horizon optimal control for nonlinear interconnected large-scale dynamical systems with an application to optimal attitude control," *Asian Journal of Control*, vol. 14, no. 5, pp. 1239–1250, 2012.

[9] S. Tong, Y. Li, and X. Jing, "Adaptive fuzzy decentralized dynamics surface control for nonlinear large-scale systems based on high-gain observer," *Information Sciences*, vol. 235, pp. 287–307, 2013.

[10] N Chen, Y Liu, B Liu, and W Gui, "Parametric absolute stabilization for interconnected lurietime-delay systems with polytopic uncertainty," *Asian Journal of Control*, vol. 16, no. 1, pp. 225–232, 2014.

[11] G. B. Koo, "Decentralized fuzzy observer-based output-feedback control for nonlinear large-scale systems: an LMI Approach," *IEEE Transactions on Fuzzy Systems*, vol. 22, no. 2, pp. 406–419, 2014.

[12] L. Zhou, H. Tao, W. Paszke, V. Stojanovic, and H. Yang, "PD-type iterative learning control for uncertain spatially interconnected systems" mathematics," vol. 8, no. 9, 2020.

[13] H. Tao, X. Li, W. Paszke, V. Stojanovic, and H. Yang, "Robust PD-type iterative learning control for discrete systems with multiple time-delays subjected to polytopic uncertainty and restricted frequency-domain," *Multidimensional Systems and Signal Processing*, vol. 32, no. 2, pp. 671–692, January 2021.

[14] R. Haber and L. Keviczky, *Nonlinear System Identification: Input-Output Modelling Approach*, Kluwer, Netherlands, 1999.

[15] L. Carassale and A. Karrem, *"Dynamic Analysis of Complex Nonlinear Systems by Volterra Approach"*, Proc., *Computational Stochastic Mechanics*, P. D. S. CSM4 and G. Deodatis, Eds., pp. 107–117, Millipress, Rotterdam, The Netherlands, 2003.

[16] W. Silva, "Identification of nonlinear aeroelastic systems based on the Volterra theory: progress and opportunities," *Nonlinear Dynamics*, vol. 39, no. 1-2, pp. 25–62, 2005.

[17] O. Tokunbo, *"Adaptive Nonlinear System Identification: The Volterra and Wiener Model Approaches"*, p. 248, Springer Science & Business Media, Berlin, Germany, 2007.

[18] M. Elloumi and S. Kamoun, "Parametric estimation of interconnected nonlinear systems described by input-output mathematical models," *International Journal of Automation and Control*, vol. 13, no. 4, pp. 364–381, 2016.

[19] J. Vörös, "Identification of nonlinear dynamic systems using extended Hammerstein and Wiener models," *Control Theory and Advanced Technology*, vol. 10, no. 4, pp. 1203–1212, 1995.

[20] H. Duwaish and M. K. Nazmul, "A new method for the identification of Hammerstein model," *Automatica*, vol. 33, no. 10, 1997.

[21] S. Rangan, G. Wolodkin, and K. Poolla, "New results for Hammerstein system identification," in *Proceedings of the 34th IEEE Conference on Decision and Control*, pp. 697–702, New Orleans, USA, December 1995.

[22] A. Wills, T. D. Schön, L. Ljung, and B. Ninness, "Identification of hammerstein–wiener models," *Automatica*, vol. 49, no. 1, pp. 70–81, 2013.

[23] M. Elloumi, "Samira Kamoun "Adaptive control scheme for large-scale interconnected systems described by Hammerstein models," *Asian Journal of Control*, vol. 19, no. 3, pp. 1075–1088, 2017.

[24] M. Elloumi and S. Kamoun, "Design of recursive parametric estimation algorithm for large-scale nonlinear systems described by Wiener Mathematical models," *International Journal of Sciences and Techniques of Automatic control & computer engineering (IJ- STA)*, vol. 8, pp. 1950–1965, 2014.

[25] S. Billings, *Nonlinear System Identification: NARMAX Methods in the Time, Frequency and Spatio-Temporal Domains*, John Wiley & Sons, New Jersey, USA, 2013.

Research Article

Collection System of Air Conditioners Remanufacturing: Development and Optimization under Probabilistic Uncertainty

Mohammed Alkahtani [ID],[1] Bashir Salah,[1] Aiman Ziout,[1,2] and Moath Alatefi [ID][1]

[1]*Industrial Engineering Department, College of Engineering, King Saud University, Riyadh 11421, Saudi Arabia*
[2]*Mechanical Engineering Department, College of Engineering, United Arab Emirates University, Al Ain 15551, UAE*

Correspondence should be addressed to Moath Alatefi; malatefi@ksu.edu.sa

The need for air conditioners (ACs) is increasing every year, particularly in the Kingdom of Saudi Arabia (KSA). The annual sales of ACs clearly indicated either buying new conditioning systems or replacing existing ACs. When air conditioners are replaced for any reason, a large number of used air conditioners are available, which leads to the necessity of remanufacturing these ACs for economic and environmental purposes. The current research focuses on investigating the collection system of used window ACs as a part of the reverse logistics of remanufacturing window ACs under the uncertainty of demand and production rate. To optimize the average inventory and fulfill the need of the ACs remanufacturing unit, this current research explained many operations in the collection system and their relationship to the remanufacturing unit. These objectives were investigated using a combination of simulation, mathematical, and optimization techniques. After developing the model using Arena software, the simulation model for the initial solution was run. The theoretical and mathematical concepts of inventory have been exploited to find an initial solution for the objectives under investigation. The Optquest tool was used for the simulation model of the initial solution to improve the iterative search technique. Finally, a sensitivity analysis was carried out to determine each input parameter's magnitude and individual impact on the results. The findings suggest that simulation and optimization strategies are effective in improving average inventory and lost demand. As a result, the average inventory has been reduced significantly.

1. Introduction and Literature Review

Remanufacturing of window air conditioners (ACs) consists of collection, remanufacturing, recycling, supplier, and distributor in which each of them is self-contained and has their own set of goals. As a result, each unit was assessed and upgraded separately in order to ameliorate the reverse logistics system. The literature on remanufacturing of ACs is part of a well-known topic called reverse logistics. It has been well investigated in the literature based on its potential importance in research and industry. It deals with the flow of material, knowledge, and money in the reverse direction, as shown in Figure 1. The researchers in the field of reverse logistics have investigated various aspects, such as reverse logistics design [1], barriers during implementation [2, 3] and optimization [4], and performance evaluation [5].

Furthermore, these studies use a variety of methodologies and investigational instruments, including fuzzy research [6], multiobjective optimization [7], and decision making [8].

The first agent in reverse logistics is the collection system, which refers to the process and location for collecting discarded window air conditioners for remanufacturing [10]. The remanufacturing of air conditioners involves multiple units or agencies that interact with one another. The collection system is the most significant component of the remanufacturing system that must be properly built to respond optimally to other system components, such as the remanufacturing unit. The consumption of air conditioners in the Kingdom of Saudi Arabia (KSA) increases every year, depending on the number of units sold. Because a substantial portion of these sales is for replacements, there are
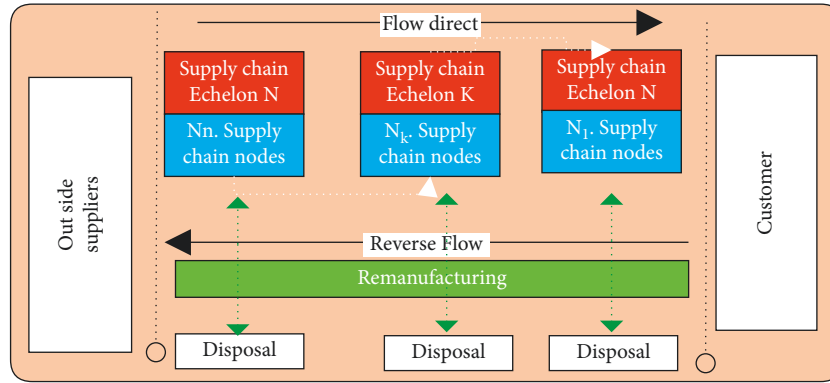
FIGURE 1: The supply chain conceptual model including the reverse flow of products [9].

many ACs that can be remanufactured. The remanufacturing of used ACs has a positive impact on the economy, environment, and society. Because they contain poisonous and other toxic components, used air conditioners are considered a waste of resources and are harmful to the environment.

In addition, remanufactured ACs provide a good alternative for low-income people. These facts mentioned above compel the researchers to look into the prospect of remanufacturing air conditioners at a lower cost and with higher output. The technique of remanufacturing air conditioners is still in its early stages and needs to be explored by research from various professions. Several aspects should be considered in this industry, including the behavior of used air conditioner owners, government laws, and remanufactured air conditioner market competitiveness [11–14]. The procedures of the collection system and its connections to other units, such as the remanufacturing unit, contain numerous interconnected tasks that impact one another, which can be assessed through a simulation method that provides an easy way of conducting many alternatives. The system's bottleneck can be pinpointed through simulation tools, recommending ways to improve performance. Because of various circumstances, factors, and high cost, this technique outperforms physical implementations and the possibility of modifying the real system. Furthermore, computer simulation saves time when it comes to investigating and comprehending model parameters for complicated systems [15].

The remanufacturing of ACs depends on the demands of the new ACs. As the demand for selling new ACs is increasing, the remanufacturing of products will be growing in which good strategic planning must be conducted for such an industry [16]. Researchers and industry experts can benefit from best practices in well-known industries like electronics remanufacturing [17–19] and household recycling [20]. In order to compare the application of numerous inventory rules, the literature has looked into reverse logistics inventory [9, 21]. Many research studies in the literature have investigated the various problems of reverse logistics. In this regard, Liao and Deng [1] provided a very good alternative to the traditional EOQ under the uncertainty of demand. They also published a recent paper [22]

and studied the uncertainty of acquisition. It mainly focuses on the tradeoff between manufacturing and remanufacturing on the basis of profitability. Furthermore, the uncertainty of demand has been investigated with environmental impacts [23]. Also, the quality of returns [24] and market demand have been investigated [25]. However, there are still many limitations in the literature in the field of reverse logistics. Some of these limitations include the need for general studies on specific product remanufacturing and the uncertainty of production rate.

This research aims to construct and evaluate the first stage of the collection procedure in remanufacturing window air conditioners. Besides, it is also directed to studying the relationships between processes in the collection system, selecting the best parameters in the direction of performance measures, and investigating its relation to other units in the remanufacturing system. Inventory expenses and the percentage of orders filled are two of the performance indicators. The model is based on the data from one of the leading ACs manufacturers in KSA and academic experts in ACs logistics. However, the study intended to provide/propose general solutions for ACs remanufacturers. To achieve the research objectives mentioned above, industry and expert opinions have been collected and converted to a computer simulation model. After the collection, the Optquest tool optimized the model by minimizing inventory costs and the percent of lost orders. Finally, the system factors have been investigated using sensitivity analysis to specify the most influential factors affecting the system to be addressed to the stakeholders to reduce costs and save time.

2. The Proposed Methodology

There are two primary stages in the proposed methodology: simulation of the collection system and optimizing the average inventory and the lost demands, as shown in Table 1. First, the collection system will be simulated using simulation software to track the system's outputs, particularly the average inventory and lost needs. After that, decision variables like reorder point, batch size, and target stock are tweaked to optimize average inventory and lost demands. Finally, the sensitivity analysis is examined in order to determine the model's robustness.

TABLE 1: The proposed methodology.

Stages	Steps	Notes
Simulating the collection system	Determining the simulation limits	Riyadh city
	Explaining the processes in the collection system	Various process from receiving ACs to storing
	Implementing the simulation	Simulation software and assumptions
	Stating inputs data	Various times and quantities
	Setting up simulation experimentation	Periods, replications, and outputs
Optimizing the collection system	Specifying the objective functions	Minimizing average inventory and lost demands
	Decision variables	Reorder point, batch size, and target stock
	Optimization method	Iterative search using the Optquest tool
	Sensitivity analysis	By reducing and increasing input parameters

The goal of the research paper is to reduce both average inventory and lost demand. The optimal solution can be researched by changing the reorder point, batch size, and target stock. However, the model's demand and production are not constant. As a result, applying exact mathematical inventory models to arrive at the best option is impossible.

Furthermore, without the use of computer optimization tools, scanning for the optimal choice factors is difficult. As a result, the Arena software's Optquest optimization tool is utilized to optimize the objectives. The mathematical model can be expressed as follows:

$$\text{minimize} \sum f(Q, R, T) S.T. \text{lost demand} \leq 1 \text{ where } Q \text{ is the batch size}, R - \text{reorder point, and } T \text{ is the target stock level.} \tag{1}$$

2.1. Simulating the Collection System

2.1.1. Simulation Limits.
The current study model was limited to the central city of KSA (Riyadh) and included only collection system-related processes involved in receiving used ACs for remanufacturing. According to the status of the AC, it can be one of the three categories when it arrives at the collection system (good, moderate, and bad). Good air conditioners arrive in a good working condition to the collection system. On the other hand, moderate air conditioners do not operate but may be remanufactured depending on the results of examinations. The ACs proceeding for the inspection process may also reveal that the inspected AC is bad and either needs to be accepted for remanufacturing or should be placed in the waste. The simulation takes 240 hours representing 30 working days at a shift of eight (8) hours, to complete from the start time (zero) when the system is inactive and the inventory is at zero. However, the first demand arrives at time zero and is registered as lost demand.

2.1.2. The Processes of the Collection System.
The demand originating from the remanufacturing unit and the collection unit are the two stages of the collection system model, as shown in Figure 2. The procedure begins with the remanufacturing unit sending the demand. When a demand request is received by the collection system, the system checks the inventory level. The request is fulfilled, and the inventory level is updated if the inventory meets the demand. Otherwise, the demand will be marked as unfulfilled. In both cases, the system will check the inventory level, and if it reaches the reorder point, it will send a request to the collection unit for ACs to be delivered until the inventory target is met.

When air conditioners arrive at the collection system, they can be in one of the three states: good, moderate, or bad. With the support of experts in the fields of conditioning, reverse logistics, and remanufacturing, the arrival rate was projected based on people's behavior in changing and selling their old air conditioners. First, the technician inspects the arriving ACs for functioning conditions, and the functional ACs are labeled as good air conditioners. Next, a skilled worker inspects those that are not working to see if the unit can be remanufactured. This process assigns the AC to one of the two categories: moderate, which means it is good for remanufacturing, or bad, which means it is difficult or expensive to remanufacture. Then, the owners of both good and moderate ACs receive their compensation, and the AC stores the collection system inventory, which is updated regularly. Finally, the system checks the inventory level once more to ensure that the inventory objective is met; otherwise, the process of obtaining ACs will stop. These regulations aim to meet the demand for the remanufacturing units without exceeding the finite capacity of the collection system inventory. Manipulation of inventory decision variables such as reorder point and batch size can help achieve this goal.

2.1.3. Simulation Implementation.
The development of this research model has been finalized with the cooperation between the authors and industrial partners, which serves as a real case study for the research model. The industrial partner is one of the leading ACs manufacturing companies in Saudi Arabia. However, independent of the manufacturer, the remanufacturing method is designed for remanufacturing numerous types of window air conditioners. After designing the actual model, Arena Simulation Enterprise Suite version 14.0 was used for the implementation. It is
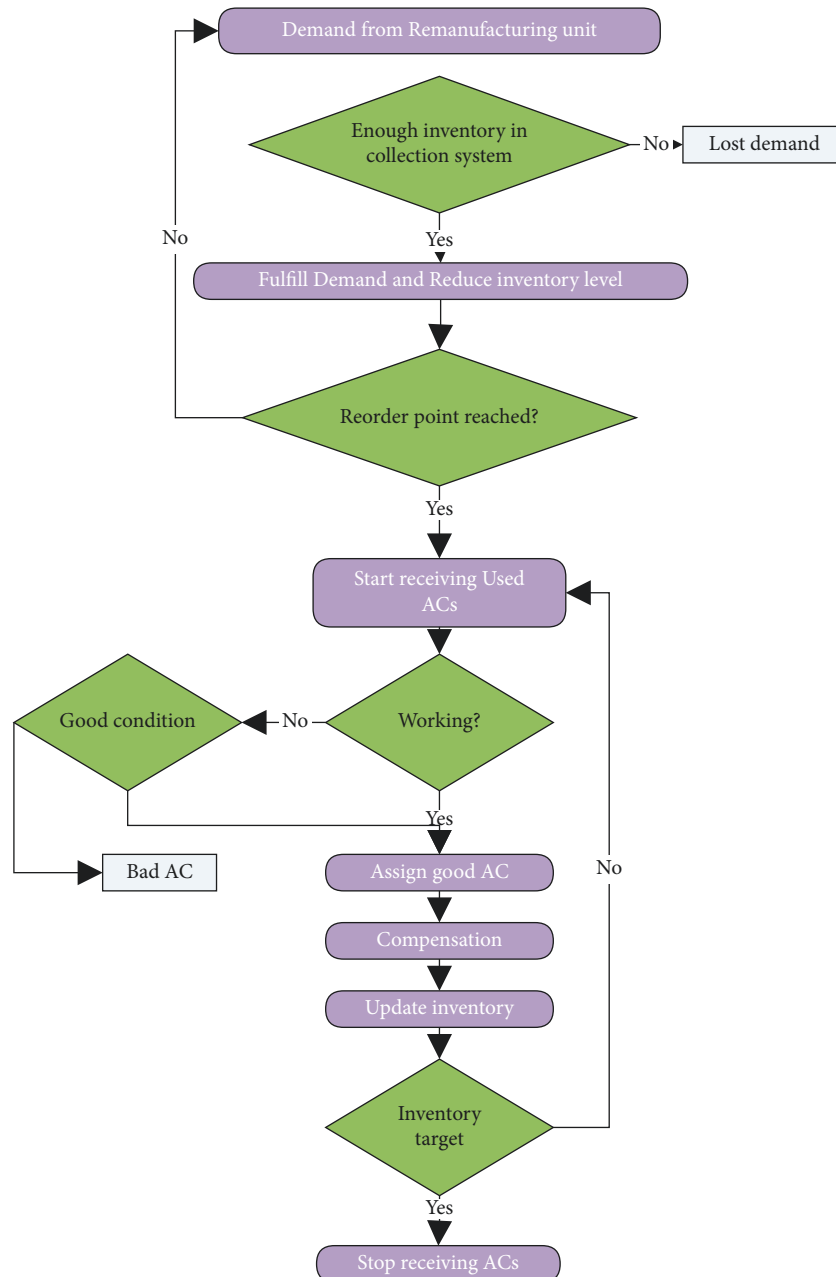
Figure 2: Activity diagram of collection system processes.

worth mentioning that any simulation model contains a number of assumptions that must be met in order for the model to be used in software to reflect the real-world system under examination. Both the authors and the industrial partners agreed with the assumptions, which include the following:

(i) The remanufacturing unit accepts only good and moderate ACs, in which bad ACs will leave the system after the inspection process without consuming any additional resources.

(ii) Regardless of the time spent in the system or any conceivable incidents that can modify their status,

the ACs' status will remain as assigned for the first time.

(iii) In the collection system, both good and moderate ACs have the same resources and priority. However, in the remanufacturing unit, they use a different remanufacturing method.

(iv) The demand of the manufacturing unit is fulfilled by good and moderate ACs randomly.

(v) The collection system's inventory was considered zero at the beginning of the system simulation, which starts with the first demand from the remanufacturing unit. As a result, the first demand

will be reinstated as a lost demand, allowing the collection system to begin accepting ACs.

(vi) Any required equipment in the collection system rather than ACs was assumed to be enough in all simulation periods.

(vii) The acquisition of ACs was assumed to be available all time, and there is a cost for storing each AC and it is computed in predetermined periods. In contrast, the inventory process requires no other resources.

(viii) The process of shipping and transferring demand to remanufacturing is not included in the collection system activities, and the remanufacturing unit handles it completely.

(ix) Only one type of the AC model is considered. This assumption seems reasonable given that many AC models available on the market have the same major components.

2.1.4. Data Inputs. The inputs required to drive the model include ACs parameters, processing time, and resource levels. The data input and simulation model are summarized in Table 2. Detailed literature review and a questionnaire survey were among the sources for the input parameters. The demand arrival is the demand that comes from the remanufacturing unit, and it might take one to three days. Furthermore, the quantity of each demand is not constant, and each demand follows a Poisson distribution with a mean of 100 ACs. Therefore, when the initial demand arrives, the system and the inventory level has zero value. With the support of industry and academic specialists, the processing timeframes for each procedure, demand, and different percentages were determined.

2.1.5. Simulation Experimentation. The goal of this study's model was to optimize the collection system's inventory problem. In terms of meeting demand with the least inventory level, the model is considered efficient. As a result, two key outcomes are used to assess the model's performance:

(i) The average inventory of the simulation period

(ii) The number of lost demands because of shortage inventory

These two measures are the objective of this research and require to be minimized. Table 3 shows the setup of the simulation parameters. At the end of the iterative search, the best 25 solutions are shown by the software. This solution is then used as input to run the simulation model. In addition to the given number of solutions, the Optquest optimization tool's stopping criteria are set to be manual and auto-stopped. Auto-stop takes place after searching 500 solutions without significant improvement using a 95% confidence level (CI). The simulation model was programmed to run for 240 hours or 30 working days at 8 hours per day.

3. Results and Discussion

3.1. Initial Solution of Decision Variables. As previously stated, the goal of this study is to reduce both average inventory and the number of lost demands. The reorder point (ROP), batch size, and goal stock are the decision variables that influence the two objectives (minimizing average inventory and number of lost demands). Before using Arena software's Optquest tool to optimize these objectives, we must first discover an initial solution to be utilized as boundaries for lowering the optimization time. The batch size equals

$$\sqrt{\frac{2 * \text{period demand} * \text{setup cost}}{\text{holding cost peritemper period}}} = \frac{2 * (66 * 30d * \$1)}{\$1} = 60. \tag{2}$$

This research model is a probabilistic inventory model since the demand and lead time are both variable (not constant). Therefore, as shown in Figure 3, the probabilistic inventory model is used when there is uncertainty in demand, lead time, or both.

To find an informative reorder quantity (batch size), the authors will use the economic order quantity (EOC) concept. As demand fluctuates and the lead time is not constant, the reorder point calculation should incorporate this variation. Moreover, since the cost of stockout cannot be determined, ROP will be calculated using a service level, which is derived using the following equation:

$$\text{ROP} = (\text{Average daily demand } x \text{ Average leadtime}) + Z\text{sdLT.} \tag{3}$$

Here, $Z -$ represents the service level sing the normal curve

$$\sigma d = \text{Standard deviation of demand per day,}$$
$$\sigma LT = \text{Standard deviation of lead time in days.} \tag{4}$$

$\sigma dLT = \sqrt{(\text{Average lead time } x\sigma d^2)}$ $+ (\text{Average daily demand})^2 \sigma_{LT}^2$. The demand in this model depends on the demand arrival distribution and the demand amount in each demand request (arrivals). The arrival of demand follows the uniform distribution with a minimum of one and a maximum of three days. The demand amount in each arrival follows a Poisson distribution with a mean of 100 ACs (pois(100)). However, this is not the daily demand since demand arrivals follow a uniform distribution with parameters 1 and 3 days (UNIF(1.3)). The mean of demand arrivals is $1 + 3/2 = 1.5$. Every 1.5 days, there are 100 demands of ACs; therefore, the daily demand is 100/1.5 = 66.667.

The lead time in this model depends on the time of the processes in the collection system. These processes include turn-on, inspection, and compensation processes. It is worth noting that 30 percent of ACs did not undergo any inspection since they are working and directly moved to the compensation process. However, the remaining 70 percent of ACs are inspected during the inspection process. Then, only 70 percent of inspected ACs are accepted for the compensation process. The remaining 30%, on the other hand, are rejected because of the significant damage they

TABLE 2: Input parameters of the simulation model.

Input parameter	Input description
Demand arrivals	Uniform distribution ($a = 1$, $b = 3$ days)
Demand quantity	Poisson distribution ($lam\ da = 100$ ACs)
Initial inventory	Zero ACs
Turn-on process	Uniform distribution ($a = 1 *$ batch size, $b = 2 *$ batch size minutes)
Expected % of working ACs	30%
Inspection process	Triangular distribution ($a = 3 *$ batch size, $c = 5 *$ batch size, $b = 7 *$ batch size minutes)
Expected % of good inspected ACs	70%
Compensation process	Uniform distribution ($a = 1 *$ batch size, $b = 2 *$ batch size minutes)
Target stock	Initial value = 215, best value = 127
Batch size	Initial value = 60, best value = 7
Reorder point	Initial value = 67, best value = 219

TABLE 3: Parameters of simulation run setup.

Parameter	Setting
Solution method	Iterative search using Optquest tool
# of searched solutions	2000 solutions
Replications for each solution	3 replications
Date and time stamp	Present day
Statistics collection	End of run
Warm-up period	0 minutes
Replication length	240 hours
Hours per day	8 hours
Base time units	Hours
Inputs	Defined in Table 1
Queue management	First in first out
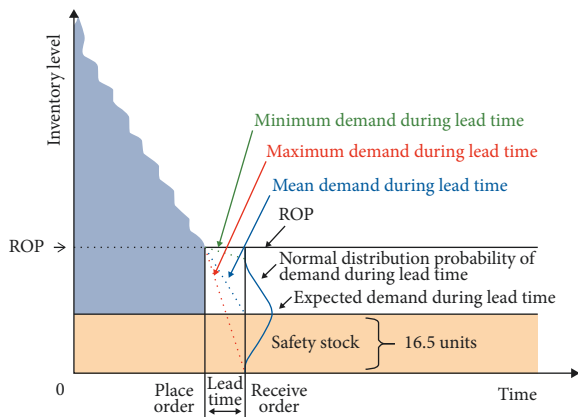
FIGURE 3: Probabilistic inventory model.

have sustained and the exorbitant expense of remanufacturing. The processing time in these processes is variable. For turn-on and compensation processes, it follows a uniform distribution with parameters of one and two minutes. At the same time, the processing time durations of the inspection process follow the triangular distribution with parameters of 3, 5, and 7 minutes. Considering all these time durations and percentages, the average, lower, and upper lead time durations for storing a batch of 60 ACs are 0.82, 0.48, and 0.99 days, respectively, where there are eight working hours in a day. Suppose we take the service level

equal to 95%; the z-value equals 1.645. Then, the reorder point is as follows:

$$ROP = (66\ x\ 0.82) + 1.64 * \sqrt{(0.82 * 370) + (66)^2 * 0.022} = 67 \text{units}. \tag{5}$$

The target inventory level can be calculated by expecting the average inventory level during the run period. The average inventory level =
Total produced during the production run −
Total used during the production run = $73 * 30$
$-66 * 30 = 215$. At this stage, the initial solution for the inventory in the collection system has been obtained, which is 60, 67, and 215 for batch size, reorder point, and target inventory level, respectively. This initial solution will be used in the next section to optimize the inventory level and the number of lost demands. Before running the optimization tool in simulation software, the initial solution will enter and register the values of our objectives (average inventory and number of lost demands). The average inventory value is 117, whereas the number of lost demands is 5, respectively. However, because we need to obtain 95%, this solution is not practical.

3.2. Iterative Search Optimization. The optimization tool included in Arena software called Optquest is used to optimize the inventory level and the number of lost demands. The Optquest optimization tool uses an iterative heuristic method to search for better solutions that optimize the given objective concerning a given constraint. This model aims to minimize the average inventory during the run time concerning the service level. The service level refers to the level of demand met, as measured by the lost demands. The model needs to meet 95% of demands as the CI, or the service level should be 95%. It is worth noting if the first arrival demand in this model is lost since the initial inventory is zero. As a result, the first demand will not be computed in the 5% lost demand range. There are 15 demands during the simulation run that allowed loss of one demand in addition to the first demand. Then, the objective of this model is to minimize the average inventory to not exceed the lost demand from two demands. Figure 4 shows the iterative solutions of Optquest that have been processed for 2000 runs. The best solution is gained by adjusting the batch size to 7, reorder point to 219,
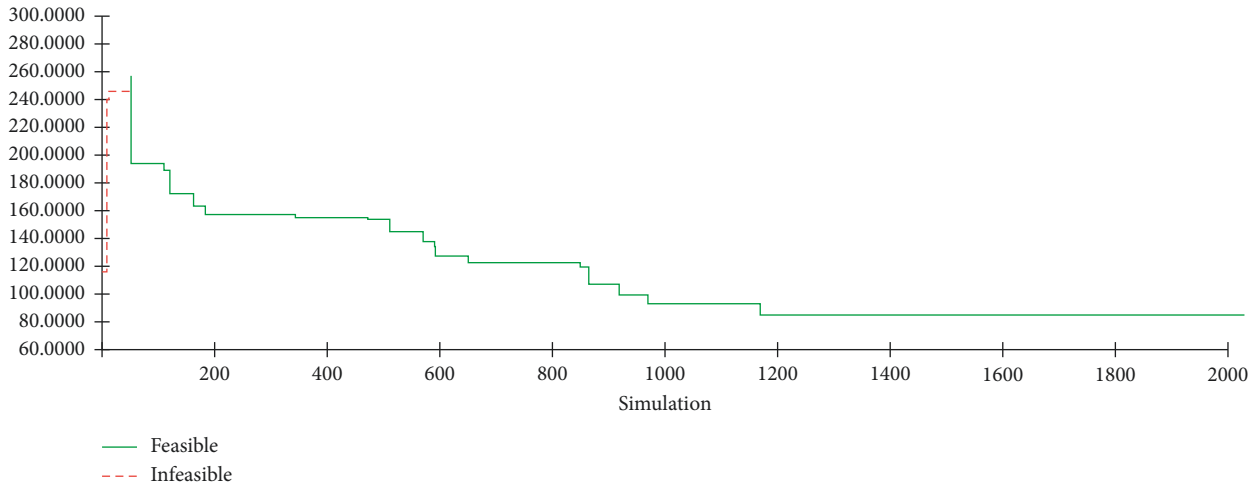
FIGURE 4: Solution improvement using Optquest optimization.

and target stock to 127. This solution reveals an average inventory of 84.72 units and two lost demands. The solution is obtained after 1352 runs, yet the simulation continues without any improvement until 1915 runs.

The idea behind improving the solution is to coincide the inventory level with the arrival demands. The concept of level of inventory for initial and improved solutions can be seen in Figure 5. Besides, Figure 5(a) shows the inventory level and demand of the initial solution along the simulation run. The inventory level itself, as well as the demand and inventory level, has high variations. However, in the optimum solution offered by the Optquest optimization program, this variance has been avoided, as shown in Figure 5(b). As a result, the inventory level variance has been decreased from a maximum of 270 units in the original/initial solution to roughly 130 units in the modified/improved solution.

3.3. Sensitivity Analysis. In this study, sensitivity analysis was used to assess the size effect of each input parameter on the outputs under consideration (average inventory and lost demand). The simulation model can be better understood by changing the input parameters. The sensitivity analysis illustrates how much changing parameters affect the model. This extent can provide an informative guide on the robustness of the model. Consequently, these changes can be used to predict the estimation of any value of the inputs.

There are many sensitivity analysis methods, which depend on the study objective [26]. In this research, one of the most popular methods has been used to conduct sensitivity analysis. This method increases and decreases the input parameters by a constant percent one input parameter at a time and records the changes in output. Based on the literature review, the current study chose to fix 20% for both increasing and decreasing changes [15, 27, 28]. The changing process was conducted for one parameter at a time to investigate the initial effect of each parameter on output. The results of sensitivity analysis on average inventory are shown in Figure 6.

The effect of reducing/decreasing input parameters on the outcomes can be classified into large, medium, and small effects depending on the percentage of change on the outcome when reducing or increasing the corresponding parameter by 20%. For example, Figure 6 shows that the large magnitude of change in average inventory has been induced by increasing the demand quantity, which reveals an increase in average inventory by 20%. However, increasing or decreasing the reorder point does not affect the average inventory.

Furthermore, changes in input parameters have had a greater impact on the number of lost customers than on average inventory, as shown in Figure 7. Therefore, changing the demand quantity is the most influential input parameter of the lost demands. Increasing the amount of demand amount by 20% resulted in a 300% increase in lost demand. It is worth noting that the model outputs are very sensitive to the change in demand quantity. Therefore, further studies in the near future are needed for the investigation of these parameters. However, lowering the majority of the input parameters leads to a significant increase in lost demand. The decrease in target stock, compensation processing time, and the percentages of good ACs demonstrate this. In general, decreasing the input parameters is more influential than increasing. It is worth noting that the changing of reorder points does not affect the lost demand.

3.4. Managerial Insights. The ACs remanufacturing in Saudi Arabia needs a lot of effort to be established among people and industry. It is a very promising sector, and many international research studies have been conducted to solve various issues in this field. The starting point of ACs remanufacturing is the collection system, in which ACs are received, inspected, and stored. The quality of received ACs is almost suitable for remanufacturing, and further inspection is needed. As the market is considered currently full of used ACs, the unit worth of received used ACs is related to the demand of the remanufacturing unit, which is constrained by the remanufacturing capacity and market demand. The collection system is
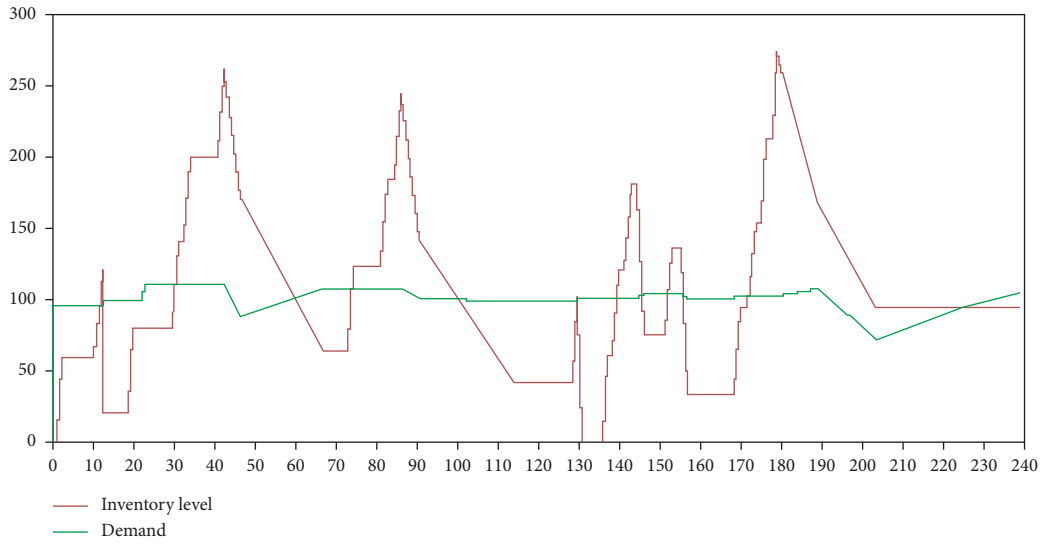
(a)
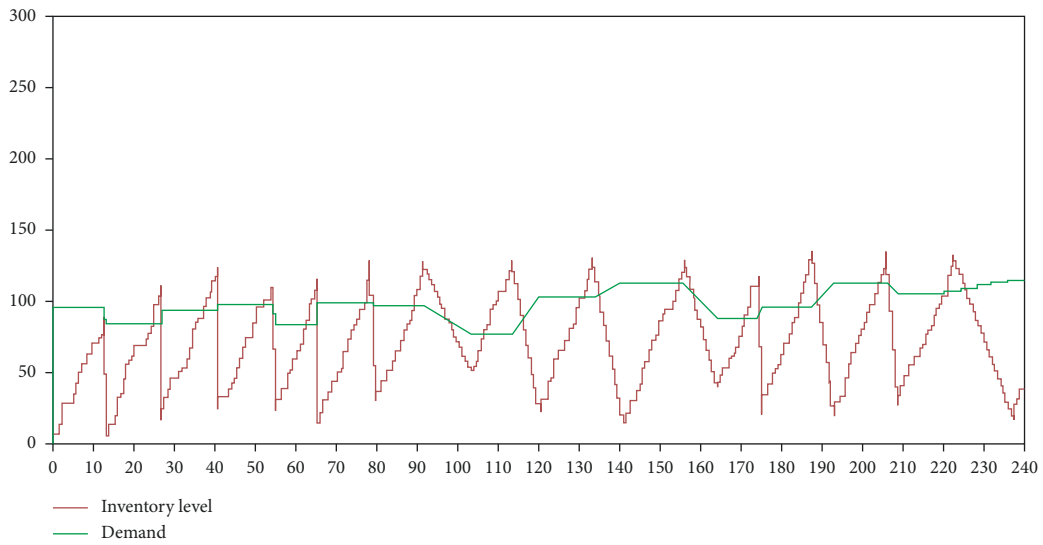
(b)

Figure 5: Level of inventory and demand for initial and improved solutions.
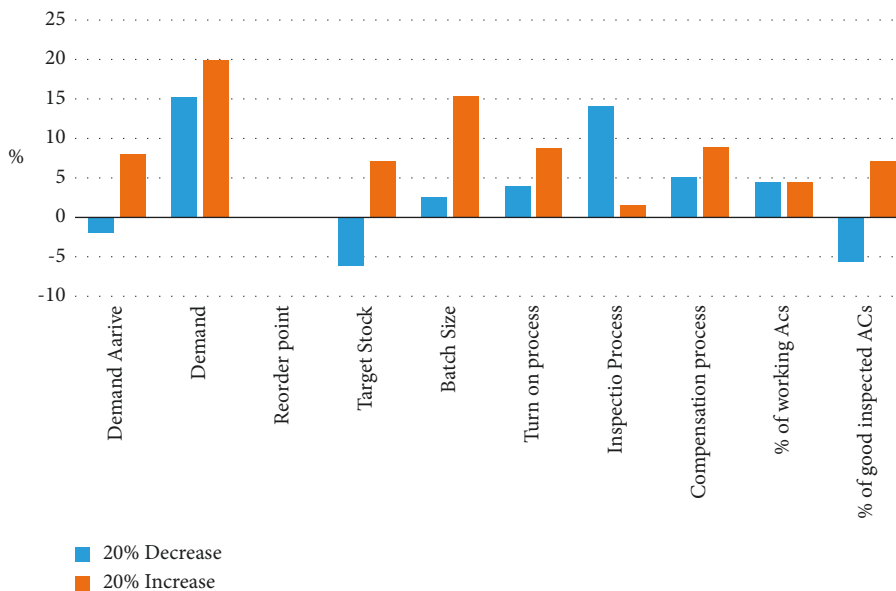
Figure 6: Percentages of changes in inventory levels.
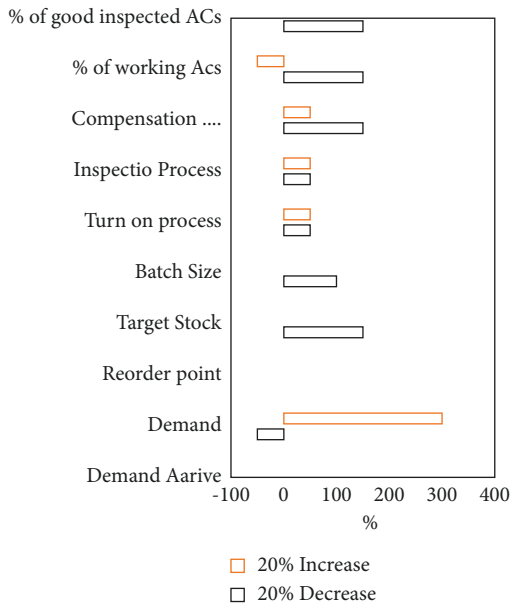
Figure 7: Percentages of changes in lost demand.

supposed to fulfil the demand of remanufacturing units along with maintaining a reasonable average inventory. The more the average inventory in the collection system, the more the expenses. To reduce the cost of the inventory, the batch size should be chosen by an appropriate method. Furthermore, the greater the batch size, the greater the average inventory, which results in great costs. Also, the reorder point plays an important role in inventory cost. On the contrary, the demand should be met to increase the service level and this will become true with more investigation of the demand curve. The presented research introduces a practical solution to these issues.

4. Conclusion

The current study investigated the collection system in ACs remanufacturing. The research was based on an actual case study from one of Saudi Arabia's largest air conditioner manufacturers. With the support of industry and academic specialists, a simulation model for the collection system was developed to optimize average inventory and lost demand. The simulation model has provided a great opportunity to improve the performance of the collection system. It is a better option because the simulation model allows for more flexibility in altering parameters and recognizing changes. Furthermore, using the Optquest optimization tool has dramatically improved the average inventory and the number of lost demands. It offers a variety of alternate ways for improving the collection system's performance. Moreover, the sensitivity analysis has provided several hints about the most influential input parameters and the most sensitive outcome to modifications, which has backed up the findings of this study.

Data Availability

No data were used to support this study.

References

[1] H. Liao and Q. Deng, "A carbon-constrained EOQ model with uncertain demand for remanufactured products," *Journal of Cleaner Production*, vol. 199, pp. 334–347, 2018.

[2] K. Govindan and M. Bouzon, "From a literature review to a multi-perspective framework for reverse logistics barriers and drivers," *Journal of Cleaner Production*, vol. 187, pp. 318–337, 2018.

[3] M. Waqas, Q.-l. Dong, N. Ahmad, Y. Zhu, and M. Nadeem, "Critical barriers to implementation of reverse logistics in the manufacturing industry: a case study of a developing country," *Sustainability*, vol. 10, no. 11, p. 4202, 2018.

[4] T. S. J. J. Sathish and J. Jayaprakash, "Optimizing supply chain in reverse logistics," *International Journal of Mechanical and Production Engineering Research and Development*, vol. 7, no. 6, pp. 551–560, 2017.

[5] H. Han and S. Trimi, "A fuzzy TOPSIS method for performance evaluation of reverse logistics in social commerce platforms," *Expert Systems with Applications*, vol. 103, pp. 133–145, 2018.

[6] P. Sirisawat and T. Kiatcharoenpol, "Fuzzy AHP-TOPSIS approaches to prioritizing solutions for reverse logistics barriers," *Computers & Industrial Engineering*, vol. 117, pp. 303–318, 2018.

[7] P. Dutta, A. Mishra, S. Khandelwal, and I. Katthawala, "A multiobjective optimization model for sustainable reverse logistics in Indian E-commerce market," *Journal of Cleaner Production*, vol. 249, Article ID 119348, 2020.

[8] N. Zarbakhshnia, Y. Wu, K. Govindan, and H. Soleimani, "A novel hybrid multiple attribute decision-making approach for outsourcing sustainable reverse logistics," *Journal of Cleaner Production*, vol. 242, Article ID 118461, 2020.

[9] F. Longo, "Testing the behaviour of different inventory control policies in case of extended reverse logistics by using simulation," *International Journal of Simulation and Process Modelling*, vol. 9, no. 3, pp. 167–180, 2014.

[10] G. R. S. Pandian and W. Abdul-Kader, "Performance evaluation of reverse logistics enterprise - an agent-based simulation approach," *International Journal of Sustainable Engineering*, vol. 10, no. 6, pp. 384–398, 2017.

[11] M. T. Islam, P. Dias, and N. Huda, "Waste mobile phones: a survey and analysis of the awareness, consumption and disposal behavior of consumers in Australia," *Journal of Environmental Management*, vol. 275, Article ID 111111, 2020.

[12] S. Pokharel and Y. Liang, "A model to evaluate acquisition price and quantity of used products for remanufacturing," *International Journal of Production Economics*, vol. 138, no. 1, pp. 170–176, 2012.

[13] Y. Ding, C. Shen, and D. Feng, "Pricing and collection for printer cartridge recycling under retailers' ordering and

collection," *Journal of Cleaner Production*, vol. 276, Article ID 122814, 2020.

[14] J. Yin, Y. Gao, and H. Xu, "Survey and analysis of consumers' behaviour of waste mobile phone recycling in China," *Journal of Cleaner Production*, vol. 65, pp. 517–525, 2014.

[15] S. M. Glasgow, Z. B. Perkins, N. R. M. Tai, K. Brohi, and C. Vasilakis, "Development of a discrete event simulation model for evaluating strategies of red blood cell provision following mass casualty events," *European Journal of Operational Research*, vol. 270, no. 1, pp. 362–374, 2018.

[16] C. Nuss, R. Sahamie, and D. Stindt, "The reverse supply chain planning matrix: a classification scheme for planning problems in reverse logistics," *International Journal of Management Reviews*, vol. 17, no. 4, pp. 413–436, 2015.

[17] J. Ylä-Mella, R. L. Keiski, and E. Pongrácz, "Electronic waste recovery in Finland: consumers' perceptions towards recycling and re-use of mobile phones," *Waste Management*, vol. 45, pp. 374–384, 2015.

[18] M. T. Islam, M. S. H. Nizami, S. Mahmoudi, and N. Huda, "Reverse logistics network design for waste solar photovoltaic panels: a case study of New South Wales councils in Australia," *Waste Management & Research: The Journal for a Sustainable Circular Economy*, vol. 39, no. 2, pp. 386–395, 2021.

[19] M. T. Islam and N. Huda, "Assessing the recycling potential of "unregulated" e-waste in Australia," *Resources, Conservation and Recycling*, vol. 152, Article ID 104526, 2020.

[20] E. E. A. Jalil, D. B. Grant, J. D. Nicholson, and P. Deutz, "Reverse logistics in household recycling and waste systems: a symbiosis perspective," *Supply Chain Management: International Journal*, vol. 21, 2016.

[21] F. Longo, "An advanced framework for inventory management in reverse logistics," in *Proceedings of the 24th European Modeling and Simulation Symposium, EMSS 2012*, pp. 591–601, Vienna, Austria, September 2012.

[22] H. Liao, Q. Zhang, N. Shen, Y. Nie, and L. Li, "Coordination between forward and reverse production streams for maximum profitability," *Omega*, vol. 104, Article ID 102454, 2021.

[23] H. Liao and L. Li, "Environmental sustainability EOQ model for closed-loop supply chain under market uncertainty: a case study of printer remanufacturing," *Computers & Industrial Engineering*, vol. 151, Article ID 106525, 2021.

[24] H. Liao, N. Shen, and Y. Wang, "Design and realisation of an efficient environmental assessment method for 3R systems: a case study on engine remanufacturing," *International Journal of Production Research*, vol. 58, no. 19, pp. 5980–6003, 2020.

[25] H. Liao and Q. Deng, "EES-EOQ model with uncertain acquisition quantity and market demand in dedicated or combined remanufacturing systems," *Applied Mathematical Modelling*, vol. 64, pp. 135–167, 2018.

[26] S. Robinson, *Simulation: The Practice of Model Development and Use*, Vol. 50, Wiley Chichester, Chichester, England, 2004.

[27] D. M. Hamby, "A comparison of sensitivity analysis techniques," *Health Physics*, vol. 68, no. 2, pp. 195–204, 1995.

[28] M. Taylor, "What is sensitivity analysis?" pp. 1–8, 2009, https://www.edupristine.com/blog/all-about-sensitivity-analysis.

Research Article

The Research of the Overlapping Decentralized Guaranteed Cost Hybrid Control Method for Adjacent Buildings with Uncertain Parameters

Qinghu Xu,[1,2,3] **Xuezhi Zhen,**[1] **Xiang Ruan,**[1] **Yutao Liu,**[1] **Xianzeng Shi** ![ORCID],[1,4] **Dawei Man** ![ORCID],[1,2,3] **Xiaofang Kang** ![ORCID],[1,2,3] **and Guanghui Xia** ![ORCID][1,2,3]

[1]*School of Civil Engineering, Anhui Jianzhu University, Hefei 230601, China*
[2]*BIM Engineering Center of Anhui Province, Hefei 230601, China*
[3]*Prefabricated Building Research Institute of Anhui Province, Hefei 230601, China*
[4]*College of Civil and Transportation Engineering, Hohai University, Nanjing 210098, China*

Correspondence should be addressed to Xianzeng Shi; shixianzeng@ahjzu.edu.cn

This paper presents an overlapping decentralized guaranteed cost hybrid control method for adjacent buildings with uncertain parameters, by combining the guaranteed cost control algorithm with the overlapping decentralized control strategy. The passive dampers are used as link members between the two parallel buildings, and the active control devices are installed between two consecutive floors in two adjacent buildings. The passive coupling dampers modulate the relative responses between the two buildings, and the active control devices modulate the interstory responses of each building. Based on the inclusion principle, a large-scale structure is divided into a set of paired substructures with common parts first. Then, the controller of each pair of substructures is designed by using the guaranteed cost algorithm. After that, the controller of the original system is formed by using the contraction principle. Consequently, the proposed approach is used to prevent pounding damage and achieve the best results in earthquake response reduction of uncertain adjacent buildings when compared with the calculation results obtained by the centralized control strategy. Furthermore, the stability and reliability of the control system are promoted by adopting the overlapping decentralized control strategy.

1. Introduction

With rapid urbanization, an increasing number of adjacent buildings are appearing in cities. These buildings are usually separated from each other without connecting members, and their seismic performance of them depends on their characteristics. However, adjacent structures with insufficient spacing may collide with each other and cause more serious damage under earthquake excitation. For instance, the results of the investigation into the 1985 Mexico City earthquake showed that more than 40% of the 330 severely damaged buildings surveyed had collided with each other [1]. During the 1989 Loma Prieta City earthquake in the United States, over 200 of more than 500 buildings surveyed

were destroyed by collision [2]. The Wenchuan earthquake in 2008 [3] and the Lushan earthquake in 2013 [4] caused adjacent buildings to be damaged by pounding. The inquiries on structural damage caused by the Christchurch earthquake in New Zealand in 2011 indicated that more than 6% of buildings had been severely destroyed by collision [5]. Previous earthquake damage investigations have shown that the collision damage to structures cannot be ignored. So, it has important research value to research how to improve the seismic performance of adjacent structures and avoid the occurrence of collision damage.

In recent years, the connected control method (CCM), which connects two independent structures by placing control equipment between adjacent buildings to resist

external disturbances such as earthquakes, has attracted widespread attention from domestic and foreign scholars. The link members between adjacent buildings can adopt passive, active, or semiactive controllers [6]. CCM has been applied in mechanical, aerospace, and civil engineering fields, the study of which is of great significance. Now, CCM cannot only reduce the dynamic response of each structure but also effectively escape the occurrence of collision damage between adjacent structures [7]. Christenson et al. [8] used CCM to study the seismic response of adjacent buildings and discussed the influence of the ratio of building height on the control effect. Roh et al. [9] considered setting a combination of linear viscous dampers and linear springs between adjacent buildings to mitigate the seismic response of the structure and analyzed the influence of the ratio of adjacent building height, the ratio of fundamental periods, damping parameters of connected dampers, and external excitation of different frequencies on the story response. Patel and Jangid [10] optimized the number and damping coefficients of viscoelastic dampers which were adopted to link two adjacent multi-degree-of-freedom buildings. Cimellaro et al. [11] considered robust control algorithms to enhance the performance of adjacent structural models connected by passive dampers. Motra et al. [12] studied the problem of adjacent buildings linked by MR dampers with LQR control, considering a modified Bouc–Wen model that relates damping force to the input voltage state. Then, the response attenuation results were compared by employing LQR-RNN and LQR-CVL. Bigdeli et al. [13, 14] discussed the number and location of connecting dampers so that the performance of adjacent buildings can be promoted. Gao et al. [15] put forward a dynamic output feedback control method for mitigating structural seismic vibration and obtaining the location of the actuators and sensors, which were placed between adjacent buildings. Gudarzi and Zamanian [16] designed an output feedback controller based on the Kalman filter and optimal control theory for three adjacent buildings under earthquake action to provide a promising means of response attenuation. Yang and Lam [17] extensively studied the vibration of two eccentric adjacent buildings linked by viscoelastic dampers under bidirectional earthquakes. Uz and Hadi [18] introduced an optimization design method of nonlinear hysteretic dampers based on genetic algorithms [19] and demonstrated that the proper number of dampers was more helpful in improving the seismic performance of two adjacent buildings.

However, the centralized control strategy has flaws such as large computation, low reliability, and poor stability. Therefore, the decentralized control strategy with the advantages of fast data transmission, less feedback delay, and strong system reliability received extensive attention [20–23]. Especially, the focus of the research is on overlapping decentralized control strategies, based on the inclusion principle, which is a method to dispose of decentralized control of a large-scale system. This approach can effectively deal with the interconnection information between substructures and realize the decoupling of the system. Besides, it can also enhance the robustness and flexibility of controller design, when a large-scale system is decomposed into several low-order subsystems, and the subcontroller design is carried out through parallel computing. First of all, a large-scale system is divided into a series of paired subsystems based on the inclusion principle, in which shared information is considered. Then, a preset control algorithm is used to design the controller for the subsystem. Finally, the contraction principle is applied to contract the extended subsystem controller to form the controller of the original system [21–24]. Palacios-Quiñonero et al. [7, 25] studied an overlapping decentralized passive-active control method of adjacent buildings under an earthquake, which integrates the high performance of an active control system with the reliability of a passive control system and allows the decentralized design and operation of an active control subsystem.

Due to the influence of model errors, material deformation, external interference, and other factors, the structural model parameters are uncertain in practical engineering. Uncertainty-based design is becoming one of the research hotspots for engineering systems [26–28]. If the influence of uncertainty is not considered in the controller design, the control effect of the system will be difficult to guarantee. Therefore, the reliability of the system becomes especially important in various fields [29–35]. So, to improve the accuracy of modeling and ensure the stability of the control system, the constructed model is made to resemble the actual model by adding uncertainty influencing factors in the process of modeling. Chang and Peng [36] first proposed the guaranteed cost control method for uncertain systems in 1972 and successfully solved this problem. This method makes the performance functions of the system have a certain upper bound and can also ensure its robust stability. Bakule et al. [37, 38] adopted overlapping decentralized guaranteed cost control methods to analyze uncertain continuous time-delay systems and uncertain discrete time-delay systems. The references [39, 40] studied uncertain discrete state time-delay systems and uncertain discrete time-delay systems with both states and inputs while proposing a guaranteed cost control method based on bilinear matrix inequality. Gyurkovics et al. [41] discussed dynamic output feedback guaranteed cost control for uncertain discrete time-delay systems. Aiming at a class of uncertain linear systems, Ahmadi et al. [42] extended the original system to a weakly interconnected system that retains all the properties of the original system based on the inclusion principle. Then, the iterative linear matrix inequality (ILMI) algorithm was applied to design the static output feedback overlapping decentralized controller of the extended system, which eventually contracted into the overlapping decentralized guaranteed cost controller of the original system.

In this paper, an overlapping decentralized guaranteed cost hybrid control method, using the inclusion principle and the overlapping decentralized control scheme with the guaranteed cost control algorithm, has been established for uncertain parameter adjacent structure systems under earthquake. The guaranteed cost control algorithm is adopted in each subsystem to get their controller, which is contracted to the original state-space to obtain the

overlapping decentralized controller, and the mitigation of responses between adjacent buildings is dependent on passive dampers linked by them. The method has been tested for two neighboring buildings with uncertain parameters, and the numerical analysis results are compared with those of the centralized guaranteed cost vibration control strategy to illustrate its effectiveness.

$$(\mathbf{M} + \Delta\mathbf{M})\ddot{x}(t) + (\mathbf{C} + \Delta\mathbf{C})\dot{x}(t) + (\mathbf{K} + \Delta\mathbf{K})\mathbf{x}(t) = \mathbf{D}_s\ddot{x}_g(t) + \mathbf{B}_u\mathbf{u}(t), \tag{1}$$

where $\mathbf{M}, \mathbf{C},$ and $\mathbf{K}$ are the total mass, damping, and stiffness matrices of adjacent buildings, respectively; $\Delta\mathbf{M}, \Delta\mathbf{C},$ and $\Delta\mathbf{K}$ are the corresponding variation matrices, respectively; $\mathbf{D}_s$ and $\mathbf{B}_u$ are the position matrices of seismic excitation and control force, respectively; $\mathbf{x}(t)$ is the displacement vector of the structure; $\mathbf{u}(t)$ is the control force vector; and $\ddot{x}_g$ is the seismic acceleration. In Figure 1, $m_i^j, c_i^j,$ and k_i^j denote the mass, damping coefficient, and interlayer shear stiffness, where $i, l, r,$ and d represent the floor, the left building, the right building, and the passive dampers, respectively. where

$$\mathbf{M} = \begin{bmatrix} \mathbf{M}_L & \mathbf{0} \\ \mathbf{0} & \mathbf{M}_R \end{bmatrix},$$

$$\mathbf{M}_L = \mathrm{diag}\{m_1^l, m_2^l, \ldots, m_{n_1-1}^l, m_{n_1}^l\},$$

$$\mathbf{M}_R = \mathrm{diag}\{m_1^r, m_2^r, \ldots, m_{n_2-1}^r, m_{n_2}^r\}, \tag{2}$$

$$\mathbf{K} = \mathbf{K}_B + \mathbf{K}_D,$$

$$\mathbf{K}_B = \begin{bmatrix} \mathbf{K}_L & \mathbf{0} \\ \mathbf{0} & \mathbf{K}_R \end{bmatrix},$$

$$\mathbf{K}_D = \begin{bmatrix} [\mathbf{k}_d]_{n_2\times n_2} & [\mathbf{0}]_{n_2\times(n_1-n_2)} & [-\mathbf{k}_d]_{n_2\times n_2} \\ [\mathbf{0}]_{(n_1-n_2)\times n_2} & [\mathbf{0}]_{(n_1-n_2)\times(n_1-n_2)} & [\mathbf{0}]_{(n_1-n_2)\times n_2} \\ [-\mathbf{k}_d]_{n_2\times n_2} & [\mathbf{0}]_{n_2\times(n_1-n_2)} & [\mathbf{k}_d]_{n_2\times n_2} \end{bmatrix}, \tag{3}$$

$$\mathbf{K}_L = \begin{bmatrix} k_1^l + k_2^l & -k_2^l & & & & \\ -k_2^l & k_2^l + k_3^l & -k_3^l & & & \\ & -k_3^l & k_3^l + k_4^l & -k_4^l & & \\ & & \cdots & \cdots & \cdots & \\ & & & -k_{n_1-1}^l & k_{n_1-1}^l + k_{n_1}^l & -k_{n_1}^l \\ & & & & -k_{n_1}^l & k_{n_1}^l \end{bmatrix}, \tag{4}$$

$$\mathbf{K}_R = \begin{bmatrix} k_1^r + k_2^r & -k_2^r & & & & \\ -k_2^r & k_2^r + k_3^r & -k_3^r & & & \\ & -k_3^r & k_3^r + k_4^r & -k_4^r & & \\ & & \cdots & \cdots & \cdots & \\ & & & -k_{n_2-1}^r & k_{n_2-1}^r + k_{n_2}^r & -k_{n_2}^r \\ & & & & -k_{n_2}^r & k_{n_2}^r \end{bmatrix}, \tag{5}$$

2. Hybrid Control of Overlapping Decentralized Guaranteed Cost for Systems with Uncertain Parameters

2.1. Systematic Description of Adjacent Buildings with Uncertain Parameters. Figure 1 shows the structural model of the adjacent buildings. Considering the uncertainties of the mass, stiffness, damping, and other factors of the structure, the motion equation of the controlled system is obtained:

$$\mathbf{k}_d = \mathrm{diag}\{k_1^d, k_2^d, \ldots, k_{n_2-1}^d, k_{n_2}^d\}, \tag{6}$$

$$\mathbf{C} = \mathbf{C}_B + \mathbf{C}_D. \tag{7}$$

The matrices $\mathbf{C}_B$ and $\mathbf{C}_D$ can be obtained by using equations (3)~(6) and replacing interlayer stiffness coefficient k_i^j with damping coefficient c_i^j. $\mathbf{M}_L$ and $\mathbf{K}_L$ are the mass and stiffness matrices of the building on the left, respectively; $\mathbf{M}_R$ and $\mathbf{K}_R$ are the mass and stiffness matrices of the building on the right, respectively; $\mathbf{K}_B$ and $\mathbf{C}_B$ are the stiffness and damping matrices of adjacent structures, respectively; and $\mathbf{K}_D$ and $\mathbf{C}_D$ are the stiffness and damping matrices of connected systems, respectively.

$$\mathbf{x}(t) = \left[x_1^l(t), x_2^l(t), \ldots, x_{n_1}^l(t), x_1^r(t), x_2^r(t), \ldots, x_{n_2}^r(t)\right]^T,$$

$$\mathbf{D}_s = -(\mathbf{M} + \Delta\mathbf{M})[\mathbf{1}]_{(n_1+n_2)\times 1},$$

$$\mathbf{B}_u = \begin{bmatrix} [\mathbf{B}_u^l]_{n_1\times n_1} & [\mathbf{0}]_{n_1\times n_2} \\ [\mathbf{0}]_{n_2\times n_1} & [\mathbf{B}_u^r]_{n_2\times n_2} \end{bmatrix}, \tag{8}$$

where

$$\mathbf{B}_u^l = \begin{cases} (B_u^l)_{i,i} = 1, & 1 \le i \le n_1, \\ (B_u^l)_{i,i+1} = -1, & 1 \le i < n_1, \\ (B_u^l)_{i,j} = 0, & \text{else}, \end{cases}$$

$$\mathbf{B}_u^r = \begin{cases} (B_u^r)_{i,i} = 1, & 1 \le i \le n_2, \\ (B_u^r)_{i,i+1} = -1, & 1 \le i < n_2, \\ (B_u^r)_{i,j} = 0, & \text{else}, \end{cases}$$

$$\mathbf{u}(t) = \left[u_1^l(t), u_2^l(t), \ldots, u_{n_1}^l(t), u_1^r(t), u_2^r(t), \ldots, u_{n_2}^r(t)\right]^T,$$

$$\Delta\mathbf{M} = \alpha\boldsymbol{\delta}_{\mathbf{M}}\mathbf{M},$$

$$\Delta\mathbf{C} = \beta\boldsymbol{\delta}_{\mathbf{C}}\mathbf{C},$$

$$\Delta\mathbf{K} = \gamma\boldsymbol{\delta}_{\mathbf{K}}\mathbf{K}, \tag{9}$$

FIGURE 1: The model of adjacent buildings.

where α, β, and γ are the maximum rate of change of mass, damping, and stiffness, respectively. $\delta_{\mathbf{M}} = \begin{bmatrix} \delta_{\mathbf{M}_L} & \mathbf{0} \\ \mathbf{0} & \delta_{\mathbf{M}_R} \end{bmatrix}$, $\delta_{\mathbf{C}} = \begin{bmatrix} \delta_{\mathbf{C}_L} & \mathbf{0} \\ \mathbf{0} & \delta_{\mathbf{C}_R} \end{bmatrix}$, $\delta_{\mathbf{K}} = \begin{bmatrix} \delta_{\mathbf{K}_L} & \mathbf{0} \\ \mathbf{0} & \delta_{\mathbf{K}_R} \end{bmatrix}$, $\delta_{\mathbf{C}}$ and $\delta_{\mathbf{K}}$ are unknown real function matrices of appropriate dimensions. Since $\delta_{\mathbf{M}}$ is a diagonal matrix [43], so

$$(\mathbf{M} + \Delta\mathbf{M})^{-1} = \mathbf{M}^{-1} + \Delta_1\mathbf{M}$$
$$\Delta_1\mathbf{M} = -\left(\alpha\mathbf{M}^{-1}\right)\delta_{\mathbf{M}}\left(\mathbf{I} + \alpha\delta_{\mathbf{M}}\right)^{-1}. \tag{10}$$

Equation (1) is transformed into a state-space model

$$\dot{Z}_p(t) = \left(\mathbf{A}_p + \Delta\mathbf{A}_p\right)\mathbf{Z}_p(t) + \left(\mathbf{B}_p + \Delta\mathbf{B}_p\right)\mathbf{u}(t) + \mathbf{E}_p\ddot{x}_g(t), \tag{11}$$

where

$$\begin{aligned}
\mathbf{A}_p &= \begin{bmatrix} \mathbf{0} & \mathbf{I} \\ -\mathbf{M}^{-1}\mathbf{K} & -\mathbf{M}^{-1}\mathbf{C} \end{bmatrix}, \\
\mathbf{B}_p &= \begin{bmatrix} \mathbf{0} \\ \mathbf{M}^{-1}\mathbf{B}_u \end{bmatrix}, \\
\mathbf{E}_p &= \begin{bmatrix} \mathbf{0} \\ -[\mathbf{1}] \end{bmatrix}, \\
\mathbf{Z}_p(t) &= \begin{bmatrix} \mathbf{x}^l(t) & \dot{x}^l(t) & \mathbf{x}^r(t) & \dot{x}^r(t) \end{bmatrix}^T, \\
\Delta\mathbf{A}_p &= \begin{bmatrix} \mathbf{0} & \mathbf{0} \\ -\Delta_{\mathbf{MK}} & -\Delta_{\mathbf{MC}} \end{bmatrix}, \\
\Delta\mathbf{B}_p &= \begin{bmatrix} \mathbf{0} \\ \Delta_1\mathbf{MB}_u \end{bmatrix}, \\
\Delta_{\mathbf{MK}} &= \Delta_1\mathbf{M}\left(\mathbf{K} + \Delta\mathbf{K}\right) + \mathbf{M}^{-1}\Delta\mathbf{K}, \\
\Delta_{\mathbf{MC}} &= \Delta_1\mathbf{M}\left(\mathbf{C} + \Delta\mathbf{C}\right) + \mathbf{M}^{-1}\Delta\mathbf{C}, \\
\left(\Delta\mathbf{A}_p \quad \Delta\mathbf{B}_p\right) &= \mathbf{D}_p\mathbf{F}_p\left(\mathbf{E}_{p1} \quad \mathbf{E}_{p2}\right).
\end{aligned} \tag{12}$$

We define a new state vector $\mathbf{Z}(t) = \overline{T}\mathbf{Z}_p(t)$, where

$$\overline{T} = \begin{bmatrix} \overline{T}^l & \mathbf{0} \\ \mathbf{0} & \overline{T}^r \end{bmatrix},$$

$$\overline{T}^l = \begin{cases} \overline{T}^l_{1,1} = 1, & \overline{T}^l_{2,n_1+1} = 1 \\ \overline{T}^l_{2i-1,i-1} = -1, & \overline{T}^l_{2i-1,i} = 1, & 1 < i \le n_1 \\ \overline{T}^l_{2i,n_1+i-1} = -1, & \overline{T}^l_{2i,n_1+i} = 1, & 1 < i \le n_1 \\ \overline{T}^l_{i,j} = 0, & else \end{cases},$$

$$\overline{T}^r = \begin{cases} \overline{T}^r_{1,1} = 1, & \overline{T}^r_{2,n_2+1} = 1 \\ \overline{T}^r_{2i-1,i-1} = -1, & \overline{T}^r_{2i-1,i} = 1, & 1 < i \le n_2 \\ \overline{T}^r_{2i,n_2+i-1} = -1, & \overline{T}^r_{2i,n_2+i} = 1, & 1 < i \le n_2 \\ \overline{T}^r_{i,j} = 0, & else \end{cases},$$

$$\mathbf{Z}(t) = \begin{bmatrix} x_1^l(t), \dot{x}_1^l(t), \left(x_2^l(t) - x_1^l(t)\right), \left(\dot{x}_2^l(t) - \dot{x}_1^l(t)\right), \dots, \left(x_{n_1}^l(t) - x_{n_1-1}^l(t)\right), \left(\dot{x}_{n_1}^l(t) - \dot{x}_{n_1-1}^l(t)\right), \\ x_1^r(t), \dot{x}_1^r(t), \left(x_2^r(t) - x_1^r(t)\right), \left(\dot{x}_2^r(t) - \dot{x}_1^r(t)\right), \dots, \left(x_{n_2}^r(t) - x_{n_2-1}^r(t)\right), \left(\dot{x}_{n_2}^r(t) - \dot{x}_{n_2-1}^r(t)\right) \end{bmatrix}^T. \tag{13}$$

The new state-space model can be expressed as

$$\dot{Z}(t) = (\mathbf{A} + \Delta\mathbf{A})\mathbf{Z}(t) + (\mathbf{B} + \Delta\mathbf{B})\mathbf{u}(t) + \mathbf{E}\ddot{x}_g(t), \tag{14}$$

where

$$\mathbf{A} = \overline{T}\mathbf{A}_p\overline{T}^{-1},$$
$$\mathbf{B} = \overline{T}\mathbf{B}_p,$$
$$\mathbf{E} = \overline{T}\mathbf{E}_p, \tag{15}$$
$$\Delta\mathbf{A} = \overline{T}\Delta\mathbf{A}_p\overline{T}^{-1},$$
$$\Delta\mathbf{B} = \overline{T}\Delta\mathbf{B}_p.$$

2.2. System Extension.

Consider the following state-space model of a linearly continuous time-invariant system

$$\begin{aligned} \mathbf{S}: \quad &\dot{Z}(t) = (\mathbf{A} + \Delta\mathbf{A})\mathbf{Z}(t) + (\mathbf{B} + \Delta\mathbf{B})\mathbf{u}(t), \\ &\mathbf{y}(t) = \mathbf{C_y}\mathbf{Z}(t), \\ \widetilde{\mathbf{S}}: \quad &\dot{\widetilde{Z}}(t) = (\widetilde{A} + \Delta\widetilde{A})\widetilde{Z}(t) + (\widetilde{B} + \Delta\widetilde{B})\widetilde{u}(t), \\ &\widetilde{y}(t) = \widetilde{C}_y\widetilde{Z}(t), \end{aligned} \tag{16}$$

where $\mathbf{Z}(t) \in \mathbf{R}^n$, $\mathbf{u}(t) \in \mathbf{R}^m$, and $\mathbf{y}(t) \in \mathbf{R}^l$ are the state, input vector, and output vector of the system $\mathbf{S}$, respectively. $\widetilde{Z}(t) \in \mathbf{R}^{\widetilde{n}}$, $\widetilde{u}(t) \in \mathbf{R}^{\widetilde{m}}$, and $\widetilde{y}(t) \in \mathbf{R}^{\widetilde{l}}$ are the state, input vector, and output vector of the system $\widetilde{\mathbf{S}}$, respectively. $\mathbf{A}$, $\mathbf{B}$, $\mathbf{C}_y$ and $\widetilde{A}$, $\widetilde{B}$, and $\widetilde{C}_y$ are $n \times n$, $n \times m$, $l \times n$, $\widetilde{n} \times \widetilde{n}$, $\widetilde{n} \times \widetilde{m}$, and $\widetilde{l} \times \widetilde{n}$ dimensional matrices, respectively. $n \le \widetilde{n}, m \le \widetilde{m}, l \le \widetilde{l}$. Based on the inclusion principle [21], for a linear uncertain system $\mathbf{S}$, a set of extended matrices $\mathbf{V}, \mathbf{R}$, and $\mathbf{T}$, and a set of shrinkage matrices $\mathbf{U}, \mathbf{Q}$, and $\mathbf{S}$, the corresponding extended system $\widetilde{\mathbf{S}}$ can be expressed as follows:

$$\begin{aligned} \widetilde{A} &= \mathbf{V}\mathbf{A}\mathbf{U} + \mathbf{M}, \\ \widetilde{B} &= \mathbf{V}\mathbf{B}\mathbf{Q} + \mathbf{N}, \\ \widetilde{C}_y &= \mathbf{T}\mathbf{C}_y\mathbf{U} + \mathbf{L}, \\ \Delta\widetilde{A} &= \mathbf{V}\Delta\mathbf{A}\mathbf{U}, \\ \Delta\widetilde{B} &= \mathbf{V}\Delta\mathbf{B}\mathbf{Q}, \end{aligned} \tag{17}$$

where $\mathbf{M}, \mathbf{N}$, and $\mathbf{L}$ are the compensation matrices [21, 44].

The system $\mathbf{S}$ is decomposed into L fully decoupled paired subsystems by extending decoupling [21].

$$\widetilde{\mathbf{S}}_D^{(i)}: \quad \dot{\widetilde{Z}}_i(t) = \left(\widetilde{A}_{ii} + \Delta\widetilde{A}_{ii}\right)\widetilde{Z}_i(t) + \left(\widetilde{B}_{ii} + \Delta\widetilde{B}_{ii}\right)\widetilde{u}_i(t),$$
$$\widetilde{y}_i(t) = \left(\widetilde{C}_y\right)_{ii}\widetilde{Z}_i(t), \quad i = 1, 2, \dots, L, \tag{18}$$

where $\widetilde{A}_{ii}$ and $\widetilde{B}_{ii}$ are known constant matrices describing the system model. $\Delta\widetilde{A}_{ii}$ and $\Delta\widetilde{B}_{ii}$ are unknown matrices that represent the parameter uncertainty in the system model. It is assumed that the parameter uncertainty under consideration is norm-bounded and has the following form:

$$\begin{bmatrix} \Delta\widetilde{A}_{ii} & \Delta\widetilde{B}_{ii} \end{bmatrix} = \widetilde{D}_i\widetilde{F}_i(t)\begin{bmatrix} \widetilde{E}_{i1} & \widetilde{E}_{i2} \end{bmatrix}, \tag{19}$$

where $\widetilde{D}_i, \widetilde{E}_{i1}$, and $\widetilde{E}_{i2}$ are matrices of constants, which reflect uncertain structural information, $\widetilde{F}_i(t)$ is an unknown matrix, and $\widetilde{F}_i^T(t)\widetilde{F}_i(t) \le \mathbf{I}$.

2.3. Design of Guaranteed Cost Controller.

It is assumed that system $\widetilde{\mathbf{S}}_D^{(i)}$ meets the quadratic performance metric

$$\widetilde{J}_i\left(\widetilde{Z}_i, \widetilde{u}_i\right) = \int_0^\infty \left[\widetilde{Z}_i^T(t)\widetilde{Q}_i^*\widetilde{Z}_i(t) + \widetilde{u}_i^T(t)\widetilde{R}_i^*\widetilde{u}_i(t)\right]dt, \tag{20}$$

where $\widetilde{Q}_i^*$ and $\widetilde{R}_i^*$ are given symmetric positive definite weighted matrices.

Theorem 1 (see [45]). *For the parameter uncertainty subsystem* $\widetilde{\mathbf{S}}_D^{(i)}$ *and performance index (20), if the following optimization problem*

$$\min_{\widetilde{\varepsilon}_i, \widetilde{Y}_i, \widetilde{X}_i, \widetilde{W}_i} \text{Trace}\left(\widetilde{W}_i\right),$$

$$(i) \quad \begin{bmatrix} \widetilde{A}_{ii}\widetilde{X}_i + \widetilde{B}_{ii}\widetilde{Y}_i + \left(\widetilde{A}_{ii}\widetilde{X}_i + \widetilde{B}_{ii}\widetilde{Y}_i\right)^{\mathrm{T}} + \widetilde{\varepsilon}_i \widetilde{D}_i \widetilde{D}_i^{\mathrm{T}} & \left(\widetilde{E}_{i1}\widetilde{X}_i + \widetilde{E}_{i2}\widetilde{Y}_i\right)^{\mathrm{T}} & \widetilde{X}_i & \widetilde{Y}_i^{\mathrm{T}} \\ \widetilde{E}_{i1}\widetilde{X}_i + \widetilde{E}_{i2}\widetilde{Y}_i & -\widetilde{\varepsilon}_i \mathbf{I} & 0 & 0 \\ \widetilde{X}_i & 0 & -\left(\widetilde{Q}_i^*\right)^{-1} & 0 \\ \widetilde{Y}_i & 0 & 0 & -\left(\widetilde{R}_i^*\right)^{-1} \end{bmatrix} < 0, \quad (21)$$

$$(ii) \begin{bmatrix} \widetilde{W}_i & \mathbf{I} \\ \mathbf{I} & \widetilde{X}_i \end{bmatrix} > 0,$$

has a solution $\left(\widetilde{\varepsilon}_i, \widetilde{Y}_i, \widetilde{X}_i, \widetilde{W}_i\right)$*, then* $\widetilde{u}_i^*(t) = \widetilde{Y}_i \widetilde{X}_i^{-1} \widetilde{Z}_i(t)$ *is the optimal state feedback guaranteed cost control law of the system, where* $\widetilde{\varepsilon}_i$ *denotes a scalar greater than 0.* $\widetilde{X}_i$ *and* $\widetilde{W}_i$ *denote symmetric positive definite matrix,* $\widetilde{Y}_i$ *denotes a matrix of appropriate dimensions. The gain matrix of subsystem decentralized controller is* $\widetilde{G}_i = \widetilde{Y}_i \widetilde{X}_i^{-1}$.

2.4. Contraction of the System. The overlapping decentralized hybrid control method is a design method that combines the passive connected damping units between adjacent buildings with the overlapping decentralized active control systems of each building. For the extended decoupling system $\widetilde{\mathbf{S}}_D^{(i)}, i = (1, 2, \ldots, L)$, the feedback gain matrices $\widetilde{G}_i$ of all subsystems are calculated by using the control algorithm, represented as a block diagonal matrix

$$\widetilde{G} = \text{diag}\left[\widetilde{G}_1, \widetilde{G}_2, \ldots, \widetilde{G}_L\right]. \quad (22)$$

The extension controller $\widetilde{G}$ can be contracted to an overlapping controller based on the contraction principle [21, 44], i.e.,

$$\mathbf{G} = \mathbf{Q}\widetilde{G}\mathbf{V}. \quad (23)$$

3. Example Simulation and Analysis

Taking 4-story and 5-story adjacent buildings (as shown in Figure 2) as an example, the corresponding parameters of the adjacent structures can be seen in reference [46].

The damping matrix is determined according to the Rayleigh damping, and the damping ratio is set to 2%. The damping coefficient of the viscous damper connecting the two structures is $c_d = 6.87 \times 10^6 N \cdot s/m$, and the stiffness coefficient is 0. The linked damper is located between the 4th floor of the two buildings.

Northridge seismic wave is used as external excitation, and its peak value is $3.0\,m/s^2$, duration is 30 s, and sampling step is 0.02 s.

Only structural stiffness variation is taken into account in this calculation example, and the maximum possible variation of stiffness is ±15% [47]. In (9), let $\alpha = \beta = 0$, so $\Delta\mathbf{M} = \Delta\mathbf{C} = \mathbf{0}$ and $\Delta\mathbf{K} = \gamma\,\mathbf{K}$, where $\mathbf{K}$ represents the nominal stiffness matrices and $\gamma = 0.15$ reflects the variation of stiffness matrix, then

$$\Delta\mathbf{A}_p^l = \mathbf{D}_p^l \mathbf{F}_p^l \mathbf{E}_{p1}^l,$$

$$\Delta\mathbf{B}_p^l = \mathbf{0},$$

$$\mathbf{D}_p^l = \begin{bmatrix} \mathbf{0} \\ -\mathbf{M}_L^{-1}\mathbf{K}_L \end{bmatrix}_{2n_1 \times n_1}, \quad (24)$$

$$\mathbf{F}_p^l = \delta[\mathbf{I}]_{2n_1 \times 2n_1},$$

$$\mathbf{E}_{pl}^l = \begin{bmatrix} \mathbf{I} & \mathbf{0} \end{bmatrix}_{n_1 \times 2n_1},$$

δ is an uncertain real scalar, $|\delta| < 1$.

In the same way, we can get $\Delta\mathbf{A}_p^r$, $\Delta\mathbf{B}_p^r$, $\Delta\mathbf{D}_p^r$, $\Delta\mathbf{F}_p^r$, $\Delta\mathbf{E}_{p1}^r$, and $\Delta\mathbf{E}_{p2}^r$.

3.1. Centralized Control. Centralized control adopts the state feedback guaranteed cost control method in Theorem 1 to design the controller for the whole multistructure system. The weighting matrices of the building on the left are $\mathbf{Q}_1^l = 1 \times 10^2 \mathbf{I}_8$ and $\mathbf{R}_1^l = 10^{-10}\mathbf{I}_4$. The weighting matrices of the building on the right are $\mathbf{Q}_1^l = 1 \times 10^2 \mathbf{I}_{10}$ and $\mathbf{R}_1^l = 10^{-10}\mathbf{I}_5$.

$\mathbf{G}^l$ and $\mathbf{G}^r$ can be obtained by solving inequality (21); then, the gain matrix of the whole multistructure structure system can be expressed as $\mathbf{G} = \text{diag}\left\{\mathbf{G}^l, \mathbf{G}^r\right\}$.

3.2. Overlapping Decentralized Control. The inclusion principle is applied to perform overlapping decomposition of the adjacent buildings, and then controller design is carried out, as shown in Figure 3. Extended decoupling of the two buildings separately: system $\widetilde{S}_1^l = [1, 2, 3]$, system $\widetilde{S}_2^l = [3, 4]$, system $\widetilde{S}_1^r = [1, 2, 3]$, and system $\widetilde{S}_2^r = [3, 4, 5]$. The overlapping layers are all set at the third layer of the structure. The state-space model of the subsystem can be expressed in the form of equation (18).
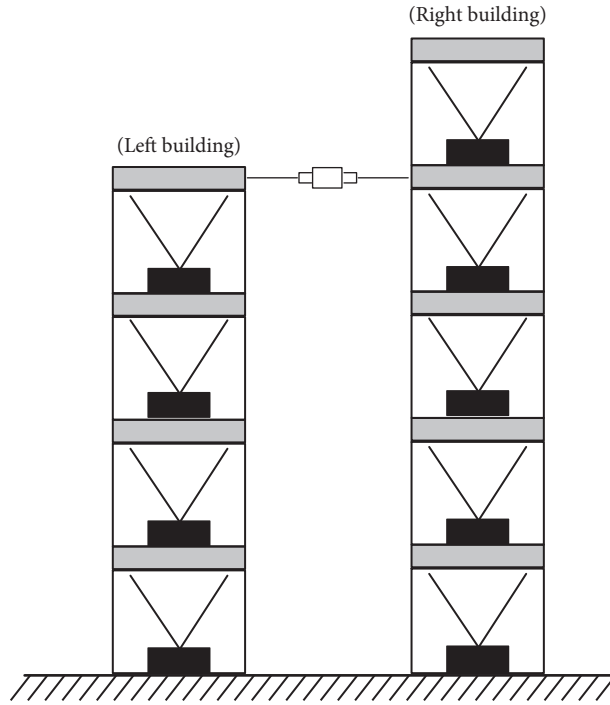
Figure 2: The model of 4-story and 5-story adjacent buildings.
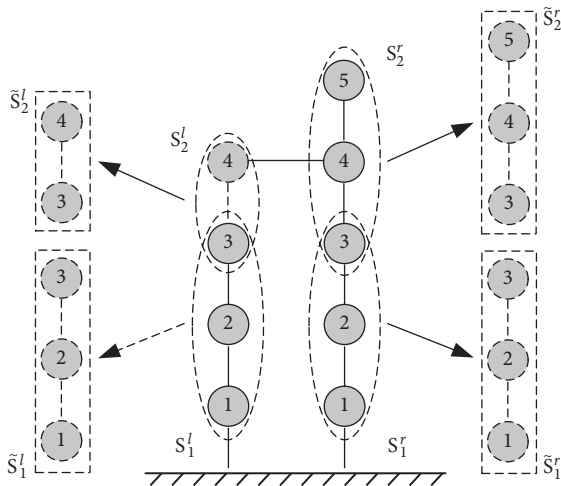
Figure 3: The design of overlapping decentralized controller.

Through the trial, the weighted matrices of the system $\widetilde{S}_1^l$ and $\widetilde{S}_2^l$ are $(\widetilde{Q}_1^l)^* = 1.0 \times 10^2 \mathbf{I}_6$, $(\widetilde{R}_1^l)^* = 10^{-10}\mathbf{I}_3$, $(\widetilde{Q}_2^l)^* = 1.0 \times 10^2 \mathbf{I}_4$, and $(\widetilde{R}_2^l)^* = 10^{-10}\mathbf{I}_2$; the weighted matrices of the system $\widetilde{S}_1^r$ and $\widetilde{S}_2^r$ are $(\widetilde{Q}_1^r)^* = 8.0 \times 10^2 \mathbf{I}_6$, $(\widetilde{R}_1^r)^* = 10^{-10}\mathbf{I}_3$, $(\widetilde{Q}_2^r)^* = 1.0 \times 10^2 \mathbf{I}_6$, and $(\widetilde{R}_2^r)^* = 10^{-10}\mathbf{I}_3$. Solving the linear matrix inequality (LMI) according to Theorem 1, we can get $\widetilde{\varepsilon}_i^l$, $\widetilde{Y}_i^l$, $\widetilde{X}_i^l$, $\widetilde{W}_i^l$ and $\widetilde{\varepsilon}_i^r$, $\widetilde{Y}_i^r$, $\widetilde{X}_i^r$, $\widetilde{W}_i^r$. The

gain matrices of the building subsystem on the left are $\widetilde{G}_1^l = \widetilde{Y}_1^l(\widetilde{X}_1^l)^{-1}$ and $\widetilde{G}_2^l = \widetilde{Y}_2^l(\widetilde{X}_2^l)^{-1}$. The gain matrices of the building subsystem on the right are $\widetilde{G}_1^r = \widetilde{Y}_1^r(\widetilde{X}_1^r)^{-1}$ and $\widetilde{G}_2^r = \widetilde{Y}_2^r(\widetilde{X}_2^r)^{-1}$.

The gain matrices of the system $\widetilde{S}^l$ and $\widetilde{S}^r$ are expressed as block diagonal matrix, so $\widetilde{G}^l = \text{diag}\{\widetilde{G}_1^l, \widetilde{G}_2^l\}$ and $\widetilde{G}^r = \text{diag}\{\widetilde{G}_1^r, \widetilde{G}_2^r\}$. The gain matrices of the original system $\mathbf{S}^l$ and $\mathbf{S}^r$ are obtained according to the contraction principle, so $\mathbf{G}^l = \mathbf{Q}^l\widetilde{G}^l\mathbf{V}^l$ and $\mathbf{G}^r = \mathbf{Q}^r\widetilde{G}^r\mathbf{V}^r$; then, the gain matrix of the entire multistructure system can be expressed as $\mathbf{G} = \text{diag}\{\mathbf{G}^l, \mathbf{G}^r\}$.

3.3. Analysis of Calculation Results.

Figures 4–6 show the peak interlayer displacement of adjacent buildings with uncertain parameters.

It can be seen from the figure that, for the building on the left, (1) when $\Delta K = 0$, the average control effect of centralized guaranteed cost hybrid control method (CHC) is 66.94%, and the average control effect of overlapping decentralized guaranteed cost hybrid control approach (ODHC) is 74.68%; (2) when $\Delta K = +0.15\,\mathrm{K}$, the average control effect of centralized guaranteed cost control method is 66.58%, and the average control effect of overlapping decentralized guaranteed cost hybrid control approach is 72.33%; and (3) when $\Delta K = -0.15\,\mathrm{K}$, the average control effect of centralized guaranteed cost control method is 65.88%, and the average
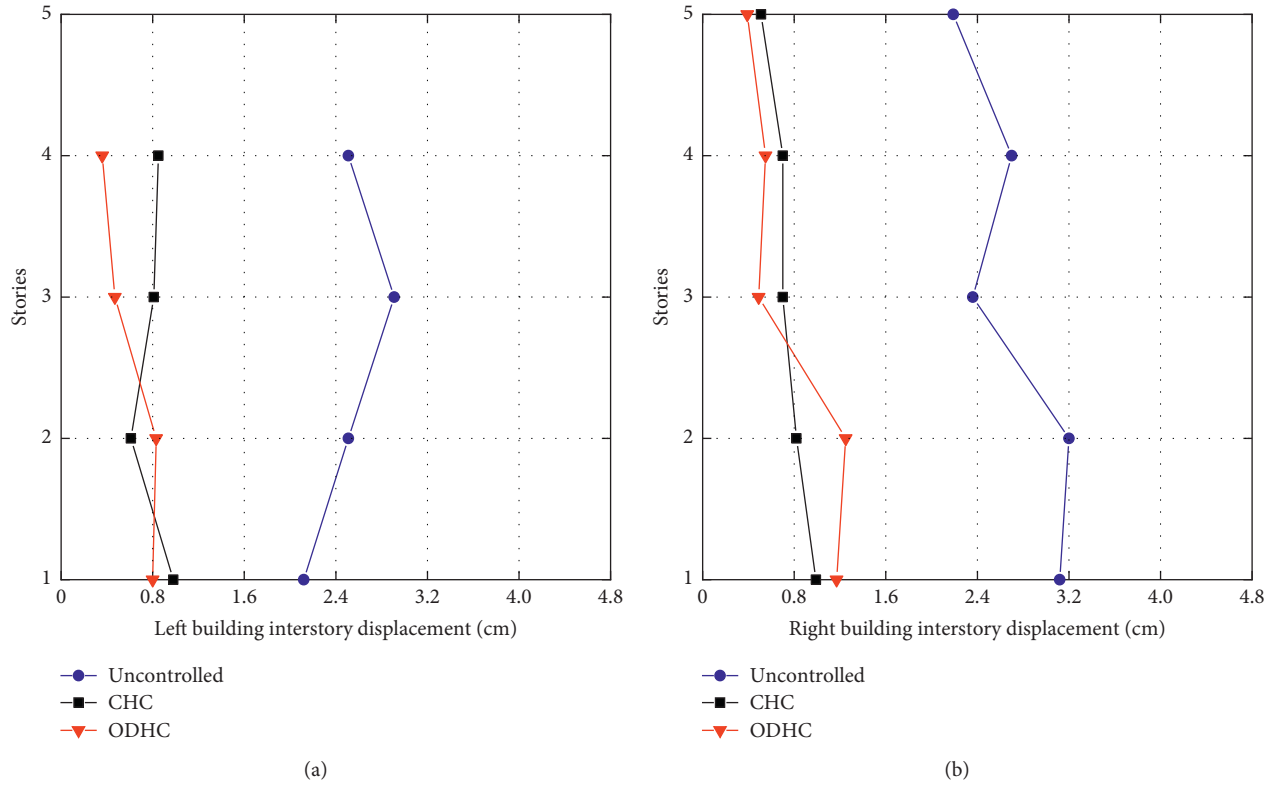
FIGURE 4: The peak interstory displacement ($\Delta K = 0$): (a) the left building; (b) the right building.
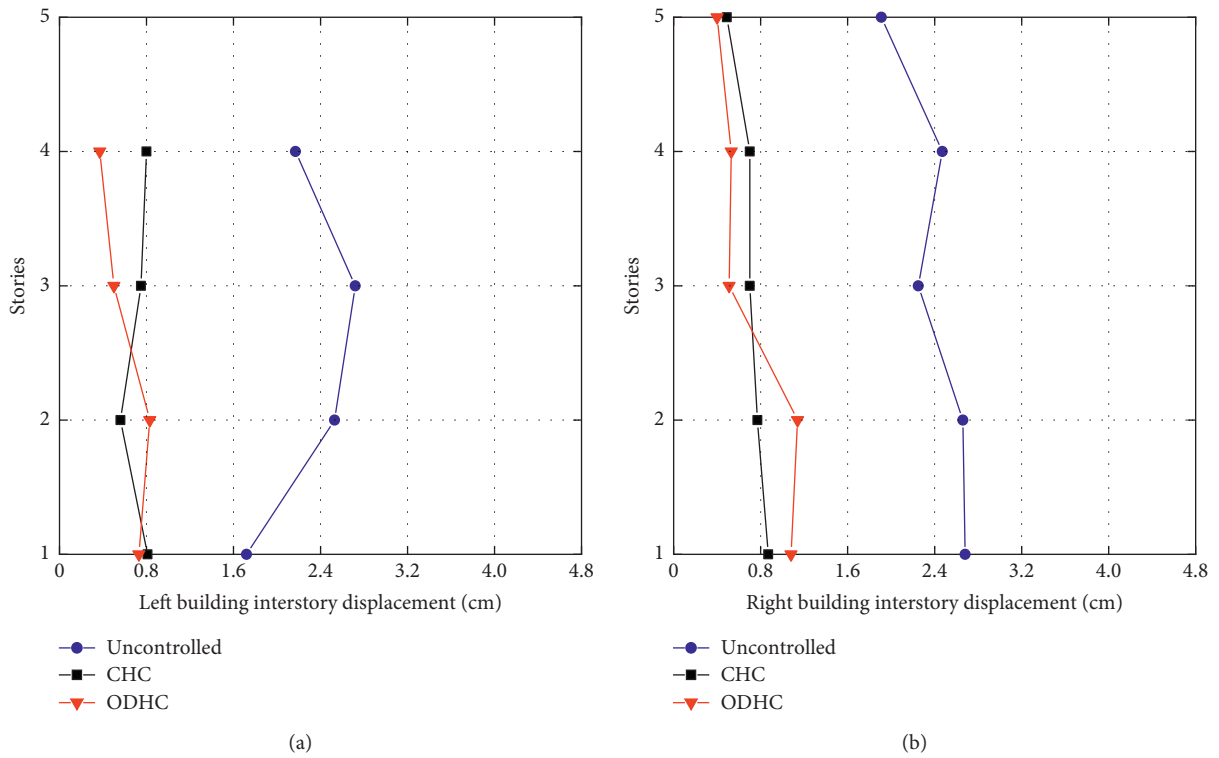
FIGURE 5: The peak interstory displacement ($\Delta K = +0.15\,K$): (a) the left building; (b) the right building.
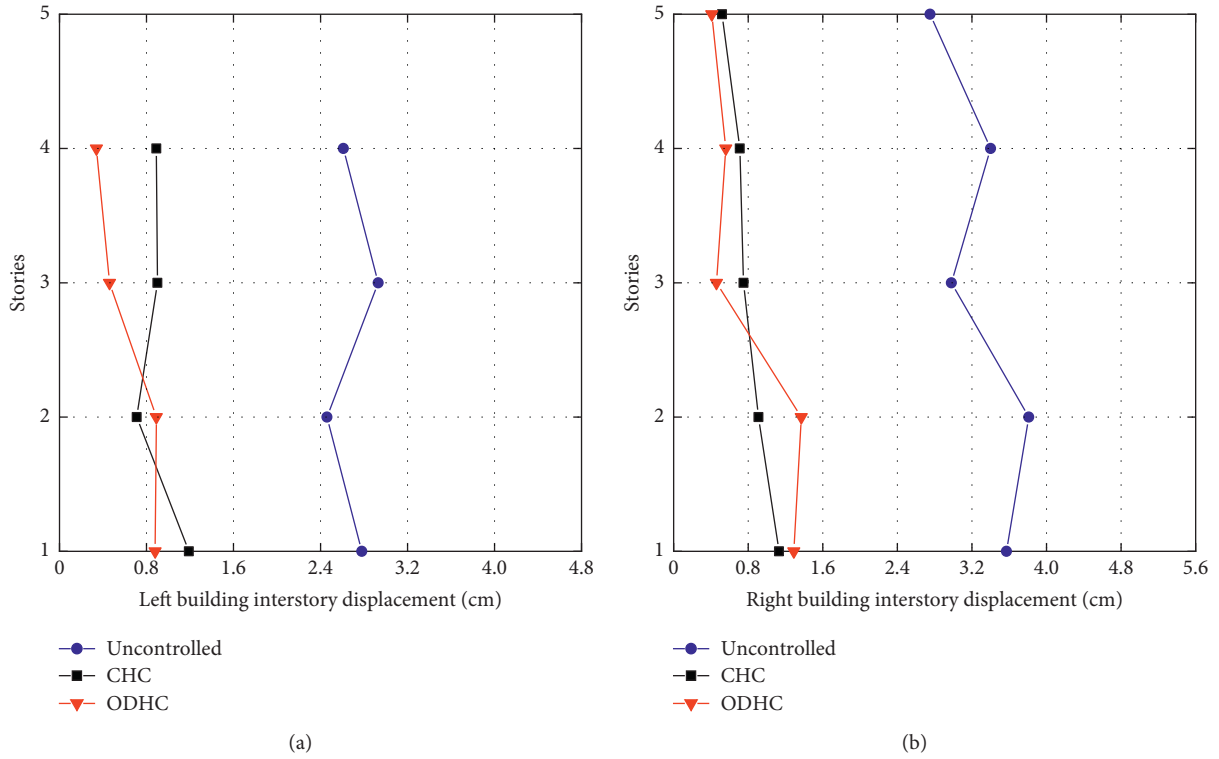
Figure 6: The peak interstory displacement ($\Delta K = -0.15\,K$): (a) the left building; (b) the right building.
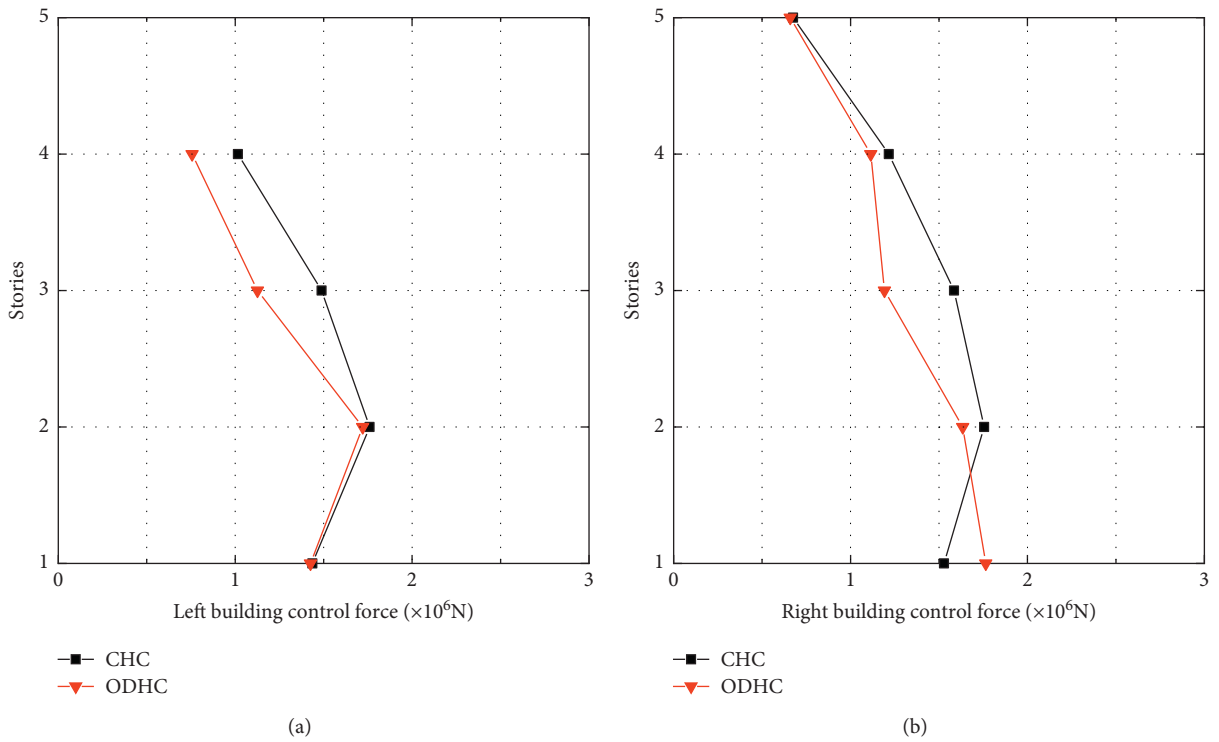
Figure 7: Maximum control forces ($\Delta K = 0$): (a) the left building; (b) the right building.

(a)

(b)
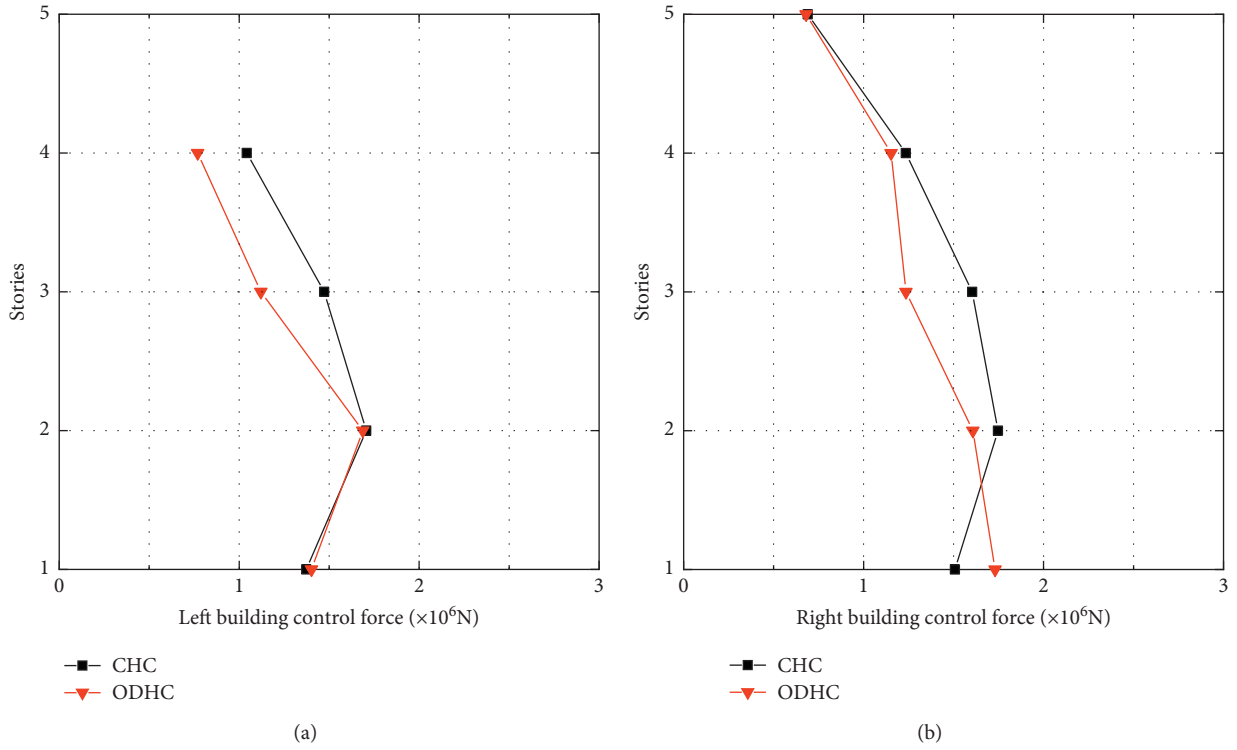
Figure 8: Maximum control forces ($\Delta K = +0.15\,K$): (a) the left building; (b) the right building.

(a)

(b)
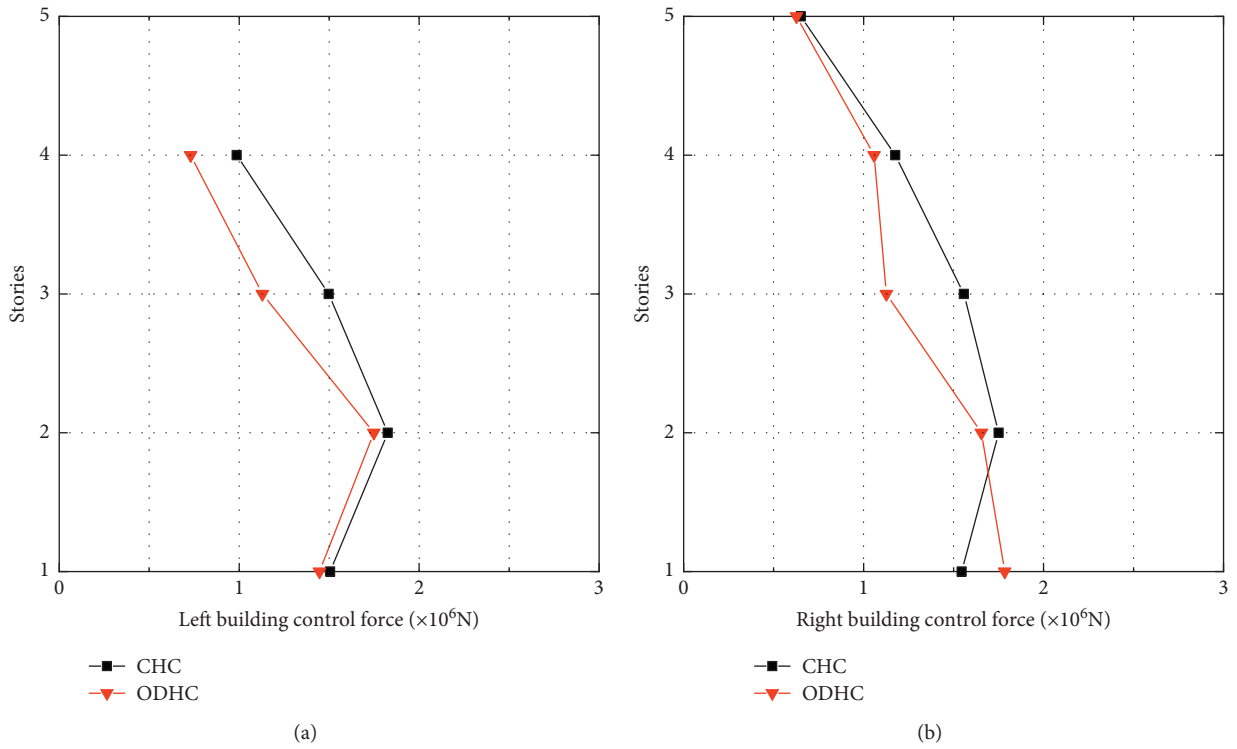
Figure 9: Maximum control forces ($\Delta K = -0.15\,K$): (a) the left building; (b) the right building.

(a)

(b)
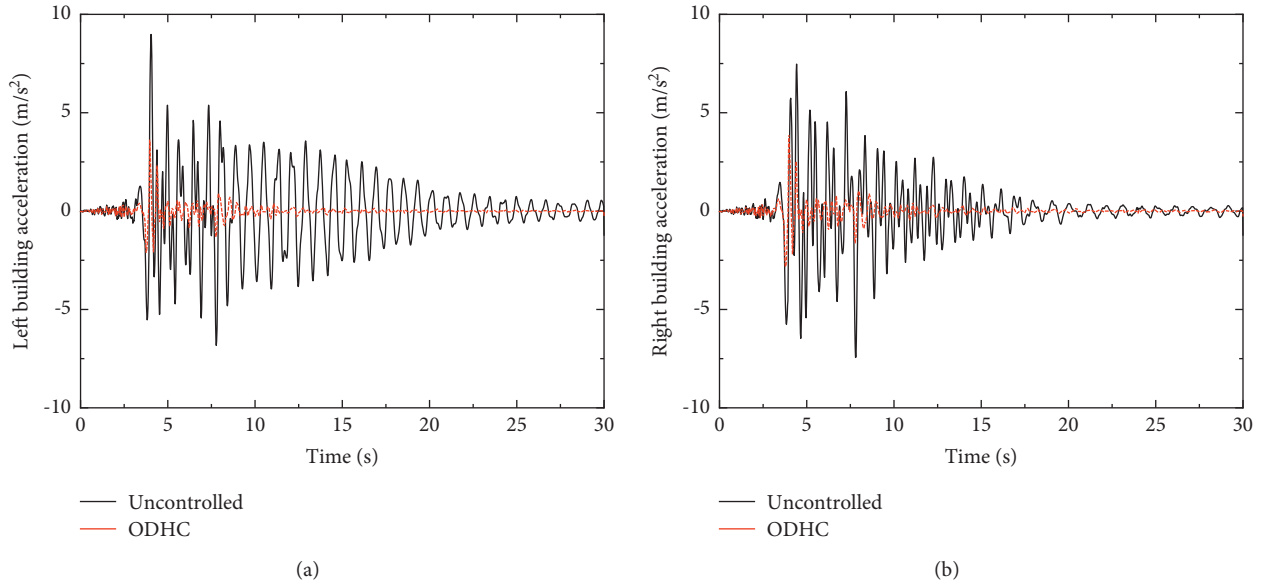
FIGURE 10: Acceleration time-history curves of the top floor ($\Delta K = 0$): (a) the left building; (b) the right building.

(a)

(b)
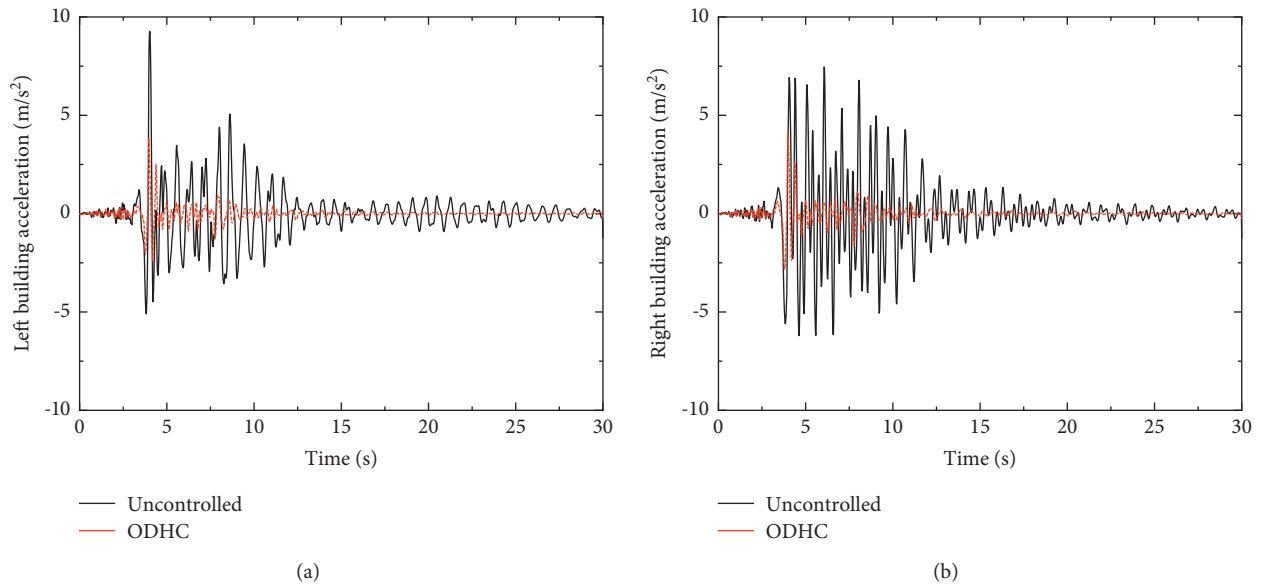
FIGURE 11: Acceleration time-history curves of the top floor ($\Delta K = +0.15\,K$): (a) the left building; (b) the right building.

control effect of overlapping decentralized guaranteed cost hybrid control approach is 75.86%.

For the building on the right, (1) when $\Delta K = 0$, the average control effect of centralized guaranteed cost control method is 72.75%, and the average control effect of overlapping decentralized guaranteed cost hybrid control approach is 72.90%; (2) when $\Delta K = +0.15\,K$, the average control effect of centralized guaranteed cost control method is 70.70%, and the average control effect of overlapping decentralized guaranteed cost hybrid control approach is 70.36%; and (3) when $\Delta K = -0.15\,K$, the average control effect of centralized guaranteed cost control method is 75.90%, and

the average control effect of overlapping decentralized guaranteed cost hybrid control approach is 76.22%.

Figures 7–12 show the maximum control force and acceleration response of uncertain adjacent building systems under seismic excitation. From Figures 7–9, it can be seen that the maximum control force of the ODHC method is not much different from that of the CHC method.

It can be seen from Figures 10–12 that the ODHC method can still effectively control the acceleration response of the structure in the case of variation of structural parameters, which illustrates the effectiveness of the ODHC method proposed in this paper.

(a)

(b)
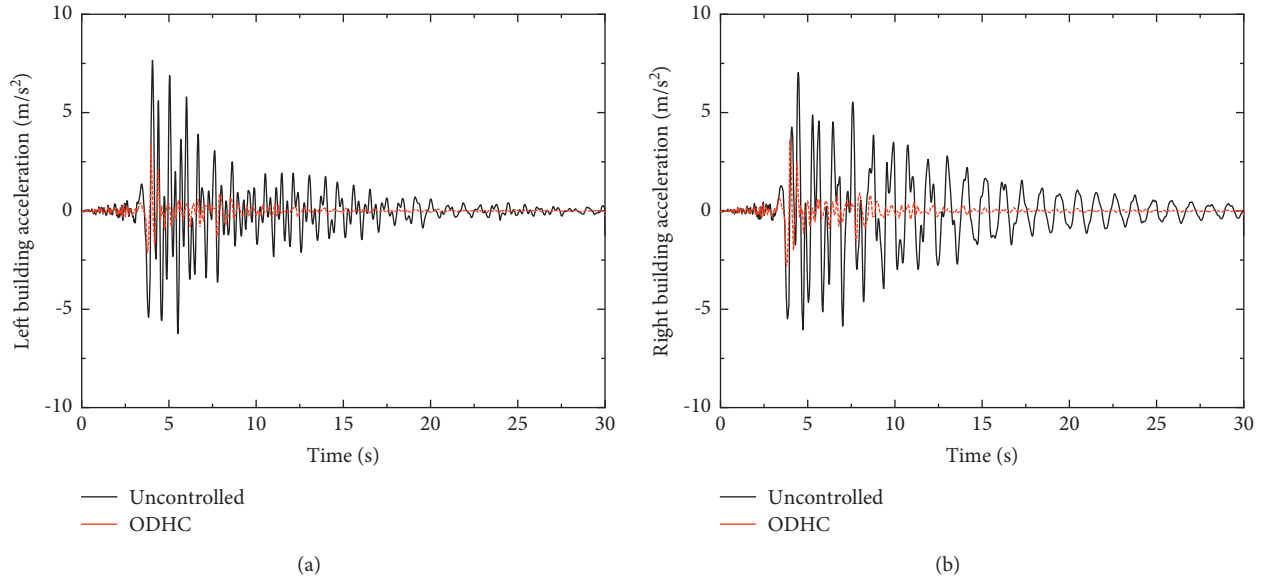
Figure 12: Acceleration time-history curves of the top floor ($\Delta K = -0.15\,K$): (a) the left building; (b) the right building.

4. Conclusions

In this paper, a new scheme to solve the problem of structural vibration control for adjacent buildings with uncertain parameters has been proposed. The pilot studies in exploring overlapping decentralized guaranteed cost hybrid control design, which integrates the high performance of active control system with the reliability of the passive control system, while allowing the decentralized design and operation of the active control subsystem, that combines the overlapping decentralized control strategy and the guaranteed cost control algorithm via LMI are carried out. The main findings are summarized as follows:

(1) The centralized control strategy can effectively analyze the structural vibration control problem, while the overlapping decentralized control strategy provides a new idea. The LMI is used as a tool that makes the design of the guaranteed cost controller easier to solve. Numerical simulation results using uncertain parameters for 4-story and 5-story adjacent buildings illustrate the feasibility of the proposed control approach, which can still effectively reduce the seismic response of a multistructure system when the structural parameters are uncertain.

(2) A comparison of performance between the overlapping decentralized guaranteed cost controllers and the centralized guaranteed cost controllers indicates that both controllers deliver the expected effect. Meanwhile, the proposed control method in this paper can improve the sampling rate and data transmission speed to ensure the reliability of the adjacent system.

(3) The overlapping decentralized control design, which overcomes the disadvantages of traditional centralized control strategies such as large computation, low reliability, and poor stability, offers promising solutions to complex structural systems.

Data Availability

The data used to support the study are available from the corresponding authors upon request.

Conflicts of Interest

The authors declare that there are no conflicts of interest regarding the publication of this paper.

Acknowledgments

References

[1] K. Kasai, V. Jeng, P. C. Patel, J. A. MunShi, and B. F. Maison, "Seismic pounding effects-survey and analysis," in *Proceedings of the 10th World Conference on Earthquake Engineering*, pp. 3893–3898, Madrid, Spain, July 1992.

[2] K. Kasai and B. F. Maison, "Building pounding damage during the 1989 Loma Prieta earthquake," *Engineering Structures*, vol. 19, no. 3, pp. 195–207, 1997.

[3] Z. Wang, "A preliminary report on the great wenchuan earthquake," *Engineering and Engineering Vibration*, vol. 7, no. 2, pp. 225–234, 2008.

[4] Y. Q. Yang, J. W. Dai, M. S. Gong, and L. L. Xie, "Investigation and analysis on adjacent buildings pounding damage in Lushan earthquake," *Journal of Harbin Institute of Technology*, vol. 47, no. 12, pp. 102–105, 2015, (in Chinese).

[5] G. L. Cole, R. P. Dhakal, F. M. Turner, and F. M. Turner, "Building pounding damage observed in the 2011 Christchurch earthquake," *Earthquake Engineering & Structural Dynamics*, vol. 41, no. 5, pp. 893–913, 2012.

[6] F. Palacios-Quiñonero, J. M. Rossel, J. Rubió-Massegú, and H. R. Karimi, "Structural vibration control for a class of connected multistructure mechanical systems," *Mathematical Problems in Engineering*, vol. 2012, Article ID 942910, 23 pages, 2012.

[7] F. Palacios-Quinonero, J. M. Rossel, J. Rodellar, and H. R. Karimi, "Active-passive control strategy for adjacent buildings," in *Proceedings of the American Control Conference (ACC)*, pp. 3110–3115, San Francisco, CA, USA, July 2011.

[8] R. E. Christenson, B. F. Spencer, and E. A. Johnson, "Semi-active connected control method for adjacent multidegree-of-freedom buildings," *Journal of Engineering Mechanics*, vol. 133, no. 3, pp. 290–298, 2007.

[9] H. Roh, G. P. Cimellaro, and D. Lopez-Garcia, "Seismic response of adjacent steel structures connected by passive device," *Advances in Structural Engineering*, vol. 14, no. 3, pp. 499–517, 2011.

[10] C. C. Patel and R. S. Jangid, "Seismic response of dynamically similar adjacent structures connected with viscous dampers," *The IES Journal Part A: Civil & Structural Engineering*, vol. 3, no. 1, pp. 1–13, 2010.

[11] G. P. Cimellaro and D. Lopez-Garcia, "Algorithm for design of controlled motion of adjacent structures," *Structural Control and Health Monitoring*, vol. 18, no. 2, pp. 140–148, 2011.

[12] G. B. Motra, W. Mallik, and N. K. Chandiramani, "Semi-active vibration control of connected buildings using magnetorheological dampers," *Journal of Intelligent Material Systems and Structures*, vol. 22, no. 16, pp. 1811–1827, 2011.

[13] K. Bigdeli, W. Hare, and S. Tesfamariam, "Configuration optimization of dampers for adjacent buildings under seismic excitations," *Engineering Optimization*, vol. 44, no. 12, pp. 1491–1509, 2012.

[14] K. Bigdeli, W. Hare, J. Nutini, and S. Tesfamariam, "Optimizing damper connectors for adjacent buildings," *Optimization and Engineering*, vol. 17, no. 1, pp. 47–75, 2016.

[15] H. J. Gao, X. B. Yang, W. Zhan, and H. R. Karimi, "Actuators and sensors allocation for adjacent buildings vibration control," in *Proceedings of the 38th Annual Conference on IEEE Industrial Electronics Society*, pp. 4821–4826, Montreal, QC, USA, October 2012.

[16] M. Gudarzi and H. Zamanian, "Application of active vibration control for earthquake protection of multi-structural buildings," *International Journal of Scientific Research in Knowledge*, vol. 1, no. 11, pp. 502–513, 2013.

[17] Z. Yang and E. S. S. Lam, "Dynamic responses of two buildings connected by viscoelastic dampers under bidirectional earthquake excitations," *Earthquake Engineering and Engineering Vibration*, vol. 13, no. 1, pp. 137–150, 2014.

[18] M. E. Uz and M. N. S. Hadi, "Optimal design of semi active control for adjacent buildings connected by MR damper based on integrated fuzzy logic and multi-objective genetic algorithm," *Engineering Structures*, vol. 69, pp. 135–148, 2014.

[19] R. Yuan, H. Q. Li, and Q. U. Wang, "An enhanced genetic algorithm–based multi-objective design optimization strategy," *Advances in Mechanical Engineering*, vol. 10, no. 7, pp. 1–6, 2018.

[20] X. F. Kang, J. G. Wang, and Q. Wang, "Study on the building structural overlapping decentralized control based on energy-to-peak control algorithm," *Chinese Journal of Applied Mechanics*, vol. 32, no. 6, pp. 9 55–961, 2015, (in Chinese).

[21] F. Palacios-Quiñonero, J. M. Rossell, and H. R. Karimi, "Semi-decentralized strategies in structural vibration control," *Modeling Identification and Control*, vol. 32, no. 2, pp. 57–77, 2011.

[22] Q. Wang, J. L. Zhuang, J. Zhang, and J. G. Wang, "Overlapping decentralized control of tall buildings under earthquakes," *Chinese Journal of Computational Mechanics*, vol. 32, no. 1, pp. 48–52, 2015, (in Chinese).

[23] R. Yuan and H. Q. Li, "A multidisciplinary coupling relationship coordination algorithm using the hierarchical control methods of complex systems and its application in multidisciplinary design optimization," *Advances in Mechanical Engineering*, vol. 9, no. 1, pp. 1–11, 2017.

[24] H. R. Karimi, F. Palacios-Quiñonero, J. M. Rossell, and J. Rubió-Massegú, "Sequential design of multioverlapping controllers for structural vibration control of tall buildings under seismic excitation," *Proceedings of the Institution of Mechanical Engineers - Part I: Journal of Systems & Control Engineering*, vol. 227, no. 2, pp. 176–183, 2013.

[25] F. Palacios-Quiñonero, J. Rodellar Benedé, J. M. Rossell Garriga, and J. Rubió-Massegú, "Control strategies for large-scale structural systems: high-raise buildings and multi-building systems," in *Proceedings of the Workshop on Control, Dynamics, Monitoring and Applications*, pp. 40–56, Barcelona, Spain, February 2011.

[26] H. Li, R. Yuan, and J. Fu, "A reliability modeling for multi-component systems considering random shocks and multi-state degradation," *IEEE Access*, vol. 7, pp. 168805–168814, 2019.

[27] P. P. Zhi, Y. Xu, and B. Z. Chen, "Time-dependent reliability analysis of the motor hanger for EMU based on stochastic process," *International Journal of Structural Integrity*, vol. 11, no. 3, pp. 453–469, 2020.

[28] R. Yuan, H. Q. Li, Z. C. Gong, M. Z. Tang, and W. Li, "An enhanced Monte Carlo simulation–based design and optimization method and its application in the speed reducer design," *Advances in Mechanical Engineering*, vol. 9, no. 9, pp. 1–7, 2017.

[29] R. Yuan, H. Q. Li, and Q. U. Wang, "Simulation-based design and optimization and fatigue characteristics for high-speed backplane connector," *Advances in Mechanical Engineering*, vol. 11, no. 6, pp. 1–10, 2019.

[30] L. Abdullah, S. S. Karam Singh, A. H. Azman, S. Abdullah, A. K. A. Mohd Ihsan, and Y. S. Kong, "Fatigue life-based reliability assessment of a heavy vehicle leaf spring," *International Journal of Structural Integrity*, vol. 10, no. 5, pp. 726–736, 2019.

[31] R. Manouchehry Nya, S. Abdullah, and S. Singh Karam Singh, "Reliability-based fatigue life of vehicle spring under random loading," *International Journal of Structural Integrity*, vol. 10, no. 5, pp. 737–748, 2019.

[32] A. A. Abd Rahim, S. Abdullah, S. Singh Karam Singh, and M. Z. Nuawi, "Reliability assessment on automobile suspension system using wavelet analysis," *International journal of structural integrity*, vol. 10, no. 5, pp. 602–611, 2019.

[33] R. Yuan, M. Tang, H. Wang, and H. Li, "A reliability analysis method of accelerated performance degradation based on Bayesian strategy," *IEEE Access*, vol. 7, pp. 169047–169054, 2019.

[34] M. Nahal and R. Khelif, "A finite element model for estimating time-dependent reliability of a corroded pipeline elbow," *International Journal of Structural Integrity*, vol. 12, no. 2, pp. 306–321, 2021.

[35] Y.-J. Yang, G. Wang, Q. Zhong, H. Zhang, J. He, and H. Chen, "Reliability analysis of gas pipeline with corrosion defect based on finite element method," *International Journal of Structural Integrity*, vol. 12, no. 6, pp. 854–863, 2021.

[36] S. Chang and T. Peng, "Adaptive guaranteed cost control of systems with uncertain parameters," *IEEE Transactions on Automatic Control*, vol. 17, no. 4, pp. 474–483, 1972.

[37] L. Bakule, J. Rodellar, and J. M. Rossell, "Robust overlapping guaranteed cost control of uncertain state-delay discrete-time systems," *IEEE Transactions on Automatic Control*, vol. 51, no. 12, pp. 1943–1950, 2006.

[38] L. Bakule and J. M. Rossell, "Overlapping controllers for uncertain delay continuous-time systems," *Kybernetika*, vol. 44, no. 1, pp. 17–34, 2008.

[39] X. Nian, Z. Sun, H. Wang, H. Zhang, and X. Wang, "Bilinear matrix inequality approaches to robust guaranteed cost control for uncertain discrete-time delay system," *Optimal Control Applications and Methods*, vol. 34, no. 4, pp. 433–441, 2013.

[40] X. Zhou, T. Dong, X. Tang, C. Yang, and W. Gui, "A BMI approach to guaranteed cost control of discrete-time uncertain system with both state and input delays," *Optimal Control Applications and Methods*, vol. 36, no. 6, pp. 844–852, 2015.

[41] E. Gyurkovics and T. Takacs, "Guaranteed cost for uncertain discrete-time delay systems," *Control Applications of Optimization*, vol. 15, no. 1, pp. 106–111, 2012.

[42] A. Ahmadi, M. Aldeen, and M. Abdolmaleki, "Robust overlapping output feedback control design in uncertain systems with unknown uncertainty bounds," in *Proceedings of the 5th Australian Control Conference (AUCC)*, pp. 69–74, Gold Coast, Australia, November 2015.

[43] S. J. Kim and J. W. Choi, "Parametric uncertainty in controlling the vibration of a building," in *Proceedings of the 39th SICE Annual Conference*, pp. 107–122, Iizuka, Japan, July 2000.

[44] X.-B. Chen, W.-B. Xu, T.-Y. Huang, X.-Y. Ouyang, and S. S. Stankovic, "Pair-wise decomposition and coordinated control of complex systems," *Information Sciences*, vol. 185, no. 1, pp. 78–99, 2012.

[45] L. Yu, *Robust Control, Linear Matrix Inequality Approach*, Tsinghua University Press, Beijing, China, (in Chinese), 2002.

[46] F. Palacios-Quiñonero, J. Rubió-Massegú, J. M. Rossell, and H. R. Karimi, "Vibration control for adjacent structures using local state information," *Mechatronics*, vol. 24, no. 4, pp. 336–344, 2014.

[47] V. B. Patil and R. S. Jangid, "Optimum multiple tuned mass dampers for the wind excited benchmark building/optimalūs masės slopintuvai vėjo veikiamuose aukštybiniuose pastatuose," *Journal of Civil Engineering and Management*, vol. 17, no. 4, pp. 540–557, 2011.

Research Article

The Optimization of Automated Container Terminal Scheduling Based on Proportional Fair Priority

Yiqin Lu (ID)

School of Economics and Management, Shanghai University of Electric Power, Shanghai, China

Correspondence should be addressed to Yiqin Lu; lu_yiqin@163.com

With the goal of maximizing the efficiency of automated container terminals, taking the loading and unloading time as the research object, the integrated optimization of automated container terminal scheduling with proportional fair priority is established by setting the priority parameters under the premise of balancing the operation efficiency of each container ship at the berth. The model considers separate assignments of general containers and special containers in the actual operation at the automated container terminal, which is never considered in other literatures. A proportional fairness algorithm (PFA) is designed to solve the problem, taking the maximum of the ratio of quantities of remaining loading and unloading containers of each container ship to the distance of empty AGVs/YTs as the proportional fair priority. The priority of all current tasks is ranked, and the highest priority task is fulfilled first. Different from the published literature, the study of this paper can be presented in two aspects. One is in the modeling. This includes (i) formalizing the description of the purpose of the model and (ii) conducting a real-world coordination of four types of equipment that incorporate at automated container terminals which considers different operations between general goods and special goods in the actual automated terminal operations. The other is that PFA is applied to deal with the integrated scheduling whose results are better with the balance of efficiency and fairness.

1. Introduction and Literature Review

As the largest automated container terminal in the world with the most advanced automatic technology, the highest level of intelligence, and zero green emissions, Shanghai Yangshan Automated Terminal adopts the automated terminal production control system and has been ranked the No. 1 in the world since 2010. The berthing time at the automated terminal of a container ship is determined directly by the loading and unloading efficiency of the automated terminal equipment. Thus, the research of the integrated scheduling of automated terminal equipment is of a great significance to improve terminal efficiency. The operation equipment at automated container terminal includes Quay Cranes (QCs), Automatic Guide Vehicles (AGVs), Automatic Stacking Cranes (ASCs), and Yard Trucks (YTs).

At present, domestic and foreign scholars have less research on the scheduling problem of automated container

terminal equipment. Studies on the optimization of terminal operations are mainly focused on the following two aspects.

The first one is about the research on the optimization of traditional container terminal scheduling. Previous studies have mostly focused on the optimization of traditional container terminals, which also has a good reference for this paper. In traditional research, there were many studies on scheduling of common container terminals, most of which concentrated on the operation of QCs, YTs, and Yard Cranes (YCs) separately. Studies of isolated scheduling mainly covered distribution and scheduling of QCs [1–3], YC allocation and work sequences [4, 5], and scheduling and path optimization of YTs [6, 7]. The joint optimization models were established for only two types of loading and unloading equipment including joint optimization of QCs-YTs [8], QCs-YCs [9, 10], and YT-YCs [11, 12]. In addition, since these three operations affected each other, the three-stage integrated optimization of the operation system was the most effective means to improve efficiency from the

perspective of system optimization [13]; Chen et al. [14], which was rare in previous literatures. When designing complex mechanical equipment, uncertainties should be considered to enhance the reliability of performance [15]. There are also many studies on optimization. Li et al. [16] realized the multiobjective optimization with a Modified Nondominated Sorting Genetic Algorithm III. A method of fuzzy optimization design-based multilevel response surface was proposed in a structural optimization design-based single-level response surface [17]. Finite element analyses are carried out, and the optimization scheme that minimizes the quality under the condition of satisfying the allowable stress is found [18].

The second aspect is about the research on optimization of the automated terminal operation system. Recent research on automated terminal horizontal transportation was mostly concentrated on the scheduling of AGVs [19–22]. The research on joint scheduling optimization of two kinds of operations includes joint scheduling of QC-AGV [23, 24] and joint scheduling of AGV-ASC [25]. To solve the cooperative scheduling of AGV-YC, the completing time under different conditions was obtained with the changes of AGVs, QCs, and container areas [25]. The abovementioned joint scheduling optimization limited to one or two types of equipment can only achieve optimal scheduling of the partial system rather than that of the entire system. As there are conflicts among the optimization objectives of the QCs-AGVs-ASCs, only a few scholars have conducted relevant research on the optimization of the overall operation system of the automated container terminal scheduling. In order to realize the optimal scheduling of the whole system, Le and Zhang [26] proposed a new joint scheduling model of QCs, AGVs, and stacking cranes, which took the whole transportation system of the automated container terminal as the research object. Zeng and Yang [27] considered the cooperation problem of terminal transportation equipment and designed a multistage optimization algorithm. Hu and Hu [28] studied the coordinated scheduling mechanism among the three devices, proposed the full-degree-of-freedom scheduling problem of integrated shore bridges, stacking cranes, and YTs, and established a mixed integer programming model, but AGV was not considered in this study. Dkhil et al. [29] proposed the QC-AGV-ASC integrated model considering the interaction and constraints among various resources of the terminals. The above literatures showed that there were only a few studies on integrated scheduling of the automated container terminal scheduling. However, studies of the loading and unloading equipment and technology mentioned above are not mature enough and do not consider different operations between general goods and special goods which exist in the actual automated terminal operations. Since AGVs cannot transport ultralong, ultrawide, and dangerous containers, these two types of special containers are transported to special yards by the queued YTs at the berth. Therefore, the integrated optimization of scheduling at automated container terminals discussed in this paper will be more comprehensive, containing not only QCs, AGVs, and ASCs but also YTs, which is never considered in other literatures.

Based on the previous research [30, 31], the innovations of this paper are as follows: One is in the modeling. This includes (i) formalizing the description of the purpose of the model. The objective is to reduce the total operating time of all seaside ships while considering the operation time control of each ship; (ii Conducting a real-world coordination with proportional fair priority of four types of equipment that incorporate at automated container terminals which considers different operations between general goods and special goods. AGVs and YTs transport standard containers and special containers, respectively, and the operation difference between AGVs and YTs at the seaside is performed by double-trolley QCs. The other is that PFA is applied to deal with the integrated problem whose results are better with the balance of efficiency and fairness. Comparing with the Greedy Algorithm (GA), which is commonly used in optimization problems, PFA improves the overall efficiency by 5%, and the fairness of loading and unloading time of each container ship is also greatly improved.

The paper is organized as follows. The problems are described and formulated in Section 2 and Section 3, respectively, and the model is proposed in Section 3. Section 4 presents the proportional fairness algorithm. Numerical experiments and results analysis are shown in Section 5 followed by conclusions in Section 6.

2. Problem Description and Assumptions

Usually, the automated production control system is adopted as the "brain" to control the automatic operation system of the loading and unloading equipment, which consists of three types of loading and unloading equipment, namely, Quay Cranes, Automatic Guide Cranes, and Automatic Stacking Cranes. Figure 1 shows the single-container operation process at the automated terminal. The loading and unloading operation is completed by the double-trolley QCs. The main trolley is controlled remotely, and the portal trolley works automatically. They interact through the transfer platform. The horizontal transportation is finished by AGVs. The assignment of the yard is operated by ASCs which are fully automated. Three types of equipment work together. The seaside ASCs can complete double-container operation. The YTs enter the berth, arriving at the designed container area. The land-side ASCs complete the unloading operation and go to the container yard. The export operation is carried out by the seaside ASCs. After the AGVs get the containers, they go to the bottom of the QCs. The automatic portal trolley hoists the containers to the transfer platform. The main trolley lifts the containers for loading and unloading operation. Thus, the entire export operation is completed. The import operation is the opposite operation process.

This paper takes the loading and unloading operation as the research object, adopts the principle of efficiency priority with consideration to fairness, and balances the containers to be transported of each ship as the constraint condition. A scheduling scheme to maximize the operational efficiency of the automated terminal is established by setting the priority parameters. In the integrated optimization model, QCs,
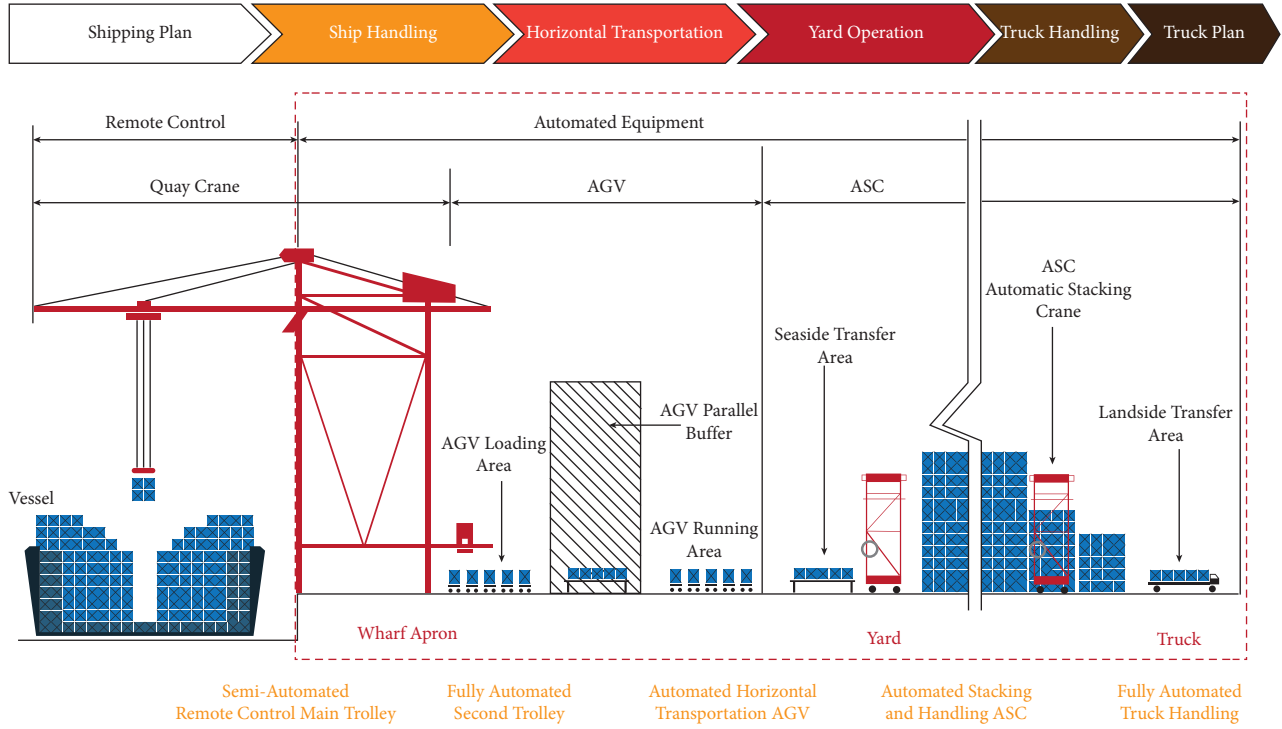
Figure 1: Single-container operation flow.

AGVs (or YTs), and ASCs cooperate with each other to maximize quantities of the loading and unloading containers per unit time, and the optimal scheduling plan of equipment scheduling is established considering the remaining container ships queued at the berth. The AGVs cannot deliver ultralong and ultrawide containers. Meanwhile, the automated container yards cannot stack these two kinds of nonstandard containers. Thus, they are transferred by YTs to the over-limit container yards. In addition, due to the related regulations, dangerous containers cannot be stored in the general container yards, so they should be transported by YTs to dangerous cargo yards. When the ship arrives, the general containers are transported by the portal trolley to the transfer platform for interaction and then transported by AGVs to the general cargo yard. The yard operation is completed by ASCs. Special containers, which are oversized or dangerous containers, will be transported to the special yards by queued YTs at the berth, not the AGVs. Figure 2 shows a full view of the automated terminal operation process. Therefore, making full use of the advantages of the double-trolley QCs to maximize the operational efficiency of the automated container terminal, the optimization model considered in this paper can satisfy different transportation requirements of all containers, not only general containers but also the other two special types of containers.

The optimization can be accomplished based on the following four assumptions:

(1) All loading and unloading tasks are completed.

(2) The operation task and operation time of each container are known, and there is no sequence for each loading and unloading task.

(3) The speeds of AGV and YT are known, and the operation speeds of QC and ASC are also known.

(4) There are no path conflicts between AGV and YT driving routes (that is, the road is wide enough).

(5) Each free AGV will find the most efficient task operation, while considering the multiship operation tasks. The optimal operating principle of AGV is to perform the task with the shortest operating time.

3. Notations and Model

The collection parameters are as follows:

K represents cargo handling tasks, $K = \{1, 2, \ldots, k\} = K_1 \cup K_2$

K_1 represents general cargo handling tasks of AGVs

K_2 represents special cargo handling tasks of YTs

N is the set of AGVs and YTs, $N = \{1, 2, \ldots, n\} = N_1 \cup N_2$

N_1 is the set of AGVs

N_2 is the set of YTs

For $i \in N$, tasks $L_i \subseteq M$ are assigned to the corresponding YTs or AGVs to satisfy the following conditions:

$L_i \cap L_j = \varnothing$, $i \neq j$; ② $\coprod_{\tau=m}^{\tau=1} L_i = M, \coprod_{\tau \in N_1} L_i = M_1$, $\coprod_{\tau \in N_2} L_i = M_2$

P is the set of the two trolleys of QC, $p \in P$, $p(t) = p_1(t) + p_2(t)$

Q is the set of ASCs, $q \in Q$

Defining time series $p(t)$ and $q(t)$ as follows:

$$p(t) = \begin{cases} 1 & \text{equipment } P \text{ is } busy \\ 0 & \text{equipment } P \text{ is free} \end{cases} \text{ and}$$

$$q(t) = \begin{cases} 1 & \text{equipment } Q \text{ is } busy \\ 0 & \text{equipment } Q \text{ is free} \end{cases}$$

M represents the tasks that need to be loaded and unloaded of container ship l

F_l is the completing time of all the loading and unloading tasks of container ship l, $F_l = \max\limits_{m \in M_l} f_m$

The decision variables are as follows:

When AGV or YT is assigned to complete task m, the completing time is $T_{m-total} = t_1 + t_2 + t_{loading} + t_{transport} + t_3 + t_{unloading}$

t_1 is the time when the vehicle arrives at the start point of the task

t_2 is the waiting time of vehicle for container loading, $t_2 = \min\limits_{loading} t_{finish}$

$t_{loading} / t_{transport} / t_{unloading}$ are given and $t_{transport} = d/v$

t_3 is the waiting time of vehicle for container unloading, $t_3 = \min\limits_{unloading} t_{finish}$

S_m is the time when each container task starts

f_m is the time when each container task finishes

The whole model is written as follows

$$\text{Min} \sum_{l=1}^{L} F_l, \tag{1}$$

$$F_l = \max_{m \in M_l} f_m, \tag{2}$$

$$f_m = S_m + T_{m-total}, \tag{3}$$

$$T_{m-total} = t_1 + t_2 + t_{loading} + t_{transport} + t_3 + t_{unloading}, \tag{4}$$

$$t_2 = \min_t \{t \geq t_1 + s_m | p_i(t) = 0\} - (s_m + t_1), \tag{5}$$

$$t_3 = \min_t \{t \geq f_m - t_{unloading} | p_i(t) = 0\} - (f_m - t_{unloading}). \tag{6}$$

Equation (1) represents the minimum time for each container ship to complete loading and unloading operations.

Equation (2) shows that the time of the container ship to complete tasks is the maximum value of the time of completing all loading and unloading tasks.

Equation (3) represents the time when each task is completed and is the start time and the time required to complete the task

Equation (4) expresses the time to complete the task, including the time for empty YT to the start of the task, loading waiting time, loading time, transporting time, unloading waiting time, and unloading time.

Equation (5) indicates the calculating method of loading waiting time.

Equation (6) indicates the calculating method of unloading waiting time.

4. The Proportional Fairness Algorithm

The key of PFA is how to determine the proportional fair priority. Considering the quantities of remaining loading and unloading tasks of each container ship and the driving distance of empty AGV/YT, the priority of all current loading and unloading tasks is ranked, and the task with the highest priority is fulfilled first. Thus, the balance between efficiency and fairness is achieved. The principle of the proportional fairness algorithm in selecting tasks is as follows:

$$\min_l \frac{\min\limits_{i \in M_l} \text{finishing time of task} i}{\text{remaining containers of ship} l}. \tag{7}$$

The flow chart of the algorithm (Figure 3) is as follows:

(1) Make the statistics of the remaining loading and unloading containers of all ships performing tasks at the current time Ni.

(2) Each container ship will find the nearest empty AGV or YT when loading and unloading containers. Calculate the time for the vehicle to reach the starting point of loading and unloading tasks Ti.

(3) Compute the proportional fair priority $Pri = \max(Ni/Ti)$ and choose the task with the highest priority.

5. Numerical Experiments and Results

In this chapter, PFA is designed for a typical business of automated container terminal. Compared with GA, which is commonly used in optimization problems, the efficiency of two algorithms is compared. The relative gain of PFA will be given through the simulation of MATLAB. The orders of job selection of two algorithms are different. In the application of GA, I first randomly selected an unfinished loading and unloading task and then selected the nearest AGV or YT to serve it. In PFA, the principles of selecting tasks are as follows:

$$\min_l \frac{\min\limits_{i \in M_l} \text{finishing time of task} i}{\text{remaining containers of ship} l}. \tag{8}$$

5.1. Data of Numerical Experiments. Suppose there are 180 loading and unloading containers to be loaded and unloaded in the designated terminal area. Loading and unloading positions of all tasks are fixed, and the quantities of AGVs, YTs, QCs, ASCs, and related parameters are known. The dataset is shown in Table 1.

5.2. Solutions of Numerical Experiments. The traditional GA and the innovative PFA are used to calculate the above
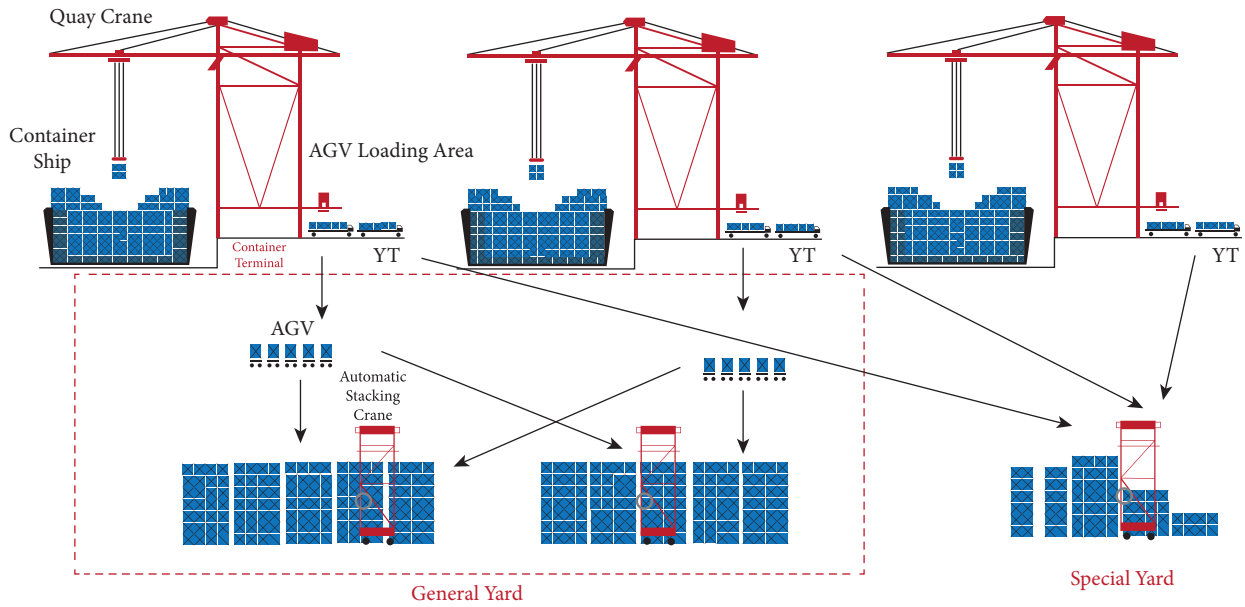
FIGURE 2: Full view of automated terminal operation process.
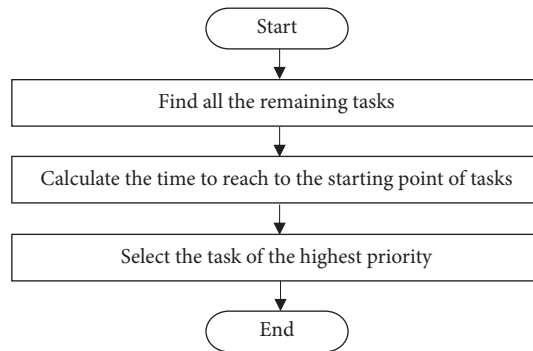
FIGURE 3: Flow chart of PFA.

TABLE 1: Dataset.

Parameter	Number	Remarks
Quantity of container ships	4	
Total loading containers	92	Quantities of loading containers by four ships are, respectively, 20, 40, 20, and 12
Total unloading containers	88	Quantities of unloading containers by four ships are, respectively, 20, 20, 40, and 8
Special containers	18	
Quantity of AGVs	6	
Quantity of YTs	4	
AGV speed	30 km/h	
YT speed	25 km/h	
Singer container operation time at the yard	45 seconds	
Singer QC operation time	35 seconds	

experiments, respectively. The results are shown in Table 2. The operation time of the four container ships of the two algorithms is listed separately. Taking the maximum value, the total operation time of GA is 1566 seconds, and that of PFA is 1479 seconds. Meanwhile, the standard deviation of operation time of four container ships is also listed in Table 2. The advantages of PFA are obvious. From Table 2, the total operation time of PFA is increased by 5% compared with that of GA. Using the standard deviation to measure fairness, the standard deviation of PFA is reduced by 50% compared with that of GA. Thus, PFA has significantly improved the efficiency and fairness. The reason is that PFA

TABLE 2: Completing time and standard deviation.

Completing time (second)	Container ship 1	Container ship 2	Container ship 3	Container ship 4	Standard deviation
GA	1523	1540	1524	1566	20.0728
PFA	1479	1461	1455	1460	10.50

gives priority to loading and unloading operations with short operation time and more remaining tasks in task selection process.

6. Conclusions

As AGVs have limitations to transport over-limit containers and dangerous containers, these two special kinds of containers should only be transported by queued YTs to special cargo yards. In this context, the advantages of the double-trolley QCs are fully utilized. By setting the priority parameters, the integrated model of QCs-AGVs (YTs)-ASCs scheduling is established under the premise of balancing the operating speed of each container ship at the berth. The model maximizes the efficiency of the automated terminal and solves the problem of fairness in operation of multiple container ships under various loading and unloading operations. PFA is designed to solve the problem, which is proved by numerical experiments with better efficiency and fairness. The integrated scheduling model helps to improve the efficiency of the automated terminals. In this paper, the choice of the task order of YT/AGV loading and unloading operation is studied. Future research will focus on scheduling at automated container terminals considering ASC-QC loading and unloading task sequence.

Data Availability

The data including models, tables, and figures which are used to support the findings of this study are included within the article.

Conflicts of Interest

The author declares that there are no conflicts of interest.

Acknowledgments

References

[1] P. Legato, R. Trunfio, and F. Meisel, "Modeling and solving rich quay crane scheduling problems," *Computers & Operations Research*, vol. 39, no. 9, pp. 2063–2078, 2012.

[2] O. Uusal and C. Oguz, "Constraint programming approach to quay crane scheduling problem," *Transportation Research Part E*, vol. 59, pp. 108–122, 2013.

[3] J. H. Chen, D.-H. Lee, and M. Goh, "An effective mathematical formulation for the unidirectional cluster-based quay crane scheduling problem," *European Journal of Operational Research*, vol. 232, no. 1, pp. 198–208, 2014.

[4] Q. Q. Shao, Q. Xu, Z. Bian, and Z. H. Jin, "Stockpiling operating optimization for yard crane with containers delivery time uncertainty," *Systems Engineering-Theory & Practice*, vol. 35, no. 2, pp. 394–405, 2015.

[5] D. Chang, Z. Jiang, W. Yan, and J. He, "Developing a dynamic rolling-horizon decision strategy for yard crane scheduling," *Advanced Engineering Informatics*, vol. 25, no. 3, pp. 485–494, 2011.

[6] Q. C. Zeng, X. J. Zhang, W. H. Chen, and X. C. Zhu, "Optimization model for truck appointment based on BCMP queuing network," *Journal of Systems Engineering*, vol. 28, no. 5, pp. 592–599, 2013.

[7] X. Guo, S. Y. Huang, W. J. Hsu, and M. Y. H. Low, "Dynamic yard crane dispatching in container terminals with predicted vehicle arrival information," *Advanced Engineering Informatics*, vol. 25, no. 3, pp. 472–484, 2011.

[8] C. Ma and C. J. Liang, "Integrated quay crane allocation and yard truck schedule problem in container terminals," *Journal of Guangxi University(Natural Science Edition)*, vol. 40, no. 3, pp. 643–650, 2015.

[9] T. B. Qin, H. Ge, and S. Mei, "Unidirectional quay crane scheduling problems solving by combination of mixed integer programming and constraint programming," *Computer Integrated Manufacturing Systems*, vol. 21, no. 2, pp. 546–555, 2015.

[10] Y. Q. Xu and X. L. Han, "United scheduling model optimization of yard truck, quay crane and yard crane," *Journal of Chongqing Jianzhu University*, vol. 32, no. 2, pp. 318–320, 2013.

[11] Y. Wu, J. B. Luo, D. L. Zhang, and D Ming, "An integrated programming model for storage management and vehicle scheduling at container terminals," *Research in Transportation Economics*, vol. 42, no. 1, pp. 13–27, 2013.

[12] W. J. Mi, Y. F. Shen, and J. X. Y. X. M. Wang, "Collaborative decision-making on container pickup operation for gateway container selection and machinery resource allocation," *Chinese Journal of Construction Machinery*, vol. 12, no. 5, pp. 454–459, 2014.

[13] X. W. Xing, J. Mao, R. Zhang, and Z. H. Jin, "Optimization of container loading/unloading integrated scheduling in a container terminal based on hybrid flow shop," *Chinese Journal of Management Science*, vol. 22, no. 10, pp. 97–105, 2014.

[14] L. Chen, A.. Langevin, and Z. Q. Lu, "Integrated scheduling of crane handling and truck transportation in a maritime container terminal," *European Journal of Operational Research*, vol. 225, no. 1, pp. 142–152, 2013.

[15] D. B. Meng, Y. Li, S. P. Zhu, G. Lv, J. Correia, and Abilio de Jesus, "An enhanced reliability index method and its application in reliability-based collaborative design and optimization," *Mathematical Problems in Engineering*, pp. 1–10, 2019.

[16] Y. H. Li, Z. Sheng, P. Zhi, and D. Li, "Multi-objective optimization design of anti-rolling torsion bar based on modified

NSGA-III algorithm," *International Journal of Structural Integrity*, vol. 12, no. 1, pp. 17–30, 2021.

[17] P. Zhi, Y. Li, B. Chen, M. Li, and G. Liu, "Fuzzy optimization design-based multi-level response surface of bogie frame," *International Journal of Structural Integrity*, vol. 10, no. 2, pp. 134–148, 2019.

[18] Y. H. Wang, C. Zhang, Y. Q. Su, L. Y. Shang, and T. Zhang, "Structure optimization of the frame based on response surface method," *International Journal of Structural Integrity*, vol. 11, no. 3, pp. 411–425, 2020.

[19] S. Y. Zhang, Y. S. Yang, C. J. Liang, B. W. Xu, and J. J. Li, "Optimal control of multiple AGV path conflict in automated terminals," *Journal of Transportation Systems Engineering and Information Technology*, vol. 17, no. 2, pp. 83–89, 2017.

[20] R. Zaghdoud and K. Mesghouni, "A hybrid method for assigning containers to AGVs in container terminal," *IFAC-papersOnLine*, vol. 49, no. 3, pp. 96–103, 2016.

[21] J. B. Xin, "Control of interacting machines in automated container terminals using a sequential planning approach for collision avoidance," *Transportation Research Part C: Emerging Technologies*, vol. 60, pp. 377–396, 2015.

[22] J. B. Luo and Y. Wu, "Modeling of integrated vehicle scheduling and container storage problems in unloading process at an automated container terminal," *Computers & Industrial Engineering*, vol. 94, pp. 32–44, 2016.

[23] C. Wei, Z. H. Hu, C. F. Gao, and X. J. Luo, "Scheduling model and algorithm of twin synchronized stacking cranes in stack yard of automated container terminal," *Journal of Dalian Maritime University*, vol. 41, no. 4, pp. 75–89, 2015.

[24] S. Y. Ma, Y. S. Yang, and C. J. Liang, "Collaborative scheduling of double-trolley quay cranes and AGV based on PSO at automated container terminal," *Computer Applications and Software*, vol. 35, no. 10, pp. 17–22, 2018.

[25] Y. S. Yang, Y. Y. Feng, C. J. Liang, B. W. Xu, and J. J. Li, "Integrated scheduling of automated guided vehicles and rail-mounted gantry cranes at automated container terminals," *Journal of Shanghai Maritime University*, vol. 38, no. 2, pp. 1–6, 2017.

[26] M. L. Le and Q. B. Zhang, "Integrated scheduling of quay cranes, automated guided vehicles and automated yard cranes at automated container terminals," *Journal of Qingdao University of Science and Technology (Natural Science Edition)*, vol. 36, no. 5, pp. 569–574, 2015.

[27] Q. C. Zeng and Z. Z. Yang, "Integrating simulation and optimization to schedule loading operations in container terminals," *Computers & Operations Research*, vol. 36, no. 6, pp. 1935–1944, 2009.

[28] S. L. Hu and Z. H. Hu, "Full freedom optimization for integrated quay cranes, Trucks and yard cranes in container port," *Journal of Wuhan University of Technology*, vol. 34, no. 5, pp. 58–63, 2012.

[29] H. Dkhil, A. Yassine, and H. Chabchoub, "Optimization of container handling systems in automated maritime terminal," *Studies in Computational Intelligence*, vol. 457, pp. 301–312, 2013.

[30] Y. Q. Lu and M. L. Le, "The integrated optimization of container terminal scheduling with uncertain factors," *Computers & Industrial Engineering*, vol. 75, pp. 209–216, 2014.

[31] Y. Q. Lu, "The three-stage integrated optimization of automated container terminal scheduling based on improved genetic algorithm," *Mathematical Problems in Engineering*, vol. 2021, Article ID , 9 pages, 2021.

Research Article

Hydromechanical Simulation of Tunnel Excavation in Rock Considering a Nearby Karst Cave

Huiling Zhao [iD],[1] **Fan Zhang** [iD],[1] **and Xupeng Yao**[2]

[1]*Department of Civil Engineering, Shanghai University, Shanghai 200444, China*
[2]*College of Civil Engineering, Tongji University, Shanghai 200092, China*

Correspondence should be addressed to Fan Zhang; fanzai@shu.edu.cn

Tunnel excavation tends to be affected by karst cavities in karst areas. Some cavities that are at low risk of causing safety issues without treatment tend to be ignored in the design and construction of tunnels to reduce costs. It is necessary to gain a better understanding of the effect of such a cavity on the seepage around a tunnel, the deformation of the surrounding rock, and the stress of the tunnel lining. In this paper, a two-dimensional rock-tunnel hydromechanical model with a karst cave was established with FLAC3D finite difference software to simulate the tunnel excavation with the consideration of seepage. Numerical simulations were performed to analyze the deformation of the surrounding rock, the seepage field of the surrounding rock, and the stress of the tunnel lining, and the results were compared for scenarios when the karst cave is at different locations relative to the tunnel. These results can provide a reference for the design and construction of tunnel engineering in rock with karst caves.

1. Introduction

With the development of the mileage and scope of tunnels, tunnels are inevitably constructed in some complicated geological areas. An increasing number of tunnels pass through karst areas, in which microscale cavities readily develop along the fault planes and joints in limestone due to weathering and chemical corrosion. The unpredictable occurrence of cavities presents challenges to tunnel construction [1, 2]. The existence of karst cavities around a tunnel certainly affects the design of the tunnel and the safety of the construction of the tunnel [3–8].

Recently, the problems associated with the excavation and support of tunnels in karst ground have attracted increasing attentions. Scholars have explored which are the main influencing factors for tunnel excavation in karst areas, and the safe distance between tunnels and karst caves has been studied. Huang et al. [9] proposed an evaluation model of karst cave development conditions, construction conditions, and control measures, performed a statistical analysis, and concluded that the groundwater level, support structure, and surrounding rock quality were the main factors

influencing the stability of tunnels in karst areas. Wang et al. [10] established a prediction model for the safe thickness of the roof of karst caves and found that the span of karst caves influenced the cave stability more significantly than the filling degree of karst caves and that the height-to-span ratio of karst caves had little relation to the safe thickness of the cave roof. Huang et al. [11] analyzed the influence of the distance between the roof and tunnel and the diameter, width, and filling degree of a karst cave on the deformation of subway tunnel segments after excavation, considering the fluid-solid coupling effect. Chen and Sha [12] studied the stress-strain characteristics of the surrounding rock and supporting structure of a tunnel with a superlarge karst cave at different distances through field tests and numerical simulations. Zhao et al. [13] studied the stability of a rock pillar on a concealed karst cave in front of a tunnel and calculated the safe thickness of the rock pillar to prevent water inrush. Shan et al. [14] analyzed the safe thickness between a tunnel and a nearby hidden cave and the factors influencing the rock-breaking mechanism and conducted numerical simulations and multiple regression analyses to study the safe distance between the tunnel and the karst cave.

Wang et a. [15] studied the influence of surrounding rock parameters on the collapse surface of a karst rock mass under a tunnel and proposed a formula for the minimum safe thickness to prevent rock pillar collapse. These studies show that some cavities with well-developed hydraulic conduits located at the key position need to be treated; without treatment, they may introduce a high risk to tunnel construction safety, possibly leading to water inrush, mud inrush, and even collapse [16–20]. Nevertheless, some cavities with a low risk of causing safety issues tend to be ignored in the design and construction of tunnels to reduce costs. Thus, it is necessary to gain a better understanding of the effect of the cavity on the seepage around the tunnel, the deformation of the surrounding rock, and the stress of the tunnel lining.

In this paper, the deformation of the surrounding rock, the seepage field of the surrounding rock, and the stress of the tunnel lining are analyzed by means of numerical simulations of several scenarios in which the karst cave is at different locations relative to the tunnel [21], and the results are compared. The results can provide some reference for the design and construction of tunnel engineering in water-rich areas with karst caves.

2. Establishment of the Coupled Hydromechanical Simulation

2.1. Establishment of the Finite Difference Numerical Model. Based on a tunnel project in Yunnan Province, China, a typical section is selected to simulate the stability of the surrounding rock and the change in the seepage field during tunnel excavation. The depth of the tunnel is 60 m. The width and the height of the tunnel are 12 m and 8.5 m, respectively. The rock range considered in the numerical model is about 4 times the diameter of the tunnel. The top boundary is the ground surface, and the bottom boundary is 36 m below the tunnel. The model is 100 m wide and 110 m high. The lateral boundaries of the model are set horizontal displacement constraints, and the bottom boundary is set a fixed displacement constraint. In order to simplify the hydrologic condition, the initial saturation of the model is set as 1.0. The initial stress is calculated according to gravity stress of rock mass. The pore water pressure on the top boundary of the model is set as 0, and the other boundaries are impermeable boundaries. The permeable boundary is set on the inner side of the tunnel during excavation, where the water pressure is initially set as 0. The karst cave is taken as the shape of an ellipse. The long axis of the karst cave is 5 m, and the short axis is 3 m. The model meshing details and geometry of rock domain and tunnel lining are displayed in Figure 1. The model meshing is according to mesh convergence study. In the zone near to tunnel lining, higher mesh density has been provided for attaining desired accuracy. The mesh size is increased away from the tunnel in order to make the model computationally efficient.

The Mohr–Coulomb elastic-plastic model is adopted for the surrounding rock, and an elastic model is adopted for the support. According to the Chinese code for the design of highway tunnels [22], the material parameters of the
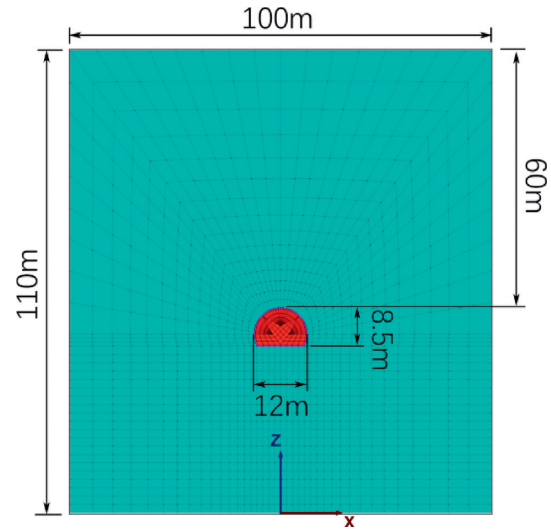
FIGURE 1: Numerical model for tunnel excavation simulation.

surrounding rock and supporting structure in the numerical simulation are shown in Table 1 [23, 24]. The primary support of this section is made of C25 shotcrete with a thickness of 0.3 m. The secondary support is a C25 mono-lithic concrete structure with a thickness of 0.7 m.

2.2. Determination of the Working Conditions. In order to study the influences of different distances and positions of a karst cave on tunnel excavation, six working conditions are established, as shown in Figure 2. For working conditions 1, 2, and 3, the karst caves are located on the left side of the tunnel, and the caves are 2 m, 4 m, and 6 m away from the left side of the tunnel, respectively. For working conditions 4 and 5, the caves are located above and below the tunnel, respectively. Under working condition 6, the center of the karst cave is 45° counterclockwise from the central axis of the tunnel. In the latter 3 cases, the karst caves are 2 m away from the tunnel boundary.

3. Comparison and Results Analysis

3.1. Influence of Distance of Cave to the Tunnel

3.1.1. Stress Field of the Surrounding Rock. The state of stress balance in the rock is disturbed due to the tunnel excavation. The redistribution of the stress in the surrounding rock has changed the permeability of the rock, accompanied by the varying pore water pressure in the surrounding rock. The variation in pore water pressure can also affect the distribution of the stress field in the surrounding rock. Actually, the pore water pressure and rock stress are interdependent. The stress field and seepage field finally have reached a relative equilibrium state under the condition of fluid-solid coupling. Figure 3 shows the horizontal and vertical stress contour plots of the tunnel and surrounding rock in the absence of a karst cave. Figures 4 and 5 show the horizontal stress contour plot and the vertical stress contour plot, respectively, for working conditions 1, 2, and 3.

TABLE 1: Material parameters of the numerical model.

	Elastic modulus (GPa)	Poisson's ratio	Friction angle (°)	Volumetric weight (kN·m^{-3})	Cohesion (MPa)	Permeability coefficient (cm·s^{-1})
Rock	6	0.25	40	26	0.9	4.5×10^{-4}
Tunnel support	30	0.2	—	24	—	1.5×10^{-8}
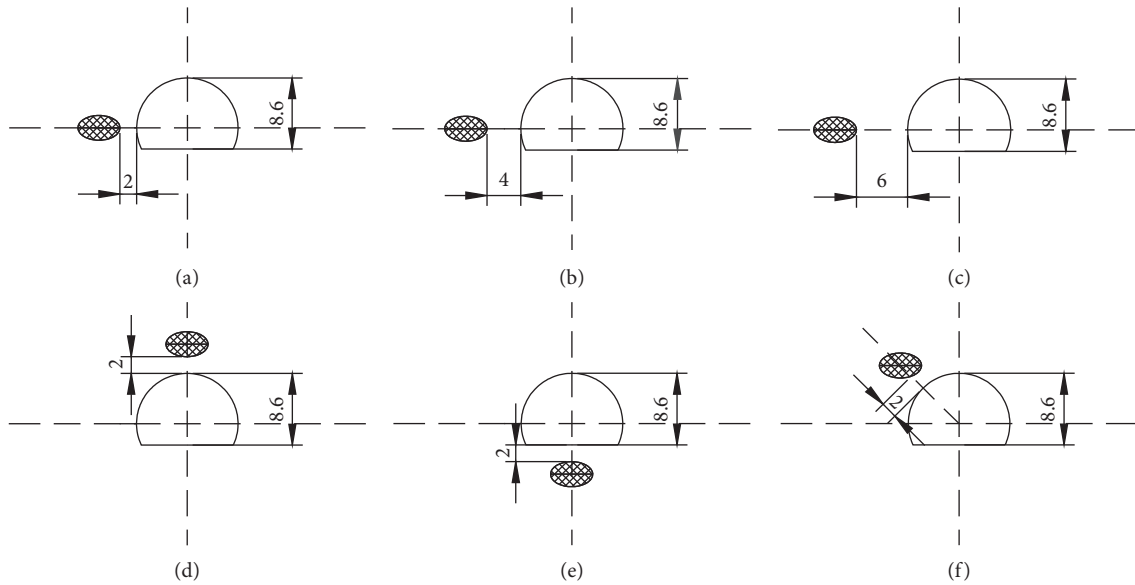
FIGURE 2: The cave location in 6 different working conditions. (a) Working condition 1. (b) Working condition 2. (c) Working condition 3. (d) Working condition 4. (e) Working condition 5. (f) Working condition 6.
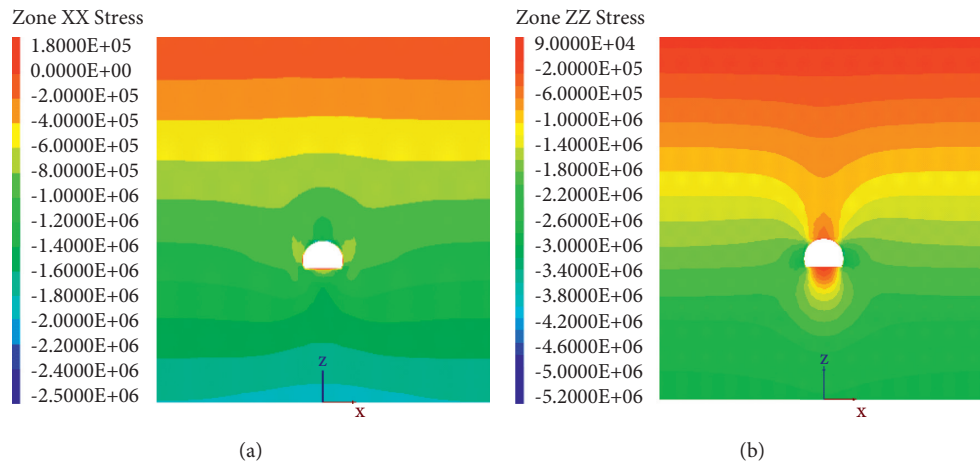
FIGURE 3: Stress contour plots without a karst cave. (a) Horizontal stress contour plot. (b) Vertical stress contour plot.

It can be seen from Figure 4 that the horizontal compressive stresses of the surrounding rock on both sides of the tunnel have changed compared with those of the working condition without a karst cave. Due to the existence of the cavern, the excavation stress release on the left and right side of the tunnel is asymmetric. When the cave is close to the tunnel in working condition 1, the excavation stress release area reaches the cave resulting in that the compressive stress decreases about 16% between the cave and the tunnel.

Figure 5 shows the vertical compressive stress of the surrounding rock in working conditions 1 to 3. The vertical compressive stress at the hance of the tunnel on the side with cave increases significantly in working conditions 1 and 2; in particular working condition 1 has increased from 2.4 MPa to 4.6 MPa. At the same time, the compressive stress of the surrounding rock directly above and below the tunnel also increases by 13% and 10% in working condition 1. Similarly, the vertical stress distribution of surrounding rock in
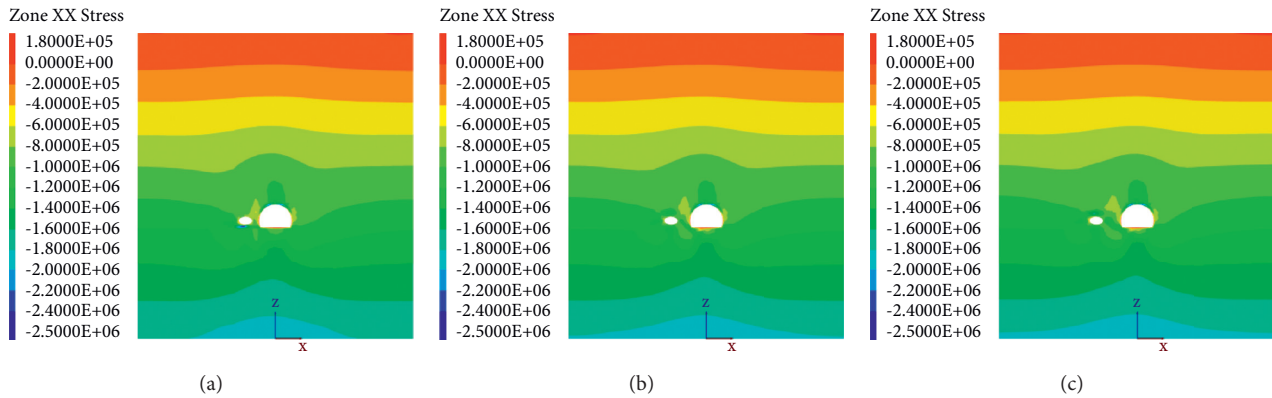
FIGURE 4: Horizontal stress contour plots. (a) Working condition 1. (b) Working condition 2. (c) Working condition 3.
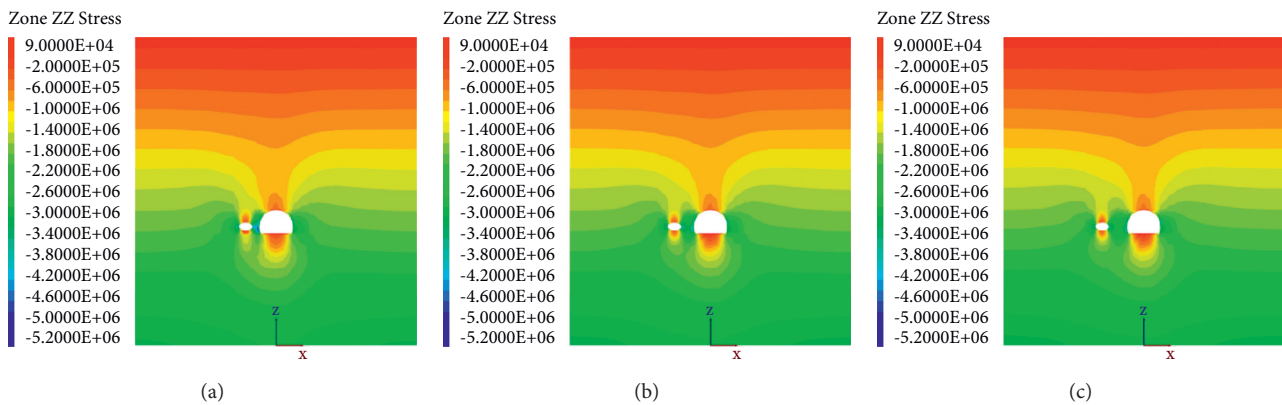
FIGURE 5: Vertical stress contour plots. (a) Working condition 1. (b) Working condition 2. (c) Working condition 3.

working condition 2 and working condition 3 is similar to that in working condition 1, but the increment decreases obviously. It can be seen that a cave near to the tunnel leads to an increase in the compressive stress of the surrounding rock at the cave side of the tunnel.

3.1.2. Seepage Field. Key points of the tunnel lining are selected to monitor the seepage field. Point A locates at the vault, point B locates at the left hance, point C locates at the right hance, point D locates at the left arch foot, point E locates at the right arch foot, and point F locates at the center of the bottom, as shown in Figure 6. The pore pressure variations of these points with time in the working conditions 1 to 3 compared with those of the working condition without a karst cave are shown in Figure 7. The solid lines in Figure 7 represent the result of the working condition without a karst cave, while the dotted lines represent the results of the working conditions 1, 2, and 3.

It can be seen from Figure 7 that, compared with the working condition with no karst cave, the pore water pressure at points B and D changes considerably in working conditions with a karst cave. When the pore water pressures are stable, the pore pressures at points A, C, E, and F under working conditions 1 to 3 are close to those without a karst
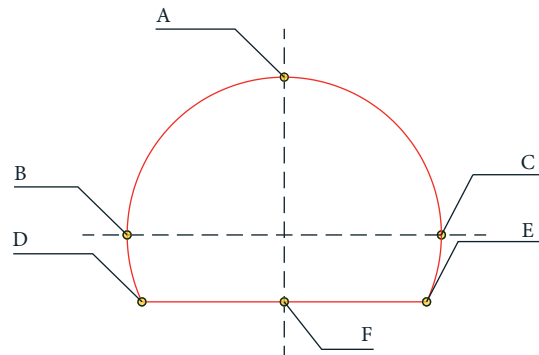
FIGURE 6: Layout of the monitoring points.

cave, while the pore pressures at points B and D decrease significantly. During the early stage of excavation, compared with the working condition without a karst cave, the pore pressures at points B and D drop significantly. The pore pressure at points C and E increases slightly in working condition 1 but basically does change in working condition 2 and working condition 3.

Figure 8 shows the flow vector distribution. When there is a karst cave, the seepage paths of surrounding rock near the cave are greatly affected, accompanied by the increase in flow vector at the arch foot of the opposite side of the cave.
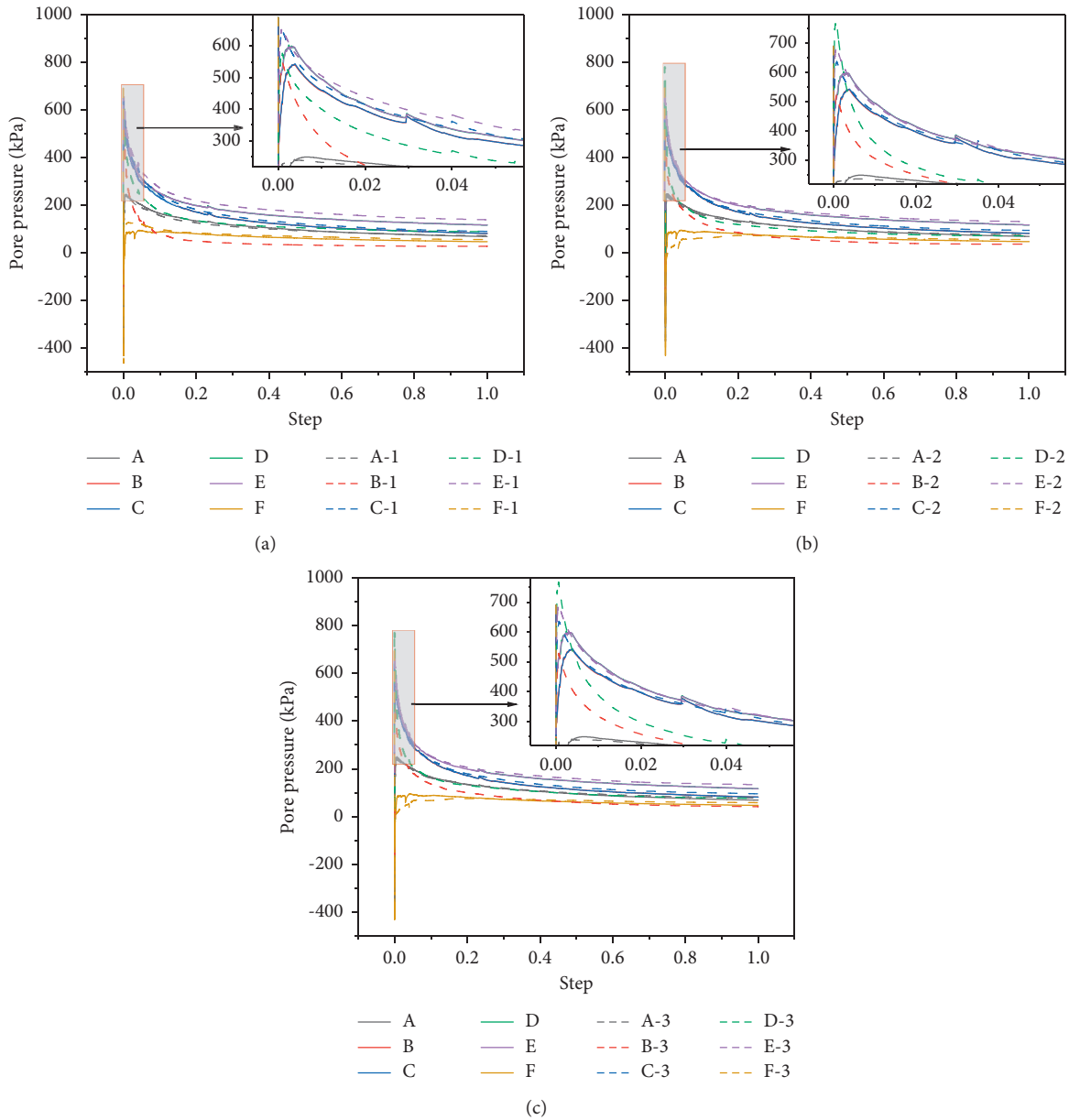
FIGURE 7: Pore water pressure variation with time of key points. (a) Working condition 1. (b) Working condition 2. (c) Working condition 3.

3.1.3. Deformation of the Surrounding Rock. To observe the deformation of the surrounding rock around the tunnel, the vertical displacement of points A and F and the horizontal displacement of points B, C, D, and E are recorded.

Figure 9 shows the development of the vertical displacement of points A and F without karst caves (the solid line) and under working conditions 1 to 3 (the dotted lines). The settlement of point A (vault) increases by 26% in working conditions 1 to 3 compared with that without a karst cave. The uplift at the bottom increases slightly, but the effect is not significant.

Figure 10 shows the development of the horizontal displacement of points B to E without karst caves (the solid line) and under working conditions 1 to 3. When there is a karst cave on the left side of the tunnel, the

horizontal displacements at point B exhibit the difference, which is the point nearest to the cave. For working condition 1, at the initial stage of excavation, the displacement of point B increases significantly. Finally, the displacement of point B increases by 45% compared with condition without cave. For working condition 2, the displacement of point B increases by 20%. For working condition 3, the increase is not obvious. It can be seen that the point B closest to the cave has an increase in horizontal displacement when the distance of cave to the tunnel is no more than 4 m.

On the one hand, the existence of the cavern itself weakens the stiffness of the surrounding rock of the tunnel, and the stability is significantly reduced. On the other hand, due to the existence of karst caves, the seepage path on the

(a)   (b)
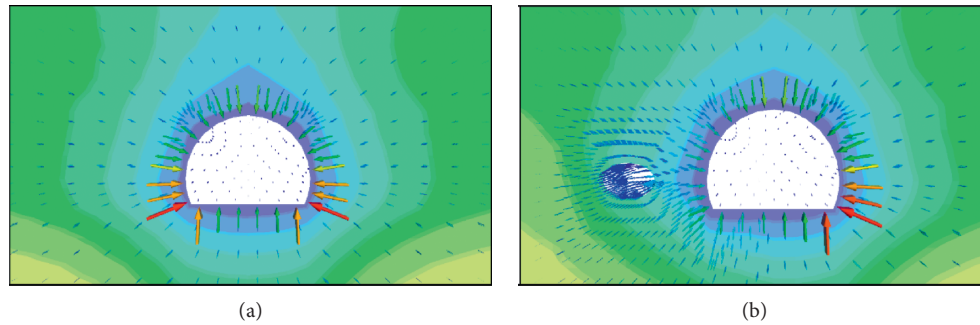
FIGURE 8: Flow vector diagram. (a) Without a karst cave. (b) With a karst cave.
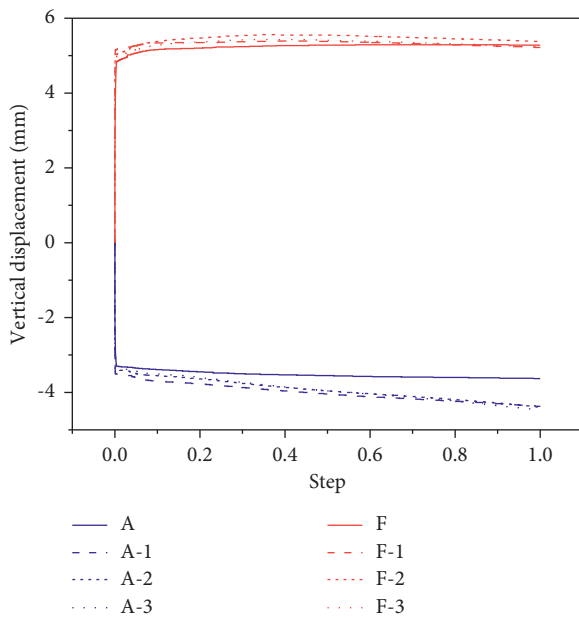
FIGURE 9: Vertical displacement at points A and F under working conditions 1 to 3.

side close to the karst cave is blocked after the tunnel is excavated, and the karst cave acts as a shield. Therefore, the pore pressure at the corresponding position is significantly smaller than the pore pressure on the symmetry side. The overlying load remains unchanged, and the reduction of pore pressure causes the skeleton stress of the surrounding rock to increase correspondingly, which reduces the volumetric strain of the surrounding rock. Therefore, the displacement of the surrounding rock near the tunnel on the side of the karst cave increases.

3.1.4. Stress of the Tunnel Lining. Figure 11 shows the 1st and 3rd principal stresses of the tunnel lining under working conditions 1 to 3, respectively, compared with the results from the working condition without a karst cave. It can be seen that the compressive stress at the vault increases while the tensile stress at the arch bottom decreases for 3 conditions due to the cave. The compressive stress at spandrel, hance, and arch foot also increases at different degree for 3 conditions due to the cave. However, there are no definite

rules for the variation in stress with the increase in the distance of cave to the tunnel. Compared with the stress distribution for the working condition without a karst cave, the principal stress distribution of the tunnel lining under working conditions 1 to 3 exhibits a nonuniform distribution.

3.2. Influence of Karst Cave Location

3.2.1. Stress Field of the Surrounding Rock. In working conditions 4, 5, and 6, the karst caves are located at different locations of the tunnel. Horizontal and vertical stress contour plots for working conditions 4 to 6 are shown in Figures 12 and 13.

It can be seen that when the relative position of the karst cave to the tunnel changed, the stress field of the surrounding rock has changed. The compressive stress near the cave decreased when the cave is directly above or directly below the tunnel in working conditions 4 and 5. The stress distribution at the upper left side of the tunnel is greatly influenced in working condition 6. For working condition 6, the horizontal stress between the cave and the tunnel increases by about 25% due to the existence of the cave. Also, a nonuniform stress distribution is found around the tunnel when the cave is not located on the axis of symmetry of the tunnel in working condition 6.

3.2.2. Seepage Field. The pore pressure variations of these points with time in the working conditions 4 to 6 compared with those of the working condition without a karst cave are shown in Figure 14. The solid lines in Figure 14 represent the result of the working condition without a karst cave, while the dotted lines represent the results of the working conditions 4, 5, and 6.

Figure 14(a) shows that when the karst cave is directly above the tunnel, the pore pressure at point A decreases significantly compared with that without a karst cave; the pore pressure at points B and C decreases slightly, while the pore pressures at points D, E, and F basically remain unchanged. Figure 14(b) shows that when the karst cave is located directly under the tunnel, the pore pressure at point F decreases significantly compared with that without a karst cave; the pore pressures at points B, C, D, and E decreases slightly, while the pore pressure at point A increases slightly.

(a)

(b)
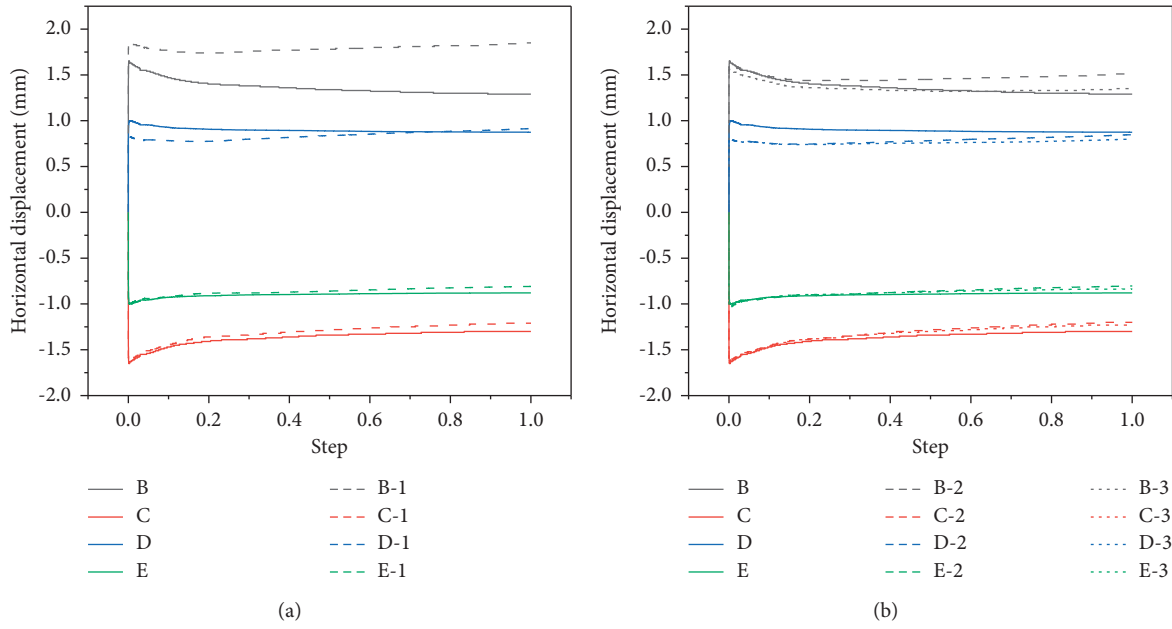
FIGURE 10: Horizontal displacement at the monitoring points B to E. (a) Working condition 1. (b) Working conditions 2 and 3.

(A) 1st principal stress (kPa)

(B) 3st principal stress (kPa)

(a)

(A) 1st principal stress (kPa)

(B) 3st principal stress (kPa)

(b)

FIGURE 11: Continued.

(c)

(A) 1st principal stress (kPa)   (B) 3st principal stress (kPa)
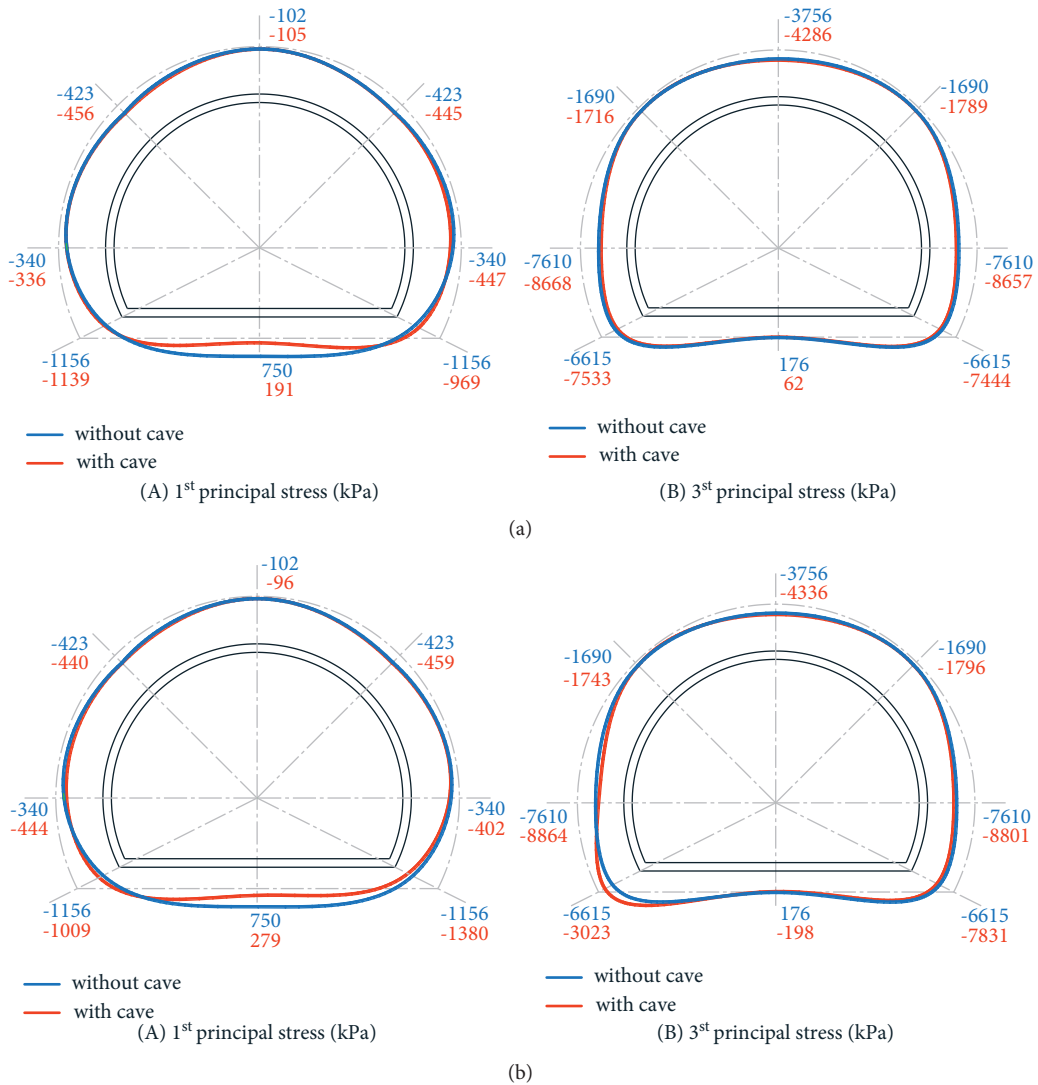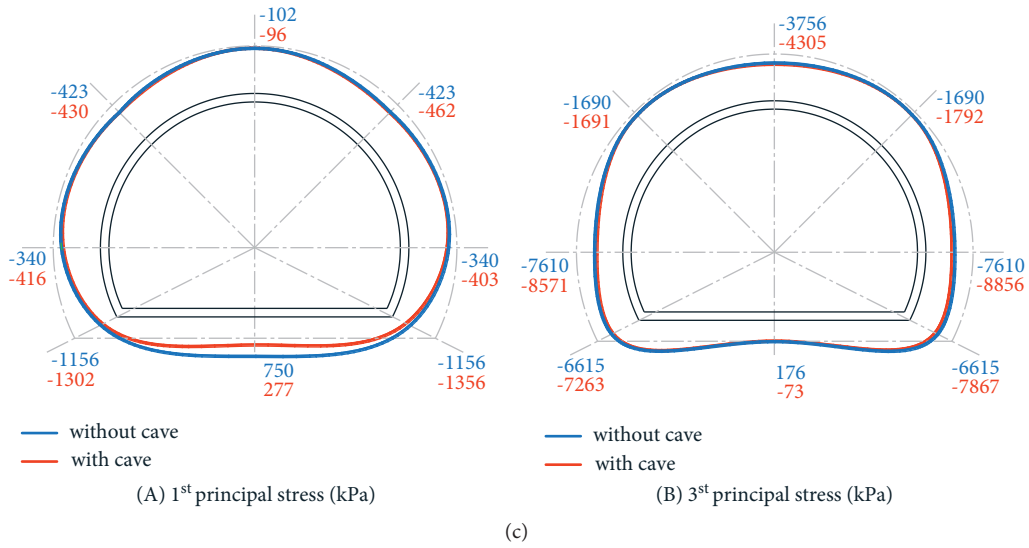
FIGURE 11: Stress distribution of the tunnel lining under working conditions 1 to 3. (a) Working condition 1. (b) Working condition 2. (c) Working condition 3.

(a)   (b)   (c)
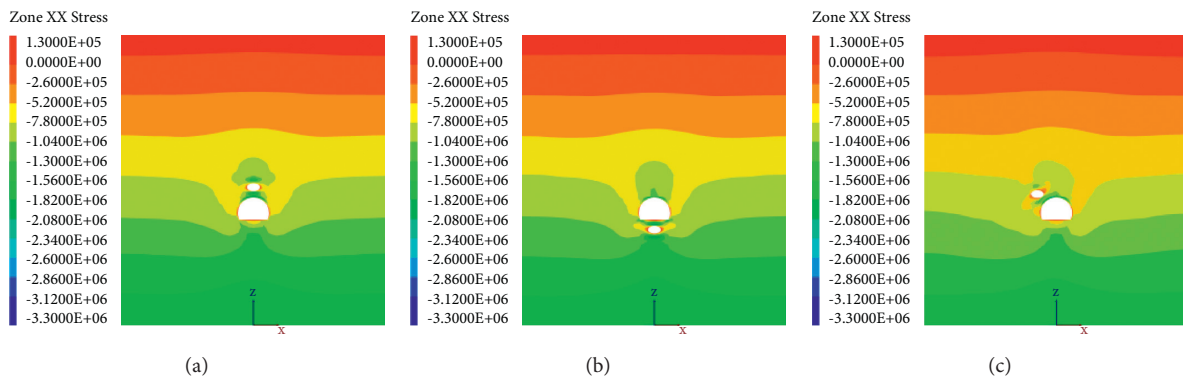
FIGURE 12: Horizontal stress contour plots. (a) Working condition 4. (b) Working condition 5. (c) Working condition 6.

(a)   (b)   (c)
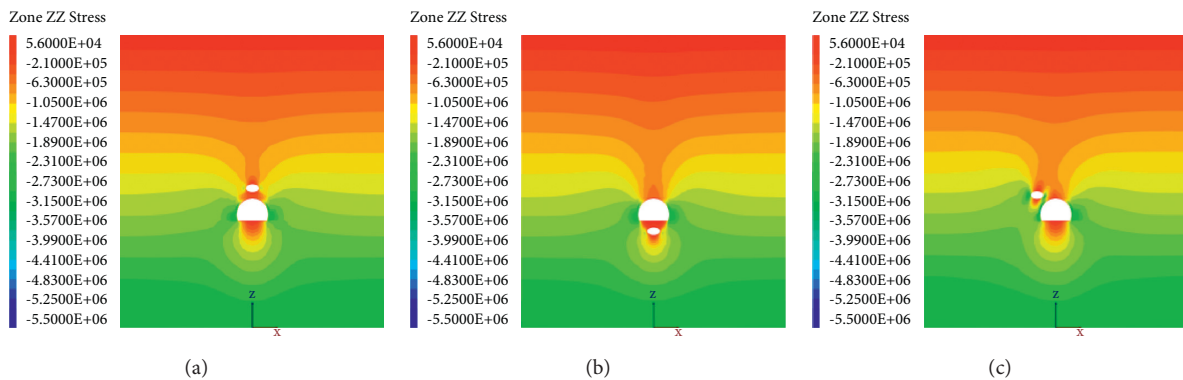
FIGURE 13: Vertical stress contour plots. (a) Working condition 4. (b) Working condition 5. (c) Working condition 6.

Figure 14(c) shows that when the karst cave is 45° to the left above the oblique tunnel, the pore pressure at points A and B decreases significantly compared with those without a karst cave, while the pore pressure at point D decreases slightly, and the pore pressure at points C, E, and F basically remains unchanged. When there is a cave, the seepage flow of the surrounding rock near the cave causes the pore pressure at this location to be relatively reduced.

(a)

(b)

(c)
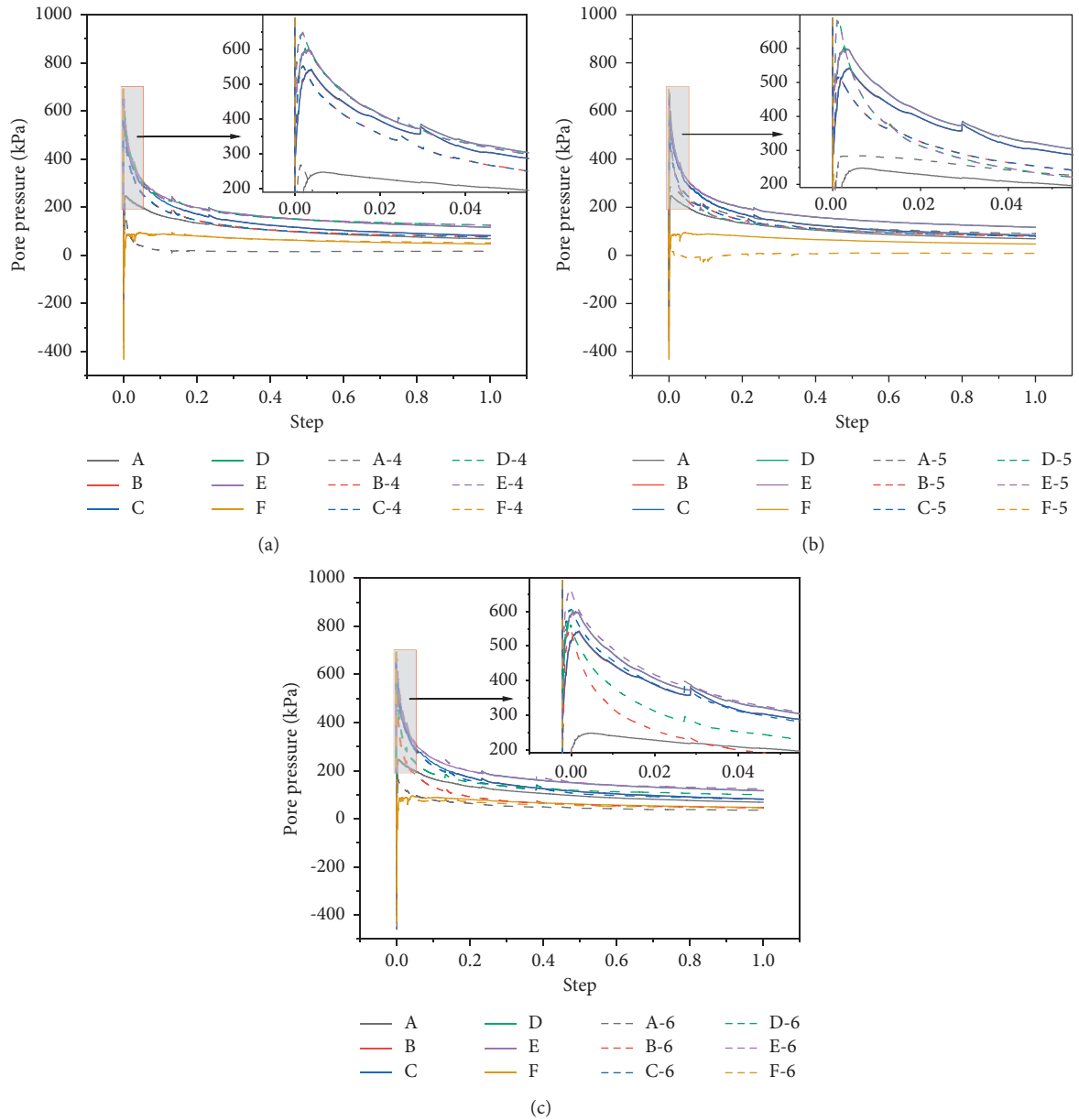
Figure 14: Comparison charts of the pore water pressure changes. (a) Working condition 4. (b) Working condition 5. (c) Working condition 6.

3.2.3. *Deformation of the Surrounding Rock.* Figure 15 shows the development of the vertical displacement of points A and F without karst caves (the solid line) and under working conditions 4 to 6 (the dotted lines). Compared with the curve without a karst cave, when the karst cave locates above the tunnel, the settlement at point A increases and the uplift at point F decreases. When the karst cave locates below the tunnel, the settlement at point A decreases and the uplift at point F increases. When the karst cave locates in the upper left of the tunnel in condition 6, the uplift at point F increases more than that in condition 4.

Figure 16 shows the development of the horizontal displacement of points B to E without karst caves (the solid line) and under working conditions 4 to 6. When the karst cave is located above or below the tunnel, it has little effect on the horizontal displacement at the monitoring points. Compared to the condition without a karst cave, under working condition 6, the horizontal displacement of points B, C, and E decreases, while the horizontal displacement of point D increases.

3.2.4. *Stress of the Tunnel Lining.* Figure 17 shows the 1st and 3rd principal stresses of the tunnel lining under working conditions 4 to 6, respectively, compared with the results from the working condition without a karst cave.
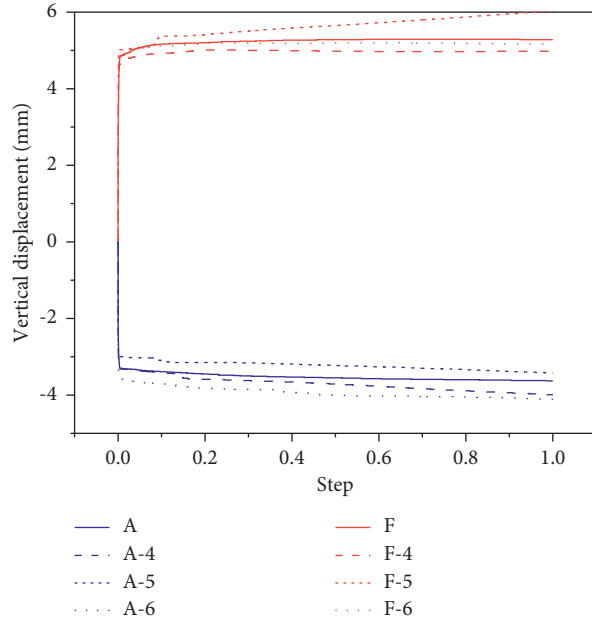
FIGURE 15: Vertical displacement at points A and F.

(a)

(b)
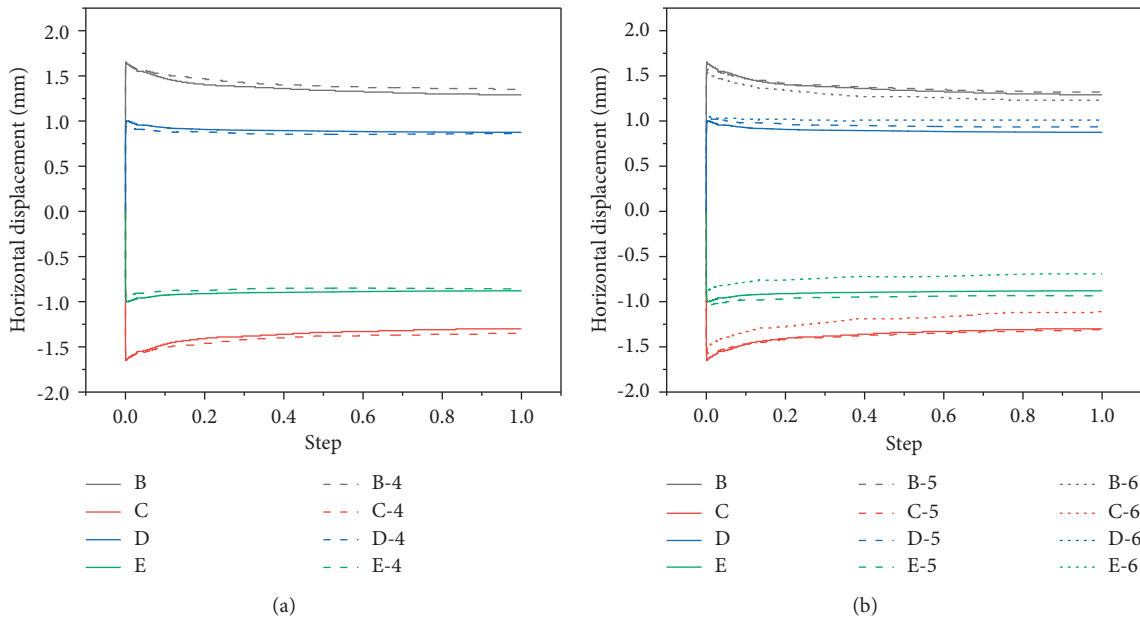
FIGURE 16: Horizontal displacement at the monitoring points B to E. (a) Condition 4. (b) Condition 5 and condition 6.

It can be seen from Figure 17 that when the cave locates above the tunnel, the compressive stress at the vault increases by 23%. When the cave was located below the tunnel, the compressive stress at the arch foot decreases significantly by 57%. When the cave locates upper left of the tunnel, the compressive stress at the vault and the left hance increases significantly by 19% and 43%, respectively.
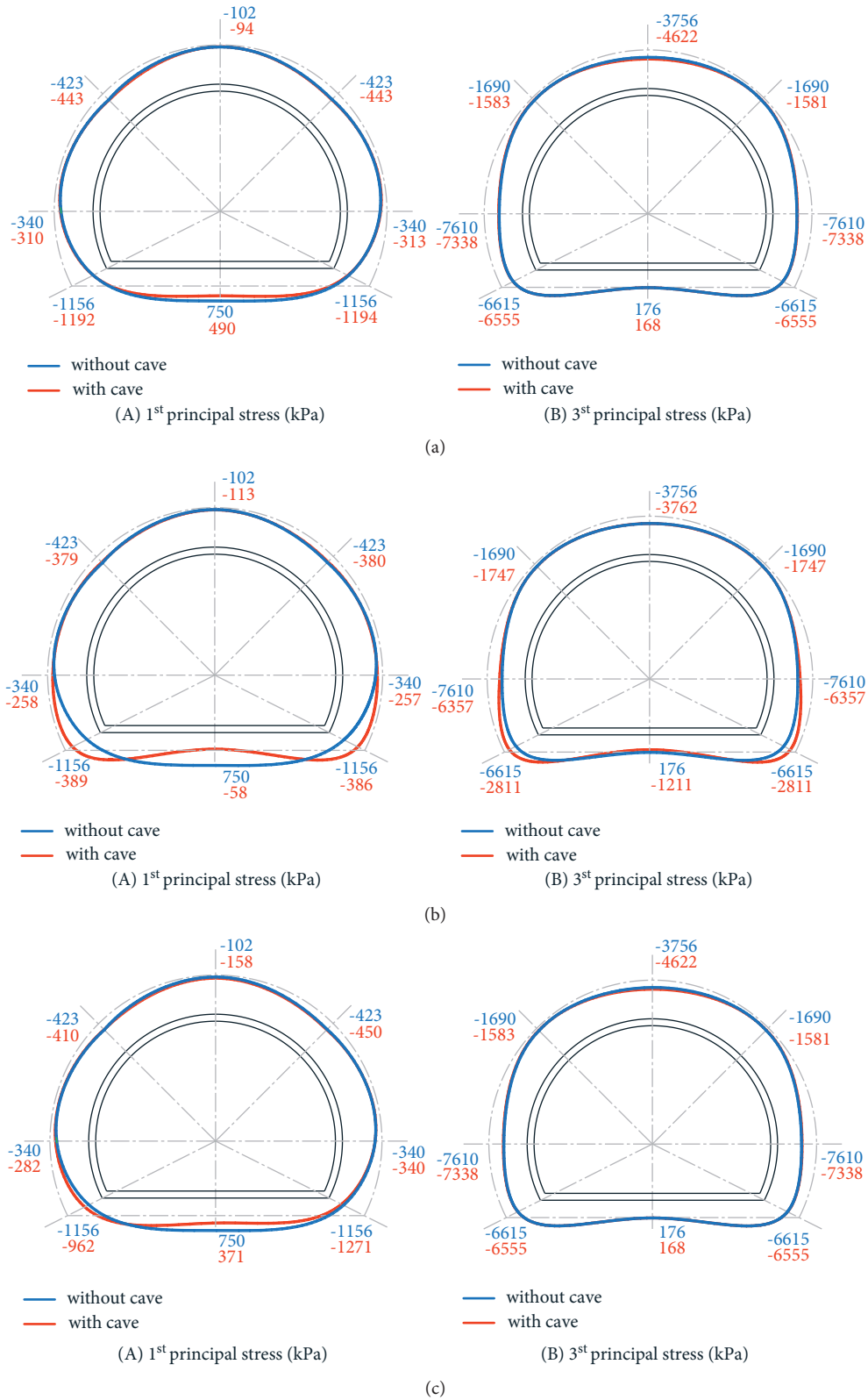
Figure 17: Tunnel lining stresses under working conditions 4 to 6. (a) Working condition 4. (b) Working condition 5. (c) Working condition 6.

4. Conclusion

A two-dimensional rock-tunnel hydromechanical model with a karst cave was established with FLAC3D finite difference software to simulate the tunnel excavation with the consideration of seepage. Numerical simulations were performed to analyze the deformation of the surrounding rock, the seepage field of the surrounding rock, and the stress of the tunnel lining, and the results were compared for scenarios when the karst cave is at different locations relative to the tunnel. The following conclusions can be obtained:

(1) Due to the existence of karst caves, the seepage path on the side close to the karst cave is blocked after the tunnel is excavated, and the karst cave acts as a shield. A cave located at the side of the tunnel results in the significant decrease of the pore pressures near the cave when the distance of the cave to tunnel is less than 2 m. When there is a karst cave, the seepage paths of surrounding rock near the cave were greatly affected, accompanied by the increase in flow vector at the arch foot of the opposite side of the cave. When a cave is at different locations of the tunnel, the seepage flow causes the pore pressure near the cave to be reduced.

(2) A cave located at the side of the tunnel also causes the increase in settlement at the vault and outward expansion at the hance near the cave. When the karst cave was located above the tunnel the settlement at the vault increased and the uplift at the bottom decreased, otherwise the opposite. When the karst cave is located in the upper left of the tunnel, the uplift at the bottom of the tunnel increased considerably.

(3) A cave located at the upper area of tunnel results in the increase of the tunnel compressive stress near the cave, while a cave located at the lower area of tunnel results in the decrease of the tunnel compressive stress near the cave.

(4) When constructing tunnels in karst areas, the relative position and distance between the karst cave and the tunnel to be built should be ascertained in advance. For the case where the distance between the karst cave and the tunnel is very close, the reinforcement measures on the karst side of the tunnel must be strengthened to prevent large uneven deformation of the tunnel. At the same time, except for the case where the karst cave is located at the bottom of the tunnel, the vault in other working conditions is a weak point, and reinforcement measures for the vault should be strengthened.

Data Availability

Some or all data, models, or codes that support the findings of this study are available from the corresponding author upon reasonable request.

Conflicts of Interest

The authors declare that they have no conflicts of interest or personal relationships that could have appeared to influence the work reported in this study.

Acknowledgments

References

[1] Y. Lu, Q. Liu, and F. E. Zhang, "Environmental characteristics of karst in China and their effect on engineering," *Carbonates and Evaporites*, vol. 28, no. 1-2, pp. 251–258, 2013.

[2] F. Gutiérrez, M. Parise, J. de Waele, and H. Jourde, "A review on natural and human-induced geohazards and impacts in karst," *Earth-Science Reviews*, vol. 138, pp. 61–88, 2014.

[3] S. Alija, F. J. Torrijo, and M. Quinta-Ferreira, "Geological engineering problems associated with tunnel construction in karst rock masses: the case of gavarres tunnel (Spain)," *Engineering Geology*, vol. 157, pp. 103–111, 2013.

[4] K. I. Song, G. C. Cho, and S. B. Chang, "Identification, remediation, and analysis of karst sinkholes in the longest railroad tunnel in South Korea," *Engineering Geology*, vol. 135-136, pp. 92–105, 2012.

[5] H. Wang, E. Binder, H. Mang, Y. Yuan, and B. Pichler, "Multiscale structural analysis inspired by exceptional load cases concerning the immersed tunnel of the Hong Kong-Zhuhai-Macao bridge," *Underground Space*, vol. 3, no. 4, pp. 252–267, 2018.

[6] H. Wang, H. Mang, Y. Yuan, and B. L. A. Pichler, "Multiscale thermoelastic analysis of the thermal expansion coefficient and of microscopic thermal stresses of mature concrete," *Materials*, vol. 12, no. 17, p. 2689, 2019.

[7] H. W. Chen and C. Sha, "Stability analysis of surrounding rock and treatment structures in superlarge karst cave of naqiu tunnel," *Advances in Civil Engineering*, vol. 2018, Article ID 4842308, 14 pages, 2018.

[8] Y. X. Lv, Y. J. Jiang, W. Hu, M. Cao, and Y. Mao, "A review of the effects of tunnel excavation on the hydrology, ecology, and environment in karst areas: current status, challenges, and perspectives," *Journal of Hydrology*, vol. 586, no. 1–15, 2020.

[9] X. Huang, S. Li, Z. Xu, M. Guo, and Y. Chen, "Assessment of a concealed karst cave's influence on karst tunnel stability: a case study of the huaguoshan tunnel, China," *Sustainability*, vol. 10, no. 7, pp. 1–26, 2018.

[10] W. Wang, S. Gao, L. Liu, W. Wen, P. Li, and J. Chen, "Analysis on the safe distance between shield tunnel through sand stratum and underlying karst cave," *Geosystem Engineering*, vol. 22, no. 2, pp. 81–90, 2019.

[11] F. Huang, L. Zhao, T. Ling, and X. Yang, "Rock mass collapse mechanism of concealed karst cave beneath deep tunnel," *International Journal of Rock Mechanics and Mining Sciences*, vol. 91, pp. 133–138, 2017.

[12] H. Chen and C. Sha, "Stability analysis of surrounding rock and treatment structures in superlarge karst cave of naqiu tunnel," *Advances in Civil Engineering*, vol. 2018, Article ID 4842308, 14 pages, 2018.

[13] Y. Zhao, Q. Peng, W. Wan, W. Wang, B. Chen, and B. Chen, "Fluid-solid coupling analysis of rock pillar stability for concealed karst cave ahead of a roadway based on catastrophic

theory," *International Journal of Mining Science and Technology*, vol. 24, no. 6, pp. 737–745, 2014.

[14] R. L. Shan, X. N. Zhang, and M. Lu, "Numerical application of safe thickness between a tunnel and surrounding concealed caves," *Geotechnical and Geological Engineering*, vol. 36, no. 1, pp. 95–104, 2018.

[15] W. Wang, S. Gao, Y. Min, L. Liu, and J. Chen, "Three-dimensional fluid-solid coupling numerical simulation of effects of underlying karst cave on shield tunnel through sand stratum," *Geotechnical and Geological Engineering*, vol. 37, no. 6, pp. 4825–4836, 2019.

[16] M. J. Day, "Karstic problems in the construction of milwaukee's deep tunnels," *Environmental Geology*, vol. 45, no. 6, pp. 859–863, 2004.

[17] V. M. Koutepov, O. K. Mironov, and V. V. Tolmachev, "Assessment of suffosion-related hazards in karst areas using GIS technology," *Environmental Geology*, vol. 54, no. 5, pp. 957–962, 2008.

[18] Q. L. Cui, H. N. Wu, S. L. Shen, Y. S. Xu, and G. L. Ye, "Chinese karst geology and measures to prevent geohazards during shield tunnelling in karst region with caves," *Natural Hazards*, vol. 77, no. 1, pp. 129–152, 2015.

[19] Q. Ai, Y. Yuan, S. Mahadevan, and X. Jiang, "Maintenance strategies optimisation of metro tunnels in soft soil," *Structure and Infrastructure Engineering*, vol. 13, no. 8, pp. 1093–1103, 2017.

[20] Q. Ai, Y. Yuan, S. L. Shen, H. Wang, and X. Huang, "Investigation on inspection scheduling for the maintenance of tunnel with different degradation modes," *Tunnelling and Underground Space Technology*, vol. 106, Article ID 103589, 2020.

[21] Z. H. Xu, J. Wu, S. C. Li, B. Zhang, and X. Huang, "Semi-analytical solution to determine minimum safety thickness of rock resisting water inrush from filling-type karst caves," *International Journal of Geomechanics*, vol. 18, no. 2, Article ID 04017152, 2018.

[22] China Merchants Chongqing Transportation Research and Design Institute Co. LTD, *Specifications for Design of Highway Tunnels*, Ministry of Communications of the People Republic of China, Beijing, China, 2014.

[23] Y. F. Zhou, *Study on Seepage-Stress-Damage/Crack Coupling Theory and Method for Hydraulic Tunnel*, Wuhan University, Wuhan, China, 2016.

[24] Z. B. Yu, *Principles of Groundwater Hydrology*, Science Press, Beijing, China, 2008.

Research Article

Requirements for the Optimal Design for the Metasystematic Sustainability of Digital Double-Form Systems

Gaurav Dhiman ⓘ,[1] **Gaganpreet Kaur** ⓘ,[2] **Mohd Anul Haq** ⓘ,[3] **and Mohammad Shabaz** ⓘ[2,4]

[1]*Government Bikram College of Commerce, Patiala, Punjab, India*
[2]*Department of Computer Science Engineering, Chandigarh University, Mohali, Punjab, India*
[3]*Department of Computer Science, College of Computer Science and Information Science, Majmaah University, Al Majmaah 11952, Saudi Arabia*
[4]*Arab Minch University, Arba Minch, Ethiopia*

Correspondence should be addressed to Mohammad Shabaz; mohammad.shabaz@amu.edu.et

The United Nations defined tenable progress as a development that responds to the demands of the current without adjusting the capacity of further generations to fulfil their own requirements; this is a fundamental idea in this article. This study recognizes three aspects, financial, social, and environmental sustainability, although its emphasis is on the latter. An electronic copy is sometimes characterized a physical thing, a real counterpart, and the data, which indicates the presence of a connector and block for effective and efficient data transmission. This article offers a systematic literature review on the sustainability of designed technology-based systems. This article also introduces the major requirements which can be helpful in designing optimal design for sustainability of a digital double-form system. Many articles on DT have also been chosen since they referenced the studied SLRs and were deemed to be significant for the objectives of this study. Selected and analysed for papers revealed so many flaws and challenges: the boons of are not clear; DTs throughout the result the wheel of life of the DTs is not adequately surveyed; DTs can contribute to cost reduction or to support decision-making is unclear; Internet practice should be improved and better integrated Moreover, it has not been feasible from our study to locate a publication which solely discusses DTs in relation with situational sustainability.

1. Introducing the Report

An electronic copy (DT) is frequently characterized as an electronic, real body with a physical counterpart and data links including connectors and blocks, which make efficient and efficient transmission of the data possible. It is an electronic representation of a more complicated physical system and despite the various explanations of DT, and it is the original one, and we accept it [1]. The pioneers of this idea are Grieves and Vickers of NASA and presented on product cycle management and recognised. They mention features such as (i) the practical output, (ii) an online representation, and (iii) bidirectional data interfaces between practical and real representation. Output design, modelling, simulation, and optimisation of assets are the primary objectives of DT development [2, 3].

Today, the use of DTs has not yet been widespread, but since 2015, scientific research has clearly increased to better grasp their potential. Common instances of DT use include machine tools and consumer products. In all instances, however, a DT must not a big-trust digital replica of a real data. For example, a DT may also be used to represent tangible assets such as whole city (urban digital twin), geographical constructions, and human organs. Other uses of building DTs have been identified for cybersecurity incidents, ergonomics monitoring virtual study, and agricultural optimisation [4]. Output style also constitutes a key and connected element of DT and environmental sustainability since it covers many complicated choices and hybrid-cutting issues, such as safety or tenability (the preference of matters or the use of energy). In addition, output style may affect the planning of a manufacturing line, an additional common use

of DTs [5, 6]. This allows mistakes and failures to be anticipated and controlled by means of DT methods utilising data analysis and machine learning techniques as well as artificial intelligence (AI). "Our Common Future" (the United Nations (1987)) defines tenable development as a development that addresses current demands minus adjusting the capacity of further procreation to fulfil needs. This framework is extremely helpful since the idea of the rounded Economics Circular Economy (CE) described as an economic model to reduce limited resource use and is becoming increasingly significant and is strongly linked with the supply chain concept [7, 8]. In 2011, Industry 4.0 has been introduced to a synonym of intelligent manufacturing/ manufacturing that corresponds to make statements, like electronic-union making, a dynamic making organisation, CE, and the management of a large volume of DT information [9, 10].

The idea of tenable product design, as described by craft of styling buildings, cities, and other artefacts to fulfil the sustainable development goals is closely related to output design optimisation and CE. Output design is not only art but also a choice as to what materials to employ, so that a product is helpful to society. A DT has a closely linked sustainable product design, as described in this study, but our emphasis will be its IT features and advantages [11, 12].

This article offers a metaphorical writings survey (i.e., an SLR on SLRs) on DT-based systems sustainability needs. In this sense, the criteria of sustainability are defined as conditions which permit sustainable development. Marten et al. attempted to use general knowledge to help with the criteria specified automatically, a list of overview and IT details for every aspect of sustainability (environmentally, technologically, socially, economically, and individually) and their impact. Furthermore, a new design and ideas have been developed like the impacts between requirements, either negate, impartial, or definite [13, 14]. This new attitude is utilised to build a system that respects the proper balance between various aspects in order to get tenability, the controlled natural language, that systematically and rigorously helps specify requirements and tests such as the IT Lingo Request-and-Status Link (RSL) and it plays an important part in explaining sustainable software needs as, for example, it helps challenges, vulnerabilities, and objectives/solutions [15, 16]. These tools are part of the model-based engineering spectrum, utilising textual and conceptual requirements to enhance the effectiveness, effectiveness, and effectiveness of the study and style and their usefulness [17, 18].

This research work introduces an optimal design for the metasystematic sustainability of digital double-form system. The major benefits of using this system are that it will provide more security than previously used systems. Also, the SLR technique developed introduces three stages, which further enhance the sustainability of the system.

In short, this article is a meta-SRL (The Saturday Review of Literature) plus an effort at adding fresh credit to the discussion on environmental sustainability. Sustainable development nowadays means responsible resource use, and

since DTs may enable the operations to be optimised, this can be a tool to that end. In testing new product, and designers may use to digitally test the new application without using raw resources and modelling the use of ecologically compatible materials; saving working times and only then if the simulation is useful [19, 20].

The current study summarises notable research publications on DT-based systems and technology, which uses the SLR technique as the primary instrument for a meta-analysis on SLR. The language that will be used to conduct research in various databases has been determined. This article provides a meta-SLR that allows us to notice and debate the major classes of needs that must be considered in sustainable DT development, also highlighting gaps and limitations in research and practise.

This paper is structured accordingly: Section 2 provides the following SLR technique; Section 3 gives the meta-SLR findings; Section 4 presents a critical analysis to suggest future work routes. Finally, the major findings of Section 5 are presented.

2. Methodology for Research

In developing this study, we examined Kitchenhand et al.'s approach for program architecture, and then we looked at the work of Escalon and Aldean, since they provided a technique that is useful in this work [21, 22]. The SLR technique developed includes three major stages: a planning phase, the execution of this plan and an analysis of the outcomes. The starting phase includes projects: (i) extracting studies from databases, (ii) removing copies from the tests, (iii) applying criteria for inclusion and exclusion, and (iv) collecting backward and forward citations, and (v) determining the end of the chosen article information sets. If fresh documents have been discovered at task IV, then the researcher reverses to task (ii) and continues the procedure as often as necessary, from task (ii) to task (iv). Additionally, we have also incorporated the backward and forward citation procedures in its selection phase [26], reported by Wolfs Winkel et al. If there is no research job in the presently chosen collection, it is deemed tenable; it should be added to those selected. Because it is a highly popular tool that enables retrospective and forward survey of citations, it is the primary tool. The entire procedure is shown Figure 1, influenced by Escalon and Aldean methodology [23].

In order to make our study more accurate, examined the trial. They specifically indicated and classified the various kinds of accessible regulated or common vocabulary and the use of software development criteria, which were essential since we wanted to concentrate on establishing sustainability needs [24, 25]. It aims to arrange information consistently in a structured way that identifies semantical connections and allows for the easy categorization, query, and retrieval of information. The most common controlled vocabularies (CVs) are ontology, taxonomy, thesaurus, and folksonomy. Natural language processing and knowledge management often utilize tools for CV assistance [26].
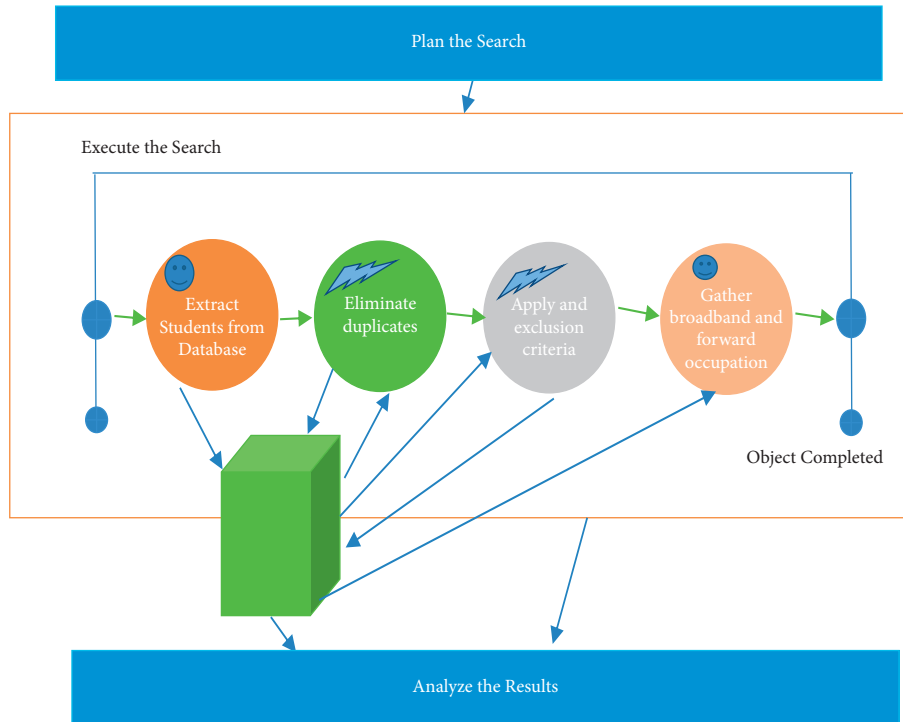
FIGURE 1: SLR's overall procedure (in BPMN notation).

2.1. Phase of Planning. The design phase is the component in which the SLR is carried out in agreement with the chosen scheme. The connection between sustainability needs and DT systems is addressed, followed by the establishment of relationships to product design. It outlines the key issues that drove this study; sections deal with scientific repositories and search queries as well as the criteria of inclusion and exclusion [27, 28].

2.1.1. Analysis of Study. We have explained survey issue (RQ1) with three sections (SQ). These queries were used to meet the major study goals:

(1) Which is the state of the art in the field of DT-based products design sustainability requirements?

(2) Which is the connection between DTs and output style?

(3) SQ2 : what are the criteria of DTs for environmental sustainability?

(4) SQ3 : what are outstanding questions and difficulties in future DT and sustainability research paths?

The search method takes account of these issues, network explanation accessible in the current literature and the following reading of the discovered work is also necessary.

2.1.2. Search Process. The following were the scientific information bases or repositories which searched for suitable documents to address the queries of this study. The information bases were chosen since they are widely known to the

scientific class and have also been utilised in previous SLR studies which we regarded to be IT domain models:

(1) ACM Electronic Library [dl.acm.org]

(2) Taylor and Francis (http://www.tandfonline.com, 4 June 2021 accessed)

(3) Science web (http://www.webofknowledge.com)

(4) ScienceDirect/Scopus (http://www.scopus.com, 4 June 2021)

(5) Exploration of IEEE (i.e., explorer. Search/advanced)

(6) Elsevier (http://www.elsevier.com)

(7) Google Scholar

These were the conditions for inclusion: (i) article written during the last period; (ii) work written in journals and in conference papers or indexed books; (iii) work written in English; (iv) SLR papers chosen in the initial research database. They were brief oppositely, these were the conditions of exclusion: (i) extremely brief (i.e., less than 6 pages) publications and (ii) repeated works united with the information base under different reference [29, 30].

2.1.3. Requests. In the first week of January 2021, we began the question "orderly survey of the literature" AND "electronic copy" (all areas) and then tried out various inquiries, not only considering the primary goal of this paper but also the articles we discovered and the potential to deepen our search. The initial work was to look for documents about a DT meta-SLR, and the second was to find sustainable criteria [31, 32]. The survey period was also examined, firstly, the

dates of publishing between 1 January 2011 and 31 January 2020, and secondly, the dates of publication between 01/01/2009 and 31 December 2020. As a result, many other inquiries have been utilised:

(1) [All: "systematic evaluation of literature"] AND [All: "Expectations"] YEAR [All: 'digital twin ∗ '] AND ("Document title": "Digi table twin • IEEE) : AND ("All metadata": ALL Metadata": ALL Metadata Review); and ("All Metadata": ALL Metadata Review") AND ("ALL Metadata": DESIGN"). ALL Metadata ("ALL DOCK Title": ALL Metainformation");

(2) (systematic review of literatures) and Name-ABS-KEY (systematic review of literature) AND ("ontology" and "electronic copy"); SCOPUS (systematic literary review).

(3) Science Web: ["electronic copy"] AND [All: "systematic review of literature"] [All: "product design"] AND TICK: (systematic review of literature "electronic copy ∗ ") and TITLE: (systematic reviews of literature AND "ontology ∗ ").

We have produced different scientific results in various databases and thus have had to utilise alternative searches. The keyword search for "milieu tenability" was unsuccessful.

2.2. Phase of Execution. The execution stage is the work in which both the findings and the execution of the SLR are described. We have followed the previously stated stages and criteria and will explain our experience and the valuable information we were able to collect throughout this procedure. The questions were given in the above information bases, and the output is shown [33, 34]. After we received the findings from these databases, the following procedures have been completed. The first is to remove duplicates; secondly, if barring criteria apply based on the titles; thirdly, on the basis of the titles, to pick articles where the criteria of inclusion and exclusion does not mention, for left out paper, examine the name section and reread steps 2 to 4; sixthly, Google Scholar will check the forward quotations for each appropriate reference and reread steps 2 to 4 for each remaining article [35].

A first search (see Table 1's column on "First search") enabled us to find works, and a second search allowed Google Scholar to identify citations (see Google Scholar columns). Relevant articles may be identified to evaluate the factors of DT use even if they are not SLRs (see column "non-SLR"). Finally, it was able to choose 29 articles, ("Selected Papers" column, including papers), to view abstracts from the papers [36, 37]. Table 2 lists SLR papers, while Table 3 lists non-SLR papers. The documents in question are article, T-these and B-Book. The SLR articles selected are relatively recent: 2020 (10 documents); 2019 (2 documents) and 2018 (18 documents).

(1 document) The same goes to chosen documents: 2020 (12 documents); 2019 (2 papers); 2016 (1 paper); 2013 (2 papers) (1 paper). This is hardly unexpected since the technology and problems examined are relatively recent as shown in Figure 2.

TABLE 1: Survey in information bases.

Data base	Survey	With Google Scholar	SLR	Non-SLR
ACM	6.2	15.4	3.1	7.3
Elsevier	19.5	10.2	1.2	2.1
IEEE Explore	13.1	34.6	1.2	4.2
Scopus	12.01	43.4	4.1	1.1
Tailor	4.02	41.2	2.1	2.2
Web Science	7.05	16.02	2.2	0.1
Total	61.01	159.01	13.1	16.1

3. Survey of the Literature and Output

This part contains documents related to (i) determination of needs for sustainability and (ii) recognition of the connection between DTs and the design of the product. The two dimensions permitted to map the responses we consider. Papers were classified according to the two dimensions, which in each study were chosen by the dominating work [38, 39].

3.1. Sustainability and Digital Twins Requirements. There are four articles and 4 non-SLR papers among our chosen papers, primarily relating to DTs and sustainability. In addition, the definitions "state of the art" on DT development is examined by Pokharel, (S3) including the noted paper of the utility of DT for cybersecurity using the SRL approach. In terms of event predictions, the situations in which are used include oddity detection; distant and monitoring; practical monitoring; predictive study; documentation; and communication. Safety is one important aspect of tenability; if equipment is hazardous, its everyday use is impossible.

3.2. SLR Application. The SLR technique is used to evaluate the connection between CE and I4.0. They emphasise hybrid categories such as rounded I4.0 and digital EC, but continue to identify the key boons and integration, like technology, economic act, market growth, supply chain management, product life-cycle management, employee power, and business patterns 40, 41, 56.

Esmond, Gladys, and Kleczka (S6) conduct a literature analysis to assess the sustainability effect of trade. They discover that CE writers often also research tenable produce chains, but themes, such as tenability, huge information, smart production, IoT, tenable progress, electronic change, and trade IoT, are often mentioned [42]. Also, prevalent ideas include internet-practical systems, sustainable production, the smart factory, and digitisation. The major conclusion of their study is may be that the good result of these technologies in terms of sustainability is not guaranteed, which means success needs encouraging measures and particular regulations to maintain the competitiveness of local players [43, 44].

Rajput and Singh (S7) propose a CE and cleaner Industry 4.0 models. Its approach is based on linear programming with mixed-integer (MILP) to optimise the allocation of the machine's production, for example, to optimise the trade in

Table 2: Chosen SLR papers.

Serial no	Reference	Name	Year	Topic
1	[1]	Electronic copy characterization: a Comprehensive art survey.	2019	DTs definition
2	[2]	Digital twin review on ideas, technology, and trade programs.	2019	DTs definition
3	[3]	Cyber security prediction electronic copy: multivocal study	2020	DTs cyber security
4	[4]	Cyber-physical systems reference framework for digital twins	2020	DTs cyber practical systems
5	[10]	Evaluation of connections between rounded financial and trade 4.0: a Comprehensive study of art	2020	DTs, CE, 14.05
6	[33]	Sustainability influence of trade 4.0 - review of library literature	2019	DTs 14.05
7	[34]	Industry 4.0 rounded financial copy and cleaner manufacturing	2020	DTs, CE 14.0
8	[35]	Digital twin systems: Cosmology and contextual framework	2019	DTs outlook
9	[36]	A study of the active trade implementation art	2019	DTs,14.05
10	[37]	Digital twins: Smart City's current challenges and future technological recommendations	2018	DTs smart city
11	[38]	Electronic copy process of steel sawing	2020	DTs. Example
12	[39]	A systemic art study on ontology software in auto application	2019	DTs ontology
13	[40]	The double electronic trade context-a study and systems review	2019	DTs

Table 3: Chosen non-slr papers.

Id	References	Title	years	Kind	Subject
NS1	[8]	Improving experimental act and output boons via the use of intelligent brewing technology	2019	J	14.0
NS2	[41]	An assessment of the potential trade to speed the transition to a rounded finance	2020	T	14.0, CE
NS3	[42]	Energy cyber-physical system IoT-based digital twin: style and practice	2018	c	DTs, energy
NS4	[43]	A quantifying power and outlook boons framework for intelligent production technology	2019	C	14.0, power
NS5	[44]	Creating electronic copy' data resources	2019	j	DTs, data
NS6	[45]	On IoT intensive electronic copy application system engineering	2018	j	DTs, IOT
NS7	[46]	Electronic copy-depends upon health application style-a new medical/medical software development approach	2019	j	DTs eHealth
NS8	[47]	Digital twins taxonomy	2019	C	DTs
NS9	[48]	Define structure needs for electronic copy	2020	T	DTs needs
NS1O	[49]	Development of a structure for digital scoping of twins in the procedure trade	2020	J	DT's structure
NS11	[50]	An agenda new da gran industries: Uma analyse da industries [4], con base elm documents *e* matters de divulgence do projector alma industrial platform +4.0	2020	T	14.0
NS12	[51]	The modernization of the archives in order to provide support to transforaminal electronic	2020	C	Organization
NS13	[52]	To the operationalisation of the methodology of socio-technical engineering	2019	J	Outlook
NS14	[53]	Ontology applications in requirements engineering: a Comprehensive literature review	2019	J	Outlook
NS15	[54]	Fusing practical and electronic copy in the practise of rounded economics:	2016	C	DTs, CE
NS16	[55]	Specification study of application needs using natural words procedure method.	2013	J	Needs

power consumption and processing costs [45]. This model uses sensors to collect practical-period data in trade emphasises the difficulty of the new I4.0 and its related new technologies, e.g., 3D printing, to optimise production. Since no generation minus energy (meaning at trade level electricity, nonuseable sources of energy are still the most important contributor to power production), the next three papers examine the general need of "energy responsibly." Spear et al. [43] (NS4) provide a methodology for quantification of the advantages of smart manufacturing technology in terms of energy and productivity [46].

The example of this framework and the use of intelligent production technology are also explained. The framework utilises CCE (energy conservation cost) as a supplementary metric to evaluate the viability of a series of intelligent manufacturing actions. The emphasis is on the measurement and analysis of energy productivity and a strategic analytical frame has been created to predict cost-effective energy and productivity gains utilising smart production [47, 48].

Saad, Fadel and Mohammed (NS3) are studying the efficient and effective application of DTs in cyber-physical energy systems. With distributed energy resources (DERs), communications and controlling complexity, it is essential to provide an effective platform capable of digesting all incoming data and ensuring a dependable power system operation. Two different DT-types have been developed to
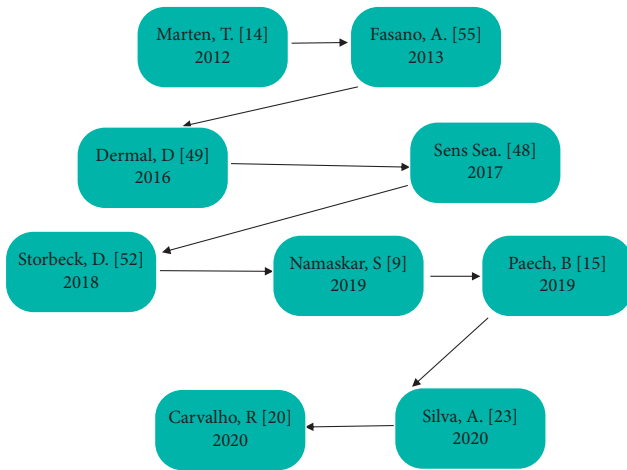
FIGURE 2: Existing work on digital twin.

construct this support technology: one for huge bandwidth applications and one for less bandwidth applications which need centralised surveillance decision-making [49, 50].

3.3. Electronic Copy and the Style of Products. The following documents are essential for a platform between DTs and product design. These articles present and evaluate issues which should be considered in actual situations while developing or constructing DTs: attempt to define the notion of DT using an SLR. The writers recognise that a range of definitions are used across business and the universities [51].

They identified thirteen features to explain the definition, namely practical/dual, virtual/dual, physical environment, virtual environment, state, metrology, twinning, twinning speed, virtual-to-virtual connection/twinning, practical process, and a whole structure and operating process of the DT [52, 53]. Literature overview of the DT based on ideas, technology and industrial applications is provided by Liu et al. (S2). They assess the present situation of the art, explain the idea of the DT, and examine several important DT enabling technologies. Furthermore, they describe 15 trade software's with their distinct life cycles, important insights and further work suggestions. Kosovska, Jigidas, and Engels (S4) are developing a DTs Reference Framework in internet-practical systems (CPSs). The writes describe CPS (characters per second) system representations that combine physical devices and processes via the Internet with computational entities that enable omnipresent research for data and duties. The framework creates a connection between the CPS architecture of 5 levels and the DT framework in order to address outstanding issues and difficulties about style and implement CPSs. Barth et al. (S8) systematises the DTs and creates a philosophical and ontological framework. In addition, the authors attempt to address three questions from the research: (i) what are the parameters for classifying and structuring DT in study literature? (ii) In these dimensions, what are the basic distinctions or specifications? And, (iii) how do the various requirements connect to one other? Bohemia and Rub (S9) explain to grasp the realities of the installation of a smart plant utilising and SLR. They highlight

a research gap associated with the choice to manufacture or purchase DTs and other key components of the smart factory. This is important since the smart factory is expected to lead to value creation, but this creation relies on how the facility is built, whether the project is done internally or utilising an external provider. Dave et al. (S10) explore the potential new reality of intelligent cities, where the latter's roles are highlighted by ideas like Big Data, Robotics, and DTs. The primary applications for DTs are smart cities, manufacturing, and healthcare. An example of how DT is used is its use in traffic management systems, employing traffic cameras that just record, but their recordings may be used to build traffic management models that help decrease traffic congestion and give more information to export and update the road network in real time. The authors suggest that demonstration sites are needed to evaluate real-life data in the new technologies and a need for broad expert panels in a variety of areas such as urban planning, IT, transportation, and environmental regulations. The DT example for the stone-sawing process is Pollini and Corrido (S11). The writer explains the DT but have reservations about the accuracy and efficiency of the apparatus. Reference [39] (S12) are using an SLR for studying potential usage of cosmology in automated programming. Ontologies that are usually regarded as technical or an artefact in one or more life cycle stages of software may be utilised to assist accomplish this. The objective of discovering greater levels of abstraction and methods to utilise application to improve its productivity and quality within the software engineering field. Jarod et al. (S3) are systematically studying the DT idea in the industry. Since 2015, the authors recognise a substantial increase in the quantity of scientific research (industry-related publications with the title "Digital Twin"). Studies demonstrate a range of DT applications from goods and processes to whole production systems [54, 55]. Explicit descriptions are somewhat contradictory, and related concepts like "Avatar product" and "Digital Shadow" have also been discovered. Their study broadened the theory and laid the groundwork further, better DT modelling and Mayrhofer (NS5) are working on data resources to generate DTs [56]. For companies transitioning from the production of products to the provision of services, DTs are regarded one of the essential technologies. The primary premise is that most of the new data or resources created while the start of phase of a product life cycle is not utilised in the middle of life (MOL). The new framework provides a better knowledge of how to utilise BOL data resources in MOL stages and enables the development of ontology of product data which facilitates DT generation and maintenance. NS6 is examining the engineering of IoT-intensive DT software systems carefully. The authors believe that the actual DT is a product equipped with several sensors or computer systems, which generates, consumes, and transfers data for diverse reasons. Because of this fact, DTs are often regarded as IoT-intensive systems. Lutze (NS7) is investigating eHealth's software design as a novel way to healthcare/medical product development. The DT idea of the writer makes on (i) personal digital twin as a patient's wife, (ii) a digital twin group that models the software's intended user group, and (iii) an electronic copy

system for the product itself. Agile development methods are believed to provide greater assistance in contrast to the classical software development based on the V-model, several aspects of DTs are identified: data connection, motive, conceptual components, interface, synchronisation, data input, and time generation. Jay (NS9) outlines the needs of infrastructure to create DTs. The author also expects that simulation is a fundamental system feature after 2015 with seamless support throughout its whole wheel of life, supporting the experiments and the service via a direct connection to operating data. Peron and Ham study manufacturing processes, and in that, setting they create a paradigm for DT scoping. Due to the uniqueness of the idea and the wide spectrum of technology it builds on, the digital scope processes.

For process businesses, dual projects may be intimidating. It attributes the new "Platform Industries 4.0″ initiative to its consequences. After a short description of its technology, (i) how existing legacy systems can be decentralised to deliver a technology solution which responds to a new user need electronic class and (ii)build a system architecture which displays the features of electronic change. Senses et al. (NS13) utilise SLR to find qualitative online engineering research. These writers' primary objective is to operationalize the socio-technical ontology approach.

Dermal [53] (NS14) utilises SLR to detect RE ontological applications (requirements architecture). The important survey of this study are (i) empirical evidence of the benefits of using ontology in RE activities is available, particularly to reduce ambiguity and incompleteness; (ii) the procedure usually is only partially dealt with, for example, only taking functional requirements into consideration; (iii) ontologies support large-scale RE modelling styles; Tools for supporting various types of RE ontology-driven approaches have been used/developed; (v) half the studies have followed recommendations on ontology-driven languages; (vi) large diversity of RE ontologies have been noticed; nevertheless; (vii) many promising research opportunities have been noticed. Other writers also provide important contribution for this debate. Rocca et al. (NS15) are trying to use VR, DT, and CE basketwork techniques and provide a scenario for laboratory applications: virtually test waste from the disassembler plant setup (WEEE) by utilising a sec of specialised simulation instruments. The authors highlight the significance of their work, owing to a growing consumer knowledge of climate change impacts, high demand instability in many industries, and the rapid simulation and digitisation of production processes. Fasano [55] (NS16) is proposing a software specification analysis utilising processing methods in the natural language. The author attempts to enhance the manufacturing process of the software product.

4. The Debate

The DT research is new, particularly after 2015, and the explanation of DT is ambiguous. However, irrespective of the ever-increasing complexity of their applications of DTs, such as industrial optimisation, and the sustainability of the product design process are agreed on. Furthermore, the absence of research with technical data may be difficult to use. A deeper examination of potential environmental sustainability advantages and product design may contribute to a visible grasp of the reality. Analysis of the literature available enables us to detect many elements of DT relationships, output style, and sustainability and, therefore, to reply to the real research question, we address the following subquestions (Qi):

(1) SQ1: how does DTs relate to product design? As for SQ1, from the chosen articles, we check that two connections with product design are mostly established: I DTs are digital goods fed with real-time data that play a vital role in understanding actual behaviours and adjustments required and (ii) DT testing are cheaper and simpler than creating latest practical copies.

(2) SQ2: what are the criteria of DT for environmental sustainability? About SQ2, the major environmental classes of sustainability criteria are based on the chosen literature: I (the management of energy use) the use of environmentally known matters. When CE is examined at I4.0, there is an obvious requirement a balance of and difficulty power consumption against the outcomes of the new application of technology. Perhaps the testing of DT and the creation of less complicated goods are the primary study issue.

(3) SQ3: what are the difficulties and risks in future DTs and sustainability research paths? As regards SQ3, the complexity reduction in building and installing DTs is just one route for future study in the first place and as previously stated. When the choice to deploy DTs at manufacturing level is considered the effect of complexity and energy consumption is crucial. This has an overall effect in terms of safety, environment, and financial sustainability on sustainability. The meta-SLR described enabled us to identify many outstanding research problems and difficulties. First, techniques and processes are required to develop and execute DTs. This should be taken into consideration because there are many application domains with their peculiarities. Although there are comprehensive explanations of DTs how to realise them is unclear, particularly if no prior experience is available. Secondly, SL R&D studies show gaps like: I the boons have not been discovered; (ii) DT is not adequately investigated life cycle or the DT life cycle (iii) It is unclear to contribute to cost reduction or improvements in service or supporting decision-making; (iv) technical implementation must be improved and detailed under IoT; (v) the loyalty standard is not assessed in terms of the number of parameters, their accuracy and levels of IoT As previously stated, DTs are a new technology, partly explaining these gaps or varied potential pathways to study.

At the same time, the DT idea is being explicitly defined, such as the classification of current levels such as "Platform trade 4.0," describing a standardised DT in the I4.0 [47]. If

DTs are identified in various ways and situations, how can the most significant break in the study of sustainability in DT use be identified? We start with the premise that DT is made up of three elements: I a physical product, (ii) a virtual product and (iii) links and data that flow between them. Then, we presume that its primary contribution to sustainability may be identified at the technical implementation and at a certain degree of accuracy. RQ1: what is the state of the art in the field of DT-based products design sustainability requirements??

Finally, we must deal with our initial research question RQ1. Despite the current limitations, the literature highlights certain sustainability criteria of DT-based product design systems: I loyalty; (ii) power management; (iii) complexity control; (iv) environmental and cost-effective material identification; and (v) simple replication of new product designs. Various researches examine different sustainability criteria and no comprehensive methodology is available to comprehend how DTs may promote environmental sustainability. For instance, a completely stringent fidelity requires extra period and further energy expenditure, and this output may produce a compromise that results in fleeting loyalty. This fluid fidelity implies that environmental costs remain external to output since assessment of these costs would likewise involve additional labour and expenses. Easy premanufacturing of new product designs may lead to a lower cost of the manufacturing level.

5. Findings

In the study, significant research paper on DT-based systems and technology may be identified utilising the SLR technique as the primary instrument for a meta-analysis on SLR. The selection of language used for research in various databases has been given consideration. Based on this study, the RQ1 and the SQ1, SQ2, and SQ3 subquestions may be answered. Five major issues must be addressed in developing a tenable:

(i) Loyalty; (ii) power control; (iii) complexity control; (iv) environmental and economically efficient material identification; and (v) simple replication of new product designs. Furthermore, research topics relating to DTs may be identified: (i) investigate their idea and description 1, 4, 35, 36, 40, 47; (ii) presenting instances 38, 56; and (iii) using SLR to analyse existing research and suggest future pathways for research [2, 10, 33, 37]. SLR research is also available. The study enables us to identify two major gaps in two potential directions of research. The first break is the lack of a comprehensive article that explains precisely what a DT is, with a rich and complete example that underlines the features of the hardware and the links between the practical and electronic dimensions may be constructed, developed, and maintained. This fact may be explained by the trade reluctance to divulge sensitive information that the school fulfils. Second, articles were found with tenability in software's and, moreover, recognise research that differentiate between various kinds of sustainability Environmental sustainability included. Moreover, we find documents where the link with the use of DTs is explicitly established in the context of Industry 4.0. However, a study could not be found

that addresses the environmental sustainability SLR of DTs alone. Is this simply a matter of language, with CE equivalent to environmental tenability? We think the result is negative because CE, on the plant level, is still a laboratory idea, and the complexity implicit in its implementation may be of the utmost importance. In other words, in order to assess this hypothesis, the issue of whether CE is ecologically sustainable when management and technically difficult is so remarkable, a future investigation route may be a scenario in which a nil environmental impact product is designed.

This article offers a (SLR) on the sustainability DT-based systems. Many articles on DT have also been chosen since they referenced the studied SLRs and were deemed to be significant for the objectives of this study. Selected and analysed for papers revealed so many flaws and challenges: the boons of are not clear; DTs throughout the result the wheel of life of the DTs is not adequately surveyed; DTs can contribute to cost reduction or to support decision-making is unclear; Internet practice should be improved and better integrated Moreover, it is not been feasible from our study to locate a publication which solely discusses DTs in relation with situational sustainability.

In summary, this article provides the meta-SLR that allows us to notice and debate the major classes of needs to be considered in sustainable DT development, but that also highlight gaps and limits in research and practise. This study can be useful in designing a frame for developing sustainable systems that can be more reliable and feasible in future in understanding SLR better. The future scope with regard to the present study is to relate the summarized findings with the recent developments capable to cater the needs of future requirements in the field of optimal design for the meta-systematic sustainability of digital double-form systems.

Data Availability

The data shall be made available on request.

Conflicts of Interest

The authors declare that they have no conflicts of interest.

Acknowledgments

References

[1] D. Jones, C. Snider, A. Nassehi, J. Yon, and B. Hicks, "Characterising the Digital Twin: a systematic literature review," *CIRP Journal of Manufacturing Science and Technology*, vol. 29, pp. 36–52, 2020.

[2] S. Tang and M. Shabaz, "A new face image recognition algorithm based on cerebellum-basal ganglia mechanism," *Journal of Healthcare Engineering*, vol. 2021, pp. 1–11, 2021.

[3] M. Liu, S. Fang, H. Donga, and C. Xu, "A digital twin review of ideas, technology, and applications for industry," *Journal of Manufacturing Systems*, vol. 2020, pp. 346–361, 2020.

[4] A. Pokharel, V. Katta, and R. Colombo-Palacios, "Digital Twin for Cybersecurity Incident Prediction: A Multivocal Literature Review," in *Proceedings of the 42nd International*

Software Engineering Workshop (ICSEW) Conference in 2020 IEEE/ACM, pp. 671–678, Seoul, Korea, June 2020.

[5] K. Mahajan, U. Garg, and M. Shabaz, "CPIDM: a clustering-based profound iterating deep learning model for HSI segmentation," *Wireless Communications and Mobile Computing*, vol. 2021, pp. 1–12, 2021.

[6] K. Kosovska, E. Jigidas, and G. Engels, "Reference framework for digital twins within cyber-physical systems," in *Proceedings of the IEEE/ACM 5th International Workshop on Software Engineering for Smart Cyber-Physical Systems (Sespe)*, pp. 25–31, Montreal, QC, Canada, May 2019.

[7] R. Minerva, G. M. Lee, and N. Crespi, "Digital twin in the IoT context: a survey on technical features, scenarios, and architectural models," *Proceedings of the IEEE*, vol. 108, no. 10, pp. 1785–1824, 2020.

[8] S. Sapsagos, "Digital twin and web-based virtual gaming technologies for online education: a case of construction management and engineering," *Applied Sciences*, vol. 10, Article ID 4678, 2020.

[9] C. Vrouw, B. Ticonderoga, A. Belen's, and S. Wolfelt, "Digital twins in farming systems," *Agricultural Systems*, vol. 189, Article ID 103046, 2021.

[10] S. Namaskar, S. Spear, W. Meadows, T. Winning, W. Guo, and J. Cresco, *Enhancing Operational Performance and Productivity Benefits by Implementing Smart Manufacturing Technologies in Breweries*, pp. 93–107, Oak Ridge National Laboratory, Oak Ridge, TN, USA, 2019.

[11] S. Deshmukh, K. Thirupathi Rao, and M. Shabaz, "Collaborative learning based straggler prevention in large-scale distributed computing framework," *Security and Communication Networks*, vol. 2021, pp. 1–9, 2021.

[12] Brundtland Commission, *Our Common Future: The Brundtland Report* Oxford University Press, Oslo, Norway, 1987, https://sustainabledevelopment.un.org/content/documents/5987our-common-future.pdf.

[13] P. Rosa, C. Sassanelli, A. Urbinati, D. Chiaroni, and S. Terzi, "Assessing relations between Circular Economy and Industry 4.0: a systematic literature review," *International Journal of Production Research*, vol. 58, no. 6, pp. 1662–1687, 2020.

[14] C. Dou, L. Zheng, W. Wang, and M. Shabaz, "Evaluation of urban environmental and economic coordination based on discrete mathematical model," *Mathematical Problems in Engineering*, vol. 2021, pp. 1–11, 2021.

[15] E. Samedi and I. Kasson, "The relationship between it and supply chain performance: a systematic review and future research," *American Journal of Industrial and Business Management*, vol. 6, pp. 480–495, 2007.

[16] A. Greco, M. Caterino, M. Fera, and S. Gerbino, "Digital twin for monitoring ergonomics during manufacturing production," *Applied Sciences*, vol. 10, no. 21, Article ID 7758, 2020.

[17] J. Massey, "The sumptuary ecology of buckminster fuller's designs," in *A Keener Perception, Ecocritical Studies in American Art History*, pp. 189–212, University Alabama Press, Tuscaloosa, AL, USA, 2009.

[18] T. Marten, T. Schäfer, and S. Burner, "Using RE knowledge to assist automatically during requirement specification," in *Proceedings of the 2012 Seventh IEEE International Workshop on Requirements Engineering Education and Training (REET)*, pp. 9–13, Chicago, IL, USA, September 2012.

[19] B. Paech, A. Moreira, J. Araujo, and P. Kaiser, "Towards a systematic process for the elicitation of sustainability requirement," in *Proceedings of the CEUR Workshop Proceedings, 8th International Workshop on Requirements Engineering for Sustainable Systems, RE4SuSy 2019*, Juju, Korea, September 2019.

[20] K. Jairath, N. Singh, V. Jagota, and M. Shabaz, "Compact ultrawide band metamaterial-inspired split ring resonator structure loaded band notched antenna," *Mathematical Problems in Engineering*, vol. 2021, pp. 1–12, 2021.

[21] D. Macie, A. Paiva, and A. Rodrigues da Silva, "From requirements to automated acceptance tests of interactive apps: an integrated model-based testing approach," in *Proceedings of the 14th International Conference on Evaluation of Novel Approaches to Software Engineering*, Heraklion, Crete, Greece, May 2019.

[22] A. Paiva, D. Macie, and A. Silva, "From requirements to automated acceptance tests with the RSL language," in *Proceedings of the International Conference on Evaluation of Novel Approaches to Software Engineering*, vol. 1172, Heraklion, Crete, Greece, May 2019.

[23] J. Karamoja, A. Silva, S. Mon fared, A. Ribeiro, P. Calando, and T. Breaux, "RSL-IL4Privacy: a domain-specific language for the specification of privacy-aware requirements," *Requirements Engineering*, vol. 24, pp. 1–26, 2019.

[24] A. Silva, "Rigorous specification of use cases with the RSL language," in *Proceedings of the International Conference on Information Systems Development'2019, AIS*, Toulon, France, August 2019.

[25] R. Carvalho and A. Silva, "Discussion towards a library of software sustainability requirements," in *Proceedings of the 9th International Workshop on Requirements Engineering for Sustainable Systems (RE4SuSy) at RE'2020*, Zurich, Switzerland, September 2020.

[26] L. Gonçalves and A. Silva, "Towards a catalogue of reusable security requirements, risks and vulnerabilities," in *Proceedings of the International Conference on Information Systems Development'2018, AIS*, Lund University, Sweden, August 2018.

[27] A. Rodrigues da Silva, "Model-driven engineering: a survey supported by the unified conceptual model," *Computer Languages, Systems and Structures*, vol. 43, pp. 139–155, 2015.

[28] A. Silva and C. Siqueira, "Towards a library of usability requirements," in *Proceedings of the ACM SAC'2020 Conference, ACM*, Brno Czech Republic, April 2020.

[29] B. Kitchenhand, P. Brereton, D. Bugden, M. Turner, J. Bailey, and S. Linkman, "Systematic literature reviews in software engineering- a systematic literature review," *Information and Software Technology*, vol. 51, pp. 7–15, 2009.

[30] R. Escalon and A. Aldea, "On enterprise architecture patterns: a systematic literature review," in *Proceedings of the 22nd International Conference on Enterprise Information Systems (ICEIS 2020)*, pp. 666–678, Setúbal, Portugal, May 2020.

[31] J. F. Wolfswinkel, E. Furtmueller, and C. P. M. Wilderom, "Using grounded theory as a method for rigorously reviewing literature," *European Journal of Information Systems*, vol. 22, no. 1, pp. 45–55, 2013.

[32] A. Ahmad, J. L. B. Justo, C. Feng, and A. A. Khan, "The impact of controlled vocabularies on requirements engineering activities: a systematic mapping study," *Applied Sciences*, vol. 10, no. 21, Article ID 7749, 2020.

[33] F. Lease, "Controlled vocabularies: an introduction," *The Indexer*, vol. 26, pp. 121–126, 2008.

[34] A. R. da Silva and D. Savić, "Linguistic patterns and linguistic styles for requirements specification: focus on data entities," *Applied Sciences*, vol. 11, no. 9, Article ID 4119, 2021.

[35] J. Pollini and A. Ghose, "An automatic elaborate requirement specification by using hierarchical text classification," in

Proceedings of the 2008 International Conference on Computer Science and Software Engineering, pp. 706–709, Hubei, China, December 2008.

[36] S. Picard and D. Valspar, "Towards a controlled vocabulary on software engineering education," *European Journal of Engineering Education*, vol. 42, pp. 927–943, 2017.

[37] National American Standards Organisation, *NISO ANSI/NISO Z39.19-2005 Guidelines for the Construction, Format, and Management of Monolingual Controlled Vocabularies*NISO, Baltimore, MD, USA, 2010, https://www.niso.org/publications/ansiniso-z3919-2005-r2010.

[38] K. Jesmond, B. Gladys, and A. Kulczyk, "Impact of industry 4.0 on sustainabilitybibliometric literature Re-view," *Sustainability*, vol. 12, Article ID 5650, 2020.

[39] I. A. Inigo, *Review of Industry 4.0 Potential to Accelerate to Accelerate the Transition to a Circular Economy*, pp. 1–122, Master's Thesis, Industrial Engineering, Universidad de Pays Vasco, Escuela de Ingenerate de Bilbao, Bilbao, Spain, 2020.

[40] A. Saad, S. Faddel, and O. Mohammed, "IoT-based digital twin for energy cyber-physical systems: design and implementation," *Energies*, vol. 13, no. 18, Article ID 4762, 2020.

[41] S. Rajput and S. P. Singh, "Industry 4.0 Model for circular economy and cleaner production," *Journal of Cleaner Production*, vol. 277, Article ID 123853, 2020.

[42] B. Wang, X. Yao, Y. Jiang, C. Sun, and M. Shabaz, "Design of a real-time monitoring system for smoke and dust in thermal power plants based on improved genetic algorithm," *Journal of Healthcare Engineering*, vol. 2021, pp. 1–10, 2021.

[43] S. Spear, D. Graziano, M. Riddle et al., "A framework for quantifying energy and productivity benefits of smart manufacturing technologies," in *Proceedings of the 26th CIRP Life Cycle Engineering (LCE) Conference, Purdue University*, pp. 699–704, West Lafayette, IN, USA, May 2019.

[44] L. Barth, M. Ehret, R. Fuchs, and J. Harman, "Systematization of digital twins: ontology and conceptual framework," in *Proceedings of the ICISS 2020*, pp. 13–23, Cambridge, UK, March 2020.

[45] L. Schweiger, L. Barth, and J. Mayrhofer, "Data resources to create digital twins," in *Proceedings of the 2020 7th Swiss Conference on Data Science (SDS)*, pp. 55-56, KKL Luzern, Switzerland, June 2020.

[46] H. Valka, H. Have, F. Moller, M. Arbiter, J. Henning, and B. Otto, "A taxonomy of digital twins," in *Proceedings of the Americas Conference on Information Systems*, pp. 1–10, Waltham, MA, USA, August 2020.

[47] M. Jay, *Defining Infrastructure Requirements for the Creation of Digital Twins*, pp. 1–47, Master's Thesis, School of Innovation, Design and Engineering, RISE Research Institutes of Sweden, Malaren University Sweden, Vasteras, Sweden, 2020.

[48] M. Peron and L. Ham, *Developing a Framework for Scoping Digital Twins in the Process Manufacturing Industry*, in *Proceedings of the Swedish Production Symposium SPS2020*, pp. 1–12, Jönköping, Sweden, October 2020.

[49] J. Rub and H. A. Bohemia, "Review of the literature on smart factory implementation," in *Proceedings of the 2019 IEEE International Conference on Engineering, Technology, and Innovation (ICE/ITMC)*, pp. 1–9, Vallone Sophia-Antipolis, France, June 2019.

[50] P. Leon and F. Horite, "Modernizes de Acquitters de Sistema's para supported à Transforaminal Digital," in *Proceedings of the Anais Extended's do XVI Symposia Brassiere de Sistema's de Infor Macao, SBC*, pp. 61–66, Brazil, November 2020.

[51] D. Sens Sea, Y. Sukanya, M. Salalah, I. Wanderrie, F. Amalaha, and H. Morrison, "Toward to opera-tonalization of SocioTechnical ontology engineering methodology," in *Proceedings of the 2017 5th International Conference on Cyber and IT Service Management (CITSM)*, pp. 1–7, Denpasar, Indonesia, August 2020.

[52] R. Rocca, P. Rosa, C. Sassan Elli, L. Fumagillin, and S. Terzi, "Integrating virtual reality and digital twin in circular economy practices: a laboratory application case," *Sustainability*, vol. 12, Article ID 2286, 2019.

[53] M. Sarod, T. Lecher, J. Fuchs et al., "The digital twin concept in industry-A review and systematization," *IEEE Explore*, vol. 1, pp. 1789–1796, 2020.

[54] A. Fasano, "Software requirements specification analysis using natural language processing technique," in *Proceedings of the 2013 International Conference on Qi*, pp. 105–110, Yogyakarta, Indonesia, June 2013.

[55] T. Y. Pang, J. D. Pelaez Restrepo, C.-T. Cheng, A. Yasin, H. Lim, and M. Miletic, "Developing a digital twin and digital thread framework for an 'industry 4.0' shipyard," *Applied Sciences*, vol. 11, no. 3, Article ID 1097, 2021.

[56] R. Carvalho and A. R. da Silva, "Sustainability requirements of digital twin-based systems: a meta systematic literature review," *Applied Sciences*, vol. 11, no. 12, Article ID 5519, 2021.

Research Article

Collaborative Evolution Mechanism of PMC Project Organizational Management System from the Perspective of Organizational Conflict

Hongyan Li [iD],[1] Jingchun Feng,[1] Ke Zhang [iD],[1] Rundong Chen,[2] Haiyu Feng,[3] and Tengfei Wang[4]

[1]*Project Management Institute, School of Business, Hohai University, International River Research Center, Nanjing 211100, China*
[2]*Department of Water Resources, Guangxi Zhuang Autonomous Region, Guangxi, China*
[3]*Guangxi Zhuang Autonomous Region Water Resources Engineering Construction Management Center, Guangxi, China*
[4]*China Water Resources Beifang Investigation, Tianjin, China*

Correspondence should be addressed to Ke Zhang; zhangke@nuaa.edu.cn

Limited by traditional construction project management ideas and systems, the implementation of the PMC model in China still has serious problems such as opposition and frequent conflicts. How to reveal the causes of organizational conflicts and explore the key mechanism of the implementation of the PMC model from the system perspective are urgent problems to be solved. Based on the idea of engineering system view, this paper abstracts the PMC project participants with self-organizing characteristics of the organizational management system, in which the internal structure is closely related, and defines the connotation of synergy and synergistic evolution of the PMC project organizational management system. Using the Cucker–Smale model to describe the group movement, the hierarchical system and the acceleration efficiency function of the project legal person's free will are constructed, and the structure, movement, and development law of the system itself are emphasized to simulate the ordered evolution trend of PMC project organizational management system and reveal the intrinsic causes of conflicts in PMC project and the key mechanisms of the PMC model application. The results show that first, the intensity of information communication between PMC subjects has a significant positive contribution to the orderliness of the organizational management system; second, too much acceleration of the project legal person's free will causes group chaos in the system, while too little slows down the group stabilization time, which has a negative impact on cost and schedule; third, the more the organizational structure of PMC contractors tends to the whole-process integrated control, the more it can drive the group to gather in an orderly manner and form a synergistic control mode combining self-organization and other organizations; and fourth, the implementation of the PMC model should focus on eliminating the traditional institutional and conceptual barriers, forming a project management model with integrated control of the whole process of the PMC project contractor and effective macro supervision of the project legal person. The research results of this paper revealed the intrinsic causes of conflicts in PMC projects and the key mechanisms of PMC model application; it can help solve the confrontational situation of PMC project participants, promote the development of the PMC model, and give full play to the investment benefits.

1. Introduction

China's construction industry is a pillar industry of the national economy and has driven a large number of related industries, making important contributions to economic and social development, urban and rural construction, and improvement of people's livelihood. About 3,424.7 billion yuan of investment in fixed assets for transportation and 770 billion yuan of investment in water conservancy were completed in 2020, and the large-scale, modern

infrastructure, industrial, and civil building construction have demonstrated the advanced and reliable nature of China's engineering technology, technical standards, and work methods. The "One Belt and One Road" initiative has been proposed for more than seven years and has won wide recognition from the international community. By the end of January 2021, China has signed 205 cooperation documents with 140 countries and 31 international organizations for the co-construction of "One Belt and One Road." China's construction industry has made remarkable achievements in the field of international engineering construction, but there is still a big gap compared with the construction industry of advanced industrialized countries; the construction labor productivity is only about two-thirds of that of developed countries; the construction industry is still big but not strong; the organization of engineering construction is backward; the level of architectural design needs to be improved; there are more market violations; the core competitiveness of enterprises is not strong; and other problems are more prominent. Under the influence of Chinese traditional thinking and traditional system, the organization and management of construction projects are still limited to the scope of project contracting business and split organization model [1]. In the traditional management model, the participants who are responsible for decision-making, construction, and operation services [2] provide services on behalf of the interests of the project legal person in the corresponding phase. Medium and large construction projects span civil, electrical, planning, environmental, and other functional departments to work together, and the connection between the participants is extensive and close and affects each other. As the project progresses, the relationship between participants changes dynamically, resulting in greater complexity of project organization and management. In addition, the different expertise and experience of each participant also increase the complexity of project coordination, which is more likely to cause problems such as confrontation and conflict among project participants. The high-quality development of the construction industry urgently needs to establish real good cooperation between all participants and improve the efficiency of organizational implementation [3]. Obviously, the traditional project management system, management style, and philosophy in China cannot meet to the needs of modern medium and large-scale project management.

Engineering practice cases showed that the PMC model (project management contracting model) has the advantages of design optimization, integrated management, risk redistribution, and cost-saving compared with traditional DB and DBB models [4]. PMC model is an organizational model to meet the market demand and implement the whole process of engineering consulting in the project decision-making and construction implementation stages [5], mainly to provide high-quality intellectual and technical services for construction activities. PMC model refers to the engineering project management enterprise (PMC contractor), in accordance with the contract, preparing a feasibility study, feasibility analysis, and project planning for the owner at the decision-making stage; providing bidding agent, design

management, procurement management, construction management, and commissioning (completion and acceptance) services for the owner at the implementation stage; and carrying out quality, safety, progress, cost, contract, and information management and control of the project on behalf of the owner. The PMC contractor shall generally bear certain management risks and economic responsibilities in accordance with the contract. Its essence is to provide high-quality whole-process intellectual and technical services for the project legal person. PMC project refers to the construction project that adopts the PMC model for the whole process integrated and professional organization and management. In February 2017, the Ministry of Housing and Construction issued document 19, the first time mentioned "whole process engineering consulting" concept, and in 2019, the National Development and Reform Commission and the Ministry of Housing and Urban-Rural Development jointly issued "Guidance on Promoting the Development of Full-Process Engineering Consulting Services" (Development and Reform Investment Regulations (2019) No. 515), which pointed out the urgent need to innovate the organization and implementation of consulting services and vigorously develop full-process engineering consulting service model oriented by market demand and meeting the diversified needs of commissioners. A series of construction project management-related regulations and practical applications have accumulated rich experience in promoting professional management of large-scale engineering project management [6]. PMC model is widely used in large-scale international project construction, for example, the South China Sea ethylene project undertaken by SINOPEC Engineering and Construction Corporation, the Bangladeshi Chittagong-Dhaka refined oil Pipeline Project undertaken by Langfang CNPC Langwei Engineering Project Management, the China-Myanmar Oil and Gas Pipeline Project undertaken by CNPC Pipeline Engineering Co., and so on [7]. The PMC model has become one of the important project management models in oil, transportation, water conservancy, and other industries [8].

The current research on the PMC model focuses on the theoretical definition and scope of the PMC model, risk study of the PMC model [9], schedule and cost control study [10], application practice study, and comparison study with other models [11]. Both domestic and foreign scholars have focused on the operational aspects of the PMC model, discussing how the PMC contractor conducts planning, design, and management scope of the PMC contractor, the risk of lump-sum contracts under unclear conditions, and institutional barriers to the promotion of the model. The research results of the PMC model have provided reference ideas for the professional management of construction projects [12], as an extension of the owner; the PMC contractor manages the whole process of project construction to achieve safe, high quality, low cost, and on-schedule completion of the project in accordance with the predetermined objectives and to optimize the technical and economic indicators over the life of the project. In the traditional project management model, the decision-making, implementation, and operation phases are independent, and the professional

engineers who undertake the tasks of different phases provide consulting services for the owner in the corresponding phases, and the antagonism between the owner and the contractor is deep-rooted. Field research on PMC projects is implemented in China, due to the lack of systematic operation norms and references, and the influence of traditional construction project management ideas and systems; conflicts between PMC contractor and owner, supervisor, designer, and constructors are frequent in the project implementation Owners and PMC contractors do not trust each other; supervisor and designer and PMC contractor constrain each other in the implementation; and constructors do not recognize PMC contractor's management. The PMC contractor is in an awkward position, and it is difficult to coordinate the relationship between all parties, and the confrontation and contradiction between the parties is intensifying as the project progresses. This is extremely mismatched with the current development demand of the construction industry; it is difficult to meet the needs of a high-quality development strategy [13]. It is urgent to introduce the system thought to explore the overall and integrated way of organization and coordination [14]. In view of this, the paper abstracts the PMC participants into an organizational management system with self-organizational characteristics from the perspective of system theory, using the Cucker–Smale group movement model, emphasizing the structure, movement, and development law of the system itself, highlighting the integrity and dynamics of the system operation, simulating the PMC participants of exchanging information and interacting with each other within the system, and identifying the underlying causes of organizational conflict among PMC project participants in the Chinese context, to facilitate in-depth study of the management mechanism of PMC projects. The paper explores the evolutionary mechanism and evolutionary dynamics of synergy formation in PMC project organizational management systems so that the PMC model can get rid of management dilemmas such as antagonistic participants, frequent conflicts, and low organizational efficiency; realize efficient collaboration among the participants, in order to promote the development of the PMC model in the field of Chinese construction project; and provide theoretical references for the revolution of the project management model.

2. Literature Review

The existing collaborative studies of construction projects were mainly based on the relationship between the participants to construct the relationship network [15]. Dogan et al. used SNA to construct an e-mail communication network between the participants of a large airport construction project and calculated closeness centrality to evaluate project coordination performance [16]. Zhao et al. constructed an organizational network between participants based on e-mail log data from a $20 million AEC project to identify inconsistencies between organizational and collaborative networks, with the aim of analyzing the patterns of collaboration achieved by the project [17]. Conflict within the organization is one of the main factors affecting project

synergy due to the diversity of interests and goals among project participants [18]. Conflict in the project construction process is dominated by interorganizational conflict, which refers to the interactive process in which actors show different interests, views, and preferences [19]. With the development of the economy, the increasing scale and technical complexity of engineering projects, the emergence of various new transaction models and project management models, the organizational conflicts of construction projects have increased dramatically. In addition to multi-cultural, multi-disciplinary, and different objectives that lead to organizational conflicts, the technical capacity or coordination ability, experience, and economic capacity of the professional team also lead to organizational conflicts [20]. In owner management, untimely owner decisions, excessive supervision, poor coordination, lack of management ability, failure to provide information or sites in a timely manner, and failure to follow procedures for handling unreasonable contractor claims can lead to conflicts [21]. This requires the project manager to have the ability to coordinate conflicts between the participants and make the project organization synergistic [22]. Most conflicts originate early in the project lifecycle, and it is important to take measures to mitigate them early on [23]. Jin et al. proposed conflict resolution strategies for the planning, construction, and handover phases by building a dynamic social network model among project participants [18]. Wang et al. discussed the causes and solutions of conflict in the construction project through multiple case studies and proposed the following six resolution strategies: (1) prevention, (2) compromising, (3) mediation, (4) resolving, (5) avoidance, and (6) smoothing [24]. Postevaluation of conflict management is also an important part, assessing the quality of conflict management in five dimensions: satisfactory resolution outcome, comprehensive resolution process, conflict prevention, perception of fairness, and postconflict effects [25]. The construction field has conducted relatively in-depth research from both the analysis of the root factors of conflict and conflict management strategies, with a focus on the study of the conflict between owners and contractors.

Construction projects are open organizational systems involving many important stakeholders, while medium and large construction projects have more complex social, cultural, and legal contexts so more complex conflict factors within the organization [26]. Most of the existing studies on conflict management are based on the local perspective of some participants or in phases, the studies on project organization issues and organizational behavior are still scattered, and there is a lack of systematic studies on conflict management in medium- and large-scale projects [27]. Systems theory stems from the investigation of natural phenomena; in 1978, Qian et al. published the article "Technology of Organizational Management-Systems Engineering," which opened a new era of systems engineering research in China [28]. In this article, a system is defined as an organic whole with specific functions, which consists of several components that interact and depend on each other, and any engineering project is a social system with continuous dynamic evolution composed of subsystems that

interact and work together. Yin et al. from the perspective of engineering ontology and engineering system view proposed to look at engineering from the perspective of human survival and development, not only recognize various elements of engineering composition but also see engineering as a system, and recognize, analyze and grasp engineering from the system viewpoint [29]. The study of construction project organizational behavior requires a broader systematic perspective. As temporary organizations, construction project organizations can be viewed as complex adaptive organizations, where the behaviors of participants at all levels interact and change dynamically [30]. Principled negotiation and joint cooperative action among participants within the project organizational system can play an important role in mediating conflicts, and interorganizational trust has direct and indirect positive impacts on improving cost performance [31].

Based on the engineering system theory, the project organizational management system is a group composed of many independent participants who depend on each other [32], which belongs to an open organizational system, and the relationship between the participants constitutes the organizational structure. In this paper, the definition of synergistic project organizational management system is as follows: under the disturbance of the external environment, the internal participants of the system have a stable connection, forming an orderly structure of internal and external energy, material and information exchange, and continuously maintaining the dynamic stability of the system structure. Definition of PMC project organizational management system synergy evolution is an organizational process in which the interactions between project participants move toward orderly and dynamic stability, forming a life-like group that combines self-organization and other organizations, in which the participants under the leadership of the commander adapt to other participants in the system by changing their rules, with the ability of self-development, self-improvement, and spontaneous synergy so that the overall system exhibits dynamic synergy. The research results help PMC projects mitigate organizational conflicts and synergize the strengths of all parties involved, provide theoretical references for innovative project management models and the implementation of specialized PMC models, open up paths for achieving integrated and specialized management of the whole process in the field of construction, and significantly improve management effectiveness and construction management levels.

3. Methodology

It is observed that self-driven particles such as flocks of birds, fish, and sheep have self-organized group behavior and can transition from disorder to orderly motion using local information and simple rules. Group behavior is characterized by certain macroscopically ordered behaviors of individuals in a group through interactions, with "order" usually referring to the same movement patterns [33]. In 1995, Vicsek et al. proposed the first numerical model to describe animal group behavior, and Jadbabaie et al. proved the correctness

of the above numerical model from the mathematical point of view [34, 35]. Based on the above research, Cucker and Smale studied the formation mechanism of orderliness and proposed the Cucker–Smale model to describe interactions between particles [36, 37]. The Cucker–Smale model analyzes the formation mechanism of group coherence by describing the position and velocity of individuals and interindividual interactions during group motion and establishing a mathematical model; the authors also demonstrate the validity of the model by using the formation of a common language in primitive societies and the emergence of the vowel system as examples.

Each individual in the Cucker–Smale model adjusts its velocity by summing the weighted average of the difference between its own velocity and that of other individuals. Given k particles in d-dimensional Euclidean space, (x_i, v_i) denotes the position and velocity of the i-th particle ($i = 1, 2, \cdots, k$), and the velocity and position updates of these k particles obey following the system of the below equation:

$$x_i(t + \Delta t) = x_i(t) + \Delta t v_i(t),$$
$$v_i(t + \Delta t) = v_i(t) + \Delta t \sum_{j=1}^{k} a_{ij}(x(t))\left(v_j(t) - v_i(t)\right), \quad (1)$$

where $x_i(t)$ and $v_i(t) \in \in \mathbb{R}^3$ denote the position and velocity of individual i at time t, respectively, and Δt is the time step.

$a_{ij}(x(t))$ quantifies the strength of interactions between individuals, and the strength of interactions between individuals is a smooth decreasing function of relative distance, as shown in equation (2). As can be seen from $a_{ij}(x(t))$, the model is a symmetric interaction model, that is, the information transfer is bidirectional, and the interactions between subjects diminish as the relative distance increases, but the interactions are always strong or weak.

$$a_{ij}(x(t)) = \frac{H}{\left(\sigma^2 + \left\|x_i(t) - x_j(t)\right\|^2\right)^{\beta}}, \quad (2)$$

where $H > 0$, $\alpha > 0$, and $\beta \geq 0$ are the system parameters and β is the decay rate.

Definition 1.1. The solution (x, v) of system (1) with asymptotic group effect means that

(1) Relative velocity tends to be 0, that is, $\lim_{t \longrightarrow +\infty} = |v_i - v_j| = 0$, $1 \leq i, j \leq k$

(2) Relative displacement aggregation, that is, $\sup_{0 \leq t < \infty} |x_i(t) - x_j(t)| < +\infty$, $1 \leq i, j \leq k$

Shen proved the correctness of the Cucker–Smale model using induction and obtained convergence results similar to the original model [38]. Cucker and Dong further explored the Cucker–Smale model with a hierarchical structure using a subsystem induction approach and using a flock of birds perched on a branch and suddenly disturbed by a predator as an empirical case [39]. Subsequent researchers have proposed various improvements to the Cucker–Smale model to suit different application scenarios and have also validated

the validity of the model from different perspectives. Cucker et al. and Dong et al. studied improved models affected by noise and time delay, giving threshold conditions for the occurrence of group behavior [40–42]. Cucker and Markou I et al. improved the model for collision avoidance by adding repulsive forces [43–45]. Cucker and Dong studied the Cucker–Smale model with the introduction of hierarchy and topologically acting neighborhoods, giving conditions for the occurrence of cluster clustering [46, 47].

Cluster dynamics models were originally used to simulate the group motion of animal groups in nature, and in recent years, such models have also been mostly used to study the control mechanisms of the asymptotic behavior in multi-intelligent body systems [48]. Examples including aircraft formations [49], robotic mass movements, and engineering science research [50] provide basic coordination and consistency algorithms for mobile autonomous individual systems. The famous Chinese economist Cheng pointed out that the most essential characteristic of a complex system is that its components have some degree of intelligence, that is, the ability to understand their environment, anticipate its changes, and act on predetermined goals, which is intrinsically responsible for biological evolution, technological innovation, economic development, and social progress [51]. The current research on the coordination of construction project participants is mostly based on SNA. SNA portrays the intersubject relationship through the network structure model and conducts a static quantitative evaluation of the density, centrality, and other indicators, but the organizational network structure changes dynamically as the project advances, and the static evaluation of SNA can hardly reflect the dynamic nature. The PMC project organizational management system is composed of several participants, who have independent interest goals and act according to the predetermined goals. As the project progresses, the interaction between the participants will prompt them to continuously receive information [52], summarize the experience, adjust action rules, improve their own adaptability, and make the system evolution more and more complex. In summary, this research introduces the Cucker–Smale cluster dynamics model, considers the characteristics of PMC project organizational structure, constructs the effectiveness function of the interaction between participants in the PMC project organizational management system, simulates the evolution process of the interaction of participants, identifies the causes of conflicts in PMC project organizational management systems, and explores the mechanisms and paths to achieve synergy and consistency. The research framework is shown in Figure 1.

4. Collaborative Evolutionary Model of PMC Project Organizational Management System

Referring to the research results of the Cucker–Smale model, a hierarchical PMC project organizational management subsystem with $k + 1$ project participants is considered, as shown in Figure 2, containing the project legal person, the PMC contractor, the design unit, the supervision unit, and the subcontractors. Project legal person refers to the highest authority group or organization that has civil rights and civil capacity, enjoys civil rights, undertakes civil obligations independently according to law, and is engaged in project management for the purpose of construction projects, and the project legal person is in a central position during the implementation stage of construction projects and is responsible for the whole process of project implementation. Therefore, in the project organizational management system, the project legal person is the general leader of the group and has the acceleration of free will. In the process of project implementation, the acceleration of free will reflects the willingness of the project legal person to lead and drive the group. The model sets the project legal person corporation code to 0 and the PMC contractor code to 1.

In Figure 2, if the adjacency matrix $A = (a_{ij})$ satisfies:

(1) $a_{ij} \neq 0$, then it means $j < i$
(2) Define $\zeta(i) = \{j : a_{ij} \neq 0\}$ as the set of leaders of behavioral agent i, for any $i > 0$, $\zeta(i) \neq \varnothing$

The rules of movement for the 2nd, 3rd up to the k-th behavioral agent are shown in the system of the following equation:

$$
\begin{aligned}
x_i(t+1) &= x_i(t) + \Delta t v_i(t), \\
v_i(t+1) &= v_i(t) + \sum_{j \in \varsigma(i)} a_{ij}(t)\big(v_j(t) - v_i(t)\big),
\end{aligned}
\tag{3}
$$

where $i = 2, \ldots, k$; $x_i(t), v_i(t) \in \mathbb{R}^3$ denote the position and velocity of behavioral agent i at time t, respectively; and Δt is the time step. The velocity update rule of the behavioral agent is to adjust its own acceleration by receiving the velocity difference information with individuals in the leader set to achieve velocity matching.

a_{ij} is a function of the intensity of the interaction between the participants, as in the set of equations (4), which is the weight function of the individual in adjusting its own speed, indicating the strength of the information received by the individual to change its speed; it also reflects the efficiency of information delivery and communication. Unlike the original Cucker–Smale model, $a_{ij}(t)$ is a one-way asymmetric decreasing function where behavioral agent i is influenced only by the individuals within its leadership set $\zeta(i)$.

$$
a_{ij}(t) = \frac{1}{\left(1 + \left\| x_i(t) - x_j(t) \right\|^2\right)^{\beta}},
\tag{4}
$$

where $\beta \geq 0$ is a system parameter indicating the decay rate.

Each participant updates their position and speed according to the difference in action with other individuals within the leadership set, and the action update rule for the total leadership project corporation 0 is as in the following equation:

$$
\begin{aligned}
x_0(t+1) &= x_0(t) + \Delta t v_0(t), \\
v_0(t+1) &= v_0(t) + \Delta t f(t).
\end{aligned}
\tag{5}
$$
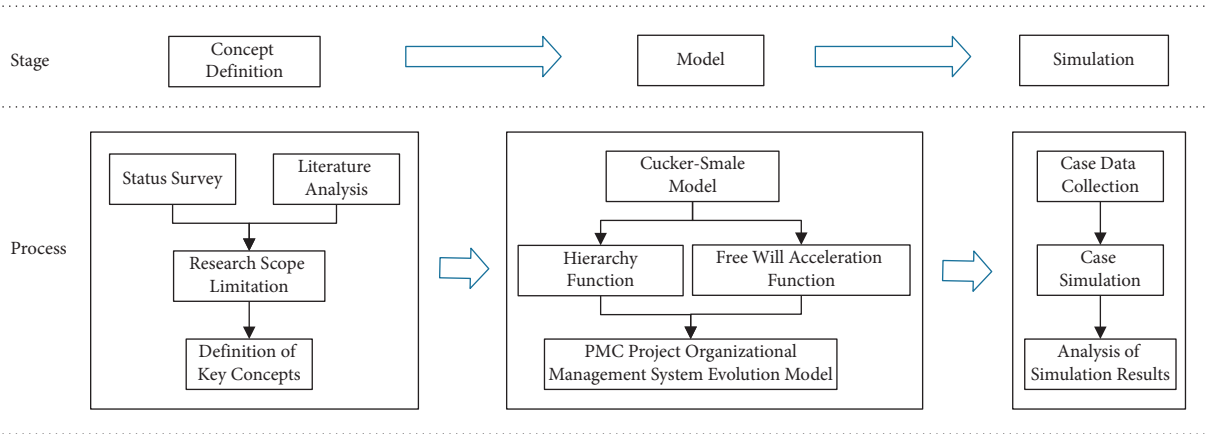
The action update rule of PMC contractor 1 is shown in the system of the following equations:

$$x_1(t+1) = x_1(t) + \Delta t v_1(t),$$

$$v_1(t+1) = v_1(t) + \sum_{j \in \varsigma(1)} a_{1j}(t)\big(v_j(t) - v_1(t)\big), \qquad (6)$$

where $f(t)$ is the free will acceleration of the project legal person, considering the actual change of the project legal person's mentality; the project legal person is more anxious to achieve the goal when the project is first started; and the anxious mentality of the project legal person decreases as the project progresses and project goals are gradually achieved. Therefore, it is assumed that the free will acceleration of the project legal person is a decaying process, reflecting the degree of control and intervention they have over the project. The greater the acceleration of free will, the greater the tendency toward a command leadership style, that is, the greater the control of the project owner over the execution of the project and the demand for immediate compliance by the other participants. The decaying process of the free will acceleration satisfies the following process:

$$\|f(t)\| = O\big((1+t)^{-\delta}\big), \quad \delta > k, \qquad (7)$$

$O\big((1+t)^{-\delta}\big)$ is an infinitesimal function of the same order as $(1+t)^{-\delta}$, that is, there exists a nonzero constant such that $\lim_{t \to \infty} O\big((1+t)^{-\delta}\big)/(1+t)^{-\delta} = c$.

Unlike the EPC model [53], the PMC contractor, as an extension of the project legal person in project management, is designed to make up for the lack of management capacity of the project legal person, fully reflecting the interests of the project legal person, whose profit comes from the management fee, and can eliminate the shortcomings of the project legal person's inexperience and inappropriate management in the coordination of management. Therefore, PMC contractor is more influenced by the free will acceleration of the project legal person than the same level of participants, and the intensity of the free will acceleration of the project legal person on PMC contractor is set twice as much as that of the same level of agents after interviews and research with PMC project managers and experts in the field of project management.

Groups have group effect, that is, they form synergies and satisfy the following conditions:

(1) The relative speed of all participants is consistent, $\lim_{t \to \infty} |v_i - v_j| = 0, 0 \le i, j \le k$

(2) All participants are bounded by their relative positions of aggregation, $\sup_{0 \le t < +\infty} |x_i(t) - x_j(t)| < +\infty$, $0 \le i, j \le k$

5. Case Study

5.1. Project Brief. PMC project of Guangxi Baise reservoir irrigation area was selected for simulation analysis (hereinafter referred to as M Project). M Project reservoir irrigation district project is located in the valley of the Right River in Baise City, involving a total of 12 towns in Baise City, which is one of the "172" major water conservation and water supply water conservancy projects determined by the State Council; the project is a large (2) type II irrigation district in general, with an investment of 414.471 million yuan and total construction period of 48 months. The project consists of two parts: reservoir diversion project and right river water lifting project, with irrigation and water supply as the main tasks, irrigating an area of 592,000 mu; the water transmission mains are divided into five pipes, including the main pipe, south main pipe, north main pipe, Lin Feng main pipe, and Baoqun main pipe.

The M Project involves many participants, a wide geographical distribution, an organizational management system across a variety of technical specialties, and cultural differences; it is difficult for the traditional project organization fragmented management approach to meet the project construction, project contracting using the PMC model. This is the first time that the PMC model is adopted for a large water conservancy irrigation project in China and the first water conservancy project in Guangxi Zhuang Autonomous Region to adopt the PMC model. The organizational structure of the organizational management system is shown in Figure 3, where the project legal person is contracted in parallel for supervision, design, tunnel construction, and PMC contracting. The PMC contractor manages the whole process of construction preparation:

FIGURE 2: Hierarchy diagram of PMC project organizational management system.

procurement of project materials and equipment, construction of main works, temporary works, soil and water conservation works, environmental protection works, acceptance of project completion, monitoring (all safety, environmental and soil and water conservation monitoring), project insurance, commissioning, 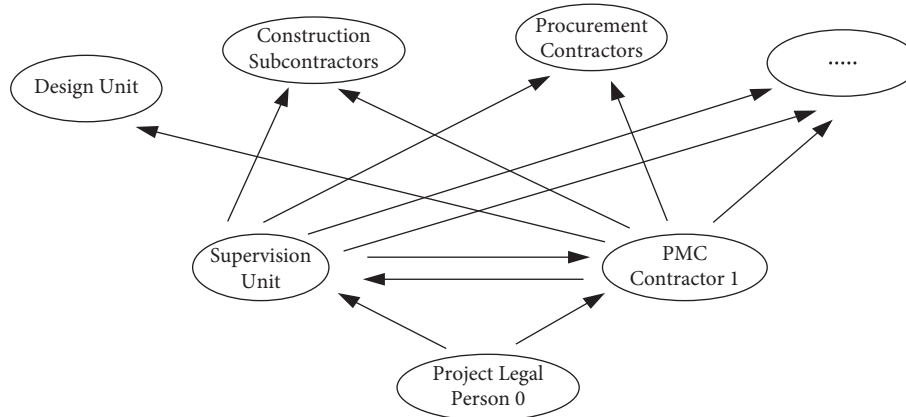and project handover in accordance with the scale, function, and technical standards defined in the approved Preliminary Design Report of M Project. During the construction period, the contractor controls and manages the project schedule, quality, safety, cost, contracts, information, and files and prepares the completion information. contractor is also responsible for coordinating supervision and design, playing the role of "control, guidance, coordination, and service." As shown in Figure 4, the PMC contractor is fully responsible for the construction management and implementation of the main project and bears the corresponding management risks and economic responsibilities according to the contract.

The conflicts between the participants in the implementation of this project are mainly manifested in the following aspects: (1) conflicts between PMC contractor and project legal person. The project legal person belongs to the command leadership style and has less experience in large-scale project management, the comprehensive strength of the PMC contractor is much higher than the project legal person, which leads to the project legal person's concern of not being able to control the moral risk of the PMC contractor. So the project legal person does not trust the PMC contractor and has greater actual control over the project, regularly bypassing the PMC contractor to organize the work of other participating entities and carry out engineering inspection independently, which makes the PMC contractor's position awkward. (2) Conflicts between the PMC contractor and the design and supervision parties. According to the contract, the PMC contractor is responsible for coordinating and managing the supervision side and the design side, but in the actual implementation of the organizational structure (Figure 3), the supervision and design are awarded by the project legal person in parallel, the supervision side is responsible for supervising and managing the PMC contractor, and it is difficult for the PMC contractor to coordinate the work of the supervision side and

the design side, so the positioning and management scope between the three is blurred. (3) Conflicts between PMC contractor and construction parties. Because the project legal person does not support the work of the PMC contractor so that the PMC contractor is in an awkward position between the project legal person and other construction sides, resulting in the construction sides do not recognize the management of the PMC contractor and autonomy and do not listen to its views, resulting in poor management of subcontracting teams; the project has more quality problems and rework.

5.2. Case Simulation Analysis. Based on Figures 3 and 4, the management level diagram of the participants in the M project organizational management system is summarized as shown in Figure 5. PMC contractor is entrusted by the project legal person to undertake the project construction management; implement the whole process management of project quality, project schedule, capital management, and production safety; and accept the supervision of higher authorities and project authorities. The project legal person is the supervision and inspection layer; the general project management contractor is the management layer; the design and supervision unit are the control layer; the construction unit and suppliers are the construction guarantee layer; and the participants are numbered.

The initial conditions of the simulation are set as follows: the number of participants is 23; the initial velocity of each individual is in the range of 0–10 m/s; the simulation duration is 100; the time step is 0.1; $\beta = 0.4$; and in order to avoid the effect of random initial distribution on the results, each simulation is repeated 100 times with random values to take the average value.

In the hierarchical diagram of individual interactions in the M Project organizational management system, each behavioral agent is influenced by the higher level of leadership, and the subcontractors and suppliers at the construction assurance level all influence each other considering the characteristics of the process crossover in engineering construction. The velocity and position trajectory evolution of the participants is shown in Figure 6, and the simulation
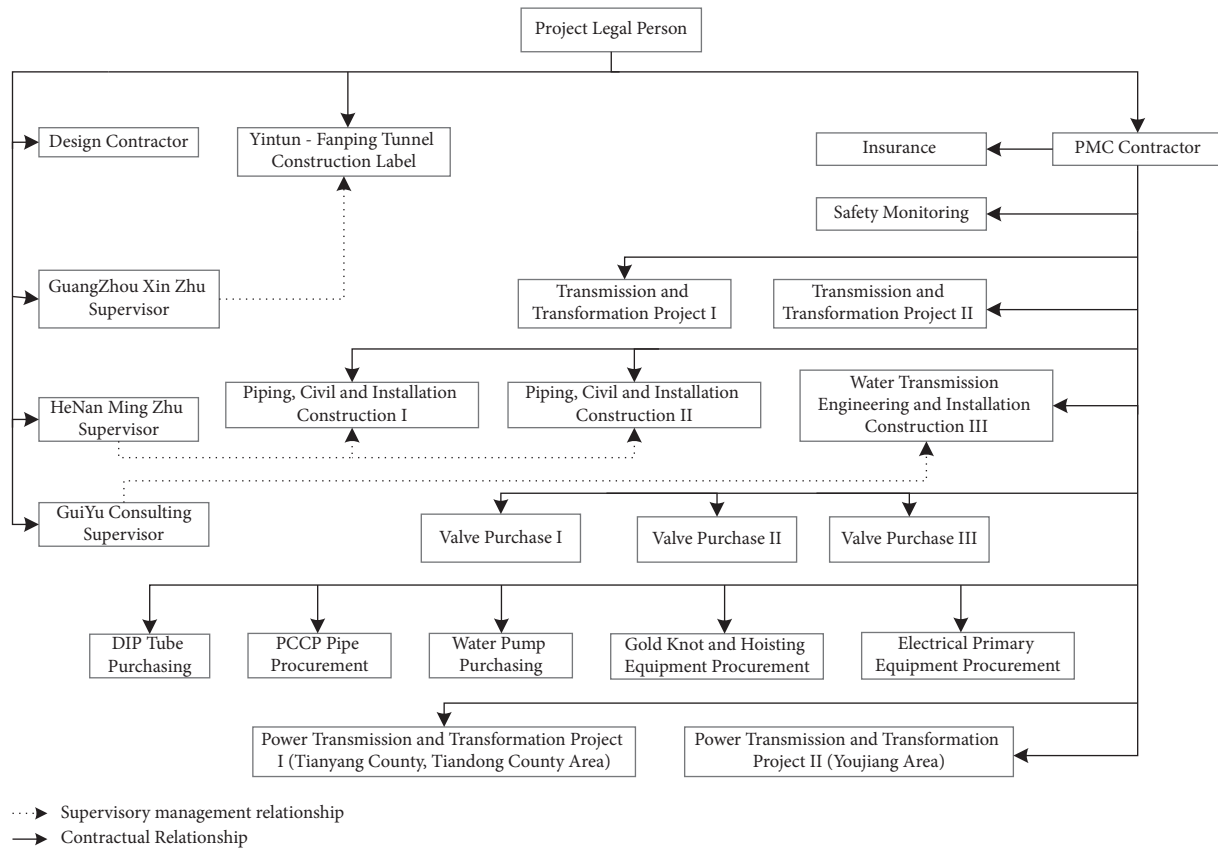
FIGURE 3: M project organization chart.

results show that there is a lack of synergy between the participants, and they cannot reach a consistent state. The position curve is more divergent; the speed matching curve in the process of movement appears obvious fluctuations; and the oscillation amplitude is larger because at the beginning of the group movement, the individuals are influenced by each other to decelerate first, making the speed gap increase, and then decrease due to the role of speed matching, and the development tends to be stable, but it cannot reach the group effect, that is, it is difficult for the participants of the project organizational management system to cooperate. The simulation results are consistent with the actual project implementation status.

The individual position trajectory curve in Figure 7 shows that the group is severely divided within the group, the organizational goals of each agent are severely divergent, and the personnel of different professions and organizations cannot coalesce in one organization to work together. Individuals only focus on their own interests, ignoring the sustainable development needs of the project, resulting in a discrete organizational management system, and the inconsistency of organizational goals will cause agents to form a situation of mutual constraints, low efficiency, and consuming a lot of costs, time, and energy to deal with work interface conflicts [54]. The individual velocity trajectory curve in Figure 6 cannot converge; there are complex connections within the organizational management system; and the velocity update of the agents depends on

information interaction to a great extent. Most parts of the M Project are managed by manual engineering information, and information communication is mostly based on paper media, lacking effective information exchange rules and information integration platforms [55]. There are information silos and information fault, which leads to inconsistent individual behavior [56], such as the lack of in-depth understanding of the requirements of the project legal person and the failure to accurately grasp the implementation plan, which increases the conflicts within the organizational management system, resulting in the project participants pursued by each subject differ greatly. Gradually reducing the decay rate β ($\beta = 0.3; 0.2; 0.1$) of the mutual influence strength function a_{ij} between agents and strengthening the strength of communication between individuals helps the group converge, but the result still cannot reach synergy, as shown in Figure 6.

The overall leader project legal person 0 has free will acceleration $f(t)$. In M Project, the project organization is complex, and the investment scale is large. The project legal person still wants to strengthen its own management and control power over the project under the PMC model due to the traditional construction ideology, so bypassing the PMC contractor to undertake many complicated and detailed management work and responsibilities, it did not reduce its own management pressure by adopting PMC model. But the project legal person does not have the management ability and experience that is compatible with this project; the free
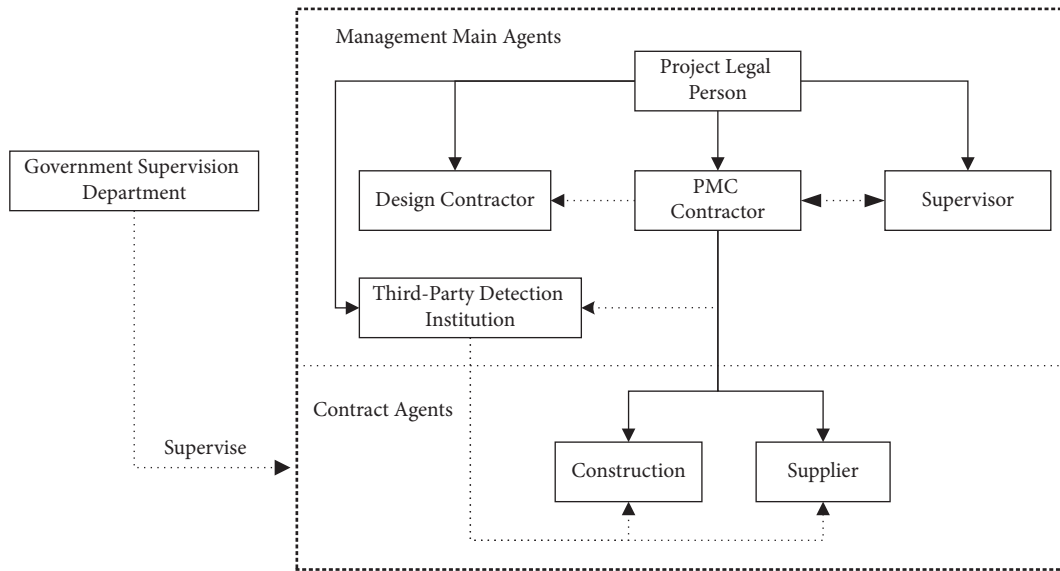
FIGURE 4: Project management model.

will affects the construction process too much, which makes the management interface blurred and increases the conflicts of the organizational management system [57]. And the project legal person belongs to the command leadership; free will acceleration is larger; coordination of problem-solving is more difficult. Adjusting the size of r in the free will acceleration of the project legal person, the simulation results are shown in Figure 8, and δ increases in (a), (b), and (c) in order. It can be seen that the larger the value of $f(t)$ taken, that is, the larger the free will acceleration of the total leader, the weaker the attraction between individuals within the group, and the more chaotic the group order of the organizational management subsystem, the more obvious the phenomenon of subgrouping appears in Figure 8(a), and it is more difficult to realize the group effect.

The existing organizational structure of the M Project is fragmented, and the PMC contractor is contracted to coordinate the supervision and design and take the overall responsibility, but in the actual organizational structure, the supervision and design are awarded by the project legal person in parallel, direct management of supervision and design by the project legal person. The PMC contractor has no management authority over the designer and the supervisor, so the designer and the supervisor restrict the professional management of the PMC contractor, which causes many obstacles to the design optimization of the PMC contractor and the control of construction sides. In addition, the project legal person has greater control over the project implementation, and the traditional engineering construction management model of the project under the PMC model is still serious; there are problems of fragmentation and disconnection between all-round management subjects, and the project implementation cannot get rid of the defects of the traditional management model of fragmentation. To adjust the hierarchical structure of the M Project organizational management system, incorporate supervision, design party, and tunnel construction into PMC management, as shown in

Figure 8, we increase the PMC contractor's control over project management and give full play to its management advantages to fully manage the project construction; the project legal person mainly assumes the responsibility of macro supervision. The simulation results shown in Figure 9 can make the group synergy consistent.

The initial conditions remain unchanged, and the simulation results of the hierarchical structure of Figure 10 are shown in Figures 9(a) and 9(b), where the group velocity tends to be consistent and the individual position curves are consistently bounded, forming a group effect, that is, reaching synergy within the system, but the curve oscillation is still large. Decreasing the decay rate r and strengthening the strength of the interaction between the agents, the amplitude of the oscillation is significantly reduced, and the time for the group to converge is shortened, as shown in Figures 9(c) and 9(d). Continuing to reduce the free will acceleration of the project legal person, as the free will acceleration tends to be 0, the oscillation gradually decreases, and the group velocity curve smoothly tends to be synergistic. The smaller the fluctuation amplitude of the velocity trajectory curve is, the more easily the velocity among individuals within the group achieves consistent, the more smooth the position trajectory change is, and the position trajectory change becomes consistent with a boundary, as shown in Figures 9(e) and 9(f). However, compared to Figures 9(c) and 9(d), the continuous reduction of the project legal person's free will acceleration in Figure 9(c) helps the group converge more gently toward synergy, but beyond a certain small range, it makes the group stabilization time slow down, and the group stabilization time in the project process has an important impact on the cost and schedule of the project [58].

6. Discussion

Participants adjust their own speed according to the speed difference information received from other individuals, reduce the decay rate of the interaction weight function between
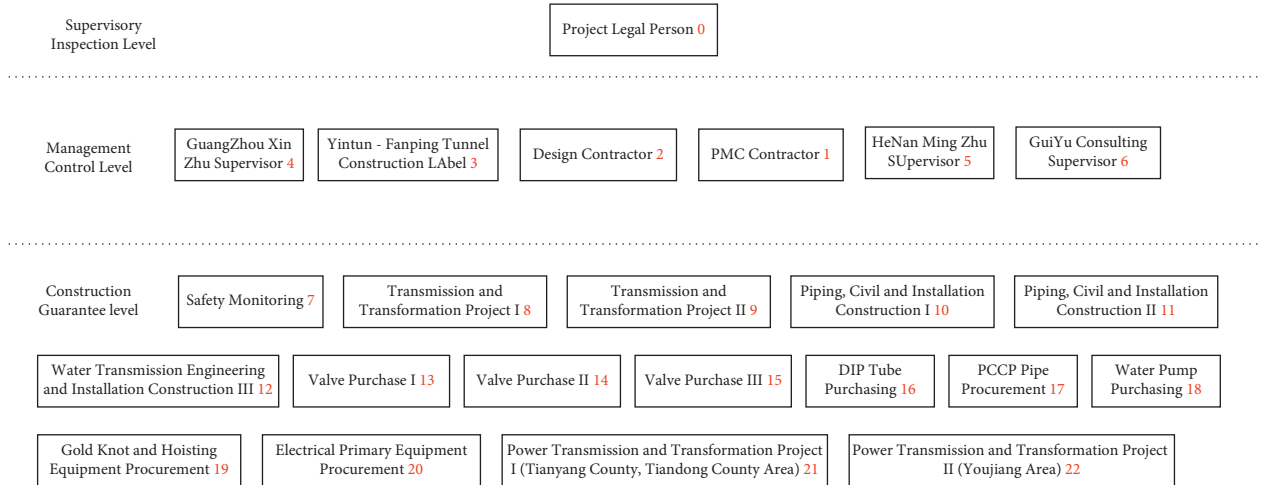
FIGURE 5: M project organizational management system hierarchy.
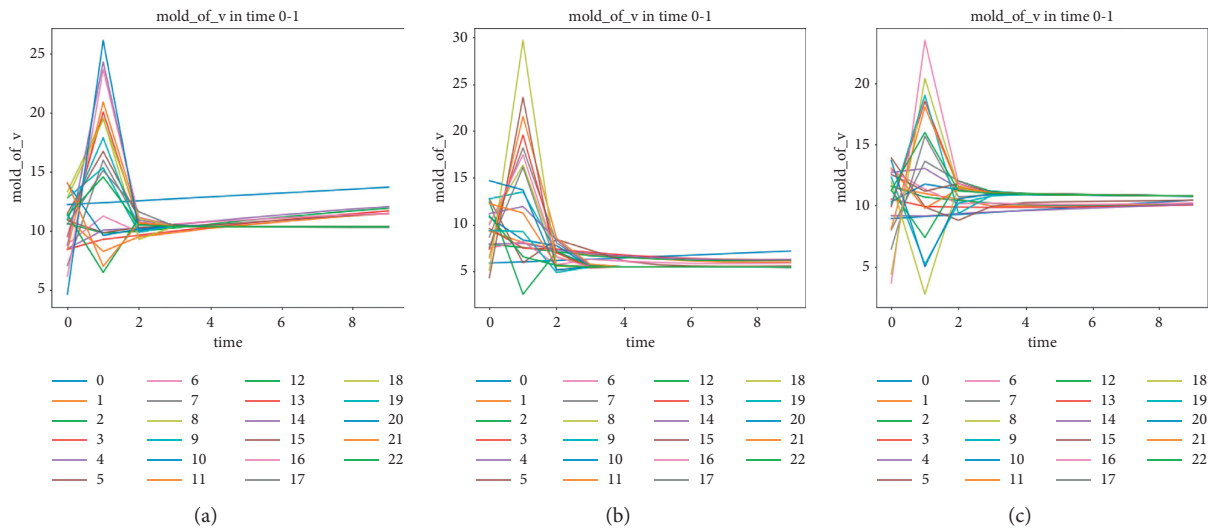
FIGURE 6: Velocity evolution curve: (a) $\beta = 0.3$, (b) $\beta = 0.2$, and (c) $\beta = 0.1$.

individuals in the organizational management system, and strengthen the interconnection, that is, increasing the efficiency of effective communication and information sharing between individuals and making the group tend to evolve in the direction of synergy. Regarding project construction from survey, design, construction, completion, and acceptance to operation, as the project progress information accumulates and is passed to the next stage, the participants involve many professions and departments, consuming a long time cycle and spanning a wide geographical area. Due to the limitations of the traditional information management and communication methods, the information transmission process may result in distortion, delay, and failure, which seriously reduces the level of group decision-making. Therefore, it is crucial for the project to achieve information sharing and effective communication in all phases of construction, and the key lies in the development and use of modern information technologies and resources such as building information model (BIM), big data, internet of things, and so on to build a whole

life cycle information management system and improve the level of information management and application [59]. It provides a guarantee for participants to make full use of information communication and sharing so as to accurately grasp the construction process; scientifically formulate plans; fundamentally solve the information fault between the stages of project planning, design, construction, and maintenance management; and realize the exchange, sharing and management of project information throughout the life cycle.

The simulation results affirm the importance of project legal person control behavior in the PMC project organizational management system. When the acceleration of project legal person free will is high, the degree of disorder within the group increases significantly, and the fragmentation phenomenon occurs; while when the acceleration of project legal person free will is reduced, the orderliness within the group increases. But too little acceleration of the project legal person's free will causes prolonged group stabilization time, which negatively affects project cost and
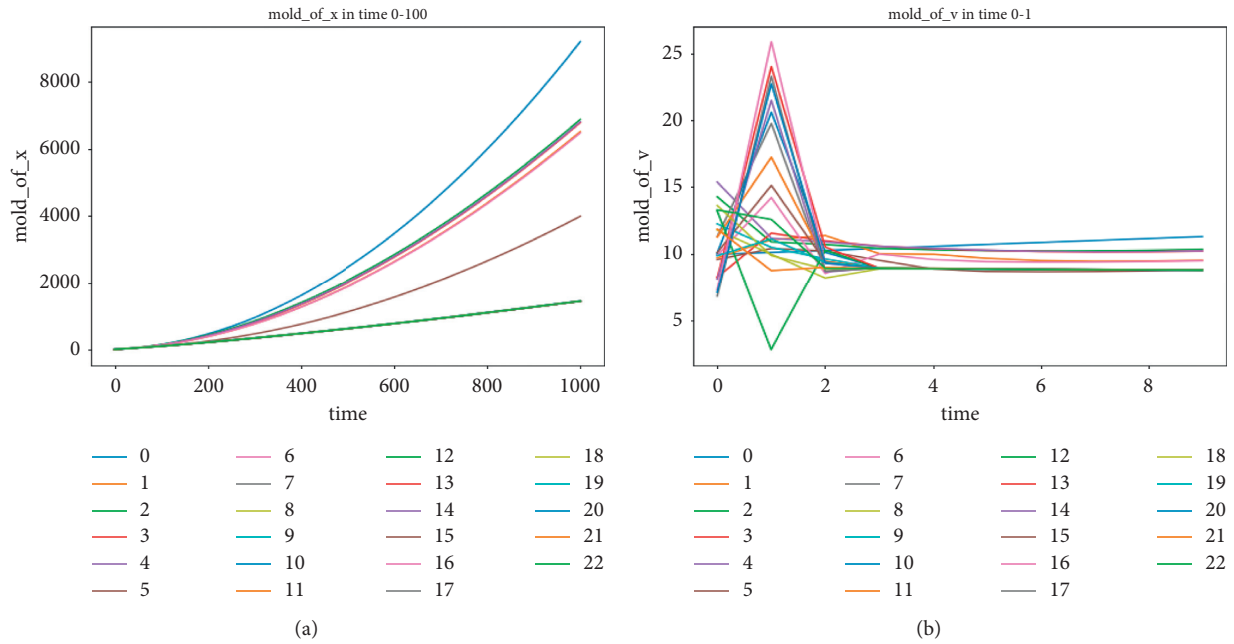
Figure 7: Evolution curve of location and velocity of M Project participants: (a) position evolution curve and (b) velocity evolution curve.
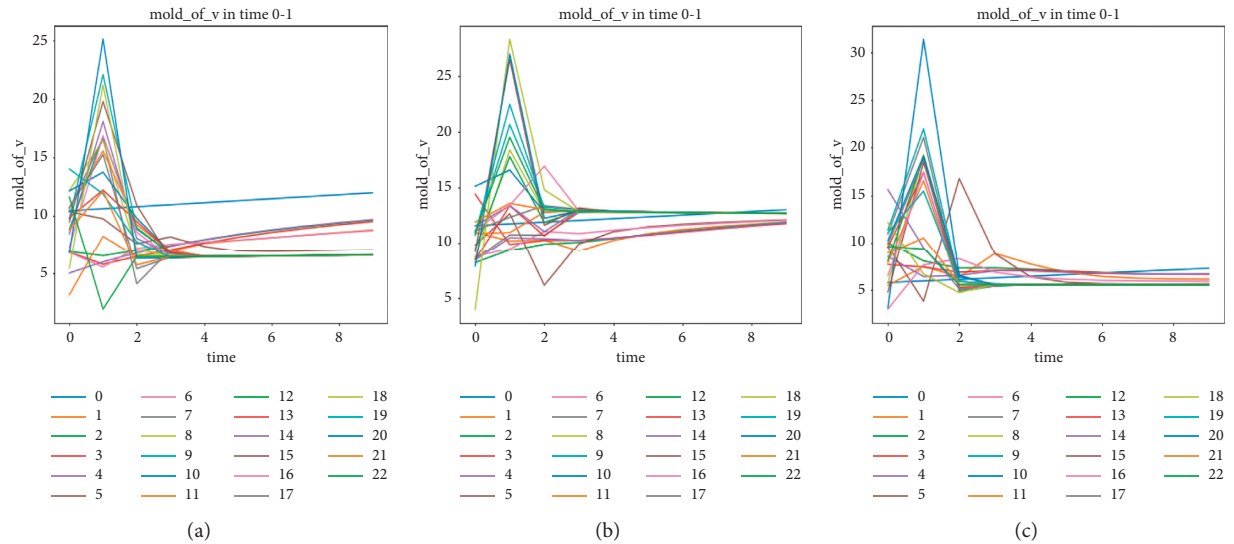
Figure 8: Velocity trajectory (δ increases in turn).

schedule. Organizational behavior theory defines leadership as the ability to influence a group to achieve a vision or goal, in order to achieve the goal most effectively; organizations need strong leadership and effective management [60]. The traditional project construction mostly adopts the control model of "project legal person + supervision," in the face of large and complex projects; the project legal person mostly lacks professional knowledge and construction experience; and the supervision unit mainly provides consulting services for the project legal person, but in fact, the supervision unit in the current market does not have the ability to control and manage the whole project, and it is difficult to provide holistic and systematic advice to the project legal person. The

PMC contractor is large engineering management consulting enterprise with strong strength and rich engineering construction experience and professional staff, which can provide high-quality project management services for the project legal person in this project. Therefore, the project legal person should change the traditional concept, give up the specialized control work beyond the capacity, focus on strategic and macroscopic planning and control for the purpose of project goal achievement and sustainable development, and support PMC contractors in their work, which not only can enhance the control power of project progress but also can give full play to the management advantages of PMC contractor to organize and coordinate
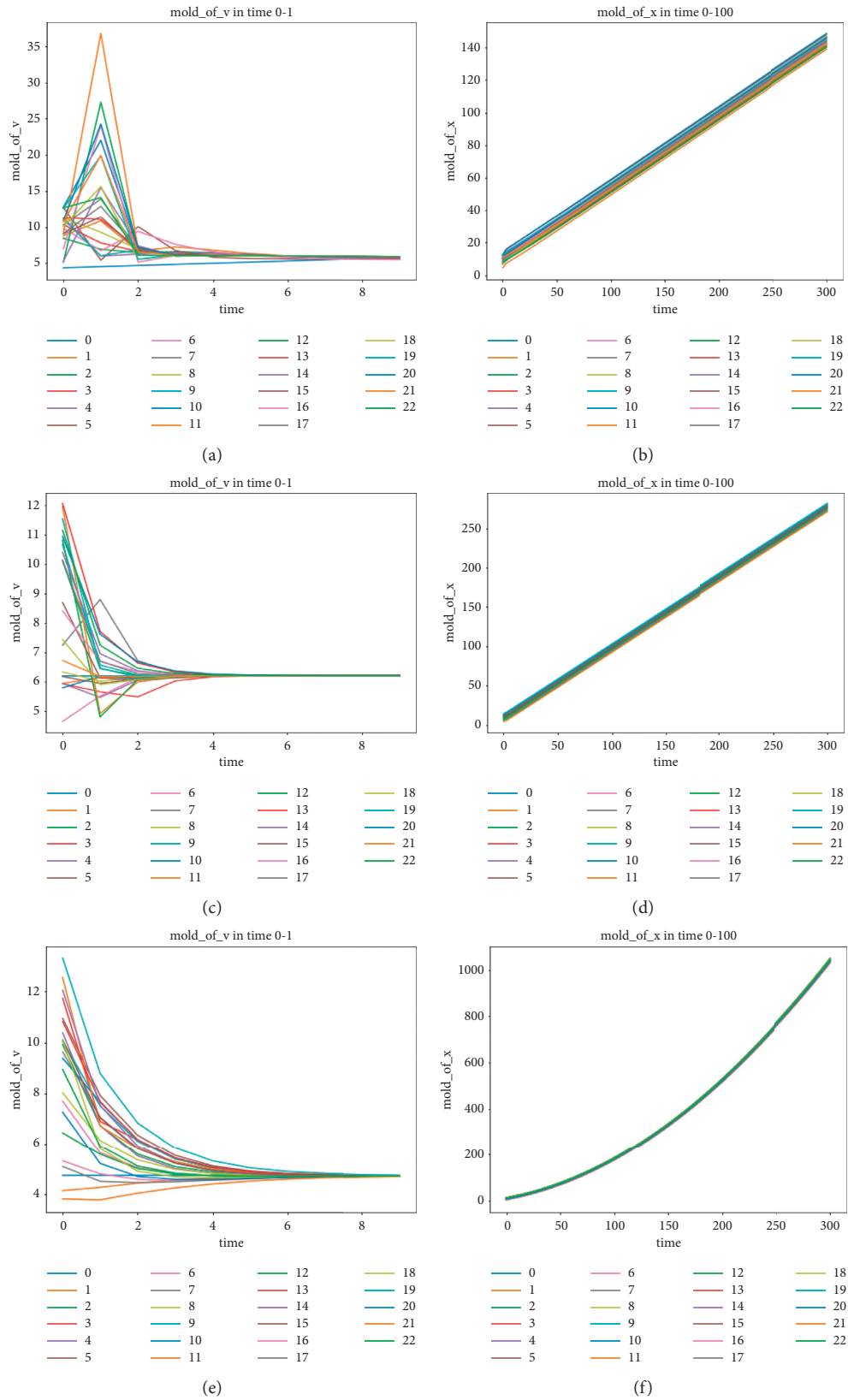
Figure 9: Evolution curve of position and velocity.
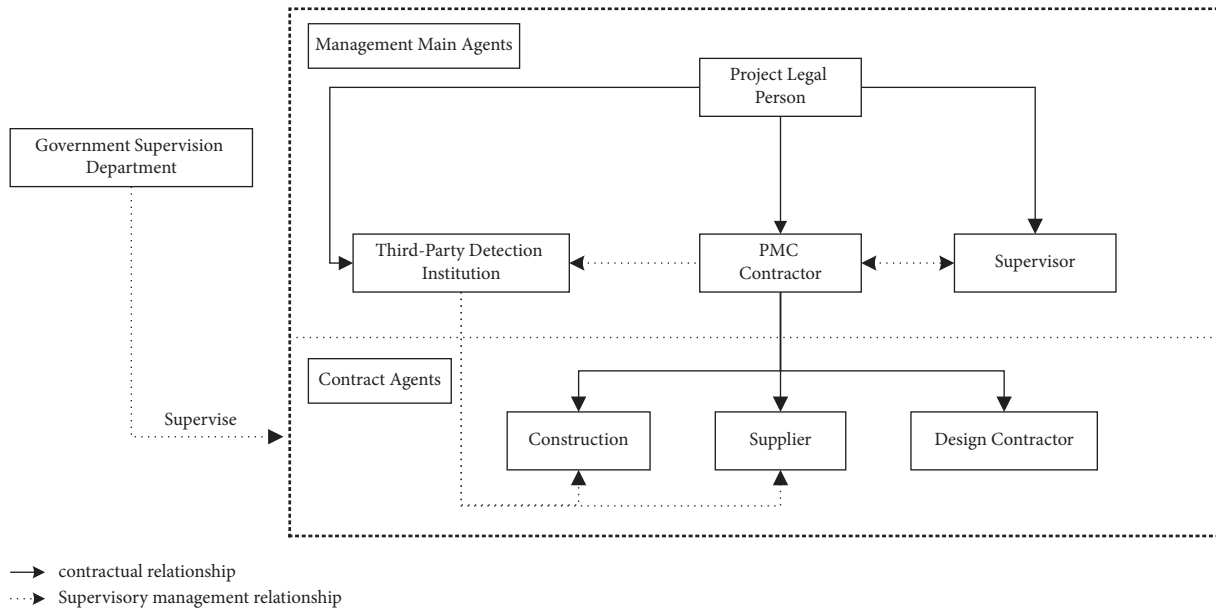
FIGURE 10: M Project management model after adjustment.

the specialized technical and construction forces in the market to cooperate with each other.

In summary, the main reasons for conflicts in the implementation of PMC projects in the Chinese context are the following three: (1) the lack of an intelligent information management platform, resulting in inefficient information communication; (2) the project legal person has too much control and tends to have a commanding leadership style, which hinders the development of the PMC contractor's management advantages; (3) the PMC project management system is too decentralized, resulting in inaccurate positioning and confusion in the scope of work of the project legal person, PMC contractor, designer and supervisor, and other major participants. In order to achieve synergy, the PMC project organizational management system must focus on breaking the institutional and conceptual barriers, strengthen the application of intelligent information technology, and construct a project management model with integrated control of the whole process by PMC contractors and effective macro supervision by the project legal person. With the gradual improvement of the construction level of fixed asset investment projects in China, when the project legal person does not have the ability to manage the project, the demand for comprehensive, cross-stage, and integrated consulting services is increasing in order to better achieve the investment purpose, and the contradiction between the real demand and the project management supply model caused by the current system is prominent. The management concept and method of the PMC model emphasizes integrated management, using systematic thinking to guide and manage practical activities, focusing on integrated management of the whole process, optimizing both design objectives and overall project benefits.

The simulation results show that to achieve synergy in the PMC model, first, to increase the PMC contractor's control over the project, the design side and supervision side

into the PMC contractor's management scope so that it becomes the overall coordinator of the project, in order to facilitate the PMC contractor to carry out design optimization and control of each construction party, and second, the project legal person should reject the traditional project management concept, break the prejudice and distrust of PMC contractors, reduce the control of the project, and give full play to the professional and integrated management advantages of PMC contractors, while the project legal person is mainly responsible for efficient macro supervision and guiding the system to evolve in the direction favorable to the project objectives.

7. Conclusion

In order to overcome the management dilemma of antagonistic and conflict-ridden relationships between the participants within the organizational management system during the implementation of PMC projects in China, based on the idea of cluster dynamics, this paper used the Cucker–Smale mathematical model, introduced a hierarchy function in the model, and made the movement rules of the total leader have a free-will acceleration.

The results show that: (1) the role of mutual exchange of motor information among PMC project participants significantly influences the consistency of group motion and the matching of intragroup individual speed. When the weight of the role of mutual exchange of movement information between individuals increases, it contributes to the convergence of group movement while significantly contributing to the matching of intragroup individual speed. (2) The free will acceleration of the legal person can have an impact on the degree of intragroup disorder. Too large free will acceleration of the overall leader project legal person may increase the degree of intragroup disorder, which in turn leads to a larger speed matching difference and the

emergence of subgroup aggregation, while too small may increase the group stability time, which has a negative impact on cost and schedule. (3) The implementation of PMC model needs to break the barriers of Chinese traditional project management concept and system; the project legal person should give up the management power beyond the capacity, include supervision and design into the management scope of PMC contractor, increase the actual control of PMC contractor to the project, and build the management system of integrated management of PMC contractor and macro supervision of project legal person, which can make the group move at the same speed and keep the cohesion; the organizational management system realize the orderly synergy; and the system forms a combined self-organized and other-organized control model.

In terms of the limitations of this study, first, the impact of the external environment on the project organizational management system is not considered, and second, the depth and scope of project management by the project legal person is not analyzed in detail. This kind of problem is worth further studying, and the subsequent study will introduce the effectiveness functions such as individual's perception ability of external environment and environmental noise impact, study the mechanism of the free will acceleration of project legal person on the system synergy in PMC model, and define its management depth and management scope quantitatively.

Data Availability

The data used to support the findings of this study are available from the corresponding author upon request.

Conflicts of Interest

The authors declare that they have no conflicts of interest.

Acknowledgments

References

[1] V. S. Anantatmula and P. F. Rad, "Role of organizational project management maturity factors on project success," *Engineering Management Journal*, vol. 30, no. 3, pp. 165–178, 2018.

[2] H. Abdirad, C. S. Dossick, B. R. Johnson, and G. Migliaccio, "Disruptive information exchange requirements in construction projects: perception and response patterns," *Building Research & Information*, vol. 49, no. 2, pp. 161–178, 2021.

[3] N. Zhao and S. An, "Collaborative management of complex major construction projects: AnyLogic-based simulation modelling," *Discrete Dynamics in Nature and Society*, vol. 2016, Article ID 6195673, 8 pages, 2016.

[4] S. Luo, P. Cheng, J. Wang, and Y. Huang, "Selecting project delivery systems based on simplified neutrosophic linguistic preference relations," *Symmetry*, vol. 9, no. 8, p. 151, 2017.

[5] R. Ruparathna and K. Hewage, "Review of contemporary construction procurement practices," *Journal of Management in Engineering*, vol. 31, no. 3, Article ID 04014038, 2015.

[6] D. Ciric, M. Delic, B. Lalic, D. Gracanin, and T. Lolic, "Exploring the link between project management approach and project success dimensions: a structural model approach," *Advances in Production Engineering & Management*, vol. 16, no. 1, pp. 99–111, 2021.

[7] Y. Huang and S. Pan, "Risk prevention strategy of international engineering project under PMC management mode," *SME Management and Technology*, vol. 21, pp. 48–50, 2021, in Chinese.

[8] Y. H. Kwak, H. Sadatsafavi, J. Walewski, and N. L. Williams, "Evolution of project based organization: a case study," *International Journal of Project Management*, vol. 33, no. 8, pp. 1652–1664, 2015.

[9] B. Lee, L. Changjun, and H. S. Heon, "International PMC project competency enhancement strategies for domestic engineering companies," *Journal of the Korean Society of Civil Engineers*, vol. 38, no. 1, pp. 121–132, 2018.

[10] T. Huang and L. Cao, "Discussion on schedule and plan management under PMC mode," *Value Engineering*, vol. 38, no. 8, pp. 75–77, 2019, in Chinese.

[11] D. Q. Tran and K. R. Molenaar, "Risk-based project delivery selection model for highway design and construction," *Journal of Construction Engineering and Management*, vol. 141, no. 12, Article ID 04015041, 2015.

[12] G. M. Winch, "Three domains of project organising," *International Journal of Project Management*, vol. 32, no. 5, pp. 721–731, 2014.

[13] M. Sanchez-Silva, "Managing infrastructure systems through changeability," *Journal of Infrastructure Systems*, vol. 25, no. 1, Article ID 04018040, 2019.

[14] M. Parchami Jalal and S. Matin Koosha, "Identifying organizational variables affecting project management office characteristics and analyzing their correlations in the Iranian project-oriented organizations of the construction industry," *International Journal of Project Management*, vol. 33, no. 2, pp. 458–466, 2015.

[15] P. Jafari, E. Mohamed, S. Lee, and S. Abourizk, "Social network analysis of change management processes for communication assessment," *Automation in Construction*, vol. 118, Article ID 103292, 2020.

[16] S. Z. Dogan, D. Arditi, S. Gunhan, and B. Erbasaranoglu, "Assessing coordination performance based on centrality in an E-mail communication network," *Journal of Management in Engineering*, vol. 31, no. 3, Article ID 04014047, 2015.

[17] D. Zhao, M. Duva, S. Mollaoglu, K. Frank, A. Garcia, and J. Tait, "Integrative collaboration in fragmented project organizations: network perspective," *Journal of Construction Engineering and Management*, vol. 147, no. 10, Article ID 04021115, 2021.

[18] J. Xue, G. Q. P. Shen, R. J. Yang, I. Zafar, and E. M. A. C. Ekanayake, "Dynamic network analysis of stakeholder conflicts in megaprojects: sixteen-year case of Hong Kong-Zhuhai-Macao bridge," *Journal of Construction Engineering and Management*, vol. 146, no. 9, Article ID 04020103, 2020.

[19] A. Singh and H. M. Johnson, "Peer-reviewed paper: conflict management diagnosis at project management

organizations," *Journal of Management in Engineering*, vol. 14, no. 5, pp. 48–63, 1998.

[20] I. U. Altuncan and A. M. Tanyer, "Context-dependent construction conflict management performance analysis based on competency theory," *Journal of Construction Engineering and Management*, vol. 144, no. 12, Article ID 04018112, 2018.

[21] A. A. Tabassi, A. Abdullah, and D. J. Bryde, "Conflict management, team coordination, and performance within multicultural temporary projects: evidence from the construction industry," *Project Management Journal*, vol. 50, no. 1, pp. 101–114, 2019.

[22] D. Özdemir Güngör and S. Gözlü, "An analysis of the links between project success factors and project performance," *Sigma Journal of Engineering and Natural Sciences*, vol. 34, no. 2, pp. 223–239, 2016.

[23] C. Lee, J. W. Won, W. Jang, W. Jung, S. H. Han, and Y. H. Kwak, "Social conflict management framework for project viability: case studies from Korean megaprojects," *International Journal of Project Management*, vol. 35, no. 8, pp. 1683–1696, 2017.

[24] N. Wang, M. Ma, G. Wu, Y. Liu, Z. Gong, and X. Chen, "Conflicts concerning construction projects under the challenge of cleaner production—case study on government funded projects," *Journal of Cleaner Production*, vol. 225, pp. 664–674, 2019.

[25] F. W. Zhu, L. Z. Wang, M. Yu, and X. T. Yang, "Quality of conflict management in construction project context conceptualization, scale development, and validation," *Engineering Construction and Architectural Management*, vol. 27, no. 5, pp. 1191–1211, 2020.

[26] Y. Li, Y. Lu, J. E. Taylor, and Y. Han, "Bibliographic and comparative analyses to explore emerging classic texts in megaproject management," *International Journal of Project Management*, vol. 36, no. 2, pp. 342–361, 2018.

[27] J. Pollack, C. Biesenthal, S. Sankaran, and S. Clegg, "Classics in megaproject management: a structured analysis of three major works," *International Journal of Project Management*, vol. 36, no. 2, pp. 372–384, 2018.

[28] X. Qian, G. Xu, and S. Wang, *Technology of Organizational Management - Systems Engineering (On Systems Engineering Revised Edition)*, Hunan Science and Technology Press, Changsha, China, 1988, in Chinese.

[29] R. Yin, Y. Wang, and B. Li, *Engineering Philosophy*, Higher Education Press, Beijing, China, 2018, in Chinese.

[30] A. Ceric, M. Vukomanovic, I. Ivic, and S. Kolaric, "Trust in megaprojects: a comprehensive literature review of research trends," *International Journal of Project Management*, vol. 39, no. 4, pp. 325–338, 2021.

[31] Q. Li, Z. M. Yin, H. Y. Chong, and Q. Shi, "Nexus of interorganizational trust, principled negotiation, and joint action for improved cost performance: survey of Chinese megaprojects," *Journal of Management in Engineering*, vol. 34, no. 6, Article ID 04018036, 2018.

[32] M. Miterev, J. R. Turner, and M. Mancini, "The organization design perspective on the project-based organization: a structured review," *International Journal of Managing Projects in Business*, vol. 10, no. 3, pp. 527–549, 2017.

[33] S. Ha, D. Ko, and Y. Zhang, "Critical coupling strength of the Cucker–Smale model for flocking," *Mathematical Models and Methods in Applied Sciences*, vol. 27, no. 6, pp. 1051–1087, 2017.

[34] T. Vicsek, A. Czirók, E. Ben-Jacob, I. Cohen, and O. Shochet, "Novel type of phase transition in a system of self-driven particles," *Physical Review Letters*, vol. 75, no. 6, pp. 1226–1229, 1995.

[35] A. Jadbabaie, J. Jie Lin, and A. S. Morse, "Coordination of groups of mobile autonomous agents using nearest neighbor rules," *IEEE Transactions on Automatic Control*, vol. 48, no. 6, pp. 988–1001, 2003.

[36] F. Cucker and S. Smale, "Emergent behavior in flocks," *IEEE Transactions on Automatic Control*, vol. 52, no. 5, pp. 852–862, 2007.

[37] F. Cucker and S. Smale, "On the mathematics of emergence," *Japanese Journal of Mathematics*, vol. 2, no. 1, pp. 197–227, 2007.

[38] J. Shen, "Cucker-smale flocking under hierarchical leadership," *SIAM Journal on Applied Mathematics*, vol. 68, no. 3, pp. 694–719, 2008.

[39] F. Cucker and J.-G. Dong, "On the critical exponent for flocks under hierarchical leadership," *Mathematical Models and Methods in Applied Sciences*, vol. 19, no. 1, pp. 1391–1404, 2009.

[40] F. Cucker and E. Mordecki, "Flocking in noisy environments," *Journal de Mathematiques Pures et Appliquees*, vol. 89, no. 3, pp. 278–296, 2008.

[41] R. Erban, J. Haškovec, and Y. Sun, "A cucker—smale model with noise and delay," *SIAM Journal on Applied Mathematics*, vol. 76, no. 4, pp. 1535–1557, 2016.

[42] J. G. Dong, S. Y. Ha, and D. Kim, "Interplay of time-delay and velocity alignment in the Cucker-Smale model on a general diagraph," *Discrete Cont Dyn-B*, vol. 24, pp. 5569–5600, 2018.

[43] F. Cucker and J. G. Dong, "A conditional, collision-avoiding model for swarming," *Discrete & Continuous Dynamical Systems*, vol. 34, no. 3, pp. 1009–1020, 2014.

[44] I. Markon, "Collision-avoiding in the singular Cucker-Smale model with nonlinear velocity couplings," *Discrete & Continuous Dynamical Systems*, vol. 38, no. 10, pp. 5245–5260, 2018.

[45] X. Yin, D. Yue, and Z. Chen, "Asymptotic behavior and collision avoidance in the Cucker-Smale model," *IEEE Transactions on Automatic Control*, vol. 65, no. 7, pp. 3112–3119, 2020.

[46] F. Cucker and J.-G. Dong, "On flocks influenced by closest neighbors," *Mathematical Models and Methods in Applied Sciences*, vol. 26, no. 14, pp. 2685–2708, 2016.

[47] C. Pignotti and I. Reche Vallejo, "Flocking estimates for the Cucker-Smale model with time lag and hierarchical leadership," *Journal of Mathematical Analysis and Applications*, vol. 464, no. 2, pp. 1313–1332, 2018.

[48] F. Paita, G. Gomez, and J. J. Masdemont, "On the Cucker-Smale flocking model applied to a formation moving in a central force field," *Marine Ecology Progress*, vol. 386, pp. 181–195, 2013.

[49] A. Belkadi, Z. Liu, L. Ciarletta, Y. Zhang, and D. Theilliol, "Flocking control of a fleet of unmanned aerial vehicles," *Control Theory and Technology*, vol. 16, no. 2, pp. 82–92, 2018.

[50] H. O. Bae, S. Y. Ha, Y. Kim, S. H. Lee, H. Lim, and J. Yoo, "A mathematical model for volatility flocking with a regime switching mechanism in a stock market," *Mathematical Models and Methods in Applied Sciences*, vol. 25, no. 7, pp. 1299–1335, 2015.

[51] S. Cheng, "Complex science and systems engineering," *Journal of Management Science*, vol. 2, pp. 3–9, 1999, in Chinese.

[52] T. Castillo, L. F. Alarcón, and E. Pellicer, "Influence of organizational characteristics on construction project performance using corporate social networks," *Journal of*

Management in Engineering, vol. 34, no. 4, Article ID 04018013, 2018.

[53] T. Wang, W. Tang, D. Qi, W. Shen, and M. Huang, "Enhancing design management by partnering in delivery of international EPC projects: evidence from Chinese construction companies," *Journal of Construction Engineering and Management*, vol. 142, no. 4, Article ID 04015099, 2016.

[54] W. Shen, B. Choi, S. Lee, W. Tang, and C. T. Haas, "How to improve interface management behaviors in EPC projects: roles of formal practices and social norms," *Journal of Management in Engineering*, vol. 34, no. 6, Article ID 04018032, 2018.

[55] D. Cao, H. Li, G. Wang, X. Luo, X. Yang, and D. Tan, "Dynamics of project-based collaborative networks for BIM implementation: analysis based on stochastic actor-oriented models," *Journal of Management in Engineering*, vol. 33, no. 3, Article ID 04016055, 2017.

[56] A. Ospina-Alvarado, D. Castro-Lacouture, and J. S. Roberts, "unified framework for construction project integration," *Journal of Construction Engineering and Management*, vol. 142, no. 7, Article ID 04016019, 2016.

[57] A. S. Hanna, "Benchmark performance metrics for integrated project delivery," *Journal of Construction Engineering and Management*, vol. 142, no. 9, 2016.

[58] D. Grau, W. E. Back, and G. Mejia-Aguilar, "Organizational-behavior influence on cost and schedule predictability," *Journal of Management in Engineering*, vol. 33, no. 5, Article ID 04017027, 2017.

[59] H. Guo, R. Yu, and Y. Fang, "Analysis of negative impacts of BIM-enabled information transparency on contractors' interests," *Automation in Construction*, vol. 103, pp. 67–79, 2019.

[60] S. P. Robbins and T. A. Judge, *Organizational Behavior*, Pearson, London, UK, 2019.

Research Article

Structural Reliability Analysis via the Multivariate Gegenbauer Polynomial-Based Sparse Surrogate Model

Yixuan Dong and Shijie Wang [ID]

School of Mechanical Engineering, Shenyang University of Technology, Shenyang 110870, Liaoning, China

Correspondence should be addressed to Shijie Wang; sjwang_syut@163.com

Structural reliability analysis is usually realized based on a multivariate performance function that depicts failure mechanisms of a structural system. The intensively computational cost of the brutal-force Monte-Carlo simulation motivates proposing a Gegenbauer polynomial-based surrogate model for effective structural reliability analysis in this paper. By utilizing the orthogonal matching pursuit algorithm to detect significant explanatory variables at first, a small number of samples are used to determine a reliable approximation result of the structural performance function. Several numerical examples in the literature are presented to demonstrate potential applications of the Gegenbauer polynomial-based sparse surrogate model. Accurate results have justified the effectiveness of the proposed approach in dealing with various structural reliability problems.

1. Introduction

Structural reliability analysis needs to recursively run a performance function $g(\mathbf{X})$ for an accurate estimation result of the structural failure probability. Herein, the vector $\mathbf{X} = [X_1, \ldots, X_d]^T$ comprises all input random variables, and each pair of X_i and X_j are assumed as independent for the sake of simplicity. Or else, statistical transformations in the literature are required to obtain equivalently independent random variables [1–3]. Note that the performance function is highly possible to be implicitly expressed and computationally expensive, which makes the corresponding structural reliability analysis be not an easy but highly demanding task in reality.

Analytical derivation for stochastic characteristics of the multivariate performance function is only feasible in rare cases. The Monte Carlo simulation (MCS) and its variants allow one to alleviate the difficulty to some extent [4–6]. However, a simulation-based approach might become tedious due to high computational efforts [7]. Approximation methods, for example, the first-order reliability method (FORM) were widely investigated [8]. This paper primarily focuses on the utility of the Gegenbauer polynomials for a sparse surrogate model to mimic the true but computationally demanding performance function in structural reliability analysis. To achieve this, the orthogonal matching pursuit (OMP) in the signal processing domain is introduced to determine the principle explanatory polynomials for a sparse model, and the chaotic Gegenbauer polynomials are Directional MCS00 introduced in this paper to realize the sparse regression, rather than ordinary polynomials $\{1, x, x^2, \ldots\}$ in conventional response surface methods (RSMs).

In reality, the RSM has received considerable attention over the past decades [9–11]. A general procedure to build the surrogate model usually comprises two aspects: (1) to locate feasible combinations of explanatory variables and their coefficients for the optimized mean response and (2) to estimate the model response in the vicinity of the optimized location for better understanding the of the "local" effect of factors [12]. Once a group of explanatory variables are available, the least-square regression and the error back-prorogation mechanism are combined to determine unknown parameters [13–16].

Consider that all explanatory variables need to be fully assessed in the conventional regression analysis. The total

number of model terms will be exponentially increased with the dimensionality of input variables. The curse of dimensionality makes the conventional RSM be usually applicable to low-dimensional problems. Instead, the sparse regression analysis aims to use a fairly small number of regressors to overcome the disadvantage. Combined with the Galerkin projection [17] or the stochastic collocation method [18] to calculate the coefficients, the determined surrogate models have been widely used for uncertainty quantification of various structural systems [19–21].

The paper proposes to build a sparse surrogate model for structural reliability analysis via the Gegenbauer polynomials. The univariate Gegenbauer polynomials $G_k^{(\beta)}(x)$ (as $k = 0, 1, \ldots$) are specified by the weight function $w(x) = (1 - x^2)^{\beta - 1/2}$ and are constituted as a complete basis to represent an arbitrary function defined on $\forall x \in [-1, 1]$ [22]. Given various realizations of the polynomial parameter β, $G_k^{(\beta)}(x)$ define a group of polynomials for the model approximation. For instance, $\beta = 1/2$ defines the Legendre polynomial, whereas $\beta = 0$ and $\beta = 1$ are related to the first and the second kinds of the Chebyshev polynomials. Flexility motivates to utilize the Gegenbauer polynomials to develop surrogate models for the structural reliability analysis in this paper.

Following the theorem of the generalized Furious expansion, a real-valued function can be exactly represented via a complete basis set. Results from the variance-based global sensitivity analysis have vividly demonstrated utilizing a small number of principle terms for an accurate estimation of the true model. This motivates developing a sparse approximation of the multivariate performance function. Once the multivariate basis set based on the Gegenbauer chaos polynomials is constituted, the method of the orthogonal matching pursuit is further introduced to select primary functions to maintain the high sparsity of the surrogate model. Similar algorithms include the basis pursuit [23] and the matching pursuit methods [24], or the method via the numerical approach of the orthogonal matching pursuit (OMP) [25].

The OMP algorithm has been widely recognized to select principle regressors that are correlated with residual errors of an engineering model. Relying on the orthogonal projection of residual errors to the linear space spanned by orthogonal polynomials, the OMP algorithm can iteratively minimize the global model error sparsely [26]. Due to its advantages in terms of simple implementation and fast convergence, the OMP has been successively used for data compression, signal recovery, image recognition, and so on. Besides, advanced algorithms such as the stagewise orthogonal matching pursuit (StOMP) and the regularized orthogonal matching pursuit (ROMP) were developed in [27, 28]. The paper introduces the Gegenbauer polynomials to constitute the basis functions, and a variety of stopping criteria are further investigated for a robust OMP-based sparse regression model in structural reliability analysis. The approach is nonintrusive, which implies the corresponding structural reliability analysis is only based on a small number of deterministic model evaluations, rather than requiring high order responses, for example, the gradients in the first-order reliability method (FORM) [29].

An objective of the paper is to utilize the multivariate Gegenbauer polynomials as the basis function for an effective surrogate model for the structural reliability analysis. The high-dimensional Gegenbauer polynomials are first presented to define the multivariate chaos terms. Combined with a variety of stopping criteria to realize the sparse regression, an effective surrogate model that mimics the true but computationally demanding performance function is determined for the structural reliability analysis.

The rest of the manuscript is organized as follows: Section 2 briefly summarizes the mathematic properties of the Gegenbauer polynomials, and the multivariate basis functions are further formulated by the chaotic multiplication of univariate functions. Section 3 presents several stopping criteria for a robust sparse regression result. Numerical examples in Section 4 are presented to demonstrate potential applications of the proposed sparse regression model, and conclusions are summarized in Section 5.

2. The multivariate Gegenbauer Polynomials

A reliable sparse regression result for a structural performance function depends largely on the multivariate basis functions to span the approximation space. The paper presents utilizing the chaotic multivariate Gegenbauer polynomials. Therefore, the section starts to introduce mathematical characteristics of the univariate Gegenbauer polynomials, and multivariate basis functions are further derived via the chaotic multiplication of one-dimensional polynomials.

2.1. The Gegenbauer Polynomial. The Gegenbauer polynomials have been widely treated as a group of basis functions for the numerical approximation in engineering realities [30]. In mathematics, $G_k^{(\beta)}(x)$ ($k = 0, 1, \ldots$) are defined as pairwise orthogonal polynomials for $x \in [-1, 1]$. They are particular solutions of the Gegenbauer differential equation [31]:

$$\left(1 - x^2\right)y'' - (2\beta + 1)xy' + k(k + 2\beta)y = 0, \qquad (1)$$

which can be further degenerated as the Legendre and Chebyshev differential equation, and the Legendre and the Chebyshev polynomials are two special cases of the Gegenbauer polynomials as shown in numerical simulations.

Besides, the Gegenbauer polynomial $G_k^{(\beta)}(x)$ can be expressed via the generating function as well [32]:

$$\frac{1}{\left(1 - 2xt + t^2\right)^\beta} = \sum_{k=0}^{\infty} G_k^{(\beta)}(x)t^k, \qquad (2)$$

and the recurrence relation of the orthogonal polynomials is given as

$$
\begin{cases}
G_0^{(\beta)}(x) = 1, \\
G_1^{(\beta)}(x) = 2\beta x, \\
kG_k^{(\beta)}(x) = 2x(k+\beta-1)G_{k-1}^{(\beta)}(x) - (k+2\beta-2)G_{k-2}^{(\beta)}(x) \quad (k \geq 2).
\end{cases}
\tag{3}
$$

Mathematically, the orthogonality of $G_k^{(\beta)}(x)$ is governed by

$$
\int_x w(x)G_k^{(\beta)}(x)G_l^{(\beta)}(x)\mathrm{d}x = C_k(\beta)\delta_{kl}.
\tag{4}
$$

Herein, $w(x) = (1-x^2)^{\beta-1/2}$ denotes the weight function $x \in [-1,1]$, and δ_{mn} represents the Kronecker delta symbol. This is further used to define the normalization constant $C_k(\beta)$:

$$
C_k(\beta) = \frac{\pi 2^{1-2\beta}\Gamma(k+2\beta)}{k!(k+\beta)[\Gamma(\beta)]^2} \quad (k = 0,1,\ldots),
\tag{5}
$$

in which the symbol $\Gamma(\cdot)$ denotes the Gamma function.

Given the parameter $\beta = 1/2, 1.0, 2.0$, and 3.0, the first six realizations of the Gegenbauer polynomial (i.e. $k = 0,\ldots,5$) are presented in Figure 1. The Legendre and the Chebyshev polynomials are two special cases of the Gegenbauer polynomial, which will be utilized to build multivariate basis functions for a sparse approximation result of the performance function $g(\mathbf{X})$ in structural reliability analysis.

2.2. The multivariate Gegenbauer polynomial.
Structural reliability analysis is always evaluated based on a multivariate performance function $g(\mathbf{X})$, and the multivariate Gegenbauer polynomials will be derived for a numerical approximation of the performance function.

Define an index vector $\theta = [\theta_1, \ldots, \theta_d]^T$ with each integral $\theta_k \in [0,p]$. Then, the degree of a d-variate chaotic Gegenbauer polynomial $\phi_\theta(\mathbf{x})$ can be measured by the length of the index vector, that is, $|\theta| = \sum_{k=1}^d \theta_k$. Specifically, the total number (N) of chaotic terms in the polynomial set $\{\phi_\theta(\mathbf{x})\}$ is determined by parameters d and the polynomial order p as

$$
N = \binom{d+p}{p} = \frac{(d+p)!}{d!p!},
\tag{6}
$$

and the vector-indexed multivariate Gegenbauer polynomials are defined via the chaotic multiplication of the univariate functions:

$$
\{\phi_i(x), i = 0,\ldots,N-1\} := \bigcup_{|\theta| \leq p}\prod_{k=1}^d G_{\theta_k}^{(\beta)}(x_k),
\tag{7}
$$

wherein $G_{\theta_k}^{(\beta)}(x_k)$ represents the θ_kth-order univariate polynomial presented in Section 2.1.

Figure 2 presents the bivariate Gegenbauer polynomials with parameters $\beta = 1/2$ and the polynomial degree $p = 4$. For other high-dimensional cases, one can refer to the tensor-product formulation in equation (7). Note that each two pair of multivariate Gegenbauer polynomials are orthogonally defined, given that

$$
\langle\phi_i(\mathbf{x}),\phi_j(\mathbf{x})\rangle = \int_\mathbf{x} W(\mathbf{x})\phi_i(\mathbf{x})\phi_j(\mathbf{x})\mathrm{d}\mathbf{x} = C_0\delta_{ij} \quad (i,j = 0,\ldots,N-1),
\tag{8}
$$

wherein $W(\mathbf{x})$ represents a d-dimensional weighting function $W(\mathbf{x}) = \prod_{k=1}^d (1-x_k^2)^{\beta-1/2}$ as $\mathbf{x} \in [-1,1]^d$ whereas C_0 denotes a normalization constant.

To illustrate the orthogonal characteristic, the original index vector of an arbitrary two orders of the chaotic polynomials are recovered as $\theta^{(i)} = [\theta_1^{(i)}, \theta_2^{(i)}, \ldots, \theta_d^{(i)}]^T$ and $\theta^{(j)} = [\theta_1^{(j)}, \theta_2^{(j)}, \ldots, \theta_d^{(j)}]^T$, respectively. Following this notation, the inner product in equation (8) is realized as

$$
\begin{aligned}
\langle\phi_i(\mathbf{x}),\phi_j(\mathbf{x})\rangle &= \int_\Omega W(\mathbf{x})\phi_{\boldsymbol{\theta}^{(i)}}(\mathbf{x})\phi_{\boldsymbol{\theta}^{(j)}}(\mathbf{x})\mathrm{d}\mathbf{x} \\
&= \prod_{k=1}^d \int_{x_k} w(x_k)G_{\theta_k^{(i)}}^{(\beta)}(x_k)G_{\theta_k^{(j)}}^{(\beta)}(x_k)\mathrm{d}x_k = \prod_{k=1}^d C_{\theta_k^{(i)}}(\beta)\delta_{\theta_k^{(i)}\theta_k^{(j)}}.
\end{aligned}
\tag{9}
$$

Note that $\forall \theta_k^{(i)} \neq \theta_k^{(j)}$ and $\phi_i(\mathbf{x}) \neq \phi_j(\mathbf{x})$ as $k = 1,\ldots,d$ and $i,j = 0,\ldots,N-1$.

Define the normalized univariate Gegenbauer polynomial:

$$
\widehat{G}_{\theta_k}^{(\beta)}(x) = \frac{1}{\sqrt{C_{\theta_k}(\beta)}} \cdot G_{\theta_k}^{(\beta)}(x) \quad (\text{for each integer } \theta_k \in [0,p]).
\tag{10}
$$

(a)

(b)

(c)

(d)
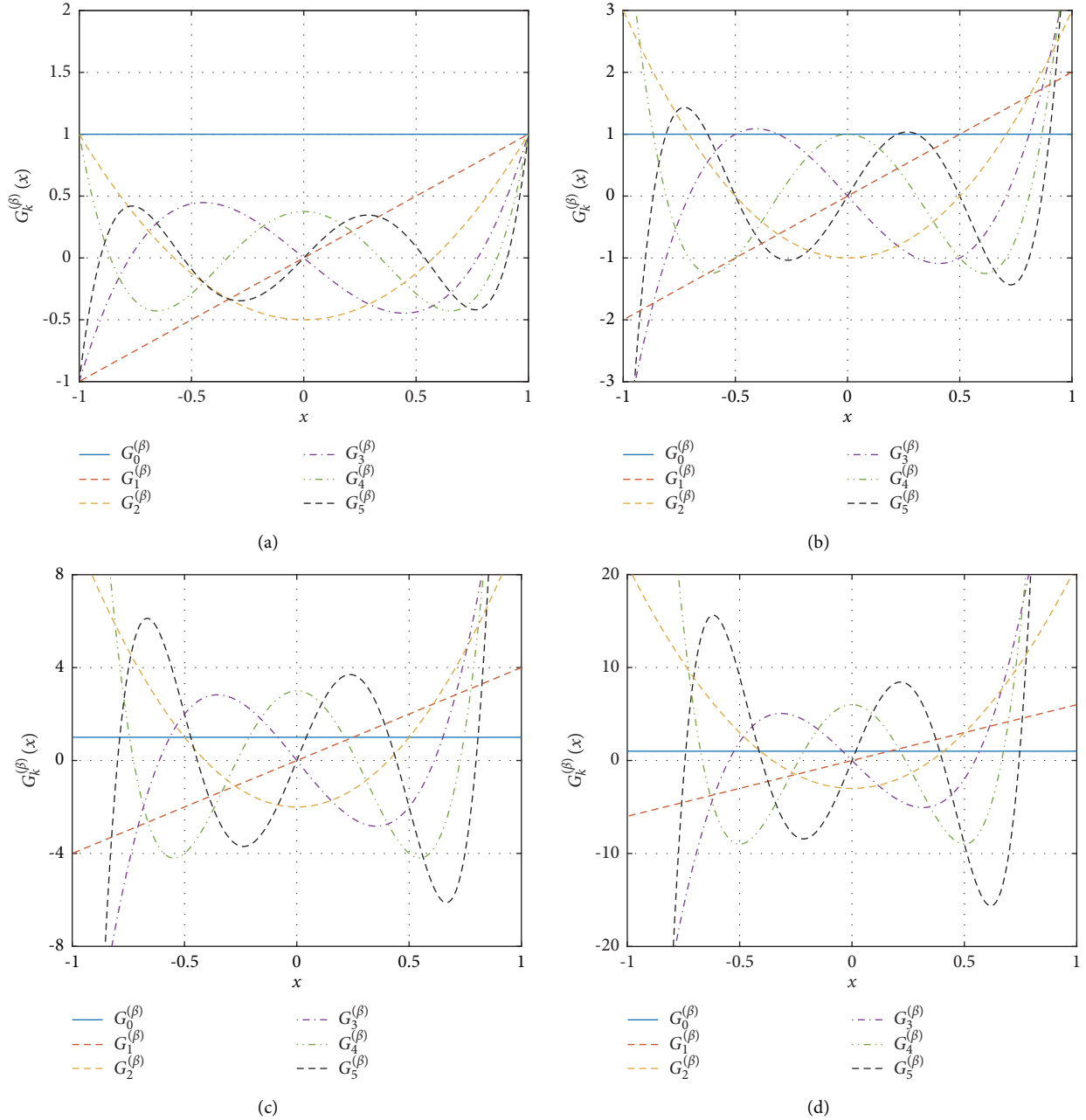
Figure 1: The first six orders of the Gegenbauer polynomial with various realizations of the parameter $\beta = 1/2, 1.0, 2.0,$ and 3.0. (a) $\beta = 1/2$: the Legendre polynomial. (b) $\beta = 1$: the Chebyshev polynomial. (c) $\beta = 2.0$. (d) $\beta = 3.0$.

Substituting $\widehat{G}_{\theta_k}^{(\beta)}(x)$ to equation (8), one can obtain the normalized multivariate set $\{\widehat{\phi}_0(\mathbf{x}), \ldots, \widehat{\phi}_{N-1}(\mathbf{x})\}$, whose elements have the property of

$$\langle \widehat{\phi}_i(\mathbf{x}), \widehat{\phi}_j(\mathbf{x}) \rangle = \delta_{ij} \quad (i, j = 0, \ldots, N-1), \tag{11}$$

and its second-norm can be defined as

$$\left\| \widehat{\phi}_i(\mathbf{x}) \right\|_2 = 1 \quad (i = 0, \ldots, N-1). \tag{12}$$

Note that the normalized multivariate Gegenbauer polynomials $\widehat{\phi}_i(\mathbf{x})$ (for $i = 0, \ldots, N-1$) will be used as the basis functions in subsequent sparse approximations, and

the normalized polynomial will be denoted as $\phi_i(\mathbf{x})$ for the sake of simplicity.

Besides the normalization issue, a linear transformation of the parameter x is required to match the definition domain of input random variables:

$$z_i = \frac{a_U - a_L}{2} x_i + \frac{a_L + a_U}{2} \quad (\text{as } x_i \in [-1, 1] \text{ and } i = 1, \ldots, d),$$

$$\tag{13}$$

and parameters a_L and a_U are empirically defined as
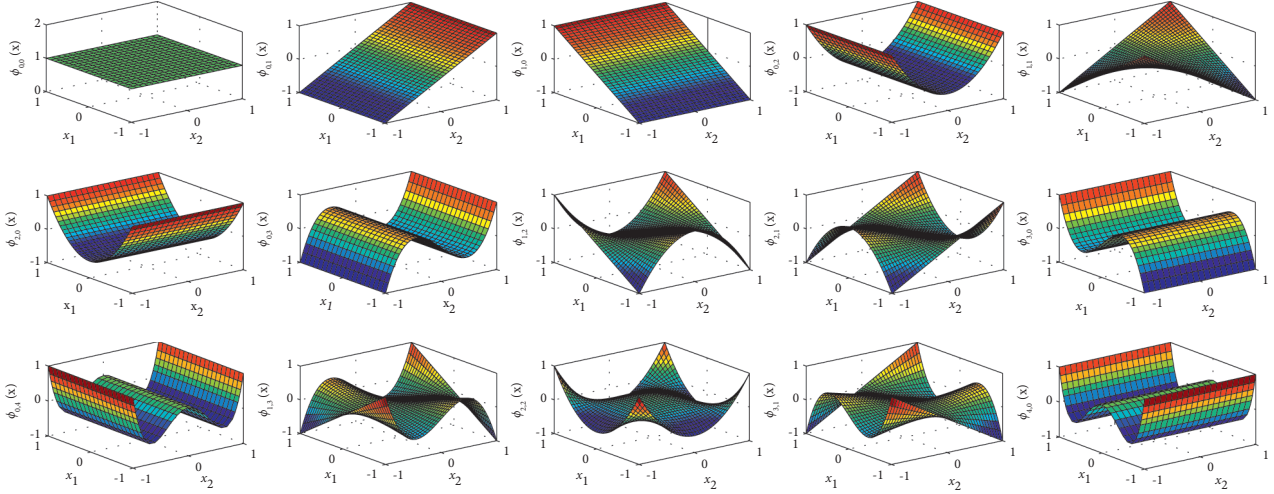
FIGURE 2: Bivariate Gegenbauer polynomials defined by parameters $\beta = 1/2$ and the polynomial degree $p = 4$.

$$\begin{cases} a_L = F^{-1}(\mu_i - k\sigma_i), \\ a_U = F^{-1}(\mu_i - k\sigma_i), \end{cases} \tag{14}$$

wherein $F^{-1}(\cdot)$ represents the inverse cumulative distribution function (iCDF) of the random variable X_i associated with the mean μ_i and the standard deviation σ_i.

The parameter k is expected to connect with the truncated probability in equation (14). If X_i is a Gaussian variable, the truncated probability $\Pr[X_i \leq a_L] + \Pr[X_i \geq a_U]$ will be less than 0.3% and 0.01%, respectively, as $k = 3$ and 4. Therefore, the linear transformation in equation (13) with the parameter $k = 4$ will be utilized in numerical examples to tackle nonuniformly distributed and skewed random variables.

3. The Gegenbauer Polynomial-Based Sparse Surrogate Model

Structural reliability simulations are always realized based on a multivariate performance function and its surrogate model. Once the surrogate model is numerically available, the subsequent reliability analysis can be alternatively realized by the brutal Monte Carlo simulation. Note that the total number of functional evaluations is limited to the development of the surrogate model $\hat{g}(\cdot)$, rather than all random samples. As a comparison, the original random simulation based on $g(\mathbf{X})$ will require $N_{MCS} \geq 100/P_F$ samples [33]. The large number of model repetitions implies a huge amount of computational cost. Therefore, the paper proposes utilizing the chaotic Gegenbauer polynomials to build the surrogate model at first, and the total number of mechanistic model reevaluations will be only limited to the number of numerical operations to develop the surrogate model, rather than directly carrying out the physical model-based random simulations.

Conventional response surface models usually contain hundreds or even thousands of polynomial terms for a robust estimation result. The global sensitivity analysis result has shown that a relatively small number of component

functions is capable of accurately approximating a complex performance function $g(\cdot)$; that is, a sparse approximation is available for the structural reliability analysis. Based on the consideration, the section presents utilizing the chaotic Gegenbauer polynomial-based sparse model to mimic the true performance function. The principle polynomials among all potential explanatory elements are detected based on a small number of model simulation results. To begin with, a standard procedure for the surrogate model developed based on the statistical regression method is briefly summarized as follows.

3.1. The Regression-Based Surrogate Model. To begin with, the set $\zeta = \{\mathbf{x}^{(1)}, \ldots, \mathbf{x}^{(n)}\}$ consists of n realizations of input random vector $\mathbf{X}$ generated based on a low-discrepancy sequence, for example, the Sobol', the Helton, or the Hammersley algorithm, whereas the corresponding realizations of the chaotic Gegenbauer polynomial set $\{\phi_i(\mathbf{x})\}_{i=0}^{N-1}$ are expressed in a matrix form as

$$\boldsymbol{\xi} = \begin{bmatrix} \phi_0(\mathbf{x}^{(1)}) & \phi_1(\mathbf{x}^{(1)}) & \cdots & \phi_{N-1}(\mathbf{x}^{(1)}) \\ \phi_0(\mathbf{x}^{(2)}) & \phi_1(\mathbf{x}^{(2)}) & \cdots & \phi_{N-1}(\mathbf{x}^{(2)}) \\ \vdots & \vdots & \ddots & \vdots \\ \phi_0(\mathbf{x}^{(n)}) & \phi_1(\mathbf{x}^{(n)}) & \cdots & \phi_{N-1}(\mathbf{x}^{(n)}) \end{bmatrix}_{n \times N}. \tag{15}$$

Following the theory of multivariate "linear" regression [34], a response surface model for the performance function $g(\cdot)$ can be obtained as

$$\hat{y} = \sum_{i=0}^{N-1} b_i \phi_i(\mathbf{x}) + \varepsilon. \tag{16}$$

Note that the vector $\mathbf{b} = [b_0, b_1, \ldots, b_{N-1}]^T$ consists of all regression coefficients that are attached to explanatory variables $\{\phi_i(\mathbf{x})\}_{i=0}^{N-1}$. In addition, the residual error is expressed as

$$\mathbf{r} = \mathbf{y} - \boldsymbol{\xi}\hat{\mathbf{b}}. \tag{17}$$

Here, the model response vector $\mathbf{y} = [g(\mathbf{x}^{(1)}), \ldots, g(\mathbf{x}^{(n)})]^T$ comprises total n realizations of the mechanistic model by continuously feeding each element of the training dataset ζ. And the unknown regression coefficients $\widehat{\mathbf{b}}$ can be expressed in terms of the training dataset ξ as

$$\widehat{\mathbf{b}} = \left(\xi^T \xi\right)^{-1} \xi^T \mathbf{y}. \tag{18}$$

Therefore, once the training matrix ξ defined in equation (15) and corresponding structural response samples $\mathbf{y}$ are numerically available, the least-square minimization based on the 2-norm of the residual error vector $\mathbf{r}$ allows deriving an empirical surrogate model noted in equation (16) for reliability analysis of the structural system.

3.2. A Sparse Regression Model Based on the OMP Algorithm.
A fundamental problem in structural reliability analysis signal processing is to develop a reliable sparse surrogate model for multivariate input uncertainties. The orthogonal matching pursuit (OMP) algorithm for the signal processing is presented with the basis dictionary defined by the chaotic Gegenbauer polynomials.

Given a realization of the polynomial parameter p, the full dictionary set can be initialized as $\phi_{(0)} = [\phi_0(\mathbf{x}), \phi_1(\mathbf{x}), \ldots, \phi_{N-1}(\mathbf{x})]^T$, together with principle components $\psi_{(0)} = \varnothing$. Based totally on n training samples in ζ generated based on the Halton or the Sobol' low-discrepancy scheme, the corresponding model responses $\mathbf{y}$ and the polynomial matrix ξ in equation (15) are prepared for subsequent model evaluations. Specifically, the residual error is initialized as $\mathbf{r}_{(0)} = \mathbf{y}$, whereas the significant elements in ξ will be $\chi_{(0)} = \varnothing$.

For a realization of the iterative counter $k \geq 1$, one could implement the OMP-based sparse regression analysis as follows:

(1) Detect the most principle polynomial $\phi_{i^*}(\mathbf{x}) \in \psi_{(k-1)}$ based on the following criterion:

$$i^* = \arg\max \left| \xi_i^T \mathbf{r}_{(k-1)} \right| \quad (\text{as } i = 0, \ldots, N-1), \tag{19}$$

wherein the symbol $\xi_i = [\phi_i(\mathbf{x}^{(1)}), \phi_i(\mathbf{x}^{02}), \ldots, \phi_i(\mathbf{x}^{(n)})]^T$ denotes an ith column of the polynomial matrix ξ that is evaluated based on n samples of the input random vector $\mathbf{X}$. Therefore, the polynomial index parameter for an i^*th significant polynomial will be updated as $\psi_{(k)} = \psi(k-1) \cup \{\phi_{i^*}(\mathbf{x})\}$ and $\chi_{(k)} = \chi_{(k-1)} \cup \{\xi_{i^*}\}$, respectively. Meanwhile, the explanatory dictionary is revised by excluding the element $\phi_{i^*}(\mathbf{x})$, that is, $\phi_{(k)} = \phi_{(k-1)} \ominus \{\phi_{i^*}(\mathbf{x})\}$ for subsequent iterations.

(2) Update the model result by calculating the coefficients $\widehat{\mathbf{b}}_{(k)} = [\chi_{(k)}^T \chi_{(k)}]^{-1} \chi_{(k)}^T \mathbf{y}$, which determines the model after a kth iteration as

$$\widehat{y}_{(k)} = \psi_{(k)}^T \widehat{\mathbf{b}}_{(k)}. \tag{20}$$

Note that the residual error will be $\mathbf{r}_{(k)} = (\mathbf{I} - \mathbf{A})\mathbf{y}$, and $\mathbf{A} = \chi_{(k)}[\chi_{(k)}^T \chi_{(k)}]^{-1}\chi_{(k)}^T$, and the symbol $\mathbf{I}$ denotes an $n \times n$ identity matrix.

(3) Evaluate the sparse regression model in equation (20) based on stopping criteria listed in Table 1. Or else, set $k = k + 1$ and repeat Steps 1–3 till the largest realization of the iterative counter $N_{\max} = \text{rank}(\xi)$.

It is observed that the OMP algorithm is a stepwise forward greedy algorithm to select principle components. In this regard, a main issue for the sparse regression can stop the greedy selection process at "a right time." However, stopping rules of the greedy algorithm are mainly defined by mathematical characteristics of the residual error. Typical realizations include the ℓ_2 and ℓ_∞ measures, that is, $\|\mathbf{r}_{(k)}\|_2 \leq \varepsilon_1$ and $\|\psi_{(k)}^T \mathbf{r}_{(k)}\|_\infty \leq \varepsilon_2$, wherein, parameters ε_i (as $i = 1, 2$) denote the predefined error thresholds. In addition, a relative-error-based measure can also be used:

$$\frac{\|\mathbf{r}_{(k-1)} - \mathbf{r}_{(k)}\|_\infty}{\|\mathbf{r}_{(k)}\|_\infty} < \varepsilon_3, \tag{21}$$

which is evaluated by two successive residual errors $\mathbf{r}_{(k-1)}$ and $\mathbf{r}_{(k)}$ (as $k = 1, 2, \ldots$) in model iterations. Note that the ℓ_∞-norm used here is much more strict than criteria based on the ℓ_2 norm.

Rather than the hard stopping criteria that are evaluated directly based on the residual error term $\mathbf{r}_{(k)}$, an F-value-based soft stopping criterion can be further used to exclude incorrectly identified component functions. This is because the multivariate Gegenbauer polynomials might not be exactly orthogonally defined with each other due to the truncated simulation domain $\Omega = \cup_i \Omega_i$ as shown in equation (14). It is highly possible that the residual error $\mathbf{r}_{(k)}$ cannot be exactly represented by the remaining polynomial set after a kth iteration. This is the motivation to utilize an F-test-based procedure to exclude spurious basis functions and maintain the high sparsity of the response surrogate model.

Recall that the covariance matrix for regression coefficients $\widehat{\beta}_{(k)}$ is estimated as

$$\text{Cov}\left[\widehat{\beta}_{(k)}\right] = \sigma^2 \left[\chi_{(k)}^T \chi_{(k)}\right]^{-1}, \tag{22}$$

wherein σ^2 denotes the variance of the error term ϵ, and its unbiased estimator is

$$\widehat{\sigma}^2 = \frac{\mathbf{r}_{(k)}^T \mathbf{y}}{n - M}, \tag{23}$$

Herein, the integers n and m represent the total number of training samples and polynomial elements in $\widehat{\beta}_{(k)}$, respectively. Then, an F-statistics for the significant test of regression coefficients are defined as

$$F_j = \frac{\widehat{b}_j^2}{\left[\text{Cov}\left(\widehat{\mathbf{b}}_{(k)}\right)\right]_{jj}} \quad \left(\text{for each } \widehat{b}_j \in \widehat{\mathbf{b}}_{(k)} \text{ and } j = 1, \ldots, M\right), \tag{24}$$

TABLE 1: Stopping criteria used in numerical simulations.

Hard rules			Soft rule
$\|\mathbf{r}_{(k)}\|_2 \le \varepsilon_1$	$\|\psi_{(k)}^T \mathbf{r}_{(k)}\|_\infty \le \varepsilon_2$	$\|\mathbf{r}_{(k-1)} - \mathbf{r}_{(k)}\|_\infty / \|\mathbf{r}_{(k)}\|_\infty \le \varepsilon_3$	$F_{j^*} < F_{\alpha^*}$

which will be used to detect the most insignificant coefficient $\widehat{b}_{j^*}$ with the minimum F-value:

$$j^* = \arg\min\{F_j, j = 1, \ldots, M\}. \quad (25)$$

Together with the significant level β^* in numerical examples, the F-value-based "soft" stopping criterion will be numerically implemented depending on the following cases:

Case 1: $F_{j^*} < F_{\beta^*}(1, n - M)$ and $i^* = j^*$. This implies that the null hypothesis $\{H_0 : \widehat{\beta}_{i^*} = 0\}$ cannot be rejected based on the F test for the $\widehat{\beta}_{i^*}$th regression coefficient, and the surrogate model $\widehat{y}_{(k-1)} = \phi_{(k-1)}\widehat{\beta}_{(k-1)}$ is the sparse regression result for the performance function $g(\cdot)$.

Case 2: $F_{j^*} < F_{\beta^*}(1, n - M)$ but $i^* \ne j^*$. One needs to update the significant polynomial set $\phi_{(k)}$ by excluding the spurious principle component $\phi_{j^*}(\mathbf{x})$ and recalculate regression coefficients $\widehat{\beta}_{(k)}$ for afterward significant tests.

Otherwise, go to Step 3 till the counting variable k reaches its upper bound $N_{\max} = \text{rank}(\xi)$.

In summary, all considered hard and soft stopping criteria are listed in Table 1. In numerical simulations, a total of eight cases about realizations of parameters ε_i and α^* will be considered, that is, $\varepsilon_1 = 0.1, 0.05$ (Cases 1 and 2), $\varepsilon_2 = 0.1, 0.05$ (Cases 3 and 4), $\varepsilon_3 = 0.1, 0.05$ (Cases 5 and 6), and $\alpha^* = 0.05, 0.01$ (Cases 7 and 8) given a realization of ε_i and α^*. Together with several examples in the literature, potential applications of the Gegenbauer polynomial-based surrogate model for structural reliability analysis will be demonstrated below.

4. Numerical Assessments of the Gegenbauer Polynomial-Based Surrogate Model

This section examines the performance of the chaotic Gegenbauer polynomial-based sparse regression method for structural reliability analysis based on several examples in the literature. In this regard, an accuracy measure of the surrogate model is defined as

$$\text{regression error} = \frac{\sum_{i=1}^{N_{\text{Test}}} \left[g(\mathbf{x}^{(i)}) - \widehat{g}(\mathbf{x}^{(i)})\right]^2}{\sum_{i=1}^{N_{\text{Test}}} \left[g(\mathbf{x}^{(i)}) - \overline{y}\right]^2}, \quad (26)$$

wherein the mean value of the model response is estimated as $\overline{y} = 1/N_{\text{Test}} \sum_{i=1}^{N_{\text{Test}}} g(\mathbf{x}^{(i)})$ based on N_{Test} realizations of the input random vector $\mathbf{X}$. In addition, a model sparsity indicator is defined as

$$\text{ratio of sparsity} = \frac{\text{the number of detected significant terms}(M)}{\text{total number of elements in}\{\phi_0(\mathbf{x}), \ldots, \phi_{N-1}(\mathbf{x})\}} \times 100\%, \quad (27)$$

and a small value of the ratio of the sparsity (RoS) (e.g., $\le 20\%$) is expected in engineering realities to reduce the total number of training samples for structural reliability analysis.

4.1. The Ishigami function. The mathematical example investigates the numerical performance of the chaotic Gegenbauer polynomial in sparse regressions analysis by considering the Ishigami function:

$$g(\mathbf{X}) = \sin(X_1) + a[\sin(X_2)]^2 + b\sin(X_1)X_3^4. \quad (28)$$

All input variables X_i are i.i.d. uniform random variables within the interval $[-\pi, \pi]$, and constants a and b are assumed as 7.0 and 0.1, respectively, in the literature. Note that the full model consists of 286 terms for the highest polynomial order $p = 10$.

Since the analytical result of the Ishigami function is available, a numerical experiment is carried out to examine the effect of various stopping criteria for uncertainty analysis of the Ishigami function. With 200 random realizations of the input vector $\mathbf{X}$, the proposed algorithm is followed to determine dominant basis functions and the corresponding sparse regression model.

Figure 3 presents simulation results of the regression error (Re) and the ratio of sparsity (RoS) for various realizations of the polynomial parameter $\beta \in [-0.8, 0.8]$ for X_1 and X_2, whereas investigated stopping criteria in Table 1 will be investigated. This allows one to determine a better stopping criterion for small realizations of the structural performance function. Results have justified that the polynomial parameter β can determine divergent surrogate models in terms of the approximation error and the sparsity ratio. Specifically, realizations $\beta = -0.6$ and -0.69 determine the minimal error and the sparsity ratio results for the uniform random variables, respectively. Besides, an increase in the absolute value of $|\beta|$ will generally increase the global errors and the sparsity ratio. In this regard, the Chebyshev polynomial determined by the parameter $\beta = 0$ will be further examined for various structural reliability problems.

Specifically, the effect of the parameter β on the numerical accuracy of the surrogate model is further investigated by considering β varying from -0.2 to 0.2 with an incremental Step 0.05. Results in Figure 4 show that there are no significant differences among prediction error results, which are less than 3×10^{-6} for all realizations cases, yet the cases $\beta = -0.05$ and $\beta = 0$ can determine relatively smaller sparsity, that is, $\le 6.7\%$.
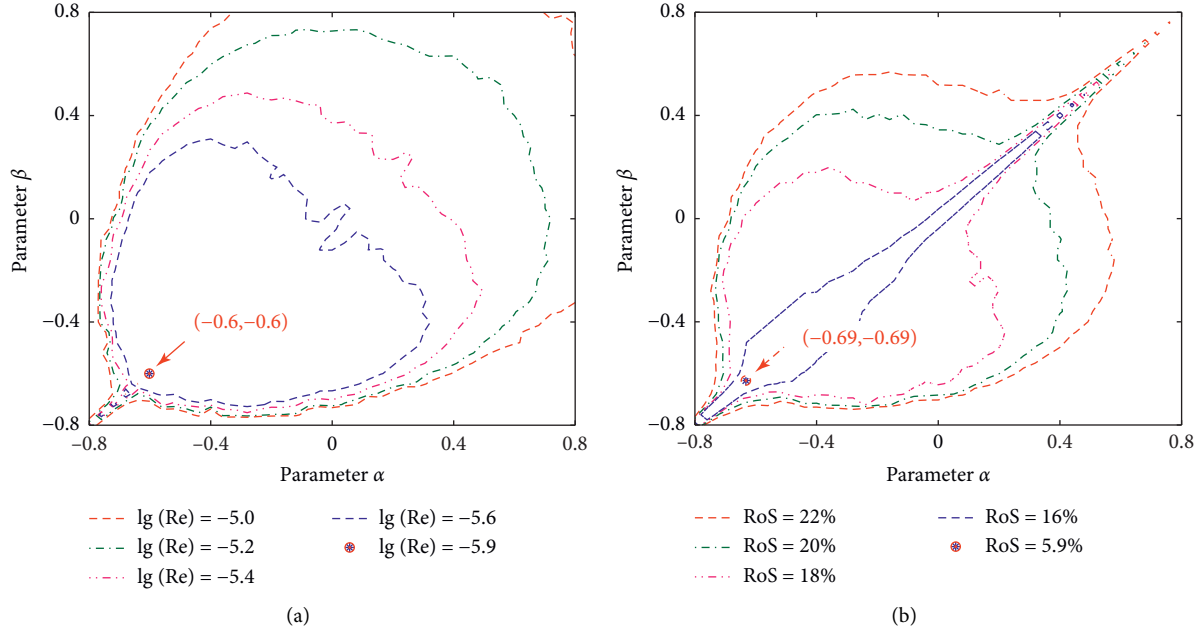
FIGURE 3: The isoline for the median values of the regression error (Re) and the sparsity ratio as $\beta_1, \beta_2 \in [-0.8, 0.8]$). (a) The regression error. (b) The sparsity ratio.
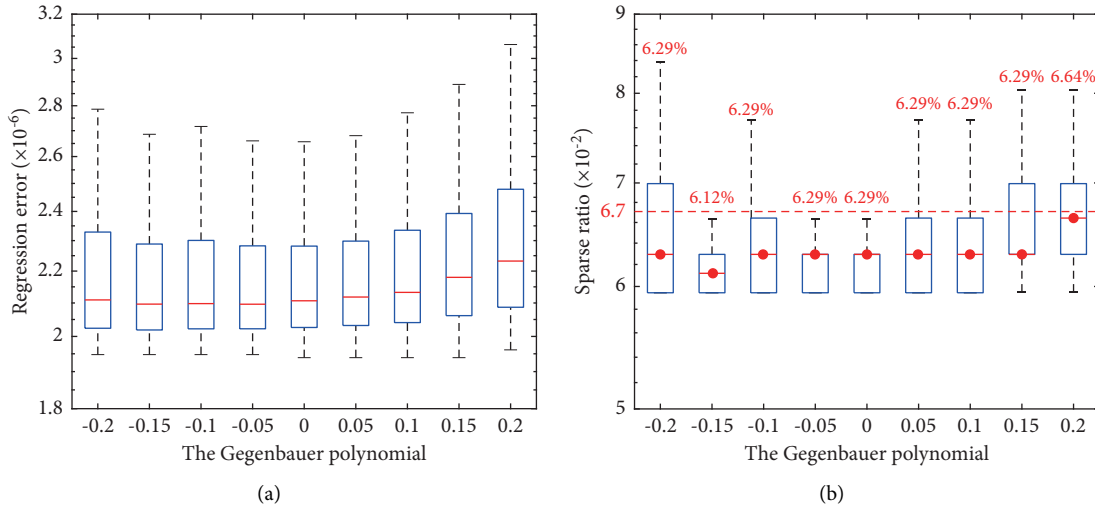

FIGURE 4: Results for the regression errors and the sparse ratio as the polynomial parameter $\beta \in [-0.2, 0.2]$. (a) The regression error. (b) The sparsity ratio.

Therefore, the case $\beta = 0$ will be used to check various stopping criteria in Table 1 as follows.

The polynomial parameter is further fixed as $\beta = 0$, numerical results of the regression error and the sparsity ratio are estimated for various stopping criteria in Figure 5. It is observed that the global regression error and sparse ratio are much higher than the average result for the hard stop criterion $\|\psi_{(k)}^T \mathbf{r}_{(k)}\|\|_\infty$ with the threshold parameter $\varepsilon_2 = 0.05$ (Case 4) and the F-value-based soft rule with the parameter $\alpha^* = 0.05$ (Case 7). Specifically, the largest regression error and the sparse ratio results are observed for

Case 2, that is, $\|\mathbf{r}_{(k)}\|_2 \leq 0.05$. In general, the optimum result is determined by the hard rule $\|\psi_{(k)}^T \mathbf{r}_{(k)}\|\|_\infty \leq 0.1$ (Case 4) and the soft criterion $F_{\alpha^*} = 0.05$ (Case 7) for the Ishigami example. The criteria will be further examined by a high-dimensional uncertain model as follows.

4.2. The High-Dimensional Function.

To further examine the performance of the proposed Gegenbauer polynomial-based regression method for uncertainty analysis of high-dimensional models, the example considers the multivariate function:

$$g(\mathbf{X}) = 3 - \frac{5}{d} \sum_{k=1}^{d} k X_k + \frac{1}{d} \sum_{k=1}^{d} k X_k^3 + \ln\left[\frac{1}{3d} \sum_{k=1}^{d} k\left(X_k^2 + X_k^4\right)\right]. \tag{29}$$

Herein, X_i are uniform i.i.d. variables within the region $[1, 2]$, and various realizations of the dimensionality parameter d are considered.

To examine the performance of the proposed sparse regression approach for a problem with various dimensions of the input random vector $\mathbf{X}$, the dimensionality parameter d is generally assumed as 10 and 20. Combining the polynomial parameter $\beta = 0$ and various stopping criteria, Figures 6 and 7 summarize simulation results for the global regression error and the sparsity ratio associated with the dimensionality parameters $d = 10$ and 20.

Results have shown that the stop criterion $\|\psi_{(k)}^T \mathbf{r}_{(k)}\|\|_\infty \leq 0.1$ (Case 4) and the F statistic-based criteria in Cases 7 and 8 are able to determine relatively small results of the regression error and the sparsity ratio. Specifically, the criterion (Case 2), that is, $\|\mathbf{r}_{(k)}\|_2 \leq 0.05$, cannot determine the surrogate model as accurate as other rules if $d = 20$. Consider a better balance of the global error and the sparsity ratio achieved by the hard criteria $\|\psi_{(k)}^T \mathbf{r}_{(k)}\|\|_\infty \leq 0.1$ and the soft rule $F_{j^*} < F_{\alpha^*}$; they will be used to build the surrogate model for structural reliability analysis in the following simulations.

To further examine the utility of various polynomials in the model approximation, the Chebyshev polynomial of the first kind, that is, the polynomial parameter $\beta = -1/2$, is further used to build a surrogate model of the high-dimensional function. Results in Figure 8 have shown that the proposed regression method is rather effective for the high-dimensional problem, for example, the dimensionality parameter $d \geq 15$. The corresponding sparsity ratio is less than 10%, and the regression errors are in the magnitude of 10^{-5}. The high accuracy ensures the numerical effectiveness of the surrogate model for structural reliability simulations.

Figure 9 finally presents numerical results for the response probability density function of the high-dimensional function. With 500 Sobol' sequences to build the sparse model at first, the brutal-force MCS is fully realized based on the surrogate model $\hat{g}(\mathbf{X})$. The close agreement of simulation results between the surrogate and the true models has confirmed the high accuracy of the proposed approach.

4.3. Reliability Analysis of a Steel Frame Structure. The example further demonstrates potential applications of the proposed Gegenbauer polynomial-based sparse regression method for reliability analysis of a two-bay six-story steel frame. As depicted in Figure 10, random variables of the frame structure include the modulus of elasticity E, the moment of inertia I, and structural external loads P_i ($i = 1, \ldots, 6$). The probabilistic characteristics of input random variables are summarized in Table 2, whereas the performance function is defined as the structural maximal interstorey drift over the limit $u_0 = 11$ cm:

$$\begin{aligned} g(\mathbf{X}) &= u_0 - D_{\max}(\mathbf{X}) \\ &= u_0 - \max\left\{\left|d_A(\mathbf{X}) - d_D(\mathbf{X})\right|, \left|d_B(\mathbf{X}) - d_E(\mathbf{X})\right|, \left|d_C(\mathbf{X}) - d_F(\mathbf{X})\right|\right\}. \end{aligned} \tag{30}$$

Herein, $D_{\max}$ denotes the maximal interstorey drift, whereas $d_{(\cdot)}$ represents the nodal lateral displacements that are explicitly evaluated based on a finite element (FE) model of the steel frame structure.

To determine the failure probability of the steel frame structure, the Gegenbauer polynomial with the parameter $\beta = 0$ is used to develop a sparse surrogate model with the polynomial order $p = 3$ and the sample size $n = 500$. Note that a similar result based on the parameter $\beta = 1/2$ is determined, yet omitted here for the sake of brevity.

Figure 11(a) depicts numerical results for the empirical PDF of the structural maximum roof drift, and 500 samples are sufficient to determine a surrogate model to mimic the true performance function. The POE result pictured in Figure 11(b) provides the estimation of the structural failure probability as 1.44×10^{-2}, which is fairly close to the benchmark result 1.49×10^{-2} in [35].

To further evaluate the robustness of the proposed approach, 100 repetitions of the sparse regression analysis have been implemented, and the corresponding results for the structural failure probability are summarized in Figure 12. Since each round of the sparse regression analysis only requires 500 nonintrusive model runs. It has exhibited the high efficiency of the proposed approach for the structural reliability analysis, whereas the small standard deviation result (3.74×10^{-4}) confirms the robustness of the proposed method as well.

4.4. Reliability Analysis of a Bar Structure with Spatially Varying Stochastic Material Properties. This section illustrates an application of the proposed approach by considering a bar structure with spatially varying Young's modulus. As depicted in Figure 13, a bar structure with unit length and cross-sectional area (i.e., $L = 1$ and $A = 1$) is subjecting axially distributed load $P(x) = x$. Specifically, the modulus of elasticity E is model via a homogeneous Gaussian random field:

$$\mathrm{Cov}(x, x') = \sigma_E^2 \exp\left(-\frac{|x - x'|}{\delta}\right) \text{ with } x, x' \in [0, L], \tag{31}$$

which is the exponential covariance function and symbols x and x' represent any two positions along the bar. The parameters $\sigma_E = 0.1$ unit and δ denote the standard deviation and correlation length of the Gaussian random field, respectively.

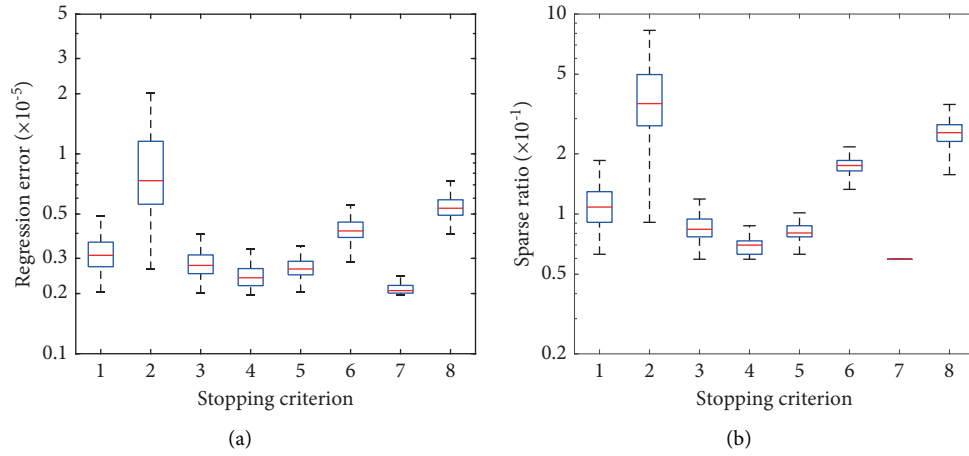FIGURE 5: Results for the regression errors and the sparse ratio. (a) The regression error. (b) The ratio of the sparsity.
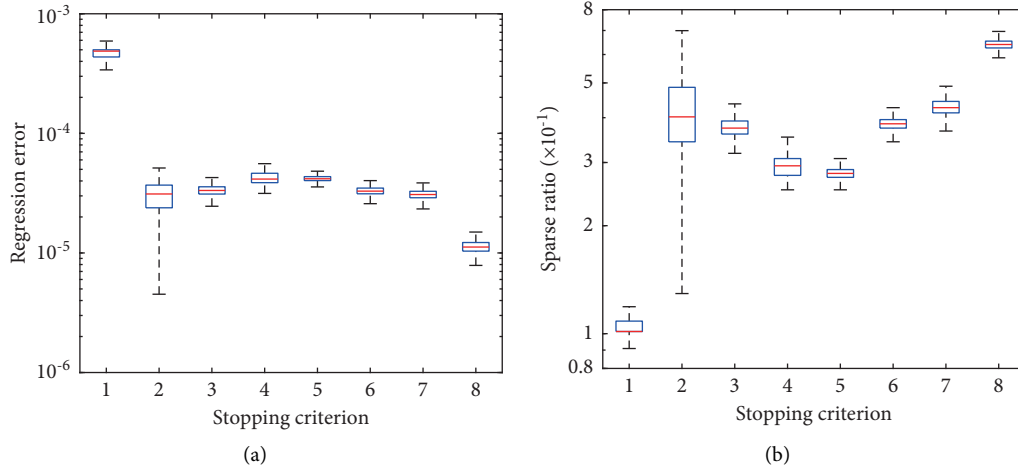
FIGURE 6: Results for the regression error and the sparsity ratio for the case $d = 10$. (a) The regression error. (b) The sparsity ratio.
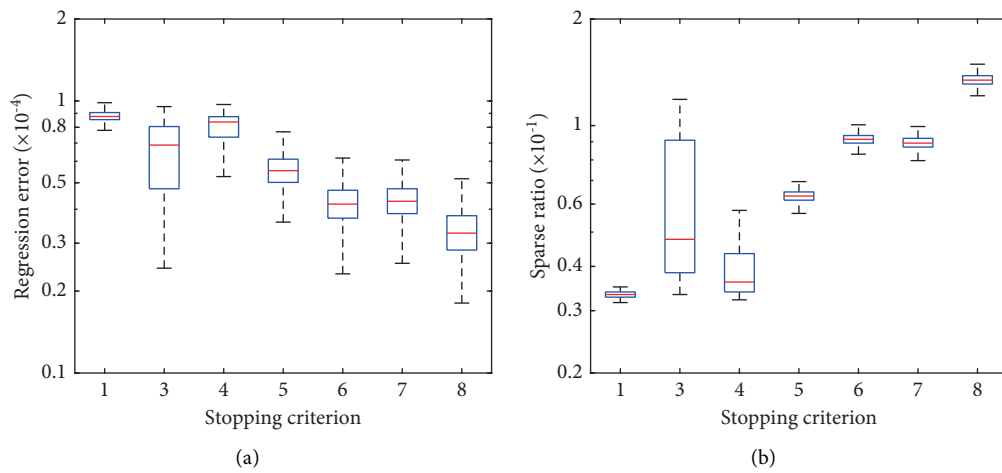
FIGURE 7: Results for the regression error and the sparsity ratio for the case $d = 20$. (a) The regression error. (b) The sparsity ratio.

(a)

(b)
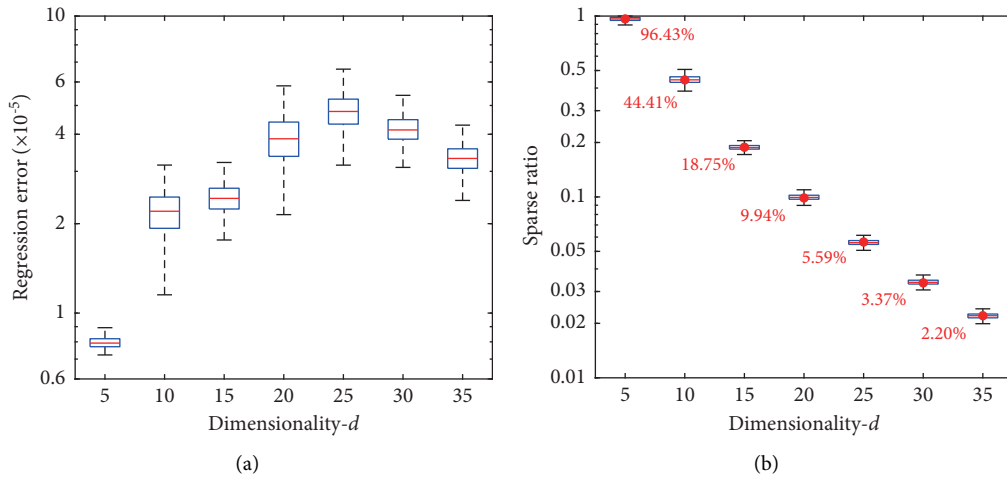
FIGURE 8: Results for the regression error and the sparsity ratio of the Gegenbauer polynomial-based surrogate model. (a) The regression error. (b) The sparsity ratio.

(a)

(b)

FIGURE 9: Results for response probability density functions (PDFs) of sparse Gegenbauer polynomial model with parameter $\beta = 0$. (a) Semilog plot of PDF: $d = 20$. (b) Semilog plot of PDF: $d = 35$.
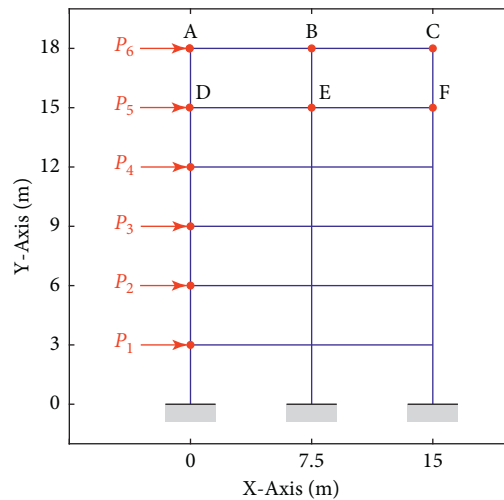
FIGURE 10: A steel frame structure subjected to lateral loads.

TABLE 2: Random variables of the steel frame structure.

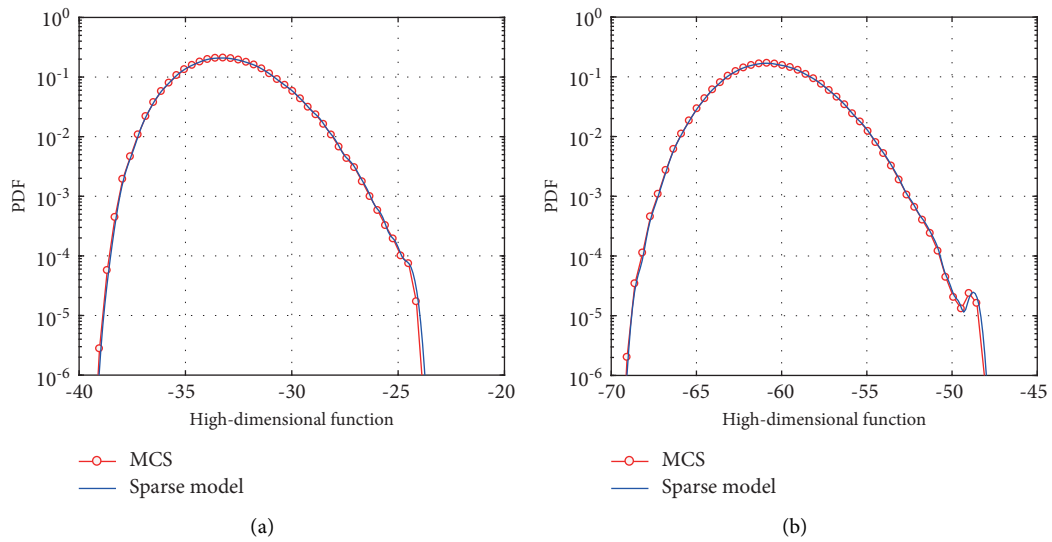| Symbol	Variable	Unit	Mean value	COV	Distribution
X_1	E_b	N/m^2	2×10^{10}	0.10	Log-normal
X_2	I_b	m^4	1×10^{-3}	0.10	Log-normal
X_3	E_c	N/m^2	2×10^{10}	0.10	Log-normal
X_4	I_c	m^4	1.5×10^{-3}	0.10	Log-normal
X_5	P_1	N	2.5×10^4	0.25	Normal
X_6	P_2	N	2.8×10^4	0.25	Normal
X_7	P_3	N	2.9×10^4	0.25	Normal
X_8	P_4	N	3.0×10^4	0.25	Normal
X_9	P_5	N	3.1×10^4	0.25	Normal
X_{10}	P_6	N	3.2×10^4	0.25	Normal

The subscripts b and c represent beam and column, respectively. COV: the coefficient of variation.

(a)

(b)

FIGURE 11: Results for structural failure probability of the steel frame structure predicted by means of the sparse Gegenbauer polynomial model with parameter $\beta = 0$. (a) Probability density function. (b) Probability of exceedance (POE).

FIGURE 12: Statistical characteristics of the structural failure probability obtained based on 100 repetitions of the sparse regression method.

FIGURE 13: A bar structure under distributed axial load.

FIGURE 14: Realizations of the modulus elasticity random field with various values of the correlation length parameter ($\delta = 0.1, 1.0, 10$, and 100).
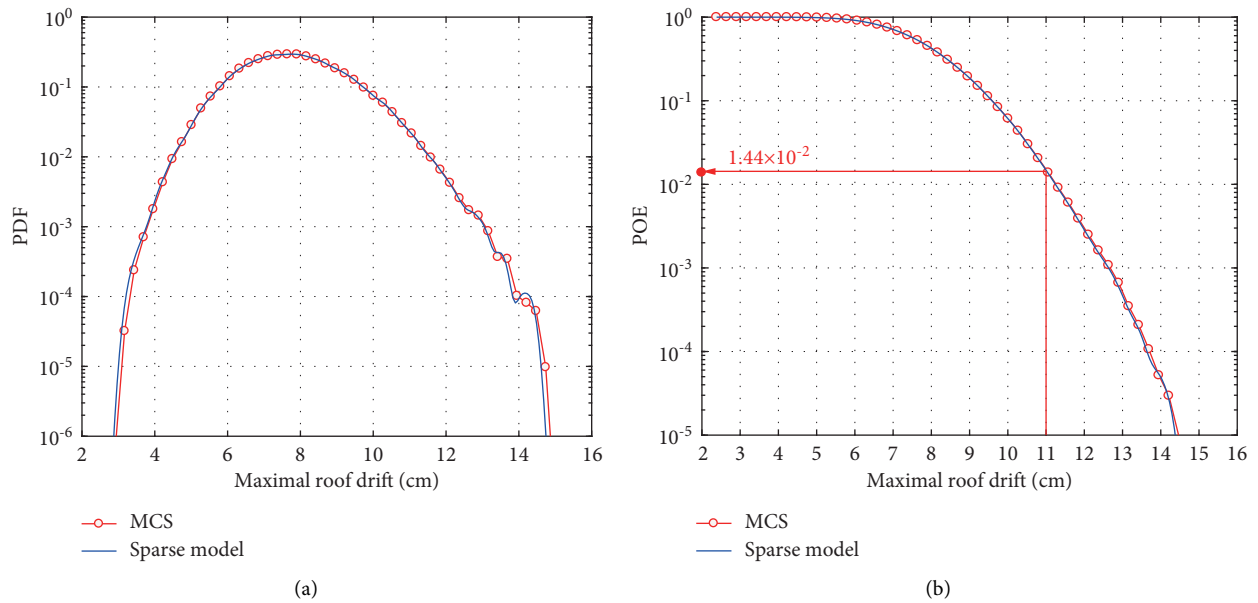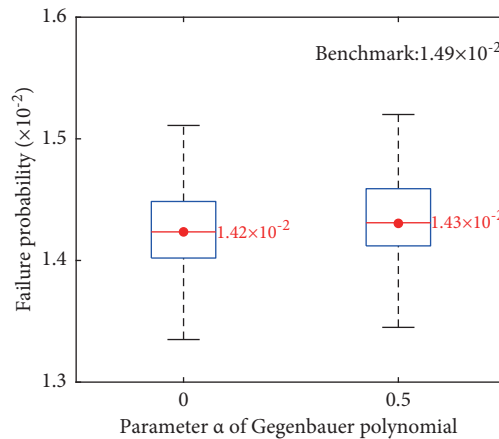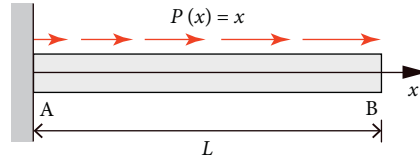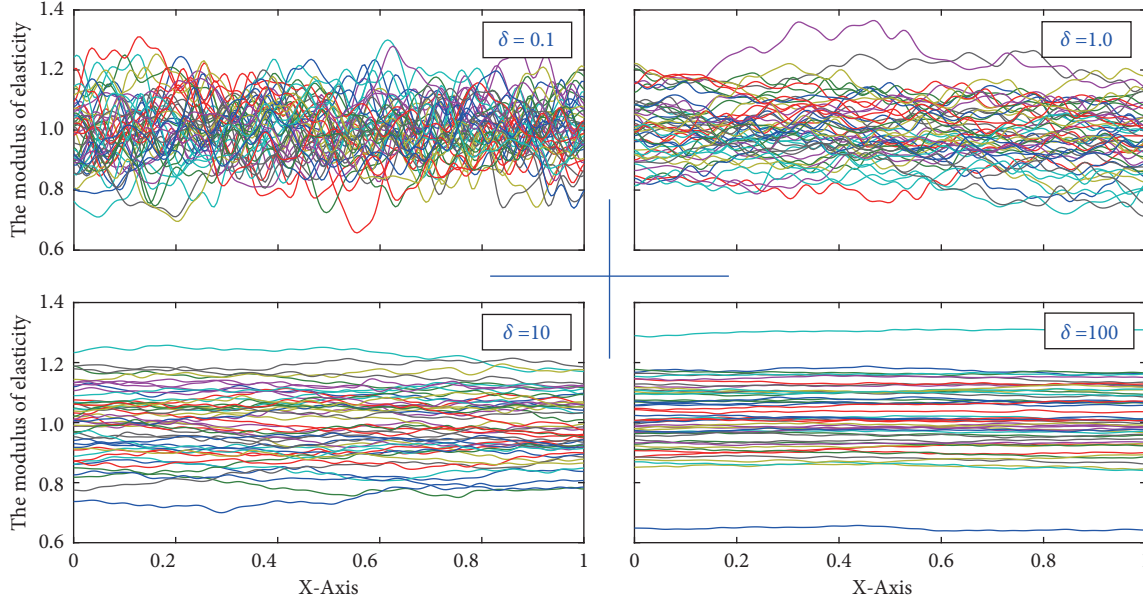
Following the theory of the Karhunen–Loève expansion, the material random field is numerically parameterized based on its first-d eigenpairs $\{\lambda_i, \phi_i(x)\}$ $(i = 1, \ldots, d)$ [36]:

$$E(x) \approx \mu_E(x) + \sum_{i=1}^{d} \sqrt{\lambda_i} \phi_i(x) X_i, \tag{32}$$

wherein X_i denote independent standard Gaussian random variables, whereas the mean value of the random field is constantly assumed as $\mu_E(x) = 1.0$.

Failure events for reliability analysis of the bar structure are defined by the maximum axial displacement $D_{\max}(\mathbf{X})$ over a threshold value of 0.40:

$$\text{failure events} = \{0.40 - D_{\max}(\mathbf{X}) \leq 0\}. \tag{33}$$

Here, random vector $\mathbf{X} = [X_1, \ldots, X_d]^T$ comprises all Gaussian random variables in equation (32) for numerical discretization of the random field.

With various realizations of the correlation length parameter, that is, $\delta = 0.1, 1.0, 10$, and 100, numerical realizations of the elasticity random field are presented in Figure 14. Note that ten random variables will be enough to represent more than 95% of the original variability. This implies that the random vector $\mathbf{X}$ consists of ten standard Gaussian random variables. In addition, a large value of the correlation length parameter (e.g., $\delta = 100$) increases the

statistical dependency between positions of the random modulus elasticity $E(x)$. This allows one to examine the numerical performance of the proposed approach in dealing with dependent input uncertainties.

To implement, the sparse regression method with the polynomial order $p = 3$ and 500 Sobol' sequences is employed to develop a surrogate model for the structural maximal axial displacement $D_{\max}(\mathbf{X})$. Results for PDFs of $D_{\max}(\mathbf{X})$ are presented in Figure 15 for various realizations of the correlation length parameter δ. It is observed that the response variability is directly related to the parameter δ in the random field model, and the case $\delta = 100$ determines the largest variation of the structural response quantity.

Based on the structural performance function defined in equation (33), Table 3 summarizes the structural failure probability for various realizations of the correlation length parameter δ. The close agreement between the estimation and benchmark results has verified the high accuracy and numerical efficiency of the sparse regression method.

Figure 16 further summarizes simulation results for the sparsity ratio and the global regression error of the surrogate model. The sparsity ratio result is dramatically decreased with an increase of the correlation parameter δ. A larger value of the parameter δ implies numerical realizations of the Young's Modulus at two different locations are strongly correlated. The statistical dependency will increase the

(a)

(b)
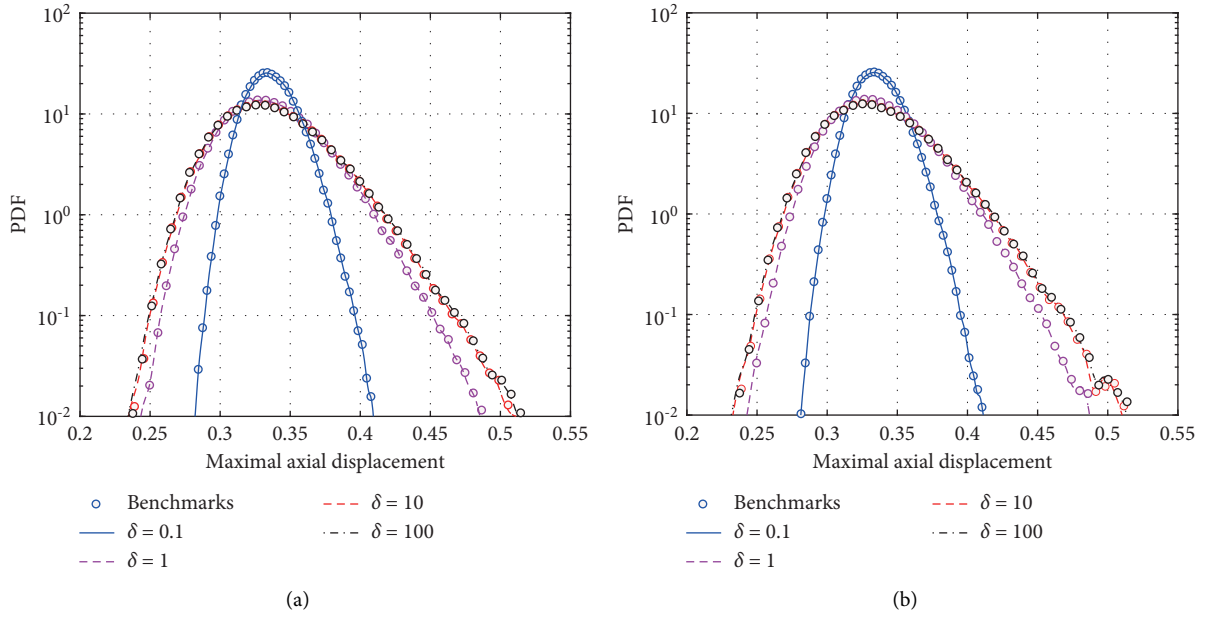
Figure 15: Results for the response distribution of the maximum axial displacement of the bar structure with various correlation length parameters. (a) The sparse surrogate model with the parameter $\beta = 0$. (b) The sparse surrogate model with the parameter $\beta = 1/2$.

Table 3: Structural failure probability for various values of the correlation length parameter (b).

	The correlation length parameter			
	$b = 0.1$	$b = 1.0$	$b = 10$	$b = 100$
MCS	3.20×10^{-4}	3.09×10^{-2}	4.63×10^{-2}	4.81×10^{-2}
Sparse model: $\beta = 0$	2.60×10^{-4}	3.10×10^{-2}	4.66×10^{-2}	4.85×10^{-2}
Sparse model: $\beta = 0.5$	2.60×10^{-4}	3.11×10^{-2}	4.66×10^{-2}	4.84×10^{-2}

(a)

(b)
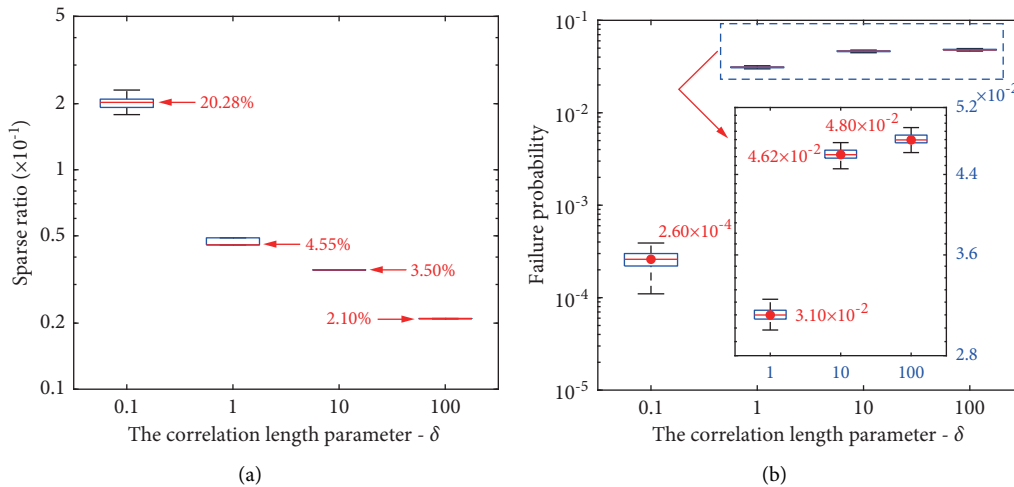
Figure 16: Results for the robustness analysis of the Gegenbauer polynomial-based surrogate model with parameter $\beta = 0$. (a) The sparsity ratio. (b) Structural failure probability.

structural failure probability as presented in Figure 16(b). Note that a small variation result for the structural failure probability further verifies the robustness of the proposed Gegenbauer polynomial-based regression method for reliability analysis of a structural model with dependent input uncertainties.

5. Conclusion

Structural reliability analysis is typically evaluated based on a multivariate performance function that defines small failure probabilities. It is significant to develop a surrogate model to mimic the true performance function as the brutal-force MCS based on the realistic model might be computationally intensive. This paper presents utilizing the Gegenbauer polynomials to constitute the explanatory dictionary, whereas principle component functions are adaptively selected via the OMP-based sparse regression algorithm. Due to the regression bias introduced by utilizing random samples, an excluding procedure to detect spuriously component functions is proposed based on the F statistics. Simulation results have shown that the Gegenbauer polynomial-based regression method can determine reliable estimation results for the investigated performance function. Small regression errors and the high sparsity of the surrogate model have demonstrated potential applications of the adaptive sparse regression algorithm for structural reliability analysis.

Data Availability

The simulation data within this submission are available based on the request.

Conflicts of Interest

The authors declare that they have no conflicts of interest.

References

[1] M. Rosenblatt, "Remarks on a multivariate transformation," *The Annals of Mathematical Statistics*, vol. 23, no. 3, pp. 470–472, 1952.

[2] P.-L. Liu and A. Der Kiureghian, "Multivariate distribution models with prescribed marginals and covariances," *Probabilistic Engineering Mechanics*, vol. 1, no. 2, pp. 105–112, 1986.

[3] S. Wang, "Reliability model of mechanical components with dependent failure modes," *Mathematical Problems in Engineering*, vol. 2013, Article ID 828407, 6 pages, 2013.

[4] R. E. Melchers, "Importance sampling in structural systems," *Structural Safety*, vol. 6, no. 1, pp. 3–10, 1989.

[5] J. Nie and B. R. Ellingwood, "Directional methods for structural reliability analysis," *Structural Safety*, vol. 22, no. 3, pp. 233–249, 2000.

[6] D. Meng, Y. Li, S.-P. Zhu, G. Lv, J. Correia, and A. de Jesus, "An enhanced reliability index method and its application in reliability-based collaborative design and optimization," *Mathematical Problems in Engineering*, vol. 2019, Article ID 4536906, 10 pages, 2019.

[7] G. I. Schuëller and H. J. Pradlwarter, "Benchmark study on reliability estimation in higher dimensions of structural systems-an overview," *Structural Safety*, vol. 29, no. 3, pp. 167–182, 2007.

[8] X. Zhang and M. D. Pandey, "Structural reliability analysis based on the concepts of entropy, fractional moment and dimensional reduction method," *Structural Safety*, vol. 43, pp. 28–40, 2013.

[9] H. P. Gavin and S. C. Yau, "High-order limit state functions in the response surface method for structural reliability analysis," *Structural Safety*, vol. 30, no. 2, pp. 162–179, 2008.

[10] X. Zhang and M. D. Pandey, "An effective approximation for variance-based global sensitivity analysis," *Reliability Engineering & System Safety*, vol. 121, pp. 164–174, 2014.

[11] X. Zhang, L. Wang, and J. D. Sørensen, "AKOIS: an adaptive Kriging oriented importance sampling method for structural system reliability analysis," *Structural Safety*, vol. 82, p. 101876, 2020.

[12] X. Zhang, L. Wang, and J. D. Sørensen, "REIF: a novel active-learning function toward adaptive Kriging surrogate models for structural reliability analysis," *Reliability Engineering & System Safety*, vol. 185, pp. 440–454, 2019.

[13] V. Cherkassky and Y. Ma, "Practical selection of SVM parameters and noise estimation for SVM regression," *Neural Networks*, vol. 17, no. 1, pp. 113–126, 2004.

[14] S. M. Clarke, M. Clarke, J. H. Griebsch, and T. W. Simpson, "Analysis of support vector regression for approximation of complex engineering analyses," *Journal of Mechanical Design*, vol. 127, no. 6, pp. 1077–1087, 2005.

[15] H. Fang and H. F. Mark, "Globle response approximation with radial basis functions," *Engineering Optimization*, vol. 38, no. 4, pp. 407–424, 2006.

[16] Y.-F. Zhang and Y.-L. Zhang, "Reliability sensitivity analysis method for mechanical components," *Mathematical Problems in Engineering*, vol. 2021, Article ID 7867003, 11 pages, 2021.

[17] O. P. Le Maîetre, M. T. Reagan, H. N. Najm, R. G. Ghanem, and O. M. Knio, "A stochastic projection method for fluid flow II.: random process," *Journal of Computational Physics*, vol. 181, no. 1, pp. 9–44, 2002.

[18] M. A. Tatang, W. Pan, R. G. Prinn, and G. J. Mcrae, "An efficient method for parametric uncertainty analysis of numerical geophysical models," *Journal of Geophysical Research Atmospheres*, vol. 102, no. 18, pp. 21925–21932, 1997.

[19] G. Blatman and B. Sudret, "An adaptive algorithm to build up sparse polynomial chaos expansions for stochastic finite element analysis," *Probabilistic Engineering Mechanics*, vol. 25, no. 2, pp. 183–197, 2010.

[20] V. Yaghoubi, S. Marelli, B. Sudret, and T. Abrahamsson, "Sparse polynomial chaos expansions of frequency response functions using stochastic frequency transformation," *Probabilistic Engineering Mechanics*, vol. 48, pp. 39–58, 2017.

[21] X. Zhang, M. D. Pandey, R. Yu, and Z. Wu, "HALK: a hybrid active-learning Kriging approach and its applications for structural reliability analysis," *Engineering with Computers*, 2021.

[22] J. Keiner, "Gegenbauer polynomials and semiseparable matrices," *Electronic Transactions on Numerical Analysis*, vol. 30, pp. 26–53, 2008.

[23] C. Ekanadham, D. Tranchina, and E. P. Simoncelli, "Recovery of sparse translation-invariant signals with continuous basis pursuit," *IEEE Transactions on Signal Processing*, vol. 59, no. 10, pp. 4735–4744, 2011.

[24] S. F. Cotter and B. D. Rao, "Sparse channel estimation via matching pursuit with application to equalization," *IEEE Transactions on Communications*, vol. 50, no. 3, pp. 374–377, 2002.

[25] J. A. Tropp and A. C. Gilbert, "Signal recovery from random measurements via orthogonal matching pursuit," *IEEE Transactions on Information Theory*, vol. 53, no. 12, pp. 4655–4666, 2007.

[26] T. T. Cai and L. Wang, "Orthogonal matching pursuit for sparse signal recovery with noise," *IEEE Transactions on Information Theory*, vol. 57, no. 7, pp. 4680–4688, 2011.

[27] D. Needell and R. Vershynin, "Uniform uncertainty principle and signal recovery via regularized orthogonal matching pursuit," *Foundations of Computational Mathematics*, vol. 9, no. 3, pp. 317–334, 2009.

[28] D. L. Donoho, Y. Tsaig, I. Drori, and J.-L. Starck, "Sparse solution of underdetermined systems of linear equations by stagewise orthogonal matching pursuit," *IEEE Transactions on Information Theory*, vol. 58, no. 2, pp. 1094–1121, 2012.

[29] A. M. Hasofer and N. C. Lind, "Exact and invariant second-moment code format," *Journal of the Engineering Mechanics Division*, vol. 100, no. 1, pp. 111–121, 1974.

[30] J. Keeiner, "Computing with expansions in Gegenbauer polynomials," *SIAM Journal on Scientific Computing*, vol. 31, no. 3, pp. 2151–2171, 2009.

[31] P. K. Suetin, *Ultraspherical Polynomials*, Encyclopedia of Mathematics, EMS Press, Berlin, Germany, 2001, https://encyclopediaofmath.org/wiki/Ultraspherical_polynomials.

[32] E. M. Stein and G. Weiss, *Introduction to Fourier Analysis on Euclidean Spaces*, Princeton University Press, Princeton, NJ, USA, 1971.

[33] G. Schuëller, "Computational stochastic mechanics: recent advances," *Computers & Structures*, vol. 79, no. 22-25, pp. 2225–2234, 2001.

[34] D. C. Montgomery, *Design and Analysis of Experiments*, John Wiley & Sons, New York, NY, USA, 7th edition, 2009.

[35] H. Dai, H. Zhang, and W. Wang, "A new maximum entropy-based importance sampling for reliability analysis," *Structural Safety*, vol. 63, pp. 71–80, 2016.

[36] R. G. Ghanem and P. D. Spanos, *Stochastic Finite Elements: A Spectral Approach*, Springer-Verlag, New York, NY, USA, 1991.

Research Article

Investigation on Deformation of the Flex-Gear and Optimization Design of Compound Curve Cam Wave Generator with Spiral

Shuyan Wang [1] **, Yudelong Zhang,** [1] **Shiteng Mao** [1] **, and Yu He** [2]

[1]*College of Mechanical Engineering, Donghua University, Shanghai 200051, China*
[2]*School of Urban Rail Transportation, Shanghai University of Engineering Science, Shanghai 201620, China*

Correspondence should be addressed to Shuyan Wang; shuyan@dhu.edu.cn

The deformation shape and mechanical property of flex-gear greatly affect the meshing accuracy and service life of harmonic drive, and the stress wave generator plays a decisive role in the deformation shape and mechanical properties of the flexible gear. The investigation on deformation of the flex-gear around the major axis is developed with comparative analysis with three kinds of traditional and commonly used wave generators. Based on the influence of the deformation around the major axis on meshing accuracy and service life, the eccentric arc cam wave generator improved by transition curve for controlling the deformation shape and reducing the deformation stress is developed. Considering the achievable flexibility of spiral with smooth curvature change rate, the contour of the compound curve cam wave generator with arc and spiral is proposed. The deformation of the flex-gear under the influence of this compound curve cam and the standard elliptic cam is further comparative analyzed. The conclusion shows that this compound curve cam can indeed reduce the deformation stress in the meshing area by increasing the meshing width, and correct deformation shape can also be gained by shape control on the whole circumference of the flex-gear's neutral layer.

1. Introduction

In harmonic drive, the flex-gear is in the severe condition of infinite alternating asymmetric cyclic stress, and the continuous deformation which affects the meshing quality and service life mainly depends on the deformation caused by the stress wave generator. Rather than the conventional single curve, the cam stress wave generator designed with the compound curve can effectively improve the mechanical deformation in the meshing area of the flexible gear. In the compound curve design, the types of curves, the parameters of curves, and even the curvature change rate of curves would all affect the mechanical property of the flex-gear [1, 2], so curve design and optimization [3–6] of the compound curve cam wave generator for lower deformation and high meshing quality is a main research domain in harmonic drive.

In order to improve the meshing performance and extend the service life of harmonic gear transmission, scholars

have made a lot of efforts in this regard. Yague [7] analyzed the von Mises stress generated by four different wave generators on the flex-gear. Gravagno [8] analyzed the kinematic errors caused by different wave generator profiles and derived the parametric equation between flex-gear and fixed circular spline. Bhabani [9] used the finite element method and experiments to compare the strain and stress of the flex-gear acted by the traditional and split cam generator. Li [10] conducted static and transient dynamic analysis of flex-gear under the action of typical contours. Routh [11] obtained the hydrodynamic lubrication equation of the interface between the flex-gear and wave generator by solving the generalized Reynolds equation. Vladis [12] discussed the angular displacement between the meshing area and the wave generator and established system equations among flex-gear, circular spline, and wave generators based on contact deformation. Fan [13] obtained the deformation relationship based on the plate and shell theory and further derived the neutral layer deformation equation.

Han [14] studied the stress and related vibration characteristics of the flex-gear with the numerical analysis tool. Hu [15] analyzed the influence of some geometric structural parameters such as the aspect ratio of the cup, the wall thickness, the round corner radius, and the width of the tooth ring on internal stress of the flex-gear. Yang [16] studied the influence of the flex-gear geometric parameters on the stress value and distribution for the short cup flex-gear. Ostapski [17, 18] proposed a method to solve the elastic deformation problem of the thin-walled shell structure with complex shape in the geometrically nonlinear shell theory. Sahoo [19] proposed a method to calculate contact tooth load and flex-gear stress by estimating the contact load of a large number of teeth pairs. Yang [20] proposed an accurate solution for the conjugate tooth profile of the cam wave generator harmonic drive. Xing [21] found that the radial displacement of the minor axis area of the flex-gear is less than the theoretical value, and there is a large film stress in the neutral layer of the flex-gear. Xin [22] simplified the gear tooth profile shape to triangle and trapezoid and compared the effect of the simplified tooth shape on the flex-gear. Zhang [23] analyzed the effect of radial deformation on the meshing performance of harmonic drive and obtained the stress distribution of the flex-gear deformed with the cam wave generator through finite element analysis. Dong [24] studied the deformation of the flex-gear and analyzed the mathematical model of the flex-gear.

In this study, main factors influencing the deformation shape and mechanical properties of the flex-gear are investigated such as the type of the stress wave generator, the curve's saturation level in the working area, and curvature change rate of the wave generator. The design principle of the wave generator for lower deformation and good meshing quality is developed. In the compound curve cam wave generator, spiral curve combined with arc is further proposed with correct parameters, and theoretical design, numerical comparative analysis, and finite element analysis on this compound curve cam wave generator have been carried out.

2. Conventional Cam Stress Wave Generator with Single Curve

Among various wave generator types, cam type can make the meshing of the flexible gear and the rigid wheel reach the ideal state with stable operation, high precision, and high efficiency. More importantly, the stress distribution of the flexible gear acted by the cam wave generator could be improved, and the bearing capacity would be higher than other wave generators. Nowadays, cam wave generators mainly include double eccentric arc cam, cosine cam, and standard ellipse. For the convenience of research, the contour equation of cam wave generators is unified as

$$\begin{cases} x = x(t), \\ y = y(t), \end{cases} \tag{1}$$

where x and y are the coordinate points of cam wave generator's profile, and t indicates the angular variable.

(1) When standard ellipse is chosen for the cam wave generator, the parametric equation is given as follows:

$$\begin{cases} x = a \cos(t), \\ y = b \sin(t). \end{cases} \tag{2}$$

Here, a is the semimajor axis of the standard ellipse, and b is the semiminor axis of the standard ellipse.

(2) When cosine curve is chosen for the cam wave generator, the parametric equation is given as follows:

$$\begin{cases} x = (0.5d_b + \omega_0 \cos(2t))\sin(t), \\ y = (0.5d_b + \omega_0 \cos(2t))\cos(t). \end{cases} \tag{3}$$

Here, d_b is the basic circle diameter of the cosine curve cam wave generator, and ω_0 is the amplitude of the cosine curve.

(3) When double eccentric arc is chosen for the cam wave generator, the parameter equation is

$$\begin{cases} x = r \cos(t); \ y = r \sin(t) + e, \\ \\ \left(\dfrac{\pi}{2} - \beta < t < \dfrac{\pi}{2} + \beta \ an \ d \ \dfrac{3\pi}{2} - \beta < t < \dfrac{3\pi}{2} + \beta \right), \\ \\ x = r \cos(\beta), \\ \\ \left(\beta - \dfrac{\pi}{2} \le t \le \dfrac{\pi}{2} - \beta \ an \ d \ \dfrac{\pi}{2} + \beta \le t \le \dfrac{3\pi}{2} - \beta \right), \end{cases} \tag{4}$$

here, r is the radius of the eccentric arc, and β is half of the arc angle.

Based on the size of the flexible gear in models 17–80 (Table 1), the basic parameters of the three cam wave generators are calculated as given in Table 2. The radial deformation and stress of the flex-gear acted by these three different wave generators are developed in FEM, as shown in Figures 1–3.

From Figure 1, the equivalent stress of the flex-gear around the major axis with the double eccentric arc wave generator is much less than with the other two cam wave generators. But from Figure 2, the radial deformation at the major axis is 0.310 mm with the double eccentric arc wave generator, 0.288 mm with the cosine curve cam wave generator, and 0.291 mm with the standard ellipse cam wave generator. The radial deformation at the major axis with the double eccentric arc wave generator is a lot different from the value given in theory, which is bigger and less accurate than with the standard ellipse or cosine curve cam wave generator. Taken together, although the double eccentric arc wave generator can effectively reduce the equivalent stress of the flex-gear around the major axis, the radial deformation of the flex-gear around the major axis is used to ensure the meshing quality deviates from the theoretical setting value. This is mainly due to the perimeter of the double eccentric

TABLE 1: The parameters of the flex-gear.

Parameters	Symbols	Values
Diameter of the neutral layer (mm)	Dm	41.98
Wall thickness (mm)	h	0.26
Width of tooth ring (mm)	bt	8
Width of cup (mm)	b	23.5
Thickness of cup bottom (mm)	hw	3
Outer diameter of cup bottom (mm)	Do	80

TABLE 2: Basic parameters.

Wave generator type	Parameters based on flexible gear in models 17–80	
Standard ellipse cam	$a = 15.418$ mm	$b = 14.88$ mm
Cosine cam	$r_b = 15.15$ mm	$\omega_0 = 0.268$ mm
Double eccentric arc cam	$r = 14.48$ mm	$e = 0.938$ mm $\beta = 30°$

arc wave generator is shorter than that of equidistant curve of the flex-gear neutrosphere, which would lead to lose control of the flex-gear's deformation shape around the minor axis, so the deformation at the major axis will deviate from the control shape set by the wave generator and the radial deformation would inevitably increase.

In addition, there is also a stress plateau phenomenon in the stress curve of the flex-gear. From Figure 1, the stress curve of the flex-gear shows a stress plateau about 50° around the semimajor axis, and then, the deformation stress reduces rapidly to another stress plateau with a much lower stress value around the semiminor axis. The value and the width of the stress plateau area around the major axis with cosine curve type is a litter bigger than with the conventional ellipse cam. It is worth noting that although the radial deformation of the flex-gear around the major axis with the double-arc wave generator is large, the value of the stress plateau is smaller and the width is bigger than with the other two cam wave generators. The analysis of the stress curve shows the following: (1) the value of the stress plateau around the major axis is mainly determined by the maximum deformation given in theory and the contour's shape of the cam; (2) the width of the stress plateau around the major axis is mainly affected by the contour's shape of the cam, which strongly affected the number of meshing teeth; and (3) the velocity of stress reduction between the two stress plateaus depends on the curvature change rate of the cam's contour.

In summary, designing a compound curve cam wave generator with shape control of full perimeter can realize high meshing accuracy, and an appropriate shape around the major axis can reduce the deformation stress and increase the number of meshing teeth to improve the service life.

3. Design Method of Combined Cam Wave Generator

There are two points in designing a good combined cam wave generator: one is to choose an appropriate curve for the deformation shape around the major axis and the other is to fit the transition curve between the appropriate curves with continuous curvature for shape control of full perimeter.

3.1. Transition Curve.
Transition curve refers to the curve with the continuous curvature set between straight line and circular curve, circular curve and circular curve in plane with the same turning direction. As shown in Figure 3, there are many types of transition curves, such as cyclotron, cubic parabola, seventh quartic, half wave sine, one wave sine, double helix, and multicenter complex curve. In road design, when the curve radius on the main line is relatively small, transition curve should be added between the circular curve and the straight line to realize the gradual transition of the curvature and reduce impact at the mutation point of the traffic. It can make the lateral force of the vehicle gradually change, which is conducive to the safety and stability of driving, and can meet the visual and psychological requirements of the driver. The commonly used transition curve of highway and ramp is spiral, also known as radial spiral, as shown in Figure 4. The curve is not only beautiful but also consistent with the trajectory of the driver turning the steering wheel from a circular curve to a straight line or from a straight line to a circular curve.

The essential characteristic of spiral is given as follows:

$$\frac{dk}{dl} = \pm \frac{1}{A^2}, \qquad (5)$$

where dk/dl means that the curvature k changes with the arc length l, and $\pm$ indicates that the curvature increases or decreases with the arc length. A is the parameter of the spiral, which is the geometric mean of the radius R of the arc segment and the total length of the spiral Ls. The larger A is, the slower the curvature changes and the slower the curve turns. And in reverse, the smaller A is, the faster the curvature changes and the faster the curve turns.

In equation (5), A cannot represent the increase or decrease of curvature. Thus, a is introduced, the relationship between a and A can be expressed as $|a|A^2 = 1$. Equation (5) can be rewritten as follows:

$$\frac{dk}{dl} = a, \qquad (6)$$

where a is the rate of curvature changing, and it can be positive or negative.
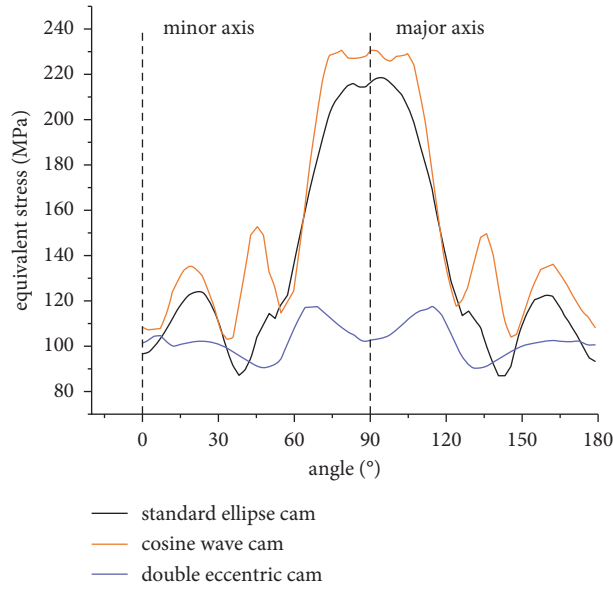
FIGURE 1: Equivalent stress of the flex-gear with three cam wave generators.

In our cam design, considering the disadvantages of the flex-gear's deformation stress with the double-arc wave generator, a compound curve with two arcs and two spiral curves is developed for the contour design of a good combined cam wave generator. Thus, the spiral is smooth and its curvature changes proportionally with the length of the curve, which can maintain the advantages of the double eccentric arc cam wave generator with lower equivalent stress and bigger width of the stress plateau around the major axis and can even more improve the accuracy of the flex-gear's deformed shape.

3.2. Contour Design of Combined Cam Wave Generator Based on Spiral.
Because the contour of the combined cam wave generator is axisymmetric, only 1/4 of the contour needs to be designed. In order to explain the combination of spiral and arc in the contour of the compound curve cam wave generator, the coordinate systems are setup as shown in Figure 5. The global coordinate system oxy is fixed at the original point of the spiral, the x axis is tangent to the spiral at the original point, and the y axis satisfies the right-hand rule. The local coordinate system $o_1 x_1 y_1$ is fixed at the center of the arc, and the local coordinate system is parallel to the global coordinate system.

General solutions of spiral's differential equation can be expressed as

$$x + iy = x_0 + iy_0 + (\cos T_0 + i \sin T_0)$$

$$\left\{ (L - L_0) \sum_{n=0}^{+\infty} \sum_{r=0}^{n} \frac{i^n \left[(a/2)(L - L_0)^2 \right]^r \left[k_0 (L - L_0) \right]^{n-r}}{r!\,(n-r)!\,(n+r+1)} \right\}, \tag{7}$$

where x and y indicate the coordinate point of spiral, x_0 and y_0 indicate the coordinate point of the spiral segment's starting point, T_0 is the forward direction of the spiral

segment's starting point. L is the arc length of the spiral segment's ending point, L_0 is the arc length of the spiral segment's starting point, and k_0 is the curvature of the selected spiral segment's starting point.

Because the starting point of the spiral segment is at the coordinate origin of the global coordinate system oxy and the direction of the starting point is tangent to axis ox, so $x_0 = 0$, $y_0 = 0$, and $T_0 = 0$. The differential equation of spiral is simplified as

$$x + y = l * \sum_{n=0}^{\infty} \sum_{r=0}^{n} \frac{(a/2 * l)^r * (k_0 * l)^{n-r}}{r!\,(n-r)!\,(n+r+1)}, \quad l \in [0, ls], \tag{8}$$

where l is the arc length of the spiral segment from the origin point to any point, and ls is the full length of the spiral segment.

In order to control the deformation shape on the whole circumference, the circumference of the compound curve should be equal to that of the neutral layer of the flex-gear. So, the length of the spiral segment can be deduced as

$$ls = r_m * \frac{\pi}{2} - r_0 * \beta, \tag{9}$$

where r_m is the radius of the flex-gear's neutral layer, r_0 is the radius of arc segment around the major axis, and β is the semienvelop angle of the arc segment.

Because the curvature at the end of the spiral segment is the same as that of the arc segment, the curvature change rate of the spiral segment is

$$a = \frac{k_s - k_0}{ls}, \tag{10}$$

where k_s is the curvature at the end of the spiral segment and $k_s = 1/r_0$, k_0 is the curvature at the start of the spiral and $k_0 = 1/r_r$, and r_r is the curvature radius of the spiral segment's starting point.
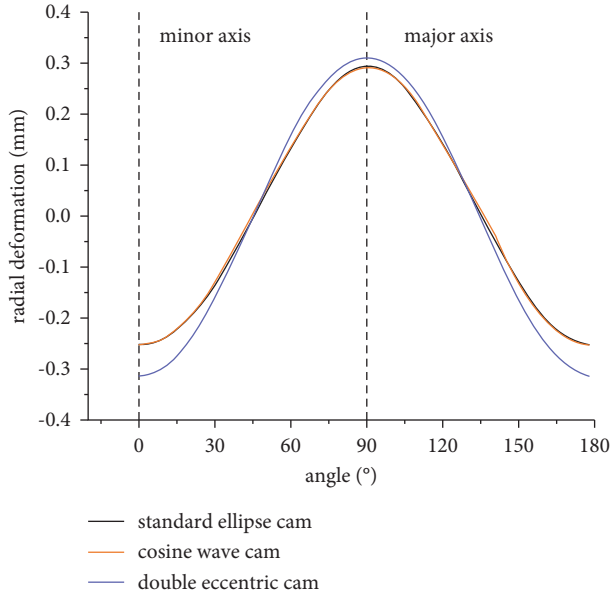
FIGURE 2: Radial deformation of the flex-gear with three kinds of wave generator.
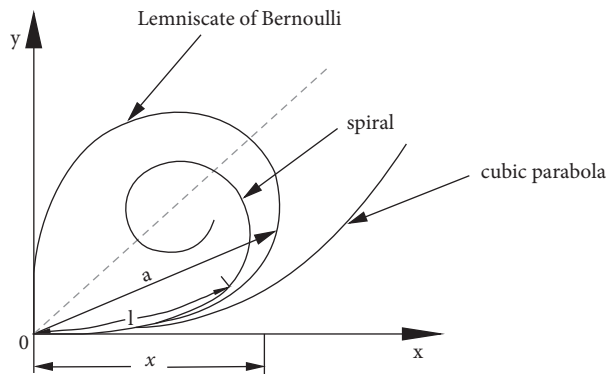

FIGURE 3: Common transition curves.

FIGURE 4: Spiral curve in road design.

The coordinates of the end point of the spiral segment in the compound curve cam wave generator can be described as

$$\begin{cases} x_z = x_e + r_0 * \cos(\beta), \\ y_z = y_e - r_0 * \sin(\beta), \end{cases} \tag{11}$$

where (x_e, y_e) is the origin of the local coordinate system $o_1 x_1 y_1$ and is also the center of the arc segment.

After solving simultaneous equations (8), (9), (10), and (11), the equations of the spiral segment and the arc segments of the flex-gear's center line layer after deformation can be obtained. The equation of the arc segment after deformation can be expressed as

$$\begin{cases} x_r = r_0 * \cos(t) + x_e, \\ y_r = y_z + r_0 * \sin(\beta) + r_0 * \sin(t). \end{cases}, \quad t \in [-\beta, \beta]. \tag{12}$$

Then, the contour curve of the compound curve cam can be obtained by using the equidistant curve, and the equation can be expressed as

$$\begin{cases} x_{wr} = x_r + \dfrac{y_r{}'(t) * h}{\sqrt{x_r{}'(t)^2 + y_r{}'(t)^2}}, \\[4mm] y_{wr} = y_r - \dfrac{x_r{}'(t) * h}{\sqrt{x_r{}'(t)^2 + y_r{}'(t)^2}}, \end{cases}, \quad t \in [-\beta, \beta], \tag{13}$$

$$\begin{cases} x_{ws} = x + \dfrac{y_s{}'(l) * h}{\sqrt{x_s{}'(l)^2 + y_s{}'(l)^2}}, \\[4mm] y_{ws} = y - \dfrac{x_s{}'(l) * h}{\sqrt{x_s{}'(l)^2 + y_s{}'(l)^2}}, \end{cases}, \quad l \in [0, ls],$$

where (x_{wr}, y_{wr}) indicates the coordinate point of the arc segment in the compound curve cam, (x_{ws}, y_{ws}) indicates the coordinate point of the spiral segment, and h indicates the equidistant distance.

4. Finite Element Analysis and Discussion of the Case Study

In this compound curve cam wave generator, the radius of the arc segment and the eccentric distance are used as variables for optimization of the deformation shape around the major axis (Table 3), and the radial deformation and the equivalent stress of the flex-gear acted by the compound curve cam with different parameters are developed in FEM, as shown in Figures 6 and 7.

From Figure 6, under the influence of this compound curve cam with arc and spiral, radial deformation of the flex-gear at the major axis varied from 0.291 mm to 0.292 mm with the value of the eccentric distance e varied from 0.95 mm to 0.7 mm. Compared with under the influence of double eccentric arc cam, the radial deformation of the flex-gear is controlled to a more accurate value from 0.310 mm to 0.291 mm or 0.292 mm, which is also less than 0.5% different from with the conventional ellipse cam. This shows that the
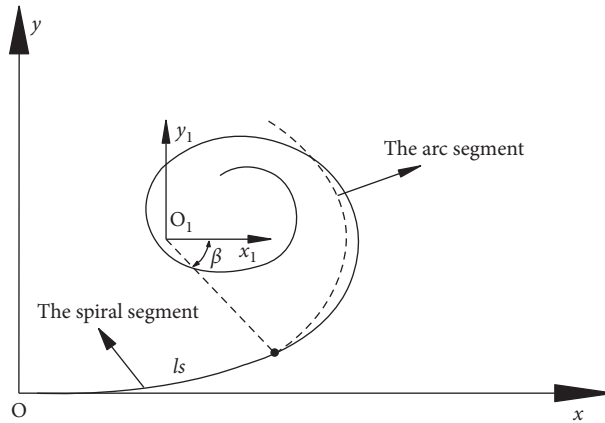
FIGURE 5: Coordinate system of the compound curve.

TABLE 3: The parameters of the wave generator.

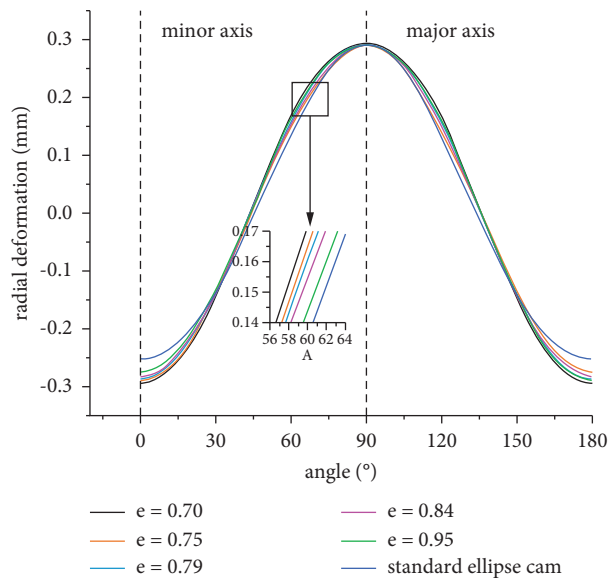|	Symbols	Values
Radius of the arc segment (mm)	r_0	20.558–20.308
Eccentric distance (mm)	E	0.7–0.95
The wrap angle (°)	β	30°

FIGURE 6: Radial deformation with different parameters.

compound curve cam with arc and spiral can effectively realize accurate deformation shape around the major axis by controlling the deformation shape of the flex-gear on the whole circumference.

From Figure 7, compared with acted by the conventional ellipse cam, the equivalent stress of the flex-gear around the major axis under the influence of the compound curve cam in different parameters showed reduction ranging from about 170 MPa to 200 MPa. Moreover, the equivalent stress of the flex-gear around the major axis decreases with the

increase of the arc segment's radius. However, if the radius of the arc segment is too large, the stress concentration near the connection point will be caused and the width of the stress plateau will be shortened. This is mainly because that increasing the radius of arc can make more teeth in meshing to gain a wider stress platform and share the load, but too large radius will lead to interference, so an appropriate radius is needed in contour design of the compound curve type. In other words, the meshing quality of the flex-gear can be easy. After parameters optimization, the equivalent stress of the
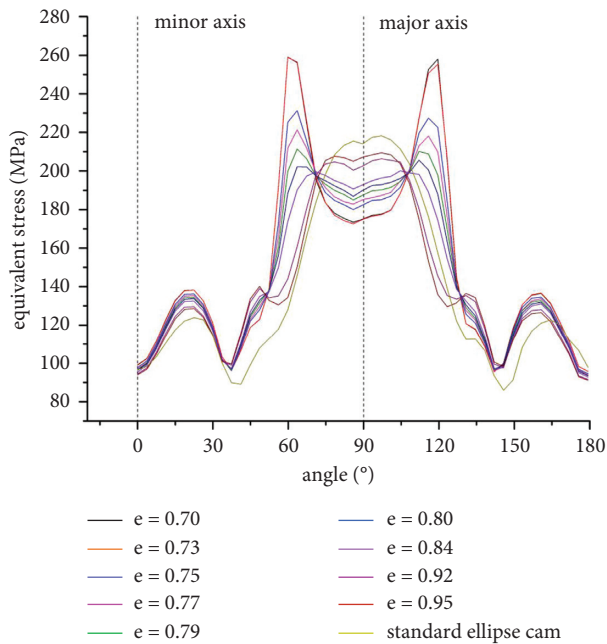
FIGURE 7: Equivalent stress with different parameters.

flex-gear around the major axis acted by the compound curve cam wave generator with $e = 0.84, r = 20.418$ can be reduced 9.92% from 214.08 MPa to 192.84 MPa, the range of stress variation is also reduced 18.91% from 132.317 MPa to 107.295 MPa, and the width of the stress plateau around the major axis is increased about from 29.89° to 48.58°.

5. Conclusion

In this study, the main factors affecting the accuracy and stress of the flex-gear are analyzed and discussed, including the type of stress wave generator, the type of the cam contour, and its parameters. On this basis, in order to obtain higher meshing accuracy and lower deformation stress, a compound curve cam wave generator is proposed with arc and spiral. The design method of this compound curve contour is established, numerical analysis is also carried out for its influence on the deformation of flex-gear, and parameter optimization is further carried out. The results show the following.

(1) The flex-gear can gain more accurate deformation shape under the action of the cam wave generator by shape control on the whole circumference, which is beneficial for the meshing accurate of the harmonic drive. The value and the width of deformation stress plateau around the major axis of flex-gear depend on the theoretical deformation value and the contour's corresponding curve of the wave generator.

(2) The compound curve cam with appropriate design not only can achieve better mechanical property around the meshing area but also can gain accurate deformation shape of the flex-gear. The double eccentric arc wave generator can indeed reduce the deformation stress in the meshing area, but the

control of the flex-gear's deformation shape is poor. Therefore, it is an effective method to improve the double eccentric arc wave generator with a compound curve.

(3) Based on the achievable flexibility of spiral with the smooth curvature change rate, a method of compound curve cam with spiral and arc is carried out. Compared with acted by the conditional ellipse cam, first of all, the deformation shape of the flex-gear around the major axis acted by the compound curve wave generator with $e = 0.84, r = 20.418$ is controlled very well. Second, the equivalent stress around major axis reduces 9.92%, the width of the stress platform around the major axis increases about from 29.89° to 48.58°, and the range of stress variation also reduces 18.91%.

Data Availability

The data that support the findings of this study are available from the corresponding author upon request.

Conflicts of Interest

The authors declare that they have no conflicts of interest.

References

[1] Y. Shen and Q. Ye, *Theory and Design of Harmonic Gear Transmission*, China Machine Press, Beijing, China, 1985.

[2] Y. He, P. Zou, Z. Zhu et al., "Design and application of a flexure-based oscillation mechanism for surface texturing," *Journal of Manufacturing Processes*, vol. 32, pp. 298–306, 2018.

[3] D. Meng, Z. Hu, P. Wu, S.-P. Zhu, J. A. Correia, and A. M. P. De Jesus, "Reliability-based optimisation for offshore structures using saddlepoint approximation," *Proceedings of the Institution of Civil Engineers - Maritime Engineering*, vol. 173, no. 2, pp. 33–42, 2020.

[4] D. Meng, T. Xie, P. Wu, S.-P. Zhu, Z. Hu, and Y. Li, "Uncertainty-based design and optimization using first order saddle point Approximation method for multidisciplinary engineering systems," *ASCE-ASME Journal of Risk and Uncertainty in Engineering Systems, Part A: Civil Engineering*, vol. 6, no. 3, Article ID 04020028, 2020.

[5] P. Zhi, Y. Li, B. Chen, M. Li, and G. Liu, "Fuzzy optimization design-based multi-level response surface of bogie frame," *International Journal of Structural Integrity*, vol. 10, no. 2, pp. 134–148, 2019.

[6] Y.-H. Li, Z. Sheng, P. Zhi, and D. Li, "Multi-objective optimization design of anti-rolling torsion bar based on modified NSGA-III algorithm," *International Journal of Structural Integrity*, vol. 12, no. 1, pp. 17–30, 2019.

[7] Y.-S. Eloy, I. Gonzalez-Perez, and F.-A. Alfonso, "Stress analysis of strain wave gear drives with four different geometries of wave generator," *Meccanica*, vol. 55, no. 11, pp. 2285–2304, 2020.

[8] G. Federico, Mucino, V. Hugo, and P. Ettore, "Influence of wave generator profile on the pure kinematic error and centrodes of harmonic drive," *Mechanism and Machine Theory*, vol. 104, pp. 100–117, 2016.

[9] Bhabani, S. Mahanto, V. Sahoo, and R. Maiti, "Effect of cam insertion on stresses in harmonic drive in industrial robotic

joints," *Procedia Computer Science*, vol. 133, pp. 432–439, 2018.

[10] L. Li, *Static and dynamic analysis of flexspline and flexible bearing under the cam with typical profile*, Ph.D. Thesis, Harbin Institute of Technology, Harbin, China, 2016.

[11] B. Routh, R. Maiti, and A. K. Ray, "Aspects of lubrication at the wave generator - flexspline interface in strain wave gearing units," *International Gear Conference*, vol. 8, pp. 26–28, 2014.

[12] V. Kosse, "Analytical investigation of the change in phase angle between the wave generator and the teeth meshing zone in high-torque mechanical harmonic drives," *Mechanism and Machine Theory*, vol. 32, no. 5, pp. 533–538, 1997.

[13] Y. Fan and H. Wang, "Study on the deformation of flexspline in the engagement output harmonic drive," *Journal of Nanjing University of Science and Technology*, vol. 20, no. 1, pp. 38–42, 1996.

[14] S. Han and S. Hoon, "A study on stress and vibration analysis of a steel and hybrid flexspline for harmonic drive," *Composite Structures*, vol. 48, no. 1, pp. 827–833, 1999.

[15] S. Hu, T. Yao, H. Qin, Y. Zhang, and B. Yang, "Research of internal stress distribution of double arc flexspline," *Journal of Mechanical Transmission*, vol. 44, no. 05, pp. 23–28, 2020.

[16] Y. Pei, *Harmonic Gear Driving Device and the Short Flexspline study[D]*, China Academy of Machinery Science and Technology, Beijing, 2006.

[17] W. Ostapski, "Analysis of the stress state in the harmonic drive generator-flexspline system in relation to selected structural parameters and manufacturing deviations," *Bulletin of the Polish Academy of Sciences, Technical Sciences*, vol. 58, no. 4, pp. 683–698, 2010.

[18] W. Ostapski and I. Mukha, "Stress state analysis of harmonic drive elements by FEM," *Bulletin of the Polish Academy of Sciences*, vol. 55, no. 1, pp. 115–123, 2007.

[19] V. Sahoo and M. Rathindranath, "Load sharing by tooth pairs in involute toothed harmonic drive with conventional wave generator cam," *Meccanica*, vol. 53, no. 1, pp. 33–394, 2018.

[20] Y. Yang, J. Wang, Q. Zhou, J. Zhu, and W. Yang, "Exact solution for conjugate profiles of zero backlash harmonic drives with elliptical cam wave generators," *Journal of Central South University*, vol. 48, no. 12, pp. 3231–3238, 2017.

[21] J. Xing, Y. Wang, and X. Chen, "Research on deformation and stress of flexspline in harmonic drive with cam wave generator. Machine Design and Research," in *Proceedings of The 10th International Conference on Chinese Institutions and Machine Science Applications (2013CCAMMS)*, pp. 147–150, Shanxi, China, December 2013.

[22] H. B. Xin, H. N. Mo, J. C. Gao et al., "Study on the gear tooth influence coefficients of flexspline of harmonic drive," *Advanced Materials Research*, vol. 774-776, pp. 144–147, 2013.

[23] L. Zhang, X. Liu, C. Wang, W. Leyu, X. Qiao, and R. Wang, "Influence of radial deformation on stress of flexspline and meshing characteristic of harmonic reducer," *Journal of Mechanical Transmission*, vol. 41, no. 9, pp. 166–169, 2017.

[24] H. Dong and D. Wang, "Elastic deformation characteristic of the flexspline in harmonic drive," in *Proceedings of the ASME/IFTOMM, International Conference on Reconfigurable Mechanisms and Robots*, pp. 363–369, London, UK, July 2009.